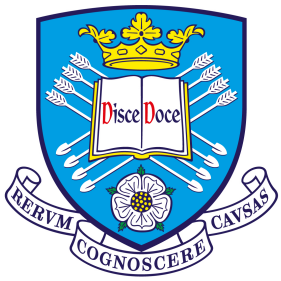

The University Of Sheffield.

Combining Extracellular Vesicles with Porous Electrospun Scaffolds for the Development of New Multifunctional Membranes for Tissue Engineering Applications

Hatim Dhaifallah Alqurashi

A thesis submitted in partial fulfilment of the requirements for the degree of Doctor of Philosophy

The University of Sheffield
Faculty of Medicine, Dentistry and Health
School of Clinical Dentistry

June 2022

الحمد لله رب العالمين

First and foremost, I would like to praise Allah the Almighty, the Most Gracious, and the Most Merciful for His blessing given to me during my study and in completing this thesis.

Acknowledgments

First and foremost, I would like to offer my heartfelt gratitude to my supervisors, Prof. Daniel W Lambert and Dr. Ilida Ortega Asencio, for their continuous encouragement, motivation, and support during my PhD. This has been a fascinating learning experience that would not have been possible without their assistance.

I would like to thank Dr. Stuart Hunt for his help with EVs isolation protocols, Prof. Fiona M Boissonade and Dr. Oscar O Solis Castro for providing me with human dental pulp cells. At the Department of Materials Science and Engineering, I would like to thank Dr. David Ramous for his training and guidance in CAM assay and Christopher Hill for his assistance with microscopy. I would also like to thank Prof. Steve Arms and Dr.Edwin C Johnson from the chemistry department, for their help with measuring the zetapotential of EVs and scaffold. A special thanks also for the technical support staff at the dental school whose training and assistance were essential for this project to be completed.

Special thanks to my funder, the Saudi Arabian Cultural Bureau in London and king Faisal University, for their financial support in making this PhD happen.

I'd like to express my deepest gratitude to my wife, Nuha, for her absolute love, patience, and care. Thank you for being with me and for your appreciated sacrifices. Special thanks also to my daughter, Deemah, I am sorry for not giving you the time you deserve.

Last but not least, I'd like to present my sincere gratitude to my dear mother and my father, for their great role in my life and their numerous sacrifices for me and my siblings. I hope that the time missed taking care of them is worthwhile. Special thanks also to my brothers, sisters and my friends for the encouragement and uplifting support throughout this journey.

Abstract

Extracellular vesicles (EVs) are membrane-enclosed vesicles that are released by cells and mediate cell–cell communication via their protein, lipid, carbohydrate, and nucleic acid (RNA, DNA) cargo. EVs are involved in a multitude of physiological processes including development, cell differentiation and angiogenesis having also been associated with tissue repair. The aim of this project was to optimise the functionalisation of electrospun scaffolds with EVs and to evaluate biological functionality for their future use in tissue engineering applications.

Extracellular vesicles were successfully isolated from oral cancer cell line (H357), normal oral fibroblast (NOF) and human dental pulp stem cells (HDPS) cells *in vitro* using ultracentrifugation (UC) and size exclusion chromatography (SEC) as assessed by NTA and determination of the presence of EV marker proteins (CD9, CD63 and CD81). Electrospun scaffolds were manufactured using an upright in-house electrospinning rig using poly(caprolactone) (PCL).

A functionalisation comparative study showed that the use of air plasma treatment (when compared to heparin treatment) increased the number of EVs attached to the scaffolds and provided homogeneous incorporation of EVs within the fibrous network. Over the course of 21 days, NTA showed a slow release of 40% of EVs from the scaffolds.

The zetapotential of EVs and scaffolds was measured to provide a better understanding of the mechanism of EVs attachment and release. All EVs exhibited anionic character regardless of the cell type (with a significantly higher anionic character of H357 EVs when compared to primary cells EVs). Plasma-treated scaffolds exhibited a positive zetapotential in comparison to the neutral charge of PCL

and highly negative charge of heparin-treated scaffolds which may explain the high attachment of negatively charged EVs on plasma-treated scaffolds.

In vitro, no effect of myofibroblast EVs or EVs-modified scaffold was found on the migration of NOF cells. When using the Chick Chorioallantoic Membrane (CAM) assay angiogenesis model, HDPS EVs modified scaffolds were able to induce vascular formation at a level comparable to the positive control, VEGF. We also found that plasma-treated PCL scaffolds promoted significant vascular formation in comparison to untreated PCL. However, an osteogenesis assay showed no significant effect of HDPS EVs on the osteo-differentiation rat bone marrow MSCs.

In conclusion, here we provide evidence that electrospun scaffolds can be functionalized with EVs and provide sustained slow release, offering an opportunity to develop novel, cell-free and tuneable approaches to tissue engineering. Furthermore, HDPS EV-modified scaffolds provide a promising way to promote vascularization, which can be used for a range of tissue engineering applications.

Publications

Alqurashi, H., Ortega Asencio, I. and Lambert, D.W., 2021. The emerging potential of extracellular vesicles in cell-free tissue engineering and regenerative medicine. *Tissue Engineering Part B: Reviews*, *27*(5), pp.530-538.

Prizes

1- 2022 IADR/Kulzer Travel Award, International Association for Dental Research (IADR)

2- First year oral presentation, School of Clinical Dentistry, Postgraduate Research Day 2020

Poster presentations

1- Combining extracellular vesicles with porous electrospun scaffolds for the development of multifunctional membranes for tissue engineering UKEV 2019, London, UK
2- Electrospun scaffolds as novel platforms for sustained release of extracellular vesicles for cell-free tissue engineering, TERMIS 2021, Online

Oral presentations

1- Sustained release of extracellular vesicles using electrospun scaffold as a novel approach for cell-free tissue engineering, BSODR 2021, Birmingham, UK
2- Sustained release of human dental pulp stem cell-derived extracellular vesicles from electrospun scaffold improves angiogenesis, Kulzer Award presentation, IADR 2022.

Table of Contents

List of Figures

List of Tables

List of abbreviations

AFM	Atomic force microscopy
ALIX	ALG-2-interacting protein X
ARF6	ADP-ribosylation factor 6
CNS	Central nervous system
CSF	Cerebrospinal fluid
CDE	Caveolin-dependent endocytosis
CIE	Clathrin-independent endocytosis
CM	Conditioned cell culture medium
CME	Clathrin-mediated endocytosis
DDS	Drug delivery systems
DNA	Deoxyribonucleic acid
ECM	Extracellular matrix
ERK	Extracellular signal-regulated kinase
ESCRT	Endosomal sorting complex required for transport
EV/ EVs	Extracellular vesicle(S)
HDSP	Human dental pulp stem cells
ILV	Intraluminal vesicle
ISEV	International Society of Extracellular Vesicles
miRNA	MicroRNA
MLCK	Myosin light-chain kinase
MP	Macropinocytosis
mRNA	Messenger RNA
MSC	Mesenchymal stromal cell
MV	Microvesicle

MVB	Multivesicular body
NTA	Nanoparticle tracking analysis
PLD	Phospholipase D
PS	Phosphatidylserine
qPCR	Quantitative polymerase chain reaction
RNA	Ribonucleic acid
SEC	Size exclusion chromatography
TE	Tissue engineering
TEM	Transmission electron microscopy
UC	Ultracentrifugation
WB	Western blot

Chapter 1

Introduction and literature review

Introduction

Tissue and organ failure or damage represents a devastating problem that affects healthcare systems. During the last century, organ transplant has been a primary solution to these problems; however, many drawbacks exist to organ transplantation, including the lack of organ donors, high costs of treatment, the rejection of transplanted tissues, and the long-term recovery process, which make this solution less than optimal (Beyar., 2011).

To overcome these problems, research and innovation have been directed toward the fabrication of bioengineered tissues and organs. Tissue engineering (TE) has become an attractive area of research and has been defined as “an interdisciplinary field that applies the principles of engineering and of the life sciences toward the development of biological substitutes that restore, maintain, or improve tissue function” (Langer *et al*., 1993). The overall requirements for TE include: 1) a appropriate source of target cells and proper isolation and cultivation methods; 2) a biomaterial device capable of transferring, supporting or encapsulating the cells, to enable their growth in the required way; and 3) the essential growth factors and signals to guide the growth and culturing process (Miller *et al*., 2003).

Because of their ability to promote regeneration, mesenchymal stem cells are one of the most commonly used approaches in tissue engineering (Pittenger *et al*., 2019). However, stem cells face a number of drawbacks, including an increased risk of contamination and damage to genetic information during isolation and expansion (Rsland *et al*. 2009), undesired differentiation as well as restricted circulation due to their very large size (Rsland *et al*. 2009; Holkar *et al*., 2020).

Although the coining of tissue engineering (TE) as a term dates back to 1987 (Berthiaume *et al*., 2011), this field has shifted dramatically throughout the last decade.

Efforts to develop biomaterials that resemble the microscopic level of native tissue have been fraught with difficulty and are generally not considered sufficient. Thus, new TE approaches aim to mimic both the microscopic and molecular *in vivo* environment, to improve the natural processes of tissue repair and development.

As a result, the concept of cell-free tissue engineering utilising extracellular vesicles has sparked attention as a unique approach to overcoming the restrictions mentioned above. Extracellular vesicles (EVs) are membrane-enclosed vesicles secreted by various cell types; they include exosomes, microvesicles and others. The function of EVs in TE can be justified by the role of EVs as paracrine mediators during cell-to-cell communication by delivering biomolecules, such as cytokines, proteins, mRNA, and regulatory micro RNAs, to target cells and modulate their behaviours (Yáñez-Mó *et al*., 2015). In addition, EVs may have an improved safety profile compared to their parent cells since they lack a nucleus, making them incapable of self-replication and preventing uncontrolled proliferation after delivery.

The aim of this project was to examine the ability to produce a novel electrospun membrane by combining extracellular vesicles (EVs) with electrospun polycaprolactone fibres and study its potential use in promoting wound healing, angiogenesis and osteogenesis.

Literature review

1.1 Extracellular vesicles

1.1.1 History of Extracellular vesicles

The field of extracellular vesicle (EV) research began in the 1940s, when the coagulation route was first revealed. EVs were first defined by Peter Wolf, in 1967, who introduced the term “platelet dust” to describe the plasma component originating from platelets (Wolf, 1967). Wolf used high-speed centrifugation to sediment platelet vesicles and identified different structures, which could be defined by electron microscopy. In 1974, Albert Claude, Christian de Duve, and George E. Palade were awarded the Nobel Prize in medicine for their work on endosomes, lysosomes and other cellular compartments, which years later established the knowledge base for understanding exosome biogenesis. In 1983, two papers were published in the same week that both described the formation of small vesicles that originated at the reticulocyte and were released into the bloodstream (Pan and Johnstone, 1983; Harding and Stahl, 1983). A few years later, the word exosome was coined by Johnstone *et al*., (1987) to describe these extracellular vesicles, although this term had been used a few years earlier to describe another membrane fragment (Trams *et al*., 1981; Harding *et al*., 2013).

Initially, EVs were believed to operate only in the removal of waste from cells and in the maintenance of cellular haemostasis; however, a clear understanding of EV roles began to appear in the late 90s. In 1996, Raposo G *et. al*., published ground-breaking findings illustrating that EVs derived from B lymphocytes play roles in the immune response. These results explained the first evidence that EVs perform important

biological functions. Furthermore, remarkable results describing the use dendritic cell -derived EVs as novel cell free vaccine were published by Zitvogel *et al*. (1998).

During the last decade, multiple studies have been published in the field of EVs, which has become an exciting area of research. In 2005, a clinical trial was published in the field of EVs examining the roles of exosomes as immunotherapy for patient with lung cancer (Morse *et al*., 2005). The next ground-breaking research in the field was published in 2007 by Valadi *et al*. This milestone report proved that EVs can deliver functional mRNA molecules to recipient cells and that this played a useful role in cell-to-cell interaction. Since then, many papers have been published that have discussed the importance of EVs in both therapeutic and diagnostic research. In 2011, Alvarez-Erviti *et al.* targeted engineered EVs to mouse brains to study their ability to deliver functional siRNA molecules. This pioneering article revealed the great potential for the use of EVs in different therapeutic approaches.

1.1.2 Nomenclature and classification of EVs

Extracellular vesicle is a hypernym that includes a large range of vesicles obtained from different types of cells. Lots of different names have been coined to define different extracellular vesicles, according to vesicle origins (e.g., platelet dust; Wolf, 1967) or particular function (e.g., calcifying matrix vesicles; Anderson, 1969). Other generic terms, including exosomes, microvesicles (MVs), microparticles, endosomes, ectosomes, and multivesicular bodies, have been used subsequently to refer to different types of EVs. Unfortunately, these terms have different definitions to different researchers. For example, the term *exosome* has been used to describe vesicles that have different sizes, biogenesis, density, or isolated by different centrifugal forces (Gould *et al*., 2013).

To resolve this misleading nomenclature, the International society of Extracellular Vesicles suggested that the term “extracellular vesicles” should be used as a generic term for any vesicles released from any cells that are delimited by a lipid bilayer and contain functional nuclei (Théry *et al*., 2018). Furthermore, they suggested that researchers should classify EVs according to the following attributes: a) size, as small (< 100 nm), medium (100-200 nm), or large (> 200 nm); b) cell of origin (e.g., hypoxic EVs and podocyte EVs); and c) the biochemical composition (e.g., $CD81^{+/-}$and $CD63^{+/}$). In addition, the guidelines suggested that researchers avoid the generic terms that have been used in the past, such as exosome and MV, unless the researchers have a clear definition and evidence to support. Thus, these guidelines will be employed throughout this study.

1.1.3 Biogenesis of EVs

EVs are categorised according to variations in their biogenesis routes, such as exosomes, MVs, and apoptotic bodies. Exosomes are formed by the endocytic pathway, beginning as intraluminal vesicles (ILVs) in multivesicular bodies (MVB), which then release exosomes into the extracellular space (Colombo, Raposo and Théry, 2014; Breakefield and Abels, 2016). In contrast, MVs form through the outward budding and fission of the plasma membrane (Raposo *et al*., 2013). Apoptotic bodies are formed by cellular disassembly during apoptosis (summarised in Error! Reference source not found.).

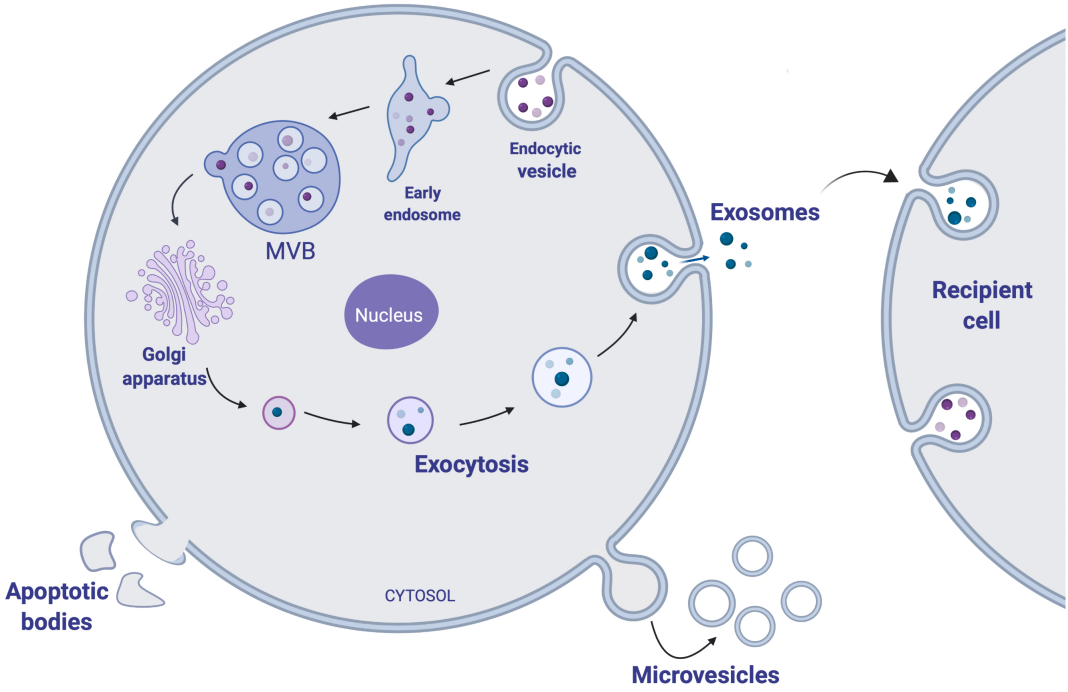

Figure 1.1. Biogenesis of various types of extracellular vesicle which showing the different route for each EVs subtype. (Alqurashi *et al*. 2020)

1.1.3.1 The formation of MVBs

During the endocytic pathway, early endosomes mature into late endosomes (Stoorvogel *et al*., 1991). Meanwhile, the formation of ILVs occurs through the inward budding of the endosomal membrane, which subsequently leads to the formation of MVBs. This process is regulated by the endosomal sorting complex required for transport (ESCRT), which includes a four-protein complex (ESCRT-0, -I, -II, and -III). First, outside of the endosomal membrane, ESCRT0 identifies ubiquitinated proteins. Then, ESCRT I bind ubiquitinated proteins, which activates ESCRT II. ESCRT III is recruited by programmed cell death 6 interacting protein (PDCD6IP, also known as ALIX) and associates with tumour susceptibility gene 101 (TSG101) on the ESCRT I

complex. PDCD6IP links ESCRT I with ESCRT III, which binds to TSG 101. Finally, the ubiquitin tag is removed from the cargo proteins to complete the process, and ESCRT III is disassembled by the ATPases associated with diverse activities (AAA)-ATPase suppressor of potassium transport growth defect 1 protein (SKD1) and recycled for another round of cargo recruitment (D'Souza-Schorey *et al*., 2018). ESCRT I and ESCRT II are believed to initiate the process of ILV membrane budding, whereas the completion of the process is performed by ESCRT III (McCullough *et al*., 2008).

In addition, the ESCRT-independent pathway can also form MVBs (Trajkovic *et al*., 2008), and this mechanism is believed to rely on lipids and lipid biogenesis.

1.1.3.2 The formation of exosomes

The biogenesis of exosomes includes the formation of MVBs and the invagination of ILVs (Abels *et al*., 2016). MVBs recycle, degrade, or exocytose proteins, nucleic acids, and lipids *via* the endosomal or lysosomal pathways. The endosomal system can be divided into early endosomes, late endosomes, and recycling endosomes (Grant *et al*., 2009). Early endosomes fuse with either endocytic vesicles, if the content is fated for degradation or secretion, or recycling endosomes, if the content is fated for recycling (Morelli *et al*., 2004). Then, residual early exosomes mature into late endosomes (Stoorvogel *et al*., 1991). Once late endosomes are formed, they accumulate ILVs that are formed by inward budding and contain cytosolic proteins, lipids, and nucleic acids sorted into small vesicles.

Late endosomes, also called MVBs, can fuse with lysosomes for degradation or with cellular membranes for the release of their contents into the extracellular space, as exosomes (Akers *et al*., 2013).

1.1.3.3 The release of exosomes

The mechanisms associated with the release of exosomes and the fusion of MVBs with lysosomes are still being dissected, and a number of mechanisms have been proposed. Different Rab GTPases are thought to direct the endosomes toward different fates (Stenmark, 2009). Each member of the Rab GTPase family localises to different membrane compartments, where they control the direction of vesicular membrane trafficking (Zhen *et al*., 2015). For example, Rab7 and Rab 9 direct late endosomes toward lysosomal degradation (Jordens *et al*., 2001), whereas Rab11 and Rab35 facilitate the release of exosomes through the fusion between MVBs and the plasma membrane (Savina *et al*., 2003). Furthermore, differences in the cholesterol levels of MVBs can also affect their trafficking, as cholesterol-enriched MVBs are directed towards the plasma membrane, whereas cholesterol-poor MVBs are directed towards lysosome fusion (Möbius *et al*., 2002).

1.1.3.4 Biogenesis and release of microvesicles (MVs)

The biogenesis of MVs, sometimes called “ectosomes”, is less well-defined and involves different pathways compared with exosomes. The outward budding and fission of the plasma membrane is thought to comprise the primary mechanism for MV formation, aided by phospholipid rearrangement and the activation of cytoskeletal proteins (Akers *et al*., 2013). The distribution of phospholipids and proteins within the plasma membrane is heterogeneous, and this asymmetric distribution is regulated by aminophospholipid translocases such as scramblases, flippases, and floppases, which can transfer phospholipids between the inner and outer surfaces (Hankins *et al*., 2015).

Different descriptions in the literature exist for the initiation of MV biogenesis. Some have suggested that the initiation step involves the exposure of phosphatidylserine (PS) to the outer surface (Akers *et al*., 2013), whereas others have shown that the redistribution of phospholipids, triggered by increases in calcium levels, result in MV release (Pasquet *et al.*, 1996). In addition, cholesterol plays a major role, as demonstrated by the impaired EV production from monocytes when cholesterol was depleted (Del Conde *et al.*, 2005).

After phospholipid redistribution, the contraction of cytoskeletal proteins completes the budding process through actin-myosin interactions. In detail, ADP-ribosylation factor 6 (ARF6) begins the process by initiating a cascade that activates phospholipase D (PLD). Then, myosin light chain kinase (MLCK) is activated via phosphorylation by the extracellular signal-regulated kinase (ERK), which triggers the release of MVs (Breakefield and Abels, 2016).

1.1.4 Isolation of extracellular vesicles

The isolation of EVs is challenging, due to their heterogeneity, small size, and physicochemical properties. However, the isolation of EVs has been performed successfully from body fluids, including breast milk (Admyre *et al*., 2007), semen (Madison *et al*., 2017), urine (Liu *et al*., 2018), saliva (Zlotogorski-Hurvitz *et al*., 2015), bile (Masyuk *et al*., 2010), and cerebrospinal fluid (Skalnikova *et al*., 2019), in addition to culture media (Pavani *et al*., 2019). Although multiples isolation techniques have been used in the literature, a “gold standard” isolation technique that provide high yield, high purity and can be used for all EV isolation events has not been established because multifactorial aspects must be considered before selecting a technique,

including the type and volume of the starting material, time, money, simplicity, yield, purity, EV integrity, and biochemical properties (Gardiner *et al*., 2016).

1.1.4.1 Ultracentrifugation (UC)

Ultracentrifugation (UC) is considered a classic method for EV isolation that utilises centrifugal forces to sediment Particles, including EVs (Monguió-Tortajada *et al*., 2019). First, large particles, including cells and cellular debris, are sedimented at 300–500 × g, followed by 2,000 × g. Next, biopolymer and apoptotic bodies are pelleted by centrifuging the supernatant at 10,000 × g, followed by the filtration of the resulting supernatant using a 0.2-μm filter. Finally, ultracentrifugation is applied, at 100,000 × g, to pellet small EVs. To increase the purity of EVs, the UC step may be repeated after resuspending the pellet (Théry *et al*., 2006). Although the general steps for UC are the same, there is no unified protocol for the UC technique. Different rotors, speeds, and times have been reported in the literature when describing the UC method.

The efficiency of the UC method relies on several factors that must be considered, including the type of rotor (radius of rotation, cleaning factor- pelleting efficiency [K factor] and sedimentation path length), centrifugation g-force, time, volume and viscosity of the sample, and sedimentation speed (g) (Konoshenko *et al.*, 2018; Livshts *et al.*, 2015).

1.1.4.2 Density gradient ultracentrifugation

The primary disadvantage of EV fractions isolated using the UC technique is that they often contain protein aggregates and other non-EV particles. Thus, density gradient UC has been used to increase the efficiency of particle separation, based on their buoyant densities (Konoshenko *et al*., 2018). This technique has been used to separate subcellular components, such as endosomes and mitochondria (Graham,

2001). Samples can be bottom-loaded or top-loaded to adjust the gradient. After centrifugation with a 30% sucrose cushion, EVs will be separated from other particles in different bands, according to the density (exosomes have densities between 1.15 and 1.19 g/ml) (Konoshenko *et al*., 2018).

This technique, however, is expensive and time-consuming, has low yield, and is operator-dependent, which makes it difficult to apply to clinical research (Webber *et al*., 2013).

1.1.4.3 Size exclusion chromatography (SEC)

In 2014, size exclusion chromatography (SEC) was recommended for the isolation of EVs from biofluids by Böing *et al*. In comparison with the UC technique, which is based on density, SEC is based on size. SEC uses a porous polymer, called a gel filtration resin, that constitutes a stationary phase through which EVs are eluted according to their sizes. In particular, The nature of the stationary phase allows differential elution: bigger particles elute first, followed by smaller vesicles, and then non-membrane-bound proteins (Monguió-Tortajada *et al*., 2019).

Sidhom *et al*., (2020) suggested after reviewing the current literature that SEC may provide an ideal EVs isolation method. They argued that SEC provide relatively pure and functional EVs. Regarding to the functionality, found that SEC may offer higher functionality of EVs compared to UC (Mol *et al*., 2017).

1.1.4.4 Precipitation technique

Volume exclusion precipitation is a polymer-based technique, most commonly performed with polyethylene glycol (PEG). In addition, multiple commercial kits use this method, such as Total Exosome Isolation™ and ExoQuick™, although they may use different polymers (PEG), dextrans or polyvinyls, (Monguió-Tortajada *et al.*, 2019). This technique has been reported to achieve the highest EV recovery rates.

However, EV purity is usually compromised by the presence of non-vesicular particles, including nucleic acids and proteins, which may be pelleted along with EVs (Van Deun *et al*., 2014).

1.1.5 Characterisation of extracellular vesicles

Because of their nanometre size range, EVs are undetectable to the human eye, even when using a light microscope. Thus, the characterisation of isolated EVs is crucial when determining whether an isolation method can reduce heterogeneity amid a complex environment. Therefore, the MISEV 2018 guideline emphasises the need to use multiple, complementary techniques to evaluate the results of the separation method (Théry *et al*., 2018).

1.1.5.1 Structure and morphology of EVs

1.1.5.1.1 Electron microscopy

Electron microscopy (EM) is the most commonly used method to investigate cellular and subcellular structures, particularly scanning electron microscopy (SEM) and transmission electron microscopy (TEM). TEM uses an electron beam that passes through the sample, providing a better representation of the internal structures, which requires ultra-thin samples that do not need to be conductive (Szatanek *et al*., 2017). Furthermore, immunogold labelling, using gold conjugated antibodies, allows detection of specific antigens (Jung *et al*., 2018). In SEM, a topographical image of a surface is achieved by sending an electron beam to a conductive surface and then detecting secondary electron emissions. Only few studies reported the use SEM to characterise EVs (Sokolova *et al*., 2011).

Extra care should be taken, however, when processing samples for EM, as the multiple and highly sensitive steps, which include fixing, staining, and dehydration,

may have negative effects on fragile vesicles. This may explain the artefact cup-shape appearance of EVs under TEM which studied well by (Chernyshev *et al*., 2015) .

To avoid damaging the sample, cryo-TEM or freeze-fraction TEM (FF-TEM) can be utilised, which uses cryofixation and the extremely rapid freezing of samples to prevent crystallisation. Therefore, using cryo-TEM increases the likelihood of imaging the vesicular lipid bilayer with clear morphology ((Rupert *et al*., 2017). Yuana *et al*., (2013) reported the highly heterogenous morphology and size of plasma EVs in under cryo-EM.

1.1.5.1.2 Atomic force microscopy (AFM)

Atomic force microscopy (AFM) uses a probing tip to detect and record 3-dimensional (3D) images of the surface topography of a sample. The sample is probed with a sharp, delicate tip mounted at the end of a cantilever, which detects the interaction force between the tip and the sample (Chiang *et al*., 2019). One advantage of using AFM is the ability to analyse a sample in an aqueous solution. However, the imaging of EVs using AFM is quite sensitive because vesicle deformation can occur when using this technique, which can affect vesicle appearance. Deformation can be prevented by functionalising the surface, using molecules that bind with EVs, to preserve the morphology (Pignataro *et al*., 2000). Moreover, monoclonal antibodies that bind to the surface of EVs can detect specific proteins, which may provide better resolution than labelling with immunogold (Creasey *et al*., 2011).

1.1.5.2 Quantity and Size characterization

The amount and sizes of EVs can be assessed using multiple techniques, including nanoparticle tracking analysis (NTA), and flow cytometry.

1.1.5.2.1 Nanoparticle tracking analysis (NTA)

NTA is a technique used to measure the different parameters of nanoparticles, including the average size and the size distribution by detecting the Brownian motion of the particle in the suspension (Dragovic *et al*., 2011). During NTA, a sensitive camera is installed on an optical microscope to record the movements of the illuminated EVs over time. Then, the sizes and size distribution are measured by tracking and plotting the displacement of each EV.

The use of NTA for EV characterisation has many advantages, including the simplicity of sample preparation and the fast acquisition of data. Furthermore, one of the most attractive features of NTA is the ability to use fluorescence to detect antigens on EVs using labelled antibodies (Gardiner *et al*., 2013)

However, detecting EVs smaller than 50 nm (van der Pol *et al*., 2014) using NTA can be difficult, and other limitations include the likelihood of detecting non-EV nanoparticles, the need for sample dilution, difficulties determining the optimal sample dilution (Rupert *et al*., 2017), and difficulties detecting some types of fluorescence (Dragovic *et al*., 2015).

1.1.5.2.2 Flow cytometry

Flow cytometry involves passing a laser beam with a specific wavelength through EVs suspended in fluid and measuring the forward-scattered light (FSC), the side-scattered light (SSC), and fluorescence to detect the size and concentration of EVs (Van Der Pol *et al*., 2012). Conventional cytometers are only able to detect large EVs, However, newer high-resolution cytometers are able to measure small EVs (van der Vlist *et al*., 2012). The simple and fast processing necessary for flow cytometry makes it an attractive method for use in a clinical setting (van der Pol *et al*., 2014).

1.1.5.3 Characterisation of EV cargo

Due to the limitations of the physical and morphological characterisation methods, characterisation of EVs composition has been suggested. EVs subtypes share common composition including outer lipid bilayer membrane and several types of lipid, proteins and nucleic acid. The specific composition of each of these cargos depend on the cell source, culture condition and biogenesis.

1.1.5.3.1 Protein Characterization

Successful purification of EVs can be assessed by detecting the enrichment of EV-associated proteins, such as tetraspanins (CD63, CD9, CD81) and biogenesis-associated proteins (TSG101, ALIX), and the absence of non-EV-associated proteins. The most common technique used for protein characterisation is the western blot (WB). However, WB requires high protein levels because it has a relatively poor detection limit. Kowal *et al.*, (2016) have explored different proteomic characterisation tools for use with heterogeneous populations of EVs.

1.1.5.3.2 Nucleic acid characterization

The presence of nucleic acids in EVs was first reported by Valadi *et al*. (2007), who proposed the name “exosomal shuttle RNA” (esRNA). The primary nucleic acid identified in EVs is RNA, and whether DNA is trafficked by EVs remains unknown (Mateescu *et al*., 2017).

However, recent findings linked the presence of DNA in EVs with tumour microenvironment (Jella *et al*., 2018). Different techniques have been used to detect EV-RNA, such as quantitative polymerase chain reaction (qPCR), microarrays, northern blotting and RNA-seq. however, detection of non-EV associated RNA can affect the characterisation results (Wei *et al*., 2016). Moreover, some EV-isolation techniques can affect the yield and purity of RNAs (Enderle *et al*., 2015). Mateescu *et*

al. (2017)reported the primary challenges associated with the characterisation of EV-RNA in their MISEV position paper.

1.1.5.3.3 Lipid characterization

Because the lipid bilayer comprises roughly two-thirds of small EVs, lipidomics in the EV field has attracted the attention of researchers, in addition to the characterisation of proteins and nucleic acids. Several methods have been used to detect lipid in EVs, such as mass spectrometry (MS), gas-liquid chromatography (GLC), and thin-layer chromatography (TLC). However, non-EV impurities can also affect the results of lipid characterisation (Skotland *et al*., 2017).

1.1.6 Role of EVs in intercellular communications

The recent surge in interest in the field of EVs began after discovering their role in cell-to-cell communications through the delivery of bioactive elements between cells. Consequently, EVs play important physiological roles, in addition to their roles in pathological conditions. The mechanisms through which EVs facilitate intracellular uptake can be divided into the following subtypes which are illustrated in **Figure 1.2**:

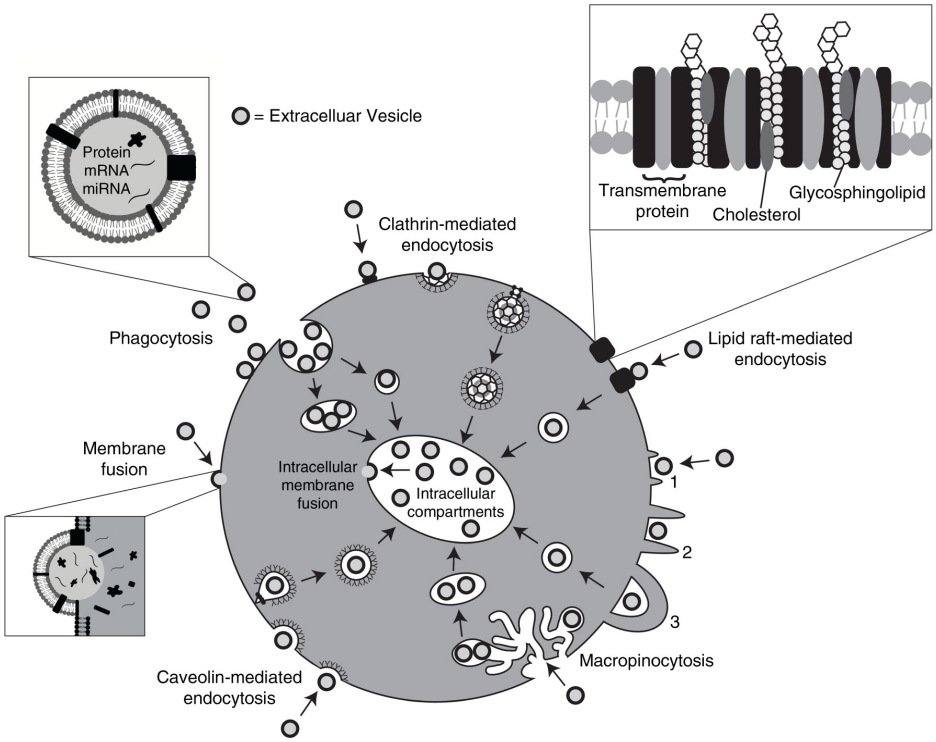

Figure 1.2. Routes of EVs uptake by target cell shows the different pathways for cellular communication. EVs uptake routes include phagocytosis, clathrin, caveolin- mediated endocytosis and macropinocytosis. EVs may also deliver their cargo by fusion with plasma membrane. Reproduced from (Mulcahy *et al.*, 2014).

1.1.6.1 Endocytosis

Most experimental evidence has suggested that endocytosis represents the primary route of EV uptake (Morelli *et al*., 2004). EV uptake is a rapid process, during which EVs can be identified after 15 minutes of initial introduction (Feng *et al*., 2010). Endocytosis is an energy-dependent process, which was demonstrated by reduced EV uptake at 4°C (Tian *et al*., 2013). Furthermore, other internalisation processes may represent subclasses of endocytosis that regulate EV uptake, including phagocytosis, micropinocytosis (MP), and clathrin-mediated endocytosis (CME).

1.1.6.2 Phagocytosis

Phagocytosis is a receptor-mediated process that involves the invagination of particles, especially large particles or materials intended for internalisation (Doherty *et al*., 2009). Although phagocytosis is employed primarily for large particles, it has been shown to internalise EVs and small particles up to 85 nm (Rudt *et al*., 1993). During the formation of phagosomes, phosphatidylinositol-3-kinase (PI3K) plays a major role by enabling the insertion of the membrane (Stephens *et al*., 2002).

1.1.6.3 Macropinocytosis (MP)

Macropinocytosis (MP) is an endocytic uptake route that involves the inward folding of the membrane, which then pinches off to form an intracellular compartment, without requiring direct contact with the internalised materials, as in phagocytosis (Mulcahy, Pink, and Carter, 2014). This mechanism relies on different molecules, including cholesterol, that play important roles in the MP process (Kerr *et al*., 2009). In addition, specific MP inhibitors have been shown to cause low EV internalisation in some cells, suggesting that MP may be a cell-type-specific process (Costa Verdera *et al*., 2017).

1.1.6.4 Clathrin mediated endocytosis (CME)

CME is a type of endocytosis that involves the formation of clathrin-coated vesicles, which contain different transmembrane receptors. The membrane is deformed by clathrin-coated vesicles, forming a vesicular bud that pinches off. Multiple studies have associated CME with EV uptake, and Escrevente *et al.* (2011) reported reduced EV uptake by ovarian cancer cells after CME was inhibited by chlorpromazine.

1.1.6.5 Membrane fusion

EVs can fuse with the plasma membrane of recipient cells, which has been observed using fluorescent lipid dequenching. Fusion events have been observed to increase under acidic conditions, which suggests this mechanism may be important in the tumour microenvironment (Parolini *et al*., 2009).

1.1.7 Role of extracellular vesicles in tissue engineering and regenerative medicine

Cellular interaction is a key pillar of TE and regenerative medicine. Therefore, the function of EVs throughout cell-to-cell communication as paracrine mediators, their release by numerous cell types, and their ability to transfer information and important molecules, such as mRNA, miRNA, and DNA, have caused in considerable interest in the efficacy of EV in TE and regenerative medicine. Potential uses of EVs in TE illustrated in **Figure 1.3.**

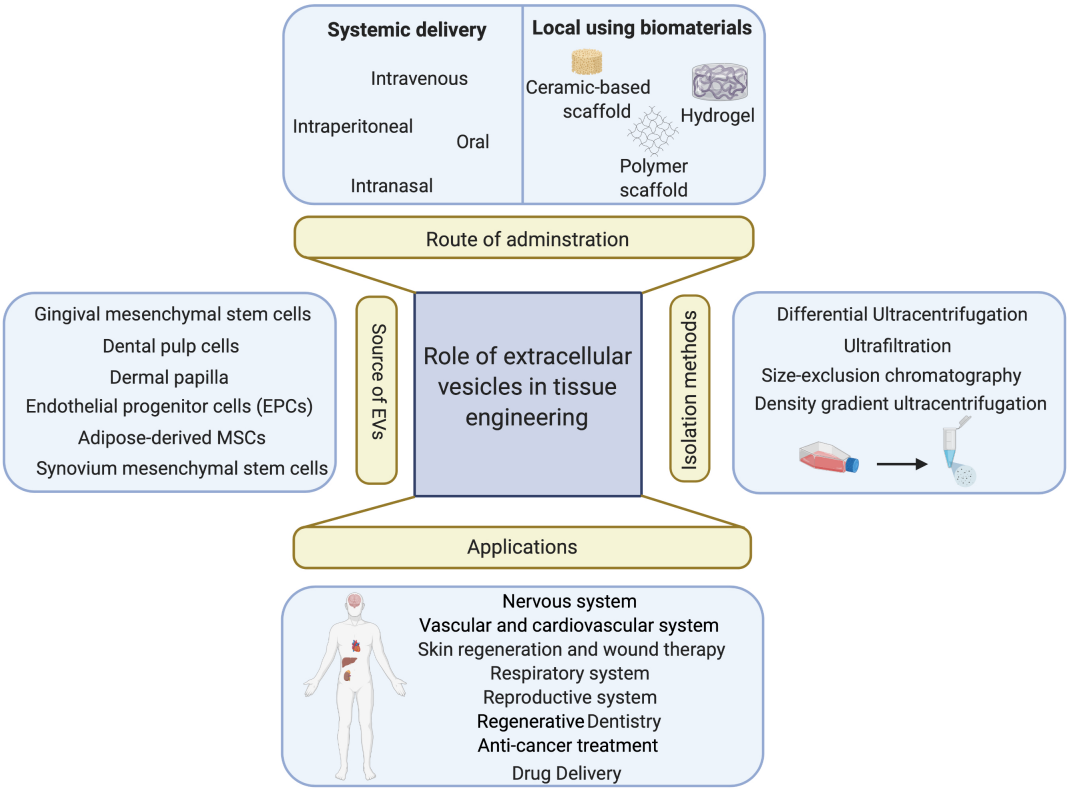

Figure 1.3. Schematic description of prospective uses of EVs in TE. Various sources of EVs have been utilized in the literature to encourage the TE process using various isolation methods. EVs can be deliver by systemic or local path. Using biomaterial to deliver EVs can improve the retention and extended the releasing activity. EVs can play major function in different area of TE and regenerative medicine. (Alqurashi *et al*., 2021).

1.1.7.1 Nervous system

In general, nerves do not have the capability for regeneration in the central nervous system due to the diminished intrinsic regenerative capacities. Peripheral nerves, however, enhance Schwann cells migration and alignment by expressing adhesion molecules that increase the communication and accordingly nerve repair. Most nervous system cells release EVs to transfer information between cells. Several recent reports have examined the possibility of utilising EVs for regenerative treatments in

the nervous system. In a rodent model, Xin *et al*. (2012) stated that mesenchymal stem cell (MSC)-derived EVs could transfer miR-133b to neural cells, which increased the likelihood of recovery from stroke. Another significant finding showed that EVs deriving from dendritic cells promoted the remyelination of nerve fibres and, therefore, can be used during the treatment of multiple sclerosis (Pusic *et al*., 2014). Furthermore, Lopez-Verrilli, Picou and Court (2013) reported that axonal regeneration can be induced by Schwann cell-derived EVs.

1.1.7.2 Vascularization and angiogenesis

Angiogenesis is the formation of new blood vessels from pre-existing vessels. To deliver nutrition and oxygen to the interior tissue, the tissue must be vascularized. An inadequate vascular network can lead to infection, loss of function and necrosis (Schreml *et al*., 2010).

Vascularisation is one of the vital stages for effective tissue regeneration. Numerous researches have examined the function played by the autocrine and paracrine signalling of EVs to enhance angiogenesis in different tissues. For example, EVs derived from endothelial cells containing miR-214 have been shown to stimulate angiogenesis and encourage the migration of endothelial cells (Balkom *et al*., 2013). In addition, placental MSC-derived EVs have been shown to stimulate placental microvascular formation (Salomon *et al*., 2013) and boost angiogenesis when administered to rats after stroke (Xin *et al*., 2013). In addition, Zhou *et al*., (2020) showed that human dental pulp stem (HDPS) cell derived EVs profoundly increase the proliferation, migration, and angiogenesis of ECs *in vitro* and were able to accelerate cutaneous wound healing and vessel formation *in vivo*.

1.1.7.3 Respiratory system

The essential functions of EVs in respiratory system physiology indicate the significance of involving them in tissue engineering development. Remarkably, EVs isolated from unhealthy lungs have been shown to have different cargo from those isolated from healthy lungs. Likewise, MSC-derived EVs showed interesting findings in the inhibition of pulmonary hypertension by suppressing the hyperproliferative pathways (Lee *et al*., 2012). Moreover, lung derived-EVs showed to reprogram marrow cells into pulmonary epithelial phenotype (Aliotta *et al*., 2007).

1.1.7.4 Wound therapy and skin regeneration

Owing to their role of improving the angiogenesis and cells interaction at wound site, EVs have sparked the attention of researchers to be applied for skin regeneration and wound therapy applications. Shi *et al.* (2017) revealed that exosomes originated from gingival mesenchymal stem cells (GMSC) and integrated into a chitosan/silk hydrogel encouraged cutaneous wound healing in diabetic rats. They proved that these EVs improved re-epithelialisation, induced angiogenesis, and remodelled collagen. Another recent experiment in diabetic rats by Wang *et al.* (2019), demonstrated that applying EVs in a bioactive hydrogel promoted the healing of chronic wound by improved re-epithelisation and provoked angiogenesis. Moreover, a recent review of this subject described the outcomes of stem-cell-derived EVs during different phases of wound healing, including the inflammatory phase, the proliferative phase, and the remodelling phase (Ferreira *et al*., 2018).

1.1.7.5 Regenerative dentistry

Dentistry is still a growing field for research in the areas of TE and regeneration. A number of studies have examined different TE approaches for application in the dental field, such as the stimulation of the regeneration of pulpal and gingival tissue (Mohammadi *et al*., 2007). Furthermore, some researches have reported the ability to construct oral mucosa TE models, which could be employed to multiple applications in dentistry (Moharamzadeh *et al*., 2007).

However, a few studies have reported the use of EVs to boost the regeneration of oral and dental tissues. A recent article by Chew *et al.* (2019) showed that the use of MSC EVs with a collagen sponge improved periodontal regeneration in a rat periodontal defect model. Moreover, EVs were found to generate cellular activity within the periodontal ligament (PDL). The amount of periodontal regeneration, however, wasn't optimum and may depend on the EV dose.

In addition, a new review of the literature on this topic highlighted the function of EVs in oral tissue regeneration, including periodontal tissue, dental pulp, cartilage, and bone (He *et al*., 2021).

1.1.7.6 Drug delivery

EVs represent a promising drug delivery system due to their capability to protect bioactive cargo, biocompatibility, and ability to cross biological membranes including the blood-brain barrier (Claridge *et al*., 2021). EVs have been examined for use as drug-delivery systems (DDSs) for various types of medications, such as curcumin (an anti-inflammatory compound), which has been shown to decrease brain inflammation (Zhuang *et al*., 2011). Furthermore, a research by Jang *et al.*, (2013) indicated the capability to load EVs with the chemotherapeutic drug doxorubicin (Dox). Additionally,

they explained that EVs travelled to tumour sites and reduced tumour growth, without any evident side effects.

The loading of EVs with various cargo and drug agents is not a simple process. However, many loading methods have been examined in the literature, including endogenous and exogenous loading approaches. The endogenous approach requires the loading of therapeutics into the parent cell, before EV isolation, while the exogenous approach involves the loading of EVs after isolation.

1.2 Routes of administration of EVs for tissue engineering and regenerative medicine purposes

Various techniques and approaches exist for the delivery of EVs to target tissues or organs; they can be classified as either systemic or local. Systemic methods include intravenous (IV), intranasal, oral, intraperitoneal, and subcutaneous, while a local delivery can be achieved through the immediate loading of EV suspensions or into biomaterials (Pinheiro *et al*., 2018). Each method of delivery has both advantages and disadvantages, which will be discussed in this section.

1.2.1 Systemic delivery of EVs

Intravenous administration is believed to be the fastest route of delivery and is the commonly used technique. Lai *et al.* (2014) proved that EVs can be found in the liver and spleen of mice after 30 min of administration. Furthermore, they confirmed that the highest levels of EV concentration after injection was detected after 30 min in blood and after 60 min in urine. However, the main limitation of employing the IV route is the short half-lives of EVs in circulation.

While the oral route is the most acceptable and accessible method of drug administration, gastrointestinal enzymes and changes in pH continue to be obstacles

to the oral delivery of EVs that must be overcome (Shandilya *et al*., 2017). Therefore, this method has been recommended for use when targeting the luminal epithelial surface of gastrointestinal tissues (Rezaie *et al*., 2018). The advantages and disadvantages of other systemic routes were discussed in depth elsewhere (Pinheiro *et al.* 2018).

1.2.2 Local delivery of EVs

Generally, the main advantages of employing a local delivery technique for any drug is to decline the systemic side effects that can arise and the enhanced retention rate of the drug of choice, which also relate to the local administration of EVs. A small number of experiments have described the use of local delivery for EVs, either via the direct application of EV suspensions or the combination of EVs into biomaterials. Kim *et al.* (2006) were the first to report the local administration of EVs derived from genetically modified murine bone marrow, which was shown to minimise the inflammation in a murine model of delayed-type hypersensitivity (DTH).

Furthermore, EVs have been discovered as potential anticancer therapies that found to be more efficient when administered locally compared with systemically (Smyth *et al*., 2015).

In tissue regeneration applications, the subcutaneous injection of EVs were shown to stimulate angiogenesis in a murine auricle wound model. Additionally, Zhang *et al.* (2016) illustrated that the direct delivery of MSC EVs, through intra-articular administration, encouraged the regeneration of both hyaline cartilage and subchondral bone after 12 weeks in rat models.

1.2.3 Using biomaterial devices for delivering EVs

The key disadvantages of systemic and direct local EV delivery are the weak retention of EVs at the target site and the failure to monitor the dose of EVs required for the therapeutic demands(Pinheiro *et al*., 2018). Subsequently, the combination of EVs into biomaterial devices as delivery systems is a robust approach to overcome this concern and to boost the effects of EVs by improving the length of EV availability at the target site. **Table 1** shows various types of biomaterials have been utilized to deliver EVs to different target tissues.

1.2.3.1 Hydrogels

Hydrogels are water-swollen polymeric material that maintain a distinct three-dimensional structure (Kopeček, 2007). In 2017, Liu *et al*. incorporated human-induced pluripotent stem cell (iPS-S-01) EVs to imine crosslinking hydrogel glue to examine the impact on the repair of articular cartilage defects(Liu *et al*., 2017). First, the hydrogel patches were made using photoinduced imine crosslinking (PIC) hydrogel by employing the o-nitrobenzyl alcohol moieties modified hyaluronic acids (HA-NB) which bonded with gelatin polymer under light irradiation to form the hydrogel. This hydrogel has been exploited because of its biocompatibility and its ability to integrate with the tissue. The constant release of EVs over the course of 14 days revealed that hydrogel degradation will progressively release EVs. According to Liu *et al*. the EV-hydrogel complex influenced cellular regulation *in-vitro* and *in-vivo* and stimulate the cartilage repair.

Using chitosan-based material as a delivery system, Tao *et al*., (2017) found that EVs can enhance the treatment of diabetic wounds. As the primary challenge of chronic diabetic wounds is inadequate perfusion, they used EVs obtained from microRNA-126-overexpressing synovium mesenchymal stem cells to boost angiogenesis.

Using various dosages of EVs, enhanced proliferation of human dermal fibroblast and human dermal microvascular endothelial cells was observed, resulting in increased angiogenesis and enhanced reepithelialisation. Another study utilised chitosan/silk hydrogel and gingival mesenchymal stem cell-derived EVs to accelerate wound healing in diabetic rats. Comparable to the previous study, encouraging effects were stated on diabetic rat skin wound repair (Shi *et al*., 2017). To examine the role of human placental MSC-derived EVs on angiogenesis, Zhang *et al*., (2018) combined them with chitosan hydrogel. This indicated that hydrogel improved the retention and slow release of EVs and enhanced the angiogenesis of ischemic hindlimbs.

Furthermore, Chen *et al*., (2018) utilized shear-thinning hydrogel to provide endothelial progenitor cell-derived EVs to improve angiogenesis after myocardial infarction. They revealed that hydrogel offers sustained release of EVs and confirmed the uptake of EVs by the endothelial cell *in vitro*. *In vivo*, they stated that EV-modified hydrogel enhanced haemodynamics in a rat model and increased the density of vessels in a peri-infarct myocardium.

Polypeptides have been employed with biomaterials to boost antibacterial activity. Wang *et al*. produced injectable poly(ethylene glycol) hydrogel with Poly-ε-L-lysine to deliver adipose-derived mesenchymal stem cells exosomes. They reported a sustained release of EVs over 21 days from the hydrogel which enhanced the impact in comparison to a one-time treatment. In diabetic wound healing model, distinguished angiogenesis was observed, leading to improve wound closure.

Self-assembling peptides (SAPs) are nano-biomaterials made of natural amino acids that form crosslinked nanofibers in aqueous solution. Zhou *et al*., (2019) utilized MMP-2 sensitive SAP hydrogel to manage the release of mesenchymal stem cell-derived extracellular vesicles (MSC-EVs). They revealed that EV-modified hydrogel declined

cell apoptosis and enhanced endothelial cell regeneration in mice with renal ischemia-reperfusion (I/R) injury.

In a recent study, oxidized sodium alginate (OSA) hydrogel was applied as EVs delivery system to promote hair growth (Chen *et al*., 2020). While aldehyde groups following alginate oxidation of OSA may trigger potential cytotoxicity, authors hypothesized that utilizing OSA hydrogel with a low level of oxidation (DO) may offer stable environment for EVs. They have shown that dermal papilla (DP) EVs increased the proliferation and migration of hair matrix cells. In addition, OSA hydrogel offered sustained release of DP-EVs, better EV retention in-vivo and greater therapeutic effect on human hair follicle growth.

1.2.3.2 Extracellular matrix (ECM) scaffolds

Extracellular matrix (ECM) scaffold has been used in tissue engineering because of its ubiquity and biocompatibility. Type1 collagen is the most widely utilised extracellular matrix (ECM) scaffold, which has numerous favourable properties (Glowacki *et al*., 2008). Huang *et al*., (2016) have utilized type 1 collagen membrane to examine the ability of EVs to encourage stem cell differentiation. In addition, they found that EVs tend to attach to matrix proteins such as fibronectin and type 1 collagen which can be utilized to promote binding to other biomaterials. Moreover, type 1 collagen-modified EVs found to stimulate the differentiation of dental pulp stem cells *in vitro*. *In vivo*, EVs prompted the regeneration of dental pulp-like tissue in a tooth root slice model. Another study evaluated the effect of human periodontal ligament stem cells, their EVs, and polyethylenimine (PEI)-engineered EVs on bone healing. (Diomede *et al*., 2018). In rat model with calvarial defects, total repair of the defect was detected after 6 weeks.

1.2.3.3 Ceramic-based scaffolds

For many years, several bone graft replacements have been used in bone regeneration, including osteoinductive materials like demineralized bone matrix (DBM) and synthetic scaffolds like tri-calcium phosphate (TCP)(Bauer, 2007). To analyze the function of EVs in bone regeneration, Zhang *et al.*(2016) combined human-induced pluripotent stem cell-derived mesenchymal stem cells exosomes (hiPS-MSC-Exos) with tricalcium phosphate (β-TCP) scaffolds. The authors discovered that EV-modified -TCP scaffolds increased the osteoinductivity of calvarial bone defects by activating the PI3K/Akt signalling pathway when compared to unmodified -TCP scaffolds. Another research combined rat bone marrow-derived MSCs- EVs in decalcified bone matrix scaffold to study their angiogenesis and bone regeneration effect (Xie *et al*., 2017a). MSCs-EVs enhanced the proliferation, migration and tube formation of human umbilical vein endothelial cells *in vitro*. Moreover, they stated that the EV-modified scaffolds encouraged angiogenesis and increased bone regeneration when planted subcutaneously into nude mice.

Table 1.1. Summary of previous publications that used different biomaterials to deliver EVs (Alqurashi *et al*., 2021).

Group	Materials	Source of EVs	Application	Result	Reference
Hydrogels	Imine crosslinking hydrogel glue	MSC derived EVs	cartilage repair	Positive results *in vitro* and *in vivo* show cellular regulation which leads to the promotion of cartilage repair	(Liu *et al*., 2017)
	Chitosan hydrogel	EV derived from miRNA-126-3p-overexpressing synovium mesenchymal stem cells	Wound healing in a diabetic rat model	Accelerate wound healing *in vivo*	(Tao *et al*., 2017)
	Chitosan/silk hydrogel	Gingival mesenchymal stem cells derived-EVs	Wound healing in a diabetic rat model	Promote wound healing of diabetic skin defects	(Shi *et al*., 2017)
	Chitosan hydrogel	MSC derived EVs	Hindlimb Ischemia treatment	Increase angiogenesis and accelerate the recovery of ischemic hindlimb	(Zhang *et al*., 2018)
	shear-thinning gel	Endothelial progenitor cells (EPCs)	rat model of myocardial infarction (MI).	Improved peri-infarct angiogenesis and myocardial haemodynamic.	(Chen *et al*., 2018)

	Antibacterial polypeptide-based FHE hydrogel	Adipose-derived mesenchymal stem cells exosomes (AMSCs-exo)	Diabetic Wound Healing and Complete Skin Regeneration	Enhance angio-genesis and diabetic wound healing	(Wang *et al*., 2019)
	self-assembling peptide (KMP2) hydrogel	Mesenchymal stem cell-derived EVs (MSC-EVs)	renal I/R injury model,	Reduce cell apoptosis/inflammation and enhance microvascular endothelial cell regeneration	(Zhou *et al*., 2019)
	oxidized sodium alginate (OSA) hydrogels	Dermal papilla DP-derived EVs(DP-EVs)	Hair regeneration	significantly facilitate the proliferation of hair matrix cells	(Chen *et al*., 2020)
Extracellular matrix (ECM) scaffold	Type 1 collagen membrane	EV derived from dental pulp cells	Dental pulp tissue regeneration		(Huang *et al*., 2016)
	collagen membrane 3-D scaffold	Human periodontal-ligament stem cells	bone regeneration	Encouraged a bone-regeneration process for the treatment of calvarium and ossification defects	(Diomede *et al*., 2018)
Ceramic-based Scaffolds	Tricalcium phosphate (β-TCP)	human-induced pluripotent stem cell-derived mesenchymal stem cells	Bone regeneration	exosomes can induce the osteo-inductivity lead to better osteogenesis activity	(J. Zhang *et al*., 2016)

	Decalcified bone matrix (DBM) scaffold	MSC-derived EV	Ectopic subcutaneous bone formation	EV influence bone formation and increased vascularization in the grafts	(Xie *et al*., 2017b)

However, although the electrospinning scaffold is one of the most common biomaterials used in TE and regenerative medicine, no study has explored its use as a delivery vehicle for EVs, to our knowledge. Thus, we are attempting to explore this possibility in this project.

1.3 Electrospinning

Many techniques can be used to fabricate fibrous scaffolds for use in TE applications. Electrospinning has several advantages over other techniques. First, electrospinning provides tunable membranes with a range of flexibilities and fibre sizes, ranging from microscale to nanoscale; electrospinning also allows to manipulate the porosity and orientation of the fibres and the incorporation of 3D complex features as well as bio-functional agents. In addition, although polymers are the most common types of material used with electrospinning, a wide range of other materials can be used, including ceramics and composites (Teo *et al*., 2006). The versatility and cost-effectiveness of electrospinning has also contributed to electrospinning being the most commonly used technique to generate fibrous scaffolds in the TE field. However, the limited control of pore structure is a significant disadvantage of the electrospinning technique.

Electrospinning is an established manufacturing technique, first studied in 1914 by Zeleny. In 1934, the first patent appeared that described the use of electrostatic repulsion for the creation of polymer filaments (Formhals, 1934). In 1990, several

research groups utilised this technique, and the term electrospinning was coined. Reneker *et al*. described the stable electrospinning technique in 1996 (Reneker *et al*., 1996).

During electrospinning, fibres can be produced by injecting the polymer through a needle at a constant rate. Once a droplet of the polymer begins to form at the end of the needle, the high voltage difference between the tip of the needle and the collector will affect the droplet, which will become highly electrically charged. Accordingly, this droplet will be exposed to two electrostatic force types, electrostatic repulsion and Coulombic forces. Consequently, a cone shape will form from the drop, which is called a Taylor cone. When the electrical force exceeds the surface tension of the solution, the charged jet of the solution is ejected. Then, this ejected liquid becomes elongated and travels toward the charged collector, which leads to the evaporation of the solvent and the formation of polymer filaments (Li and Xia, 2004; Bhardwaj and Kundu, 2010). **Figure 1.4** shows the different parts of electrospinning system.

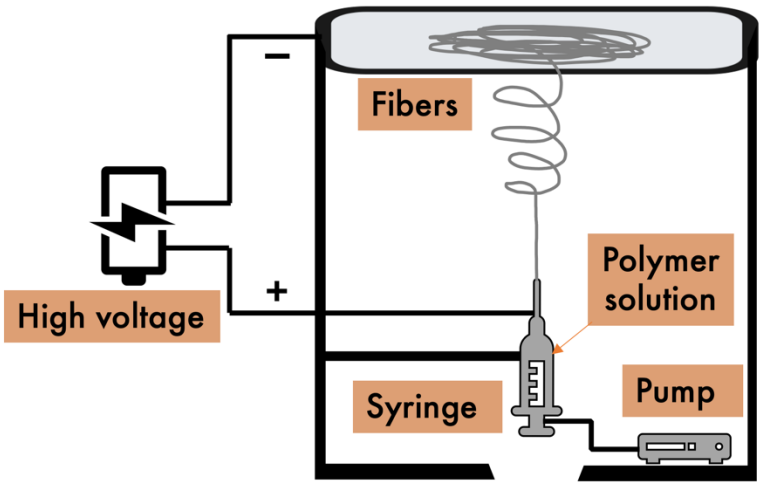

Figure 1.4. Schematic diagram of the vertical electrospinning system.

1.3.1 Polymers used in electrospinning

Several types of polymers can be used during electrospinning to manufacture fibrous scaffolds for use in different applications. Polymers that have been used in the literature can be divided into several categories, including natural, synthetic, or both (Bhardwaj *et al.*, 2010).

A wide range of natural biopolymers, such as cellulose, hyaluronic acid (HA), and chitosan as well as proteins including, fibrinogen, collagen, and gelatin, have been identified. There are many advantages to the use of these polymers to fabricate scaffolds for TE applications, including the high likelihood of biocompatibility compared with synthetic polymers and the ability of these polymers to enhance cell attachment and proliferation. However, the primary drawback of using natural polymers is the difficulty modifying the properties of these polymers to accommodate the targeted use (Agarwal *et al.*, 2008). Associated costs, availability and in some cases disease contaminations are other important issues with natural sources

However, the ability to tailor a wide range of properties, including the desired degradation rate and mechanical properties, represents a great advantage of synthetic polymers over natural polymers (Bhardwaj *et al*., 2010). During biomedical applications, the typical synthetic polymers used in the literature are biodegradable hydrophobic polyesters, including poly (ɛ- caprolactone) (PCL)(Cipitria *et al*., 2011), poly (glycolic acid) (PGA)(Boland *et al*., 2004), poly (lactic acid) (PLA)(Yao *et al*., 2017), and copolymer poly (lactide-co-glycolide) (PLGA).

1.3.2 Solvents used for electrospinning

To prepare the polymer solution for electrospinning, many solvents can be used, which have significant effects on the spinnability of the fabricated scaffold. The vapour pressure, volatility, and the preservation of polymer integrity are the primary properties associated with solvent use during electrospinning. Thus, several articles have explored the different types of solvents and their effects on the properties of the resulting scaffolds. Chloroform, ethanol, dimethylformamide (DMF), a mixture of trifluoroacetic acid and dichloromethane (DCM), and water are the most common solvents used, and each has different effects on the mechanical, morphological and thermal properties of the (Asran *et al.*, 2010; Luong, Moon and Nam, 2009; Wannatong, Sirivat and Supaphol, 2004).

1.3.3 Parameters of electrospinning process

As mentioned above, the electrospinning process is governed by several parameters that can affect the properties of the fibres, including solution parameters and processing parameters.

1.3.3.1 Solution parameters

1.3.3.1.1 Concentration

The optimal solution concentration is the primary factor that determines the ability to electrospin a polymer. At low concentrations, more beads will form instead of fibres because fibres break before reaching the collector. In contrast, with high concentrations, the solution can have difficulties flowing through the needle, which is necessary for the fibres to form (Sill *et al*., 2008). Furthermore, several articles found a power law relationship between the concentration of the polymer and the diameters of the resulting fibres, where increasing the concentration leads to increasing the fibre diameter (Ki *et al*., 2005).

1.3.3.1.2 Molecular weight

Because the molecular weight of a polymer plays an important role in other properties, such as surface tension, viscosity, and conductivity, it represents an important solution parameter (Haghi *et al*., 2007). Molecular weight can have a large effect on the morphologies of electrospun fibres because it also determines the viscosity. Thus, beads instead of fibres have been observed when the molecular weight of the solution was too low. However, a high-molecular-weight solution forms larger fibre diameters (Bhardwaj *et al*., 2010). Furthermore, molecular weight appears to control the chain entanglement for the electrospun fibre (Gupta *et al*., 2005).

1.3.3.1.3 Conductivity

The conductivity of a solution is a crucial element for successful electrospinning. Most polymers are conductive, with a few exceptions, and the type of polymer, type of solvent, and the availability of ionisable salt are the primary determinants of the solution conductivity (Bhardwaj *et al*., 2010). Moreover, a significant decrease in the

electrospun fibre diameter has been found with increased solution conductivity (Haghi *et al*., 2007).

1.3.3.2 Processing parameters

1.3.3.2.1 Flow rate

The flow rate is an important processing factor, as it determines the amount of the polymer jet. Many authors have studied the relationship between the flow rate, the morphology of electrospun fibres, and the possibility of bead formation. Yuan *et al.* (2004) stated that reducing the flow rate gives the solvent more time to evaporate and may reduce the formation of beads. Moreover, fibres decrease in size with a decrease in the flow rate (Pham *et al*., 2006).

1.3.3.2.2 Applied voltage

The applied voltage is one of the most-studied parameters, although how applied voltage affects the electrospinning process and resulting nanofibers remains under debate. Some authors have suggested that the effects of voltage on the diameter of nanofibers are minimal (Reneker *et al*., 1996), whereas other authors have suggested that the ejection volume increases with high voltage, which leads to larger fibre diameters (Zhang *et al*., 2005).

However, some researchers have reported that increases in the repulsive forces when using a high electric field tend to narrow the fibre diameters (Haghi *et al*., 2007). Likewise, high voltage may increase the chance of bead formation (Bhardwaj *et al*., 2010).

1.3.3.2.3 Tip to collector distance

The distance between the tip and the collector is another important factor that affects electrospun nanofibers. A minimum distance is required to provide sufficient time for the solvent to dry. When the tip is too close or too far from the collector, the formation

of beads may occur (Bhardwaj *et al*., 2010). Additionally, some studies have concluded that as the distance between the tip and the collector increases, the fibre diameters decrease (Doshi and Reneker, 1995).

1.3.3.2.4 Types of collectors

The types and shapes of the collectors are important processing factors that can affect the quality of the nanofibres. Generally, the most common collector used in the literature has been aluminium foil. However, due to the difficulty transferring collected fibres, other collectors have been used, such as wire mesh and conductive paper (Wang *et al*., 2005). Furthermore, the shape of the collector can affect the orientation of the fibres. Thus, a rotating wheel has been used to produce aligned fibres (Xu *et al*., 2004).

Electrospun scaffolds are one the most successful tissue engineering devices and provide a suitable substrate for the incorporation of biofunctional agents. In addition, EVs have been shown to have an important role for promoting tissue engineering processes. To our knowledge, the potential of electrospun scaffolds functionalised with EV in tissue engineering applications has yet to be explored.

1.3.4 Surface treatment of electrospun scaffold

After producing electrospun scaffold that replicates the ECM structure, biofunctionalization is required because cells not only recognise topographical stimuli but also biochemical stimuli that have a substantial impact on their behaviour. Surface modifications to the scaffold have been shown to increase both wettability and cell attachment (Cipitria *et al*., 2011). In addition, surface modification of the scaffold found to induce drug delivery by enhancing the incorporation of the drugs (Seeram Ramakrishna *et al*., 2013). It was also found to overcome the issues of short release time and first burst release(Im *et al*., 2010). The choice of an appropriate surface

modification not compromising the delicate structure of nanofibers is a challenging. Ion-beam, X-ray, ozone oxidation, and gamma radiation can create reactive chemical functionalities on polymer surfaces, however, they often degrade the polymer and damage nanofibers(Rosario-Meléndez *et al*., 2011). In addition, wet chemical treatment is used to provide functional groups to biomaterial surfaces. Despite improving surface wettability, chemical treatments might reduce mechanical performance and promote degradation, destroying fine structures of nanofibers (Chong *et al*., 2007). On the other hand, plasma treatment found an alternative surface modification technique that to incorporate functional groups on polymer surfaces without the use of solvents which can be very adequate to treat delicate structures such as nanofibers (Wulf *et al*. 2011).

1.3.4.1 Plasma treatment

Plasma is a totally or partially ionized gaseous mixture of ions, radicals, and free electrons (Petlin *et al*. 2017). Plasma treatment can activate a polymer surface by forming new polar functional groups, such as carbonyl, carboxyl, ether, amine, and hydroxyl, therefore significantly boosting the free polymer surface energy, increase surface adhesion and the hydrophilic chemistry of materials (Nair *et al*., 2015; Vijayalakshmi et al., 2011). The capability of plasma treatment to obtain ultra-thin films and maintain perfect control during the treatment process provides justification for the treatment's practicability (Morent *et al*., 2011).

Activation of PCL fibres has been reported by several research groups to improve the biocompatibility of the materials or establish delivery platforms for biomolecules (Sandoval-Castellanos *et al*., 2020). Depending on the choice of the working gas, different functional groups will be added directly or indirectly on the surface. For example, a plasma generated in air, O_2, N_2 or NH_3 will incorporate oxygen and/or

nitrogen-containing functionalities during the plasma exposure and can create free radicals that could serve after the treatment for the grafting or cross-linking (Morent et al., 2011).

1.3.4.2 Heparin treatment

Heparin is a linear polysaccharide made up of repeating units of uronic acid and glucosamine (Sakiyama-Elbert, 2013). The anticoagulation effect of heparin increased its use for vascular tissue engineering. Scaffolds functionalized with heparin exhibit a hydrophilic and negatively charged surface that prevents thrombus formation by hindering the adsorption of proteins such as albumin and fibrinogen (Ye *et al*., 2012). Beside its anticoagulation characteristic, it was found to provide a drug delivery mechanism. Heparin-based delivery systems have proven useful for the delivery of a wide range of growth factors for diverse biomedical applications since a significant number of growth factors bind to heparin with either moderate or high affinity (Sakiyama-Elbert, 2014). Different methods of incorporating heparin to the biomaterials have been extensively reviewed elsewhere(Sakiyama-Elbert, 2013).

1.4 Hypothesis, Aim and Objectives

1.4.1 Hypothesis

We hypothesise that EVs can retain their functionality after being attached to fibrous membranes via a simple one-step functionalisation protocol based on electrostatic interactions rather than covalent bonding.

1.4.2 Aim

The aim of this project is to examine the ability to produce a novel electrospun membrane by combining EVs with electrospun polycaprolactone fibres and study its potential use for wound healing, angiogenesis, and osteogenesis.

1.4.3 Objectives

1- Isolate and characterise EVs from cells *in vitro*.

2- Manufacture and characterise a set of Polycaprolactone electrospun scaffolds

3- Treatment of the surface of scaffolds with air plasma and heparin to enhance wettability and EV attachment.

4- Modify the scaffold with different types of EV e.g: fibroblast- and MSC-derived EV, with relevance to specific tissue engineering applications and quantify EV attachment and release kinetics from the scaffold.

5- Assess the ability of myofibroblast-derived EVs to induce myofibroblastic differentiation of NOF cells using qPCR and immunofluorescence.

6- Examine the ability of HDPS EVs and conditioned media to induce angiogenesis using Chorioallantoic membrane (CAM) assay and to induce osteogenic differentiation of rat MCS cells.

Chapter 2

Materials and methods

2.1 Cell culture and propagation

2.1.1 Cell culture

The laminar flow hoods, equipment and reagents utilized during cell culture practice were sterilised using autoclave-based sterilisation or by industrial methylated spirit (IMS) 70% in dH2O (v/v). Media was replaced every three days unless otherwise indicated. Cells were incubated in a 5% CO_2 humidified incubator at 37°C. Primary cells were cultured and passaged between passage 3-12. Cells were passaged when reaching 80-90% confluency. Cell lines were regularly checked for mycoplasma infection on conditioned media collected from confluent cultures.

2.1.2 Cell lines and primary cell

2.1.2.1 H357

The human OSCC-derived cell line H357 was retrieved from the School of Clinical Dentistry biorepository. The H357 cell line was initially obtained from a well-differentiated OSCC of the tongue excised from a 74-year-old Caucasian male patient (Prime *et al*., 1990) The primary tumour width was 20 mm in diameter with no regional lymph node spread or distant metastases.

2.1.2.2 NOF

Primary normal oral fibroblasts NOF were isolated from connective tissue biopsies taken from the buccal oral mucosa of patients during routine dental practices with written, informed consent (ethical approval number 09/H1308/66). NOF 822 were used at passage 3-7 to exclude the possibility of senescence (Hearnden *et al*., 2009).

2.1.2.3 HDPSC

Human dental pulp cells, a gift from Dr. Oscar O. Solis-Castro and Prof. Fiona M. Boissonade, were isolated from samples collected with written informed consent from patients at the Charles Clifford Dental Hospital, Sheffield, UK. HDPS-5 cells were isolated from non-carious molar tooth from a female patient, 22yrs old in accordance with ethical approval granted by the Leeds East Research Ethics Committee of the UK National Research Ethics Service (reference: 15/YH/0308; protocol: STH19019) (Solis-Castro *et al*., 2020).

2.1.2.4 HUVEC

Primary Human Umbilical Vein Endothelial Cells isolated from the vein of the umbilical cord of single, pooled or pre-screened donors were acquired from PromoCell (catalogue number: C-12200).

2.1.2.5 MG 63

MG 63, a human osteosarcoma-derived osteoblastic cell line isolated from osteosarcoma of a 14-year-old male patient, was acquired from Sigma-Aldrich, (catalogue number: 86051601).

2.1.2.6 rBM-MSCs

Mesenchymal stromal cells (MSCs) were taken from the bone marrow of 4-5 weeks old male Wistar rats tibia according to the method described by Maniatopoulos *et al*., (1988). Isolation method was described by Santocildes-Romero *et al*., (2015).

Human cells and cell lines used in this study and their source are summarised in **Table 2.1.**

Table 2.1. Cell lines and primary cells cultured

Cell name	Tissue site origin	Source
H357	OSCC tongue keratinocyte cell line	Health protection agency culture collections, Salisbury, UK (Yeudall *et al*., 1993)
NOF 822	Normal buccal fibroblasts	Charles Clifford Dental Hospital, The University of Sheffield, UK
HDPS	Dental pulp cells from non-carious molar tooth	Charles Clifford Dental Hospital, The University of Sheffield, UK
HUVEC	The vein of the umbilical cord	PromoCell®, C-12200
MG 63	Human osteosarcoma-derived osteoblastic cell line	Sigma-Aldrich®, 86051601
rBM-MSCs	Male Wistar rats, 4-5 weeks of age	School of clinical dentistry, University of Sheffield

2.1.3 Culture media

The cells were cultured in their corresponding culture media as summarised in **table 2.2**. The cells were passaged when they reached 70-80% confluency (section 2.1.4.1). All media was warmed in a 37°C water bath before use.

Table 2.2. Media used to culture the specific cell strains

Cell name	Nutrient Media
H357 **NOF 822**	Dulbecco's Modified Eagle's Medium (DMEM) 10% (v/v) Foetal Bovine Serum (FBS) 1% (v/v) Penicillin/ Streptomycin 1% (v/v) Amphotericin B (250 µg/ml) 1% (v/v) L-Glutamin
HDPSC	Dulbecco's Modified Eagle's Medium (DMEM) 15% (v/v) Foetal Bovine Serum (FBS) 1% (v/v) Penicillin/ Streptomycin 1% (v/v) L-Glutamine Ascorbic acid 100 uM
HUVEC	PromoCell Endothelial Cell Growth Media, C-22010
MG 63	Minimum Essential Medium Eagle (MEME) (Sigma-Aldrich) 10% (v/v) Foetal Bovine Serum (FBS) 1% (v/v) Penicillin/ Streptomycin 1% (v/v) L-Glutamin
rBM-MSCs	Minimum Essential Medium Eagle (MEME) (Sigma-Aldrich) 10% (v/v) Foetal Bovine Serum (FBS) 1% (v/v) Penicillin/ Streptomycin 1% (v/v) L-Glutamin

2.1.4 Cell maintenance

2.1.4.1 Cell subculture and propagation

After reaching near confluence (70-80%), all cells were trypsinised, reseeded, and allowed to further propagate. After removing the medium, the cells were washed twice in 5 ml of sterile modified Dulbecco's PBS, without calcium or magnesium chloride (catalogue number D8537, SigmaAldrich). Following rinsing twice, PBS was removed, 5 ml trypsin ethylenediaminetetraacetic acid (EDTA) solution (catalogue number T3924, Sigma-Aldrich) was applied, and cells were allowed to detach in the incubator for 5 min at 37°C. Then, the supernatant was discarded carefully and 10 ml of fresh medium was added to neutralise the trypsin before centrifugation, at 1,000 × g for 5 min. The cell pellet was re-suspended in 10 ml fresh DMEM+ FBS, then reseeded in a new flask (T 75, T175) at the required density ($1x10^6$, $3x10^6$ cells).

2.1.4.2 Counting cells

Cell counts were performed using a modified Neubauer haemocytometer. The number of cells in four 1 mm^2 (volume 1 x 10^4 ml) squares of the grid were counted and the mean was taken. Cell number was calculated as follows:

Average No cells counted per $1mm^2$ x dilution factor = cells/ml

2.1.4.3 Freezing cells for storage in liquid nitrogen

For cryopreservation, cells were resuspended in freezing media (90% FBS, 10% di-methyl sulfoxide (DMSO) in a concentration of $1x10^6$ cell/ ml. Then, cell suspension (1 ml) was transferred to a cryovial and placed in a freezing container with 250 ml isopropanol at -80° C. After 24 hours, vials were moved to a liquid nitrogen dewar **(-196° C**).

2.1.4.4 Thawing cells

After thawing cryovials in a 37 °C water path, the cell suspension was diluted in appropriate culture media and centrifuge for 5 min at 1000 rpm. The pellet was then resuspended in a cell culture medium after discarding the supernatant.

2.2 Isolation of extracellular vesicles

2.2.1 Ultracentrifugation (UC)

Cells were serum starved for 27 h before the isolation of EVs, by replacing the FBS-containing medium with a serum-free medium. To isolate EVs, the conditioned medium from a T175 flask was transferred to a 50 ml Falcon tube, which was centrifuged for 10 min at 3,000 × g to remove dead cells. Following centrifugation, the supernatant was filtered with a 0.22-µm filter and transferred to a 70 ml centrifuge bottle (Beckman Coulter). The supernatant was then centrifuged using a Beckman Optima LE-80k Ultracentrifuge (Beckmann Coulter), with a Ti45 fixed-angle rotor, at 100,000 × g (29,000 rpm) for 1 h. The supernatant was discarded, and the EV pellet was re-suspended in 60 ml PBS and centrifuged again for 1 h at 100,000 × g (29,000 rpm). Finally, the supernatant was discarded, and the pelleted EVs were re-suspended in 50 µl PBS and stored at -80°C.

2.2.2 Size exclusion chromatography (SEC)

The conditioned medium was prepared as described above and then filtered using a 0.22 µm filter. Serial centrifugation cycles, at 6,000 × g for 25, 30, 35, 10, and 5 min, in sequence, using a Vivaspin 20 (100 kDa molecular weight [MW] cut-off) centrifugal tube, were performed to concentrate the 60 ml conditioned medium down to < 1 ml. A size exclusion chromatography (SEC) column was prepared by adding 14 ml Sepharose CL-2B (GE) to an Econopack column (Biorad), which was allowed to settle for 2 h under normal gravity conditions. Then, a polystyrene fret was placed

horizontally just above the gel layer. The bottom cap was removed to allow the ethanol to drain, and the column was washed twice with 10 ml 0.03% Tween 20 (v/v) in PBS. After the column was washed, 0.75-1 ml of the concentrated medium was top-loaded and allowed to enter the Sepharose before using 10 ml 0.03% Tween 20 (v/v) in PBS to elute the column. Immediately, twenty 0.5 ml fractions were collected and stored at -80°C.

2.3 Characterisation of EVs

2.3.1 Quantification and size distribution

2.3.1.1 Nanoparticle tracking analysis (ZetaView)

Nanoparticle tracking analysis (NTA) uses the Brownian motion of EV, captured on video, to determine their hydrodynamic diameter. The diffusion movement of the small and large particles in the liquid is measured to determine the size and size distribution of the nanoparticles (**Figure 2.1**). In this study, A ZetaView Video Microscope PMX-120 (Particle Metrix, Germany) was used to perform nanoparticle tracking analysis. Before measurements were performed, the system was washed three times with Milli-Q water (MQH_2O). Pre-testing was performed to identify the ideal concentrations necessary to achieve the recommended particle per frame value (140-200). Each sample was measured three times by scanning 11 different cell positions and capturing 60 frames per position. All measurements were performed using the following settings: focus: autofocus; shutter: 70; temperature: 23°C; and scattering intensity: 5.7. All resulting data and video were analysed by ZetaView (8.04.02, SP2), which measures the particle size, size distribution, and zeta potential.

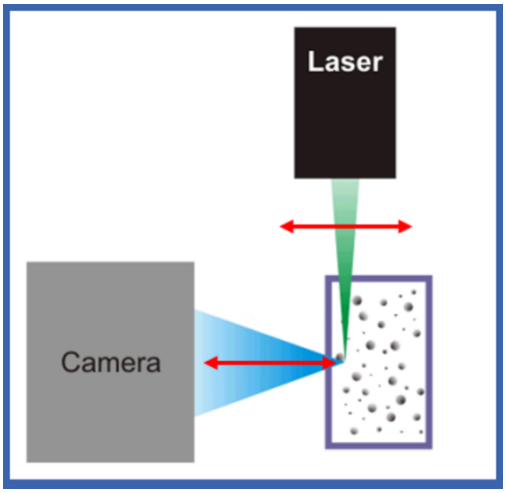

Figure 2.1 Schematic diagram of how ZetaView measure the size of the EV by hitting them with laser then detect the light scattered on the attached camera.

2.3.2 Zetapotential measurement using Zetasizer

The zetapotential (ZP), also known as electrokinetic potential, is the potential at a colloid particle's slipping/shear plane when it is moving in an electric field (Kaszuba et al., 2010). The zeta-potential (ζ-potential) of EVs was measured using a Malvern Zetasizer NanoZS 3000-HA (Malvern Instruments, UK). The Zetasizer Nano Series uses a combination of laser Doppler velocimetry and phase analysis light scattering (PALS) in a patented technique called M3-PALS to measure particle electrophoretic mobility. For measurements, EV isolated by SEC were diluted at 10:1000 in PBS. The diluted PBS buffer solution acted as an electrolyte for the measurements (pH ~ 5.5, 25 °C). All data were averaged over 100 consecutive runs.

2.3.3 Protein analysis

2.3.3.1 BCA Assay

Total protein in SEC fraction was detected and quantified using Pierce BCA protein assay kit (catalogue number 23225, Thermo Fisher Scientific, UK). This kit is a colorimetric protein assay which detects protein based on the bicinchoninic acid (BCA) by combining the reduction of Cu^{2+} and Cu^{1+} by peptide bonds in an alkaline medium with the highly sensitive and selective colorimetric detection of the cuprous cation (Cu1+) by bicinchoninic acid (BCA). To detect the protein in SEC fraction, Bovine serum albumin (BSA) standards of known concentration (0, 0.125, 0.5, 0.75, 1, 1.5, 2 mg/ml of BSA) were prepared in PBS. After adding 200 µl of assay working reagent (consisting of A and B solution 50:1 ratio) to 96 well plates, 10 µl of each sample and standards were added to each well. All standards and samples were run in triplicate. Following mixing each well by pipetting up and down, the plate was sealed with plastic film cover and incubated at 37 °C for 30 min. After the incubation, the plate was cooled to room temperature then the optical density of the standard and samples were measured using a spectrophotometer plate reader TECAN (Magellan V7.2 software, Infinite M200). Using the BSA standard curve and a polynomial equation, protein concentrations of SEC fractions were determined.

2.3.3.2 Western blot

2.3.3.2.1 SDS-PAGE Gel preparation

12% Acrylamide gels were cast between glass plates using the following quantities to produce two gels **Table 2.3.**

Table 2.3. Regents for 12% acrylamide gel

resolving gel		Stacking gel	
40% Acrylamide (37.5:1 acrylamide: bis-acrylamide)	3.0 ml	**40% Acrylamide (37.5:1 acrylamide: bis-acrylamide)**	975 µl
H2O	4.3 ml	**H2O**	4.725 ml
pH 6.8 Tris Page SDS buffer	2.5 ml	**pH 6.8 Tris Page SDS buffer**	2.1 ml
10% Ammonium persulfate	350 µl	**10% Ammonium persulfate**	100 µl
TEMED	5 µl	**TEMED**	17 µl

Once prepared, the resolving gel was pipetted between the plates. Then, the stacking gel was poured on top of the set resolving gel. Before allowing the gel to polymerise, the sample comb was immediately inserted. After 10 min, the comb was removed, and each well was washed out with copious amounts of distilled water.

SEC fractions (4-10) were concentrated using ultracentrifugation then the pellet was suspended in 100µl loading buffer. The samples were then heated for 5 min at 95 °C. The separation was done using 12% polyacrylamide SDS-PAGE in Biorad tanks filled with 1X running buffer (88 g Glycine, 10% W/V SDS and 32 g Tris Base in 1 L dH_2O). 20 µl of sample was loaded in each well alongside Precision Plus prestained protein ladder (Biorad) in the outside wells. Separation was carried out at 150 V until the dye had reached the bottom of the plate.

2.3.3.2.2 Bio-Rad transblot Turbo transfer

The gel was put on the nitrocellulose membrane of a pre-prepared stack (iBlot transfer system (Bio-Rad, UK)) after SDS-PAGE. The sandwich was put together by adding the top layers and removing the bubbles. Proteins were transferred using a programme that was appropriate for the gel thickness. This was 28 V for 7 minutes for 1.0 mm gels and 28 V for 10 minutes for 1.5 mm gels.

2.3.3.2.3 Blocking and antibody incubation

The nitrocellulose membrane was blocked for 1 h on a rocker shaker in 5% (w/v) skimmed milk in TBST (8 g NaCl 3 g Tris base 0.2 g KCl in 1L dH2O and 0.1% Tween-20). Following the preparation of the primary antibody in accordance with the manufacturer's instructions (**Table 2.4**), the membrane was incubated overnight on a rocker shaker at 4°C. The next day, the membrane was washed three times for 15 mins in TBST before being incubated with the secondary antibody (**Table 2.5**) for 1 h at RT. After washing again three times with TBST for 15 min, the membrane was incubated in a 1:1 ratio (500 µl volume of each) of Westra Supernova substrates (CYANAGEN, XLS3,0100) for 5 min to increase the intensity of the signals. After removing the excess, the membrane was placed in cling film inside an x-ray cassette. In the dark room, the x-ray film was placed inside the cassette for exposure and then developed with an automated processor (Xograph Compact X4).

Table 2.4. Details of all primary antibodies used in western blot experiment

Antibody (clone)	Blocking buffer	Dilution	Manufacturer (Antibody number)
CD63 (EPR5702) rabbit monoclonal	5% milk in TBST	1:1000	Abcam (ab134045)
CD9 antibody [EPR2949]	5% milk in TBST	1:2000	Abcam (ab92726)
CD81 antibody [M38]	5% milk in TBST	1:1000	Abcam (ab79559)

Table 2.5. Details of all secondary antibodies used in western blot experiment

Antibody	Blocking buffer	Dilution	Manufacturer
Anti-mouse	5% milk in TBST	1:3000	Cell Signalling (New England Biosciences)
Anti-rabbit	5% milk in TBST	1:3000	Cell Signalling (New England Biosciences)

2.3.3.3 Nano flow cytometry

A NanoAnalyzer U30 instrument (NanoFCM Inc.) equipped with dual 488/640 nm lasers and single-photon counting avalanche photodiode detections (SPCM APDs) was used for simultaneous detection of side scatter (SSC) and fluorescence of individual particles. Bandpass filters allowed for collection of light in specific channels (SSC - 488/10; FL1 – 525/40; FL2 – 670/30). HPLC-grade water served as the sheath-fluid via a gravity feed, reducing the sample core stream diameter to ~1.4 µm. Measurements were taken over a 1-min interval at a sampling pressure of 1.0kPa, maintained by an air-based pressure module. All samples were diluted to attain a particle count within the optimal range of 2000-12,000/min. During sample acquisition, the sample stream is fully illuminated within the central region of the focused laser beam, resulting in approximately 100% detection efficiency, which leads to accurate particle concentration measurement via single-particle enumeration.

The concentration of samples was determined by comparison to 250 nm silica nanoparticles of known concentration to calibrate the sample flow rate. EV isolates were sized according to standard operating procedures using a proprietary 4-modal silica nanosphere cocktail (NanoFCM Inc., S16M-Exo). Using the NanoFCM software (NanoFCM Profession V1.8), a standard curve was generated based on the side scattering intensity of the four different silica particle populations of 68, 91, 113 and 155nm in diameter. Silica provides a stable and monodisperse standard with a refractive index of approximately 1.43 to 1.46, which is close to the range of refractive indices reported in the literature for EVs (n = 1.37 to 1.42). The laser was set to 10 mW and 10% SSC decay.

EVs presenting core tetraspanins were labelled with the following antibodies: FITC-conjugated anti-human CD63 (clone MEM-259; Abcam), FITC-conjugated anti-human CD9 (clone MEM-61; Abcam), and FITC-conjugated anti-human CD81 (clone M38;

Abcam). 1e8 EVs/particles in PBS was mixed with a cocktail of the 3 antibodies (1:50, or 1:150 each) before incubation for 30 minutes at room temperature. After incubation, the mixture was resuspended to 1ml PBS and Ultracentrifugation at 100,000 x g was performed for 1 hour in a BC Optima™ TLX Tabletop centrifuge with a TLA-120.2 rotor. Pellets were resuspended in 50ul PBS and diluted to 1e8-5e8 particles/ml for immediate phenotypic analysis.

Data processing was handled within the nFCM Professional Suite v1.8 software, with dot plots, histograms, and statistical data provided in a single PDF. Gating within the software allows for proportional analysis of subpopulations separated by fluorescent intensities with size distribution and concentration available for each sub-population.

2.3.3.4 ExoView characterisation of EV markers

EVs suspended in PBS were analysed using an ExoView R100 (NanoView Biosciences) to determine the presence of selected tetraspanins, established markers of EV (Lai *et al*., 2016). According to manufacture instructions, 35 µl of EV diluted 1 to 400 using proprietary incubation solution was directly pipetted onto a chip. Using a humidified 24-well plate, the chips were incubated in dark, overnight at room temperature. The humidified plate used for incubation was filled by adding diH2O to the outer wells and covered with foil. The following day, using a proprietary washing solution, chips were washed three times for 5 min each. Next, chips were incubated with the secondary antibody, conjugated to a fluorophore, for 1h at room temperature. After incubation, chips were washed three times for 5 min each and then allowed to dry at room temperature. Then, chips were loaded into a metal cassette and placed in the ExoView R100. Samples were examined in the fluorescence and label-free mode to obtain high-resolution images. Images, then, were acquired using proprietary software.

2.4 Manufacturing of electrospun scaffolds

The electrospun scaffolds used in this project were manufactured using an upright in-house developed electrospinning set-up. A 10% polymer solution of (w/v) poly(caprolactone) (PCL) (Average Mn= 80,000 g/mol; Sigma Aldrich, UK) was prepared by dissolving the PCL in a solvent mixture containing 90% dichloromethane (DCM) (Fisher Scientific, UK) and 10% dimethylformamide (DMF) (Fisher Scientific, UK). The solution was prepared and stirred at room temperature for 24 hours before electrospinning was performed, to ensure that the polymer dissolved completely. The electrospinning system was composed of an Alpha IV Brandenburg power source (Brandenburg, UK) and a PHD2000 infuse/withdraw syringe pump (Harvard Apparatus, UK). For each scaffold, 1 ml of the solution was electrospun using a plastic syringe (1 ml; Becton Dickinson, UK), during which the solution flowed into a metallic 20-gauge needle (Intertronics, UK), with a flow rate of 1.5 ml/h. The voltage used was 21 kV, and the needle tip-collector distance was 17 cm.

2.5 Surface treatment of PCL scaffold

2.5.1 Plasma treatment

To increase the hydrophilicity of the PCL scaffold, plasma treatment was performed using a low-pressure plasma system (plasma cleaner, model 2 base unit type, ZEPTO, Diener Electronics, Germany). First, the scaffold was placed on a petri dish and then it was inserted into the glass cylinder chamber of the plasma instrument. After the evacuation of the chamber, the air plasma was generated for 2 min using a power of 10 watt. The plasma-treated scaffold was then removed and stored in a sealed plastic bag at 4°C.

2.5.2 Heparin treatment

Heparin treatment was performed according to a previously described protocol (Wang *et al*., 2013). First, Scaffolds were immersed in an ethylenediamine (EDA) solution (0.1 M) (Sigma-Aldrich, E26266-500ML) by gently shaking at room temperature to introduce amino group on the surface . After 30 min, scaffolds were rinsed three times in phosphate-buffered saline (PBS). Then, samples were treated with 2- (N-Morpholino) ethanesulfonic acid (MES) buffer saline solution (pH = 5.6) (ThermoFisher, 28390) containing 1-Ethyl-3-(3-dimethylaminopropyl) carbodiimide hydrochloride (EDC) (0.144 mg/ml) (ThermoFisher,28390), N-hydroxysuccinimide (NHS) (0.144 mg/ml) (ThermoFisher, 24500), and heparin sodium salt from porcine intestinal mucosa (10 mg/ml) (Sigma, H5515-100K). The heparinisation proceeded for 3 h on a shaker. After washing three times with PBS, treated scaffolds were air-dried at room temperature then stored in a sealed plastic bag at 4°C.

2.6 Characterization of scaffolds

2.6.1 Fibre Diameter

Using SEM images at a magnification of x800, the fibre diameter of each scaffold was measured using ImageJ, Version 2, 1.52 P. Three different samples from three different scaffolds were analysed and a total of 4 random areas per sample were examined. Average fibre diameter was measured from total of 60 fibres for each scaffold.

2.6.2 Wettability- Contact angle measurement

To measure the wettability of the scaffold and study the effect of plasma treatment on its hydrophilicity, computer-aided contact angle measurements were used to measure the contact angle of deionized water (DI water) using a Drop Shape Analyzer

(DSA100- KRÜSS- Germany). Three samples from each scaffold were randomly selected and the mean of right and left angle of three drops (5 µl) per sample were measured using Drop Shape Analysis Software (KRÜSS, V1.72-02).

2.6.3 Mercury intrusion porosimetry (MIP)

Mercury intrusion porosimetry (MIP) is a method using the non-wetting property of the mercury to determine the total pore volume, pore size and pore size distribution of 3D material (Loh *et al*., 2013). During the measurement, the samples are placed in an evacuated chamber mercury penetrometer then the mercury is introduced into the chamber. Under increasing pressure up to a maximum of 414 MPa, mercury is forced to penetrate the pores of the sample. Meanwhile, the intruded volume of mercury and applied pressure are recorded. This technique has been used to determine the pore characteristics of various scaffold types including electrospun scaffold (Brennan *et al*., 2015).

In this experiment, measurements were obtained using a MicroActive AutoPore V 9600 Version 1.02 (Micromeritics, USA). First, a 3 mg sample of each type of scaffold was introduced to the system. The pressure was applied gradually up to 61 psia to analyse the different pore sizes. A detailed report was generated showing the pore size, pore size distribution, density and surface area.

2.6.4 Surface Zetapotential of electrospun scaffold

Electrospun scaffolds' surface zeta potentials were determined using laser Doppler electrophoresis measurements with a Malvern Surface Zeta Potential ZEN1020 cell. Scaffolds were adhered to the sample holder using ethyl cyanoacrylate "superglue" (Gorilla Super Glue, Gorilla Glue Europe A/S), and the sample holder holding the scaffolds was inserted into a Malvern ZEN 1020 surface zeta-potential cell. The

Zetasizer was configured to detect forward-scattered light at an angle of 13°, with the attenuator set to position 11 (100 percent laser transmission). Automatic voltage was chosen (typically 10 V was selected). The dip cell was inserted in a cuvette containing 1 mL of spherical nanoparticles containing 0.003% w/w PGMA-PBzMA in the presence of 1 mM KNO3 at 25 °C. The apparatus was configured to do five slow-field reversal measurements at four distances from the sample surface (125 mm, 250 mm, 375 mm, and 500 mm), with 15 sub-runs and one minute between each measurement. In order to quantify the electro-osmotic mobility of the tracer nanoparticles, three fast-field reversal measurements were conducted at a distance of 1000 m from the sample surface. In this instance, each measurement consisted of 100 sub-runs separated by a 20-second delay. The zeta potential of the particles was computed utilising the Henry equation and Smoluchowski approximation.

2.7 Fabrication of EV-modified scaffolds

Two methods were utilised to modify the scaffold with EVs. The incubation method by incubating the scaffold after fabrication with EVs suspension. This method was used to modify the plasma-treated scaffold (our approach) and heparin-treated scaffold (Wei *et al*., 2019) with EVs. Spinning EVs with polymer solution (EV-spun method) was used according (Trindade *et al*., 2021). **Figure 2.2** illustrates the manufacturing routes of EVs modified scaffold used in this project.

2.7.1 Incubation method

Before each experiment, the scaffold samples were prepared by cutting them into 8-mm circles for use in 96-well plates. After washing the samples with 70% IMS then thoroughly with PBS to remove IMS remnants, samples were placed in 96 well plates, loaded with EV suspension, and incubated for 24 h at 4°C. The concentration of EVs

used for each assay is described in the result section. Three control samples (scaffold in PBS) were also included.

2.7.2 EV-spun method

Following preparing the polymer solution as described in **section 2.4,** 500 µl of EV suspension were added to the solution before spinning. After spinning, scaffolds were left in the ventilation fume hood for 24 hours to allow the remaining solvent to evaporate. Scaffolds were then stored at 4 °C.

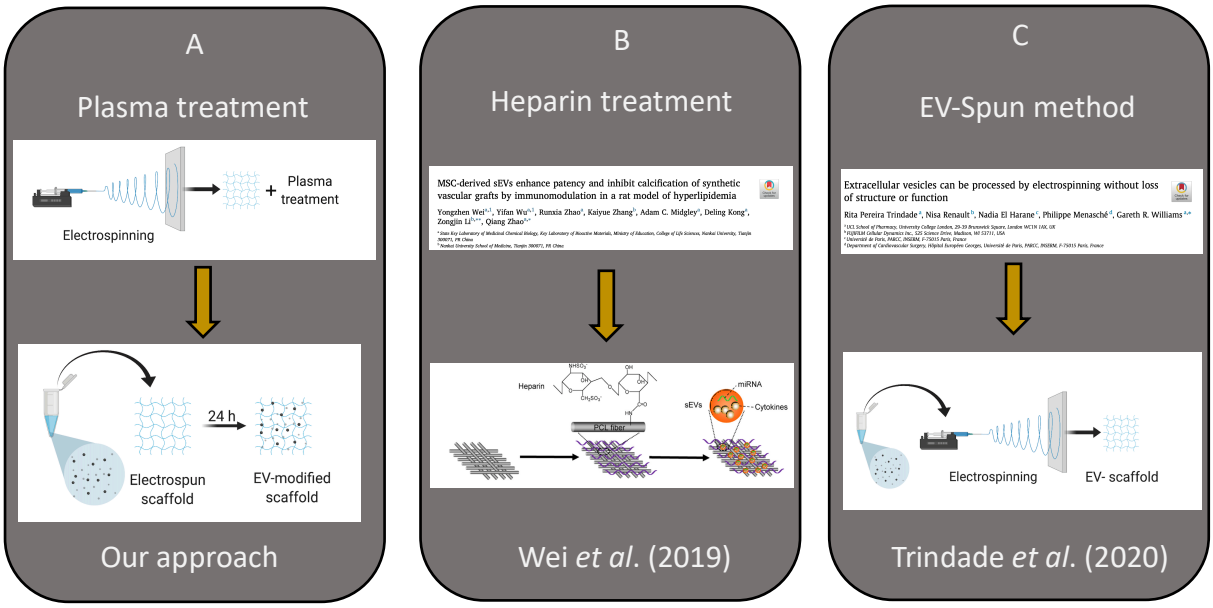

Figure 2.2. Schematic illustration of the manufacturing routes of EVs-modified scaffold. (A) In our approach to modifying scaffolds with EVs, PCL scaffolds were manufactured, treated with air plasma the incubated with EVs suspension. (B) Scaffolds were treated with heparin and then incubated with EV suspension. (C) EVs suspension was added to electrospun polymer solution before spinning.

2.8 Microscopic characterisation of EVs, scaffolds, and EVs-modified scaffolds

2.8.1 Scanning electron microscopy (SEM)

2.8.1.1 Electrospun scaffolds

After the fabrication of PCL scaffolds, the morphologies and sizes of electrospun fibres were examined in detail using SEM. Three samples from three different areas of the scaffold were obtained and mounted onto a pin-stub, using a Leit-C sticky tab, for coating and SEM imaging.

2.8.1.2 EVs on coverslips

To study the morphologies of EVs alone using SEM, 13-mm coverslips were used in 24-well plates. First, coverslips were washed with acetone, methanol, isopropanol, and deionised (DI) water, sequentially, and then dried with an air stream. Then, $6x10^7$ EV suspension was loaded onto the coverslips and incubated at room temperature for 24 h.

2.8.1.3 Fixation and dehydration protocol of EVs-modified scaffold

After each experiment, all EV-modified scaffold samples, including control samples, were fixed with 3% (v/v) glutaraldehyde in 0.1 M sodium cacodylate buffer for 1 h. Then, the samples were washed three times with sodium cacodylate buffer for 10 min and then dehydrated in a graded ethanol series (50%, 70%, 95%, 100%) for 15 min each. Following that, samples were dried with 50:50 ethanol:hexamethyldisilane (HMDS) before being dried with 100% HMDS for 15 min.

After the removal of HMDS, the samples were left to dry overnight in a fume hood. Samples were mounted onto a pin-stub, using a Leit-C sticky tab, and then gold-coated, using an Edwards S150B sputter coater. Finally, using a Tescan Vega3 LMU Scanning Electron Microscope, samples were examined at an operating voltage of 12 kV.

2.8.1.4 Immunogold labelling

Scaffolds containing EV were fixed with a mixture of formaldehyde 4% (v/v) and glutaraldehyde 1% (v/v) in 0.1 M sodium cacodylate buffer, for better structural preservation and rapid stabilisation (Murtey, 2016). Then, samples were incubated in the blocking reagent Sorensen's phosphate buffer (0.2 M pH 7.6) for 30 min. Next, samples were incubated in 10 % (v/v) primary antibody (recombinant Anti-CD9 antibody [catalogue number: ab92726], Abcam, UK) for two hours at room temperature. After washing with TBS-Tween 20 buffer 5 times, for 5 min each time, samples were incubated in a 2% (v/v) secondary antibody (goat anti-rabbit IgG H&L [20 nm gold] preadsorbed [catalogue number ab27237], Abcam, UK) for 1 h at room temperature. Samples were then washed again with TBS-Tween 20 buffer 5 times, for 5 min each time. Finally, the samples were washed with distilled water for 5 min, followed by dehydration, coating, and imaging, as described above.

2.8.2 Transmission electron microscopy

2.8.2.1 EVs

To investigate EV morphology using TEM, a 200-mesh carbon-coated copper grid was glow discharged for 1 min. Purified EVs were fixed with 2% formaldehyde for 5 min. Then, $4.2x10^6$ EV suspension was loaded onto the grid and incubated for 1 min. Immediately afterwards, 20 drops of filtered 1% uranyl acetate (UA) solution were added on the EM grid for staining. Following the removal of excess of UA with filter paper, the grid was rinsed with distilled water to remove excess staining solution. Holding the grids with tweezers, the grids were covered with a culture dish and left to dry for 10 min. Finally, the grids were examined using TEM at 80 kV.

2.8.2.2 Scaffolds and EV-modified scaffolds

All EV-modified scaffold samples, including control samples (plain scaffolds), were fixed initially with 2.5% glutaraldehyde and then with 2% osmium tetraoxide for 1 h each. After washing three times with 0.1 M sodium cacodylate buffer, for 10 min each time, the samples were fixed with 2% osmium tetroxide for 1 h and then washed three times with 0.1 sodium cacodylate, for 10 min each time. Next, the samples were incubated in a graded acetone series (70%, 80%, 85%, 95%, and 100%, sequentially), for 10 min each. After the removal of acetone, the samples were incubated in a graded series composed of acetone: low-viscosity embedding resin (3:1, 1:1, and 1:3, sequentially), for 30 min each, at room temperature. Then, the samples were baked in 100% low-viscosity embedding resin for 24 h at 65°C. The next day, the samples were sectioned using an ultramicrotome to create 60-nm-thick sections, prior to being observed using TEM at 80 kV.

To study the morphologies of the fibres, plain scaffolds were embedded in pure low-viscosity embedding resin for 24 hours at 65°C. Then, the samples were sectioned into 60-nm-thick sections before being observed using TEM at 80 kV.

2.8.3 Fluorescent microscopy

2.8.3.1 Labelling of EVs

A total of 1.16×10^8 EVs in PBS, isolated by UC, were labelled using a lipid dye (5-(and-6)-carboxyfluorescein diacetate succinimidyl ester [CFSE], Abcam, catalogue number ab113853). To stain EVs, 1 µl CFSE dye was added to 300 µl PBS. Then, 20 µl EVs in PBS were added to the solution and incubated for 2 hours, in the dark, at room temperature, according to manufacturer's instructions and as previously described by Morales-Kastresana *et al.* (2017).

2.8.3.2 labelled EVs with scaffolds

To study the overall distribution of EVs within the scaffolds, the scaffold samples were loaded with labelled (CFSE) EVs in PBS for 24 hours. After observing that unbound dye in the PBS was sticking to the scaffold, stained EVs were re-purified using SEC to remove residual non-EV associated CFSE. Stained EVs were found in the 3rd and 4th fractions as suggested by Morales-Kastresana *et al.* (2017). After incubation for 24 hours at room temperature, samples, including control samples (unmodified scaffold), were examined under a a Zeiss Axioplan 2 fluorescent microscope. Images were analysed using ImageJ 1.52 P.

2.9 Attachment and Release Kinetic of EVs

EV suspension (100 µl of 9.3×10^9 EVs / ml), isolated by SEC, was added to each scaffold sample in a 96 well-plate and incubated at 37ºC. After 4 hours, the PBS containing EVs has been removed and examined using NTA (ZetaView, 8.04.02, SP2) to calculate the number of EVs attached to the scaffold.

To assess the time courses of EV release, 70µl of PBS was loaded onto the top of each scaffold and incubated at 37ºC. Releasates were collected on days 4,7,14 and 21 without disturbing the scaffold, stored at -80ºC and replaced with fresh PBS. Using NTA (ZetaView, 8.04.02, SP2), Releasates were analysed to determine EV release kinetics.

2.10 Role of myofibroblast EVs in wound healing

2.10.1 Differentiation of NOF cell to myofibroblast

Normal oral fibroblast was differentiated to a myofibroblast phenotype as previously reported (Melling *et al*., 2018). Once cells cultured in T75 flask reached 70-80% confluency, the media was discarded, and cell harvested using 3 ml of trypsin for 3 min. Following neutralizing trypsin with nutrient media and centrifugation (1000 rpm for 5 min), cells were counted using a haemocytometer. On sterile coverslips (VWR) in 6 well plate, 250,000 cells (2ml/well) were seeded to determine α-SMA expression and localisation using immunofluorescence (**2.10.2**)

Following allowing the cells to adhere to the well for 24 h, spent media was aspirated and the cells were washed 3X with PBS. Serum-free media was added to the cells (2 ml/ well). The next day, three well were treated with 5 ng/ml recombinant human TGF-β1 (Catalogue number 240B, R&D Systems, UK) diluted in serum-free media (Bhowmick *et al*., 2004). Three wells of cells in serum-free media served as a negative control.

2.10.2 Immunofluorescence (IF) of αSMA staining

After 72 hours of treating cells with TGF-β1, condition media was discarded then cells were washed using 1 ml methanol. Cells then were fixed with fresh absolute methanol for 15 min. The fixed cells were permeabilized in 0.02% Triton™ X-100 in PBS (v/v) for 15 min. Then, blocking buffer 2.5% bovine serum albumin (BSA) in PBS) was added to fibroblast at RT for 15 min. After discarding the blocking buffer, cells were incubated for 1h at 37° C with monoclonal alpha smooth muscle actin FITC murine antibody (catalogue number A2547, Clone 1A4, Sigma-Aldrich), prepared in 1:100 v/v in 2.5% BSA in PBS.

After incubation, each well was washed three times with PBS before transferring coverslips and mounting them on glass slides (catalogue number 631-0108, VWR International) using a drop of Prolong gold DAPI containing mountant (catalogue number P36931, ThermoFisher Scientific). Images were taken at x20 and x40 magnification using an Axioplan 2 fluorescent microscope.

2.10.3 Scratch healing assay

The scratch assay is a simple and inexpensive method for determining cell migration *in vitro*. The main premise of this assay is based on the fact that when an artificial gap (scratch) is created on a confluent cell monolayer, cells on the border of the scratch travel towards the gap to close it until new cell to cell contacts are created. The assay was preformed in 24 well plates by seeding 50,000 cells per well. The selection of this seeding density was based on preliminary experiments examining various cell densities (30,000- 80, 000 cells/ well). Plates were kept at 37°C and 5% CO_2 to facilitate cell adhesion and the creation of a confluent monolayer. Once become confluent, media was removed and a scratch 'wound' was made by scraping off the monolayer cells using 200 µl pipette tip. After washing each well twice using PBS to remove unattached cells, fresh media was added to each well. The cells then were treated with EVs, or EVs-modified scaffold then incubated at 37° C. Wound closure was tracked microscopically for 24 h. Images were taken at x10 magnification and analysed using ImageJ (1.8.0). Wound closure was calculated according to the calculation below:

wound closure rate(%) = ((A0 − At)/A0)*100

A0= Area at time 0

At= Area at time point

2.10.4 PrestoBlue® cell viability assay

After assessing the ability of different samples in inducing cell migration using scratch assay, fibroblast viability was measured using PrestoBlue Cell Viability reagent (Invitrogen Thermofisher, UK). The PrestoBlue assay is based on resazurin which functions as a cell metabolism indicator. Resazurin is a weakly fluorescent protein that is reduced to resorufin in living cells during cellular respiration and serves as an electron acceptor for NADPH, FADH, FMNH, NADH, and cytochromes. PrestoBlue changes from a weak-fluorescent to a strong-fluorescent form as a result of this reaction. The number of metabolically active cells is then directly proportional to the fluorescence conversion. The cells were incubated with 1:10 PrestoBlue reagent in conditioned media (600 µl/ well) according to manufacturer's instructions. The 24 well plate was covered in aluminium foil and allowed to incubate in a humidified incubator for 1 h. After incubation, media from each well was transferred to 96 well plate in triplicate (200ul/ well). Control wells with only cell culture media were included to correct the background error. To measure the fluorescence, a TECAN (Magellan V7.2 software, Infinite M200) plate reader was used with an excitation wavelength of 560 nm with an emission wavelength of 590 nm. After deduction the reading of the no cell controls, relative fluorescence was measured of each treatment group.

2.10.5 Quantitative Real-Time Polymerase Chain Reaction (qPCR)

2.10.5.1 RNA extraction

After removing the media and washing the cells twice with PBS, 350 µl of RNA lysis buffer containing β-mercaptoethanol (10 µL/ml) was added to each well and cells were harvested using a cells scraper. Total RNA was extracted using RNeasy mini kit (QIAGEN, 74104) following the manufacturer's instructions. First, 350 µl of 70%

ethanol was added to the homogenized cell lysate. To remove contaminants, 700 µl of the mixture was applied to the mixture and centrifuged for 15 seconds at 8000g. Then, 700 µl of RW1 buffer was added to the tube and centrifuged for 15 seconds at 8000g. 500 µl of RPE buffer was added to the column and centrifuged for 15 seconds at 8000g then another 500 µl was added to the column and centrifuged for 2 min at 8000g. Finally. The collection tube was replaced and 50 µl of nuclease-free water was added to the tube and centrifuged for 1 in at 8000g. The eluted RNA was immediately placed on ice, ready for RNA quantification.

The concentration and purity of extracted RNA were observed at wavelength 260nm/280nm, with an optimum ratio of 2.0, using a Nanodrop (ND-1000) spectrophotometer (Thermo Scientific, VWR International; Illinois).

2.10.5.2 Reverse Transcription (RT) of RNA to complementary DNA (cDNA)

High Capacity cDNA Reverse Transcription Kit (Applied Biosystems, USA) was used to reverse transcribe RNA according to the manufacturer's instructions. Total volume 10 µl of reverse transcription master mix was prepared according to **Table 2.6** below:

Table 2.6. Reverse Transcriptase (RT) master mix components

Master mix reagents	Volume (total volume 10 µl)
Random primers	2 µl
Reverse transcriptase buffer	2 µl
Reverse transcriptase Multiscribe	1 µl
Deoxynucleotides (dNTPs)	0.8 µl

Each PCR tube (VWR International, USA) received a total volume of 250ng of RNA, with 10 µl of the prepared master mix added to each sample. Samples were centrifuged for 15 seconds at 10,000 rpm to ensure that all samples collected at the bottom of the tubes were collected. The samples were then placed in a DNA Engine DYAD (Bio-Rad Laboratories, USA) thermo-cycler and programmed at 25°C for 10 minutes, 37°C for 2 hours, and 85°C for 5 minutes, before being kept at 4°C, ready for use, or frozen at -80°C for cDNA preservation.

2.6.1 qPCR protocol

Following reverse transcription to cDNA, real time qPCR was done using Rotor-Gene Q PCR system (Qiagen, Germany). TaqMan primers (Life Technologies, Thermo Fisher Scientific, USA) were used for DNA amplification **Table 2.7 and Table 2.8**

Table 2.7. TaqMan probe/ primers

TaqManprimer	Details
a-SMA	alpha smooth muscle actin, Thermo-fisher Catalogue number: 4331182 (Hs00426835) Thermo Fisher Scientific, USA
VCAN	Versican, Thermo-fisher Catalogue number: 4351372 (Hs01007940) Thermo Fisher Scientific, USA
B2M	Human beta-2 microglobulin Catalogue number Hs00187842_m1, Thermo Fisher Scientific, USA

Table 2.8. Real time qPCR TaqMan master mix components

Real time qPCR master mix	Volume (total volume 9.5 µl)
Primer/probe	0.5 µl
B2M reference gene	0.5 µl
Nuclease free water	3.5 µl
TaqMan Gene Expression Master Mix (Applied Biosystems, Catalogue number 4369016, Thermo Fisher Scientific)	5 µl

Human beta-2 microglobulin B2M (Catalogue number Hs00187842_m1, Life Technologies, Thermo Fisher Scientific, USA) was used as a reference gene (Kabir et al., 2016). Nuclease free water was used as a negative control. Samples were loaded in triplicate into 0.2 ml PCR tubes (catalogue number 14230225, Fisherbrand) and centrifuged to collect the sample at the bottom of the tube. The qPCR was run in a two-step method (denaturation stage for 10 s at 95°C, followed by a decrease in temperature to 60°C for 45 s for annealing and extension stage, this was repeated for 40 cycles). To obtain ΔCt, each sample's gene expression was normalised to the endogenous gene B2M. Finally, 2-ΔΔCt method was utilized to calculate fold-change of gene of interest to related untreated samples (Livak, 2001).

2.11 Osteo-differentiation of HDPS

To assess the ability of human dental pulp stem cells to differentiate to osteoblast, cells were analysed using STRO-1 and Alizarin red staining.

2.11.1 Immunofluorescence of STRO-1 staining

Cells were seeded on sterile coverslips in 6-well plates until reaching 80% confluency. Cells then were fixed with 4%PFA for 20 min at RT then washed twice with PBS. Then, washing was done using in 0.02% Triton™ X-100 in PBS (v/v) for 10 min. For immunohistochemistry, cultures were blocked using 5% normal donkey serum (NDS)-PBST (Sigma; Blocking solution) for 1 h at RT. Following blocking, Primary antibody Anti-MSE STRO-1 (R&D Systems, MAB1038) [1:100] in 5% NDS in PBST was added and incubated overnight at 4°C. Next day, cells were washed twice with PBS 0.02%Triton then incubated for 90 min with DNK anti-mouse FITC [1:500] 1.5% NDS in PBST at RT. Then, cells were washed twice with PBS and coverslips were mounted on glass slides using a drop of Prolong gold DAPI containing mountant (catalogue number P36931, Thermo Fisher Scientific). Images were taken at x20 magnification using an Axioplan 2 fluorescent microscope.

2.11.2 Alizarine red staining

Cells were cultured in 12-well plates at a density of 5×10^3 cells/cm^2. After 48 hours, the growth media was replaced with an osteogenic media (StemPro Osteogenesis Differentiation Kit, Gibco, A1007201) for 21 days. Cells cultured in growth media were used as a control. The media was changed every 3 days. After 21 days, media was removed and cells were washed twice with PBS. Cells then were fixed in 4 % PFA in PBS (Thermo Scientific J19943.K2). The mineralized matrix formed was assessed by staining using Aizarine Red S (Sigma, A5533). To make an Alizarin Red dye solution,

342 mg of Alizarin Red S was dissolved in 25 ml of distilled water. The pH was then adjusted to 4.1 using HCL and NaOH. The solution was added to the cells and incubated for 20 min at RT. After removing the excess dye, cells were washed twice with distal water until clear. The cells were then imaged using light microscopy.

2.12 *Ex-ovo* study of angiogenic response using a Chorioallantoic membrane (CAM) assay

The *ex ovo* chick Chorioallantoic membrane (CAM) assay is an extraembryonic membrane that serves as an organ for gas exchange between the embryo and the natural environment. CAM assay was employed to examine angiogenesis as described by Mangir *et al*., (2019). Pathogen-free fertilised white leghorn chicken eggs (Gallus gallus domesticus) supplied from Henry Stewart Co. Ltd (UK) were incubated and handled in accordance with the instructions of the Home Office, UK (in compliance with UK Home Office Animals [ScientificProcedures] Act 1986 and definition of chicken as a Protected Animal from development day 14). Every day, the temperature of the incubator was monitored, and any damaged embryo were discarded. The eggs were kept at 10°C for no more than 10 days before being used in the experiment. The CAM approach used to measure angiogenic activity is schematically represented in **Figure 2.3.**

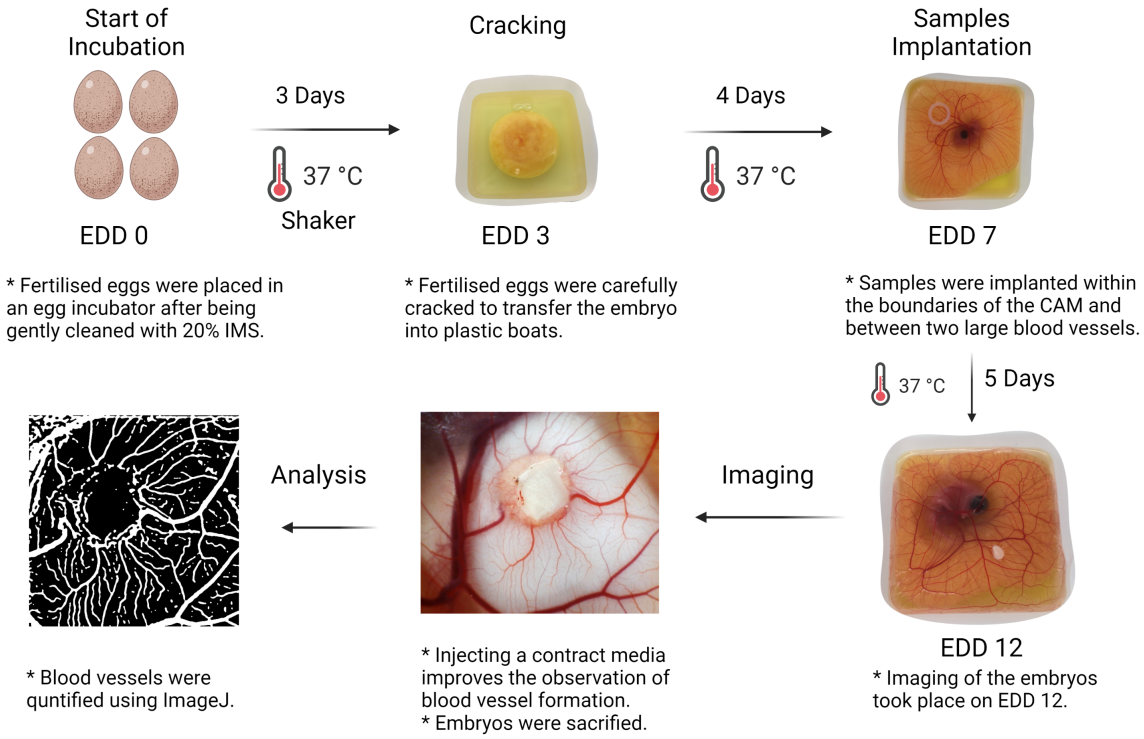

Figure 2.3. Schematic representation of the CAM methodology used to evaluate angiogenesis. EDD: embryonic development day.

2.12.1 Chick embryo incubation

Eggs were carefully cleansed with a 20 % industrial methylated spirit (IMS) solution (Fisher Scientific, UK) on embryonic development day0 (EDD 0) and incubated at 37°C in a humidified hatching incubator (Rcom King Suro Max-20, P&T Poultry). Before incubation, incubators were cleaned with 70% IMS and air-dried for 24 hours in a class II biosafety cabinet. Each incubator was fitted with a 120 ml pot containing 50 ml of dH20 to maintain a humidified atmosphere during the incubation time. Three independent experiments were conducted, each with five samples (N = 3, n = 5).

2.12.2 Egg cracking – *ex-ovo* culture

Egg cracking was performed on EDD 3. On the day before, 100 ml square weigh boats (Starlabs, UK) were prepared to receive the embryo. The edges were trimmed then they were cleaned with 70% IMS followed by a wash with PBS. Then, the weighting boats were put in sterile petri plates with 3 ml PBS + 1% penicillin-streptomycin solution (100 IU/ml - 100 mg/Ml). On the day of cracking, the incubator was turned off and the tops of the eggs were marked with a pen to indicate where the embryo would be during the process. After turning off the incubator, 10 minutes passed before the eggs were cracked. The eggs were broken in the weighing boats and immediately placed in a 37°C humidified incubator (Binder, Tuttlingen). During cracking, any damaged (**Figure 2.4, B)** or dead embryo (**Figure 2.4, C)** was disposed of immediately.

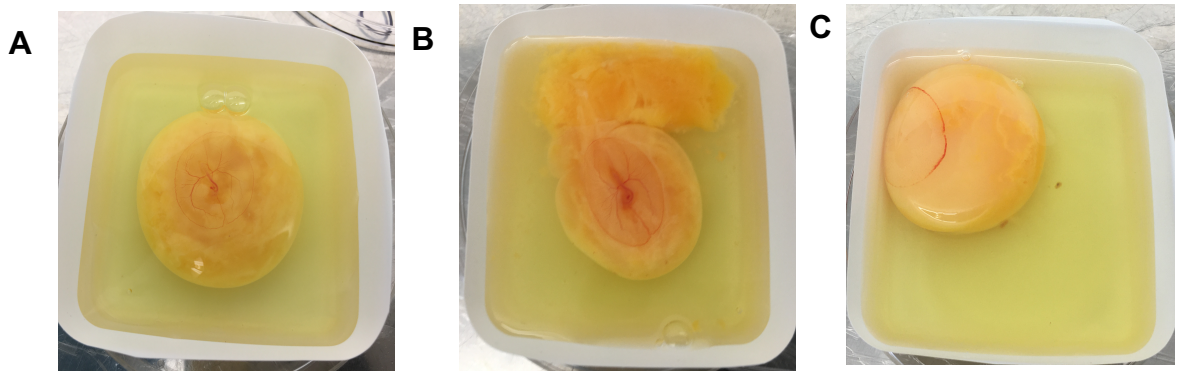

Figure 2.4. Observation of successful embryo transfer. (A) Successful embryo transfer with an intact egg yolk and a live embryo. (B) Unsuccessful embryo transfer with a live embryo. (C) Successful embryo transfer with an intact egg yolk but a dead embryo.

The embryos were kept inside the incubator for the rest of the experiment (from EDD 3 to EDD 12). Embryos were checked every day for any malformation or infection. Damaged embryos were discarded accordingly.

2.12.3 Implantation of scaffolds and application of bioactive compound

Samples were implanted on EDD 7 within the boundaries of CAM between large two blood vessels. **Table 2.9** shows the samples and concentration of the compound used in the CAM assay. 8 mm ID silicone rings were used to hold VEGF, EVS, and condition media solutions. These rings were sterilized with 70% IMS and washed with PBS before being implanted on the CAM. Electrospun scaffolds were cut using 8 mm disks cut from the electrospun mats before being incubated with EVs or used in CAM assay.

Table 2.9. Samples and concentrations used to assess their angiogenic potential on the CAM assay

Sample	Concentration
VEGF	80 ng/day
HDPS condition media	100 µl/ day
HDPS EVs	$5.3x10^8$ EVs /ml
HDPS EVs- scaffolds	$5.3x10^8$ EVs /ml (Incubated for 24 with plasma treated scaffold prior the assay)
Plasma PCL scaffold	N/A
PCL scaffold	N/A

2.12.4 Imaging and analysis of angiogenesis

On EDD 12. a digital camera and MicroCapture software (version 2.0) were used to capture images. A white moisturising body lotion (Neutrogena, UK) was injected into the surrounding area of the sample to increase the contrast between the blood vessels and the sample **(Figure 2.5**). To avoid any injury to the blood vessels around the sample, this media contrast was carefully injected from a corner area.

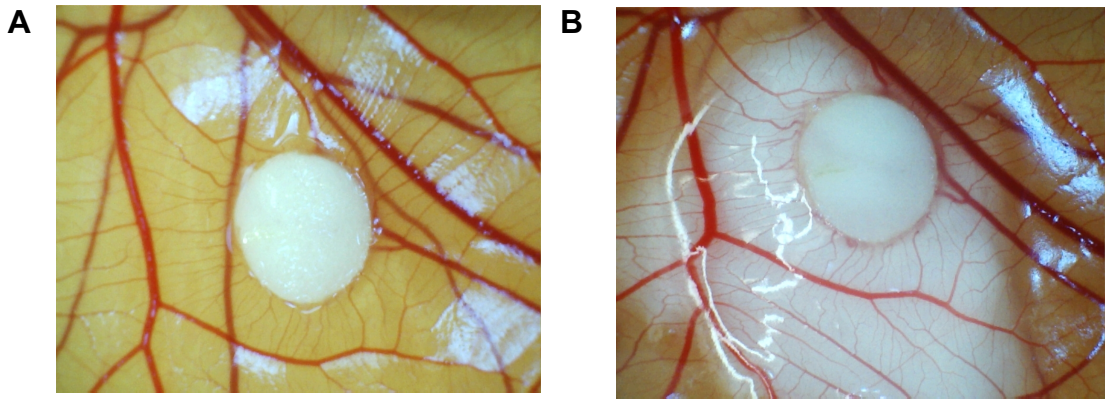

Figure 2.5. Comparison of vessel visibility between an electrospun scaffold implanted on CAM without media contrast (A) and the use of media contrast (B).

Embryos were sacrificed by decapitation or bleeding after imaging. Blood vessel formation was processed and analysed using ImageJ software version 1.52. The image was divided into its RGB components, with the green channel preserved for "Mexican Hat" filtering, contrast enhancement, and unmask filtering. The image was then converted to binary before being analysed with the vessel analysis tool (Elfarnawany, 2015) to determine vascular density. **Figure 2.6** shows an overview of the image processing used to analyse the CAM data.

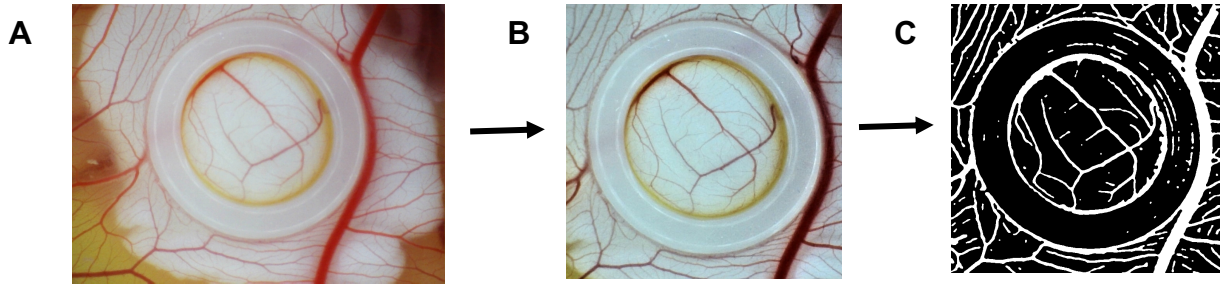

Figure 2.6. Image processing used to analyse the CAM data. (A) CAM image with contrast media. (B) Images was cut and contrast was enhanced. (C) black and white image of capillary network profile used to quantify the vessels.

2.13 Assessment of the ability of EVs and EVs-modified scaffold to induce osteogenic differentiation

The osteogenic potential of HDPS EVs was assessed by studying their ability to induce differentiation of rat bone marrow MSC (rBM-MSC). First, cells were seeded in 24 well plates 30,000 cells/well until reaching 80% confluency. The cells then treated with HDPS EVs, HDPS EVs-modified scaffold as described in **Table 2.10**.

Table 2.10. Samples and concentrations of media and EVs used in osteogenic assay.

Samples	Concentration
Osteogenic media (StemPro Osteogenesis Differentiation Kit, Gibco, A1007201)	1ml/ well Replaced every 3 days
HDPS condition media	100 µl/ every 3 days
HDPS EVs	$5.3x10^8$ EVs /ml (every 3 days)
HDPS EVs- scaffolds	$5.3x10^8$ EVs /ml (Incubated for 24 with plasma-treated scaffold prior to the assay)

Plasma PCL scaffold	N/A
PCL scaffold	N/A

Cells were cultured for 21 days and osteo-differentiation was assessed using alizarin red staining (as described in **Section 2.11.2**) and Alkaline phosphatase activity on days 7, 14 and 21.

2.13.1 Alkaline phosphatase activity (ALP) measurement

The alkaline phosphate activity was measured using Alkaline Phosphatase, Diethanolamine Detection Kit, Sigma-Aldrich, AP0100 according to the manufacturer. On days 7, 14 and 21, media was removed and cells were washed with distilled water twice. Then, 0.5 mL distilled water was added to each well of rMSC cultures in a 24-well plate and placed at -20 °C. Before, the measurements, cells were thawed then frozen again. The standard curve and pNPP were prepared according to the manufacturer. Cells then were incubated in the dark at 37 °C for 1 hour and monitored for colour change. The absorbance was then read using a plate reader TECAN (Magellan V7.2 software, Infinite M200) at 405 nm.

2.14 Statistical analysis

Data were showed as mean ± standard deviation (mean ± STDV). Student's t-test for two groups and ANOVA for three groups or more were utilized to define the statistical significance of the data. Data determined to be significant if the p-value was lesser than 0.05. Every experiment was carried out with three or more repeats and three separate runs. P-values were determined in order to quantify the concept of statistical significance, and the following symbols were utilised in order to graphically display p-values in a decimal format: ns for p>0.05, * for p0.05, ** for p0.01, *** for p0.001 and **** for p0.0001. Graphpad Prism was utilised for all of the graphical data and analysis that was conducted. (Versions 7.0-9.0).

Chapter 3

Extracellular vesicles: Isolation and characterisation

3.1 Introduction

Extracellular vesicles are membrane-enclosed vesicles released by various cell types which include exosomes, microvesicles and others. Since 2007, when Valadi *et al.*, (2007) discovered the role of EVs in transferring mRNA between cells which induce cell–cell communication, a considerable number of articles have been published that studied the role of EVs in tissue engineering and regenerative medicine (Lamichhane *et al*., 2015; Cunnane *et al*., 2018).

In the past, EVs were extracted only using ultracentrifugation, which frequently resulted in the co-purification of small quantities of contaminating debris (Gardiner *et al*., 2016). Size exclusion chromatography (SEC) is a column-based approach for extracting EVs from a variety of sources such as plasma or serum samples, urine, saliva, and conditioned medium (Böing *et al*., 2014). Smaller molecules, such as proteins, follow tortuous paths through the porous beads, whereas bigger objects move around the beads in a straight line, eluting purified EVs early with no impact on EV integrity (Monguió-Tortajada *et al*., 2019).

The characterisation of isolated EVs is crucial when determining whether an isolation method can reduce heterogeneity amid a complex environment. Therefore, the MISEV 2018 guideline emphasises the need to use multiple, complementary techniques to evaluate the results of the separation method (Théry *et al*., 2018). Here, we isolated EVs from different sources and characterised their concentration, size, size distribution, protein marker, zetapotential and microscopic topography.

The mode of delivery of EVs to target tissue or organ is crucial as it controls the bioavailability, duration of action and therapeutic outcomes. Several methods and strategies exist for the delivery of EVs; these can be categorised as either systemic or local. Systemic routes include intravenous (IV), oral, intranasal, intraperitoneal, and

subcutaneous, whereas local delivery can be achieved through the direct loading of EV suspensions or the loading of EVs into biomaterials (Pinheiro *et al*., 2018). Generally, the primary advantages of utilising a local delivery route for any drug are the reduction in systemic side effects and the increased retention rate of the drug of choice, which also apply to the local administration of EVs. A small number of studies have reported the use of local delivery for EVs, either through the direct application of EV suspensions or the incorporation of EVs into biomaterials. We are aiming to assess the ability to functionalise electrospun scaffolds, a widely used biomaterial in tissue engineering, with EVs as a novel cell-free tissue engineering approach.

3.2 Aim

The aim of this experimental chapter is the assess the ability to isolate EVs from various cell sources using different isolation method and characterise them to be used for modifying scaffolds to enhance tissue regeneration. To achieve this aim, the following objectives were established:

1- Isolation of EVs using ultracentrifugation and size exclusion chromatography
2- Characterisation of concentration and size distribution of EVs.
3- Assessment of SEC elusion profile using NTA and BCA assay.
4- Assessment of enrichment of the EV markers CD9, CD63 and CD81 to confirm EV isolation using western blot and flowcytometry.
5- Measurement of EV zetapotential.
6- Assessment of microscopic structure of EVs using SEM, TEM and fluorescent microscope.

3.3 Experimental approach

According to the objectives above, the experimental approach was established and performed according to the schematic diagram illustrated below (**Figure 3.1**).

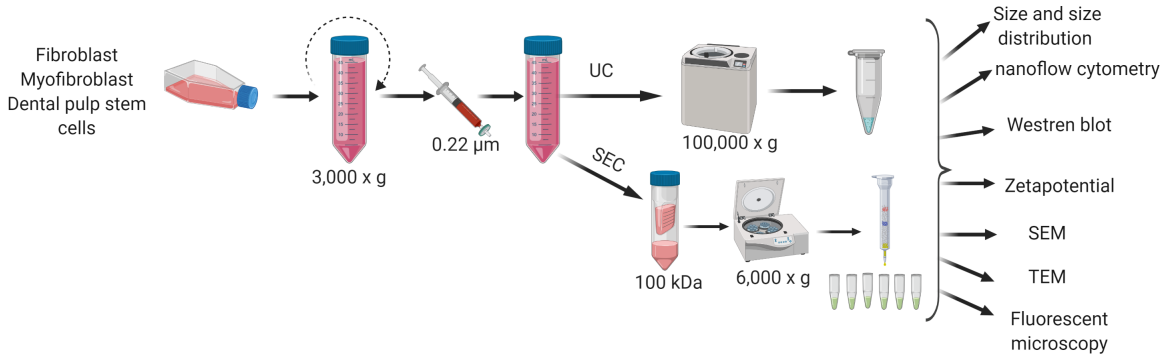

Figure 3.1. Schematic representation of EVs isolation and characterisation. Cells were cultured to 70% confluency then serum starved for 72 hours. The media them collected, centrifuged to get rid of cells debris. The supernatant was then flited twice with a 0.22 µm filter. 60 ml media then become ready for EVs isolation. EVs were isolated using UC or SEC isolation method then characterized using NTA, nFCM, western blot, SEM, TEM and fluorescent microscope.

3.4 Collection of condition media for EVs isolation

Cells were grown in serum free culture media (DMEM) in tissue culture flasks. Upon reaching 70- 80 % confluency, condition media was collected for EV isolation. To

maximize the yield, 60 ml of condition media from 3xT175 flasks were used for EV isolation.

3.5 Isolation methods

Ultracentrifugation (UC) is the most commonly used protocol for EVs isolation. Non-EV contamination, however, is a main drawback of this technique (Gardiner et al., 2016). Size exclusion chromatography (SEC) is widely regarded as one of the most reliable EV isolation methods to isolate relatively pure and functional EVs. Here, the two isolation techniques were compared to determine the most suitable for this project.

3.6 Quantification and size distribution of EVs

Nanoparticle tracking analysis (ZetaView Basic NTA- Nanoparticle Tracking Video Microscope PMX-120, Particle Matrix) was used to determine the concentration, size and size distribution of EV isolated from H357, NOF, NOF-derived myofibroblasts and HDPS cells. Following isolation, EVs were diluted in Milli-Q water to adjust the concentration for the measurement using Zetaview. Then, each sample was measured three times by scanning 11 different cell positions (in triplicate) and capturing 60 frames per position. Brownian motion of particles was analysed to acquire an average measurement of the particles. The number of EVs generated per ml was estimated by multiplying the sample dilution factor by the particle concentration.

H357 EVs were isolated using UC and SEC to optimise the most effective isolation method for the project. The total number of EVs isolated by UC was 5.8×10^9 EV/ml which was significantly lower than total number isolated by SEC ($4x10^{10}$; fractions 4-11) (**Figure 3.2**). Particles were detected for all cell types, with H357 oral cancer cells producing a significantly highest yield of EVs. Among primary cells, HDPS produced

highest number of EVs compared to NOF and NOF-derived myofibroblast **(Figure 3.3**). The size profile of EVs was similar in all cell types. The modal size of EVs was observed as follows H357 UC (105 nm), H357 SEC (105 nm), NOF (135 nm), Myofibroblast EVs (105 nm) and HDPS (175 nm) (**Figure 3.4**).

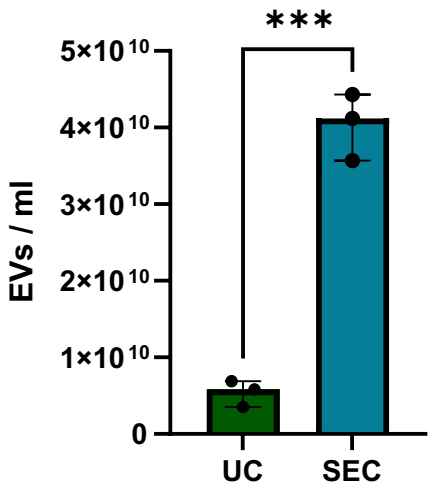

Figure 3.2. Total yield of H357 EVs isolated by UC and SCE. After collection of serum-free condition media of H357 cells. EVs were isolated by UC and SEC isolation method. Following the unpaired student t-test, the total number of EVs isolated by UC was significantly lower than the total number of EVs isolated by SEC (Fractions 4-11). Values are expressed as (mean± SD). Error bar = SD. (*p≤0.001).**

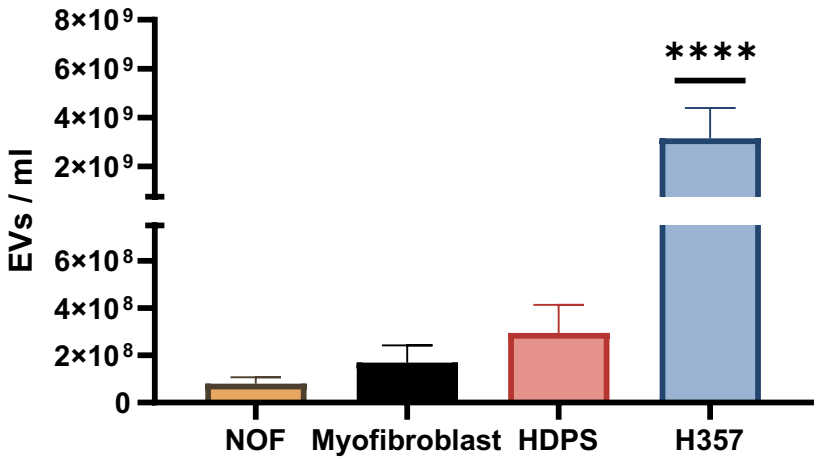

Figure 3.3. The average number of EV produced by different cell types using SEC. Zetaview instrument was used to determine the number of EV produced, H357 ($3.1x10^9$), NOF ($8x10^7$), NOF derived myofibroblast ($1.6x10^8$) and HDPS ($2.9x10^8$). H357 produced significantly higher numbers of EVs compared to other cell types when tested using a one-way ANOVA with Tukeys multiple test correction (**$p \leq 0.0001$). Values are expressed as mean± SEM. Error bar = SEM. Testing was conducted in triplicate.**

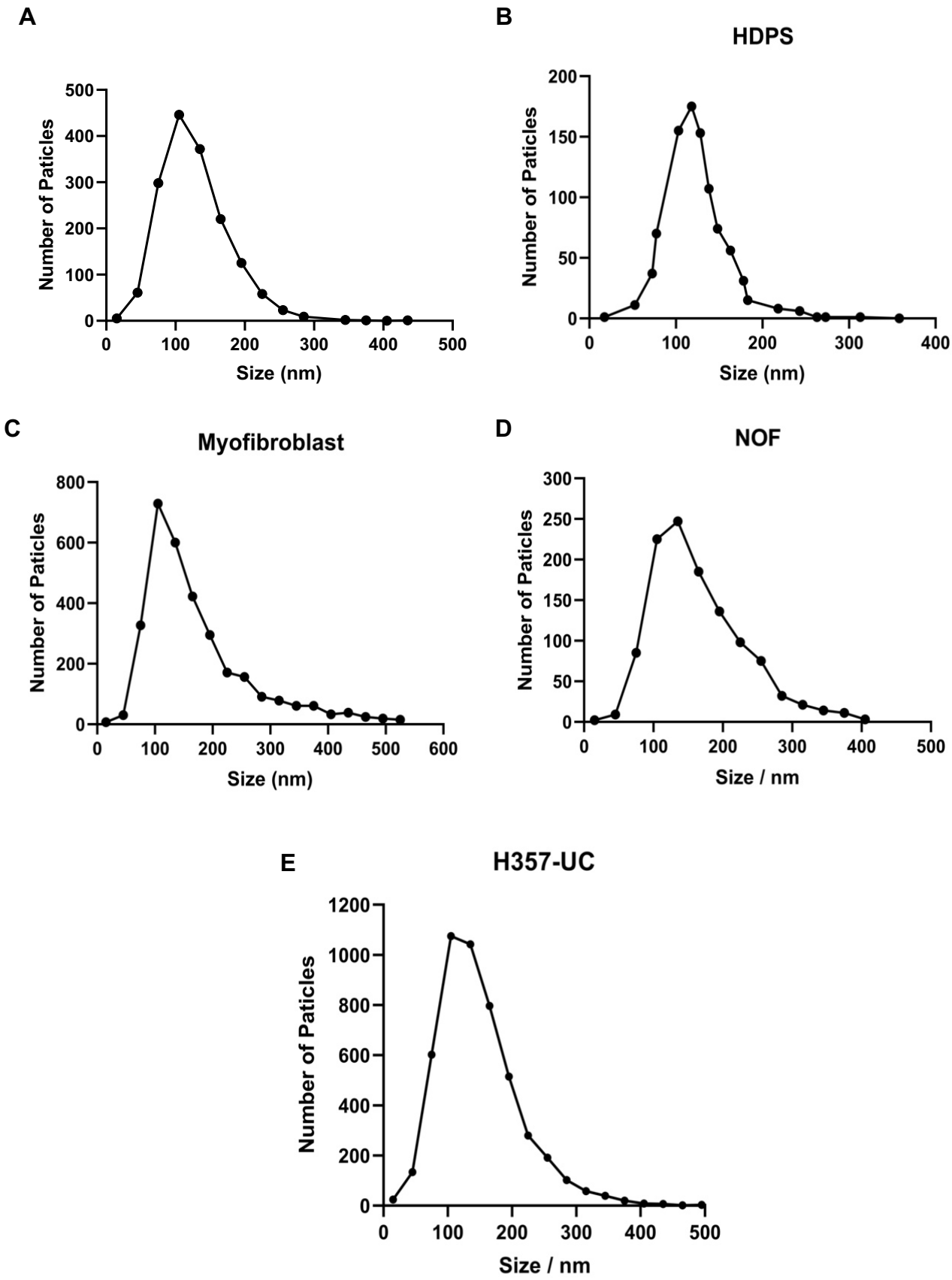
A
Number of Paticles
Size (nm)
B
HDPS
Number of Paticles
Size (nm)
C
Myofibroblast
Number of Paticles
Size (nm)
D
NOF
Number of Paticles
Size / nm
E
H357-UC
Number of Paticles
Size / nm

Figure 3.4. EV size distribution analysis using the ZetaView instrument. Following 72 hours of serum starvation, culture media was concentrated to >1 ml then applied to SEC column for EV isolation. SEC fractions were then analysed by NTA (ZetaView) to obtain particle measurements. (A) Representative size distribution profile of H357 EVs isolated by SEC. (B) Representative size distribution profile of human dental pulp stem cells (HDPS) EVs isolated by SEC. (C) Representative size distribution profile of NOF-derived myofibroblast (NOF treated with TGF-β (5 ng/ml)) EVs isolated by SEC. (D) Representative size distribution profile of normal oral fibroblast (NOF 822) EVs isolated by SEC. (E) Size distribution profile of H357 EVs isolated by UC.

3.7 SEC fraction analysis

3.7.1 SEC elution profile

SEC fractions (1-20) were analysed using a ZetaView instrument. EVs were found between fraction 4-11 in all cell types. The highest EVs concentration was found in fractions 9 for HDPS and NOF, fraction 8 for H357 and fraction 7 for myofibroblast. **Figure 3.5** shows the elution profile and the concentration of EVs in each fraction.

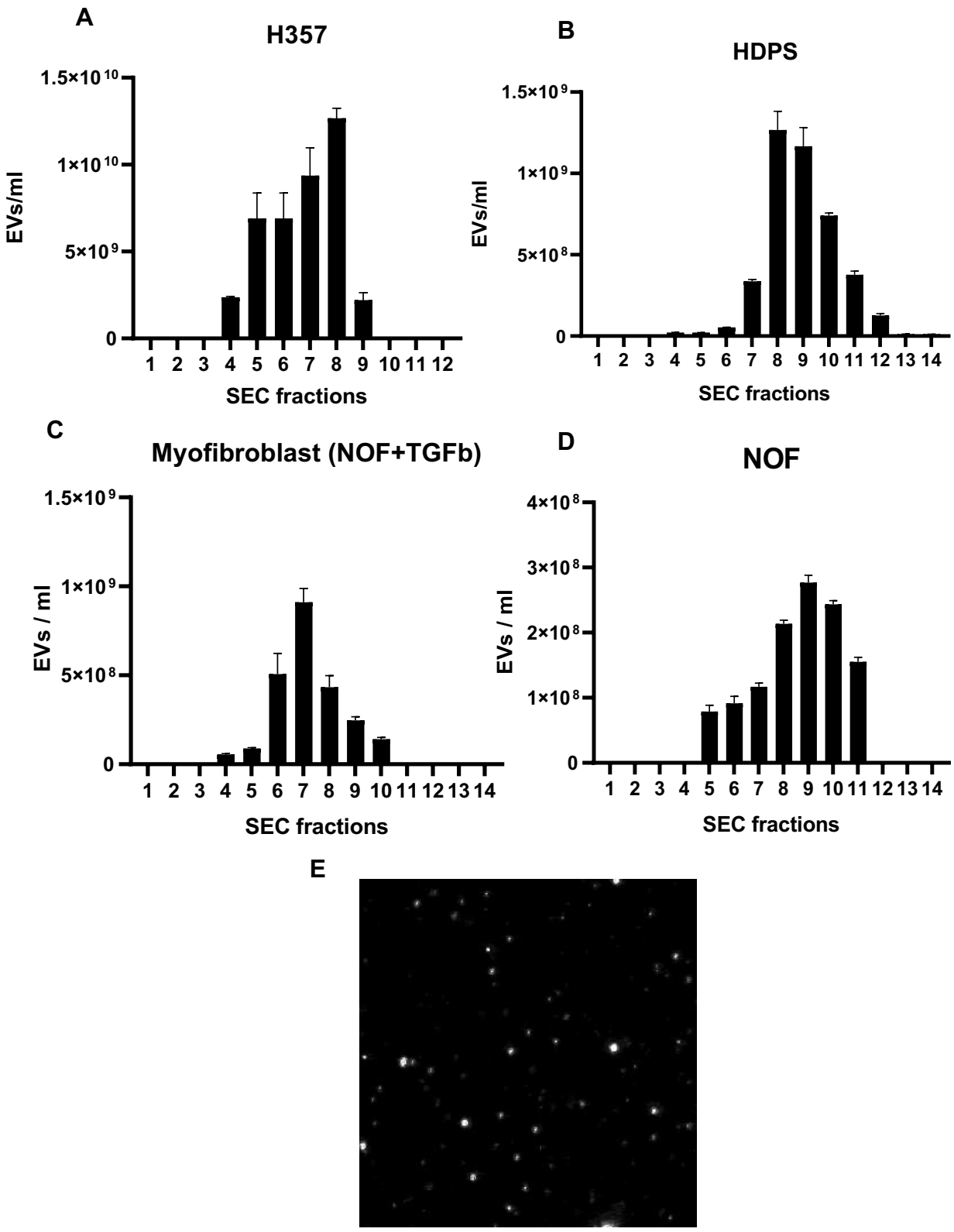
A
H357
EVs/ml
1.5×10 10
1×10 10
5×10 9
0
1 2 3 4 5 6 7 8 9 10 11 12
SEC fractions
B
HDPS
EVs/ml
1.5×10 9
1×10 9
5×10 8
0
1 2 3 4 5 6 7 8 9 10 11 12 13 14
SEC fractions
C
Myofibroblast (NOF+TGFb)
EVs / ml
1.5×10 9
1×10 9
5×10 8
0
1 2 3 4 5 6 7 8 9 10 11 12 13 14
SEC fractions
D
NOF
EVs / ml
4×10 8
3×10 8
2×10 8
1×10 8
0
1 2 3 4 5 6 7 8 9 10 11 12 13 14
SEC fractions
E

Figure 3.5. EVs elution profile isolated by SEC analysis by nanoparticle tracking using ZetaView instrument. 60 ml of culture media was concentrated down to <1 ml in volume then applied to Sepharose gel. Twenty 0.5 ml fractions were collected using PBS + 0.03 Tween 20. Fractions were then analysed by Zetaview instrument. EVs are in fractions four through eleven. (A) H357 cells with peak concentration at fraction 8 which significantly higher than total number of EVs isolated by UC. (B) HDPS cells with peak concentration at fraction 8. (C) NOF cells with peak concentration at fraction 9. (D) NOF derived myofibroblast (NOF+ TGF-β) cells with peak concentration at fraction 7. (E) Representative image of EVs detected using Zetaview instrument. Error bar = STDV.

3.7.2 SEC soluble protein elution profile

BCA assay was utilised to assess the level of protein in SEC fractions. Protein elution profiles of SEC were all similar in all cell types. Proteins were detected starting from fraction twelve to twenty, with no detectable soluble protein below fraction twelve.

The highest soluble protein concentration for H357 cells was detected at fraction 19 (~ 780 µg/ml) and the lowest was ~100.9 µg/ml in fraction fourteen. For NOF and HDPS, the highest concentrations were in fraction 20 (~720 and 800 µg/ml) and the lowest were in twelve and fourteen (50 µg/m and 142 µg/ml) respectively (**Figure 3.6).**

Collectively, these data suggested that EVs were predominantly eluted in fractions 4-11 while soluble protein was eluted in fractions 12-20. The EVs were enriched between fractions 4-11 with less than 10% of EVs detected at fractions 4,12 and the highest EV concentration in fractions 8 and 9 (apart from H357, where the highest EV concentrations were found in fractions 7&8). The percentage of EVs and soluble protein in each fraction is shown in (**Figure 3.7**).

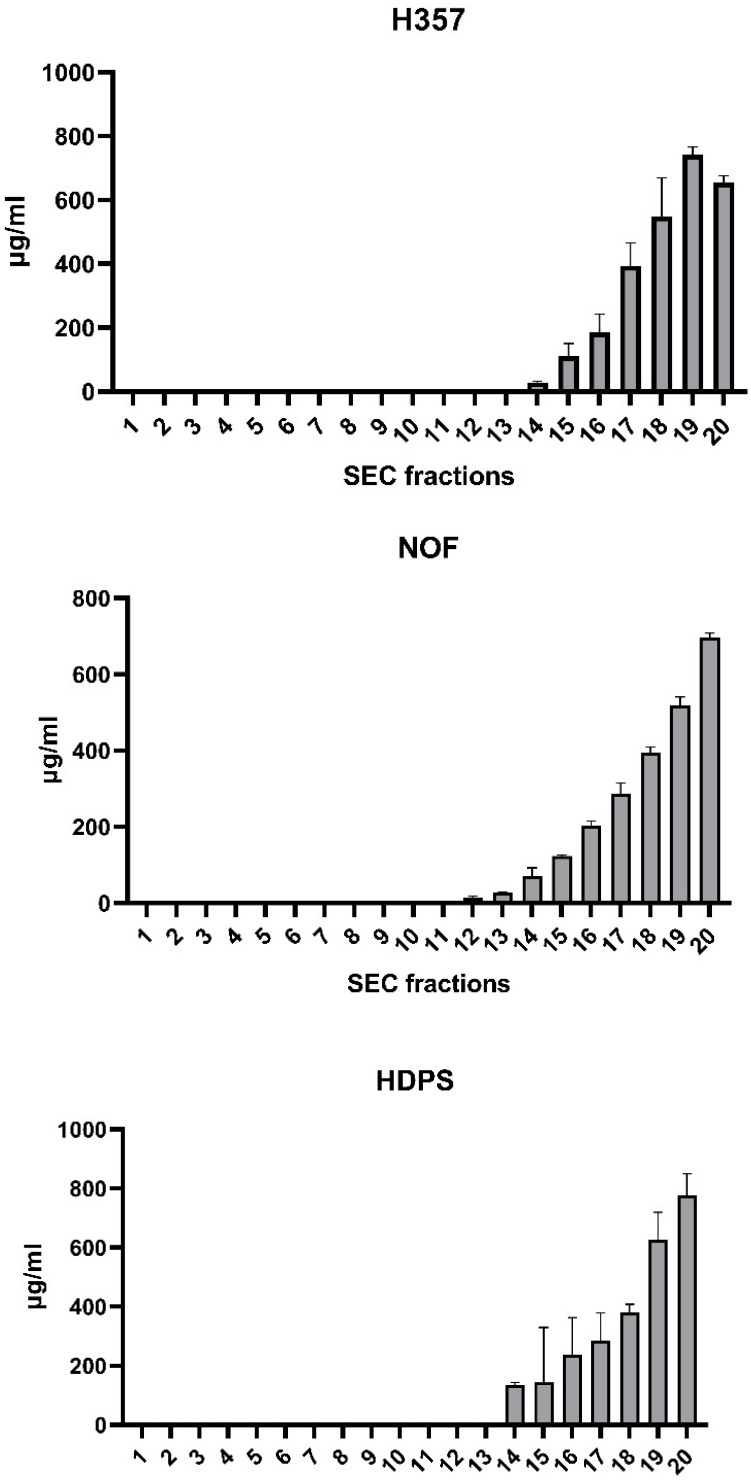

Figure 3.6. SEC protein elution profile. Following EV isolation using SEC, total protein in SEC fractions was detected and quantified using BCA protein assay kit. Using a BSA standard curve and a polynomial equation, protein concentration of SEC fraction was determined. The majority of protein elute in fractions eighteen to twenty. Testing was conducted in triplicate. Values are expressed as (mean ± SD). Error bar = SD.

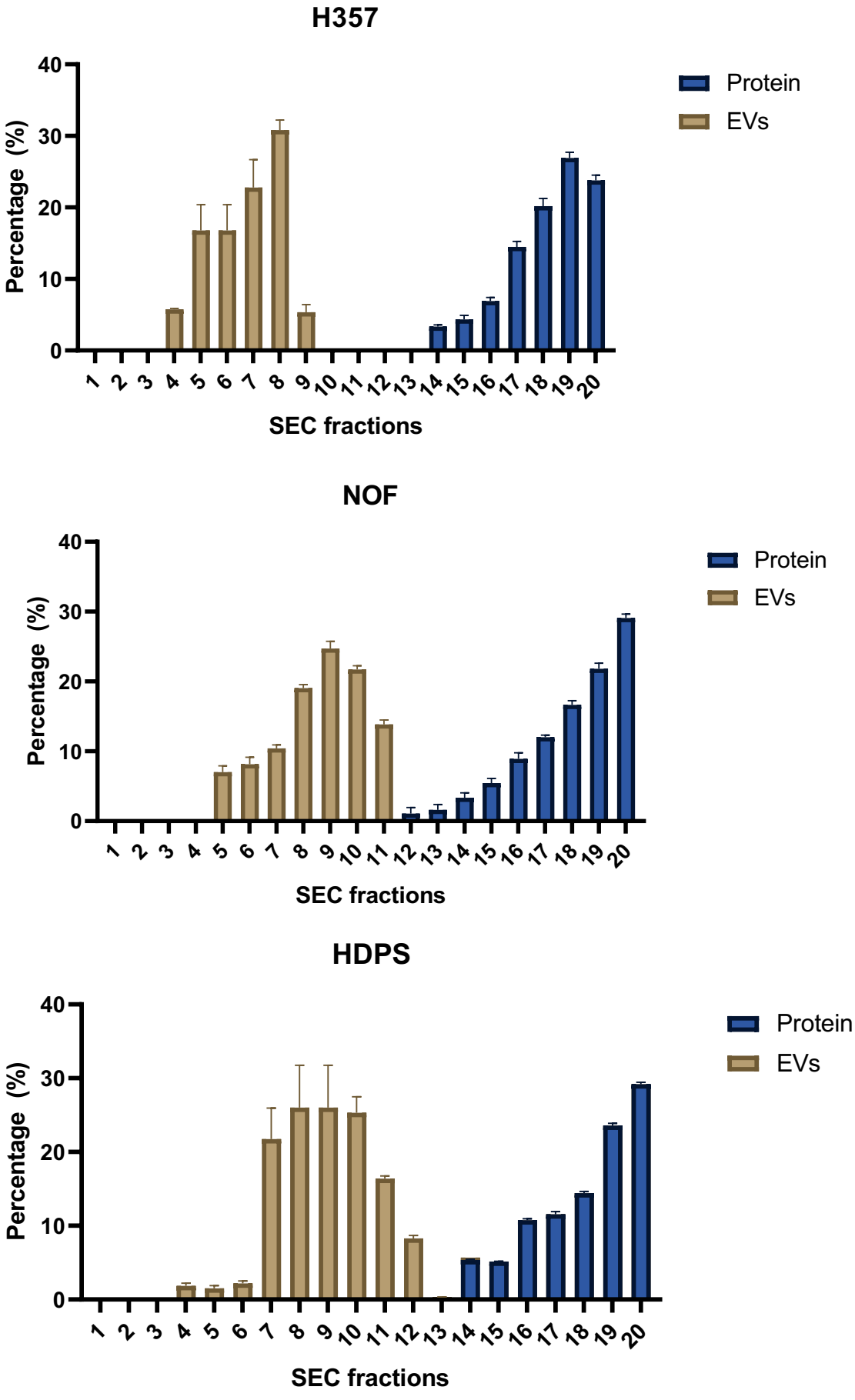
H357
Percentage (%)
SEC fractions
Protein
EVs
NOF
Percentage (%)
SEC fractions
Protein
EVs
HDPS
Percentage (%)
SEC fractions
Protein
EVs

Figure 3.7. Elution profile of EVs in comparison to soluble contaminate protein. Brown bars show EVs fractions and the percentage of EVs in each fraction of total EVs that would be collected if fractions were pooled. Blue bars show the soluble protein and the percentage in each fraction that would be in the pooled fractions.

3.8 EV Characterisation

3.8.1 Tetraspanins as exosome markers

Due to the difficulty of distinguishing EVs from other non-EVs contaminants of similar size (large protein complexes, lipoproteins, etc) using NTA, specific protein markers are helpful to assess the purity of EVs. Tetraspanin markers including CD9, CD63 and CD81 are specifically enriched in the membrane of EVs and are often used as EVs biomarkers (Tian *et al*., 2020).

3.8.2 Western blot

To assess whether the particles isolated by SEC were in fact EVs by analysing the expression of EV tetraspanins markers, SEC fractions (4-11) were pooled. Then, pooled fractions were centrifuged at 100,000 g for 1 h. The pellet was then solubilised using RIPA buffer and tetraspanins protein markers for western blot analysis. Using 12 % SDS-PAGE gel, proteins were separated and transferred to nitrocellulose membranes. Primary antibodies were incubated overnight at 4°C on blocked membrane. Only CD9 and CD63 were detected in H357 EVs. In NOF EVs, only CD63 was detected. After several attempts, no bands were detected for any of the markers in NOF derived myofibroblast or HDPS EVs (**Figure 3.8**).

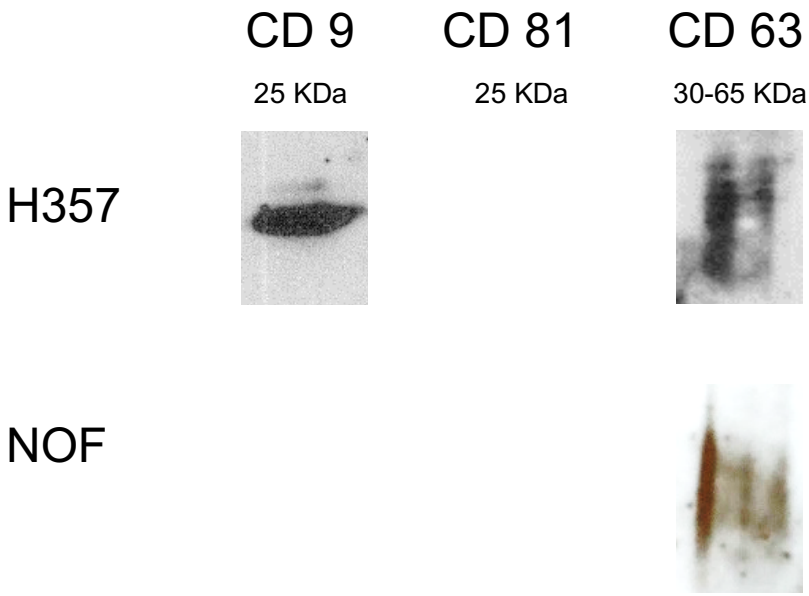

Figure 3.8. EV tetraspanins marker (CD9, CD81 and CD63) analysis using western blot. After isolation by SEC, EVs were loaded on SDS-PAGE and immunoblotted tetraspanins CD9 Abcam (ab92726), CD81 Abcam (ab79559) and CD63 Abcam (ab134045). Only CD9 and CD63 were detected in H357 derived EVs. Only CD63 was detected in NOF derived EVs.

3.8.3 Nano flow cytometry

As ZetaView nanoparticle tracking detects EV and non-EV nanoparticles such as salt aggregates, non-EV lipoproteins, or other contaminants, further investigation was performed to confirm enrichment of EV. Phenotyping of single EVs was done using nFCM (Nanofcm, analysis was conducted by Ben Peacock) by measuring the presence of a cocktail of tetraspanins (CD9, CD63, CD8) via immunofluorescent labelling. Pooled SEC fractions (4-11) were centrifuged at 100,000 g for 1 h then suspended in 500 ul of PBS+ 0.03 % tween. EVs/particles in PBS (2.1e8) were mixed with a cocktail of the 3 antibodies (1:50) before incubation for 30 minutes at room temperature.

Total gated events of H357 EVs detected by nFCM were 5366. Around 7% (374) were positive for tetraspanins. HDPS EVs showed higher expression of tetraspanins; 1202 particles (26.3 %) were positive. **Figure 3.9** shows the plot of positive particles (highlighted in red) in comparison to total number detected by nFCM.

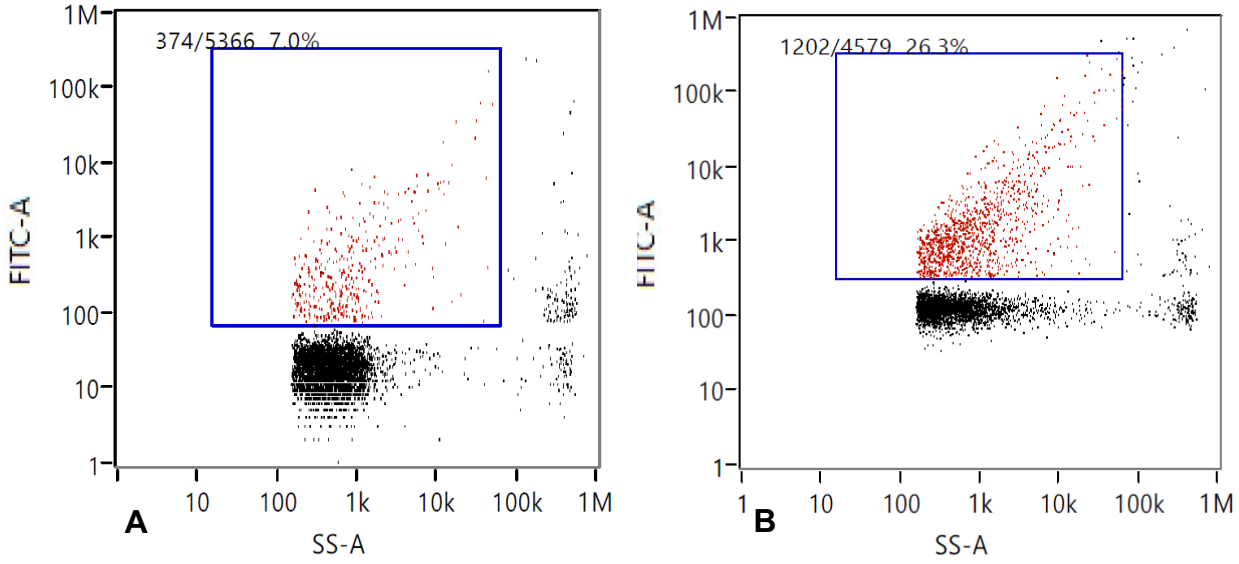

Figure 3.9. EV surface protein marker characterisation using nano flowcytometry (nfCM). EV SEC fractions were pooled then stored at -80° C for EV marker analysis. (A) representative dot-plots show 7% of H357 EVs population (RED) were positive for tetraspanins marker CD9, CD63 and CD 81. (B) representative dot-plots show 26.3% of HDPS EVs population (RED) were positive for tetraspanins marker CD9, CD63 and CD 81.

3.8.4 ExoView characterisation of EV markers

To further assess the quality of EVs isolation, an ExoView R100 was used to characterise the H357 and NOF EVs. Samples were probed for CD9, CD63 and CD81 and murine IgG was used as a negative control. H357 derived EVs were positive for CD9 and CD63 and, to a lesser extent, CD81 (**Figure 3.10**). NOF derived EVs were positive for CD9, CD63 and CD81 (**Figure 3.11**). H357 cells produced 10 times more EV than NOF (**Figure 3.10 E**). This data agrees with those acquired using the ZetaView nanoparticle tracking equipment (**Section 3.7.1**).

A

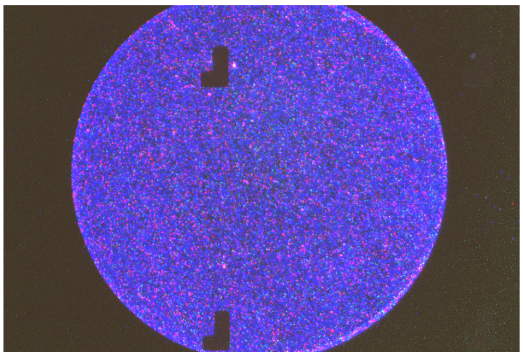

B

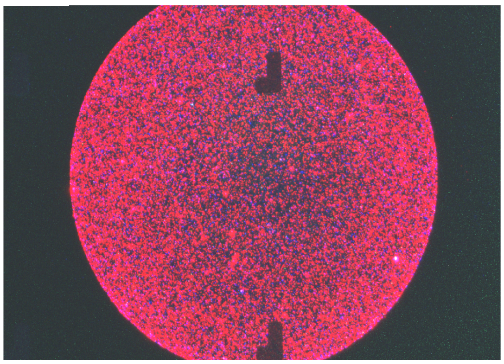

C

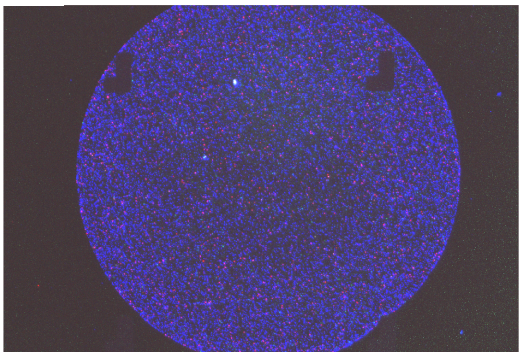

D

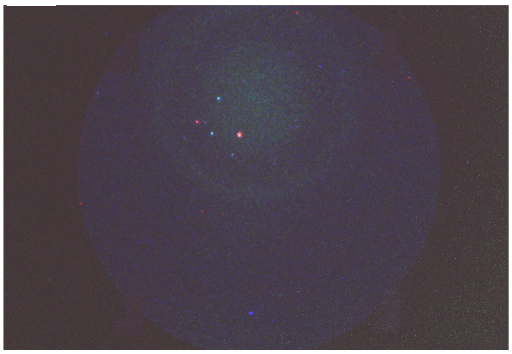

E

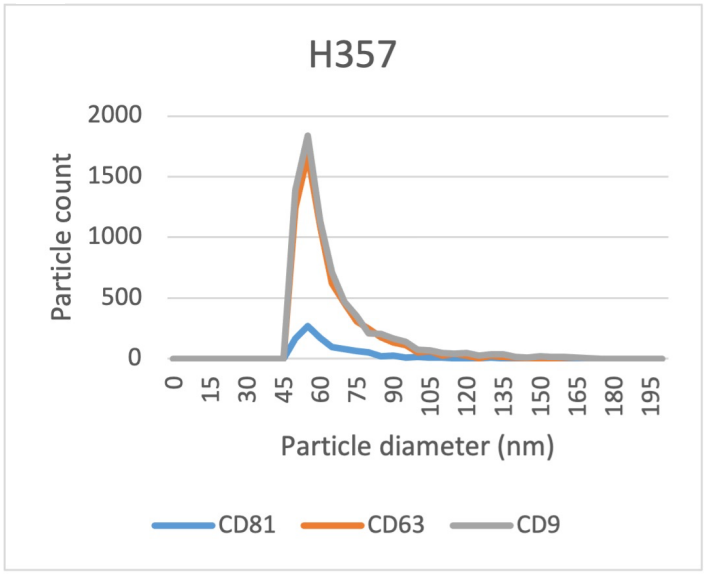
H357
Particle count
2000
1500
1000
500
0
0
15
30
45
60
75
90
105
120
135
150
165
180
195
Particle diameter (nm)
CD81
CD63
CD9

Figure 3.10.Characterisation of H357 derived-EV by ExoView. EV tetraspanin markers (A) CD9 (blue), (B) CD63 (red), (C) CD81 (green) (D) Murine IgG negative control. (E) EV population size distribution showed an amplified expression in EV with a size range of 45 to 100 nm, with a specific EV profile of CD9 (57.1 nm), CD63 (54.3 nm), and CD81 (55.9 nm)

A

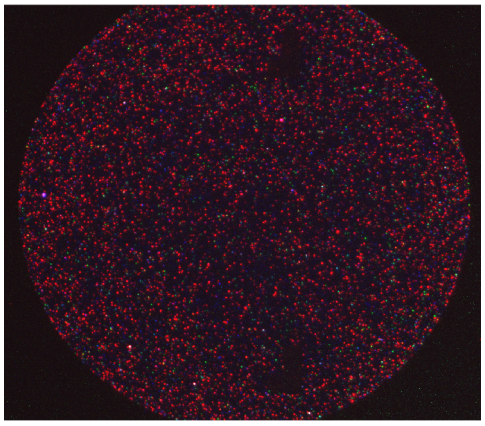

B

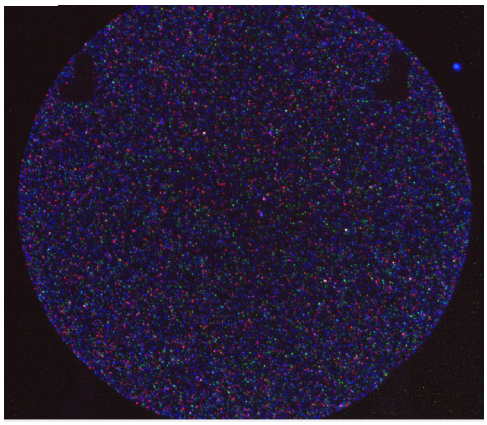

C

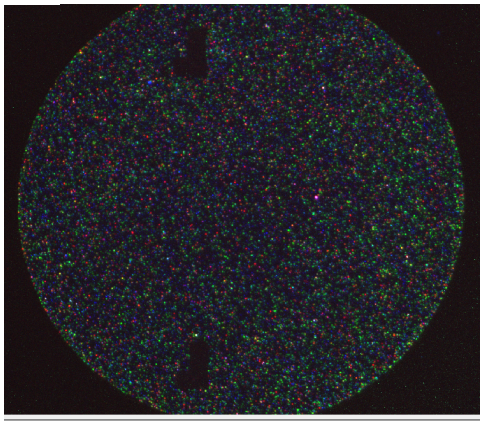

D

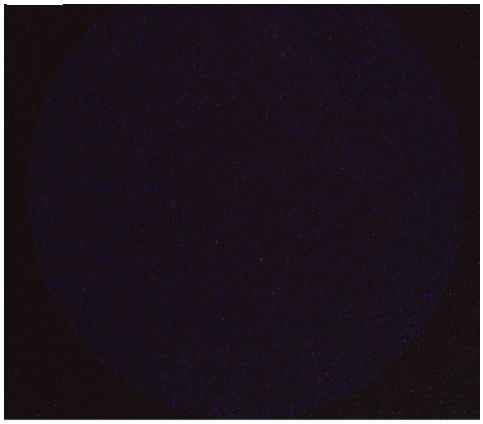

E

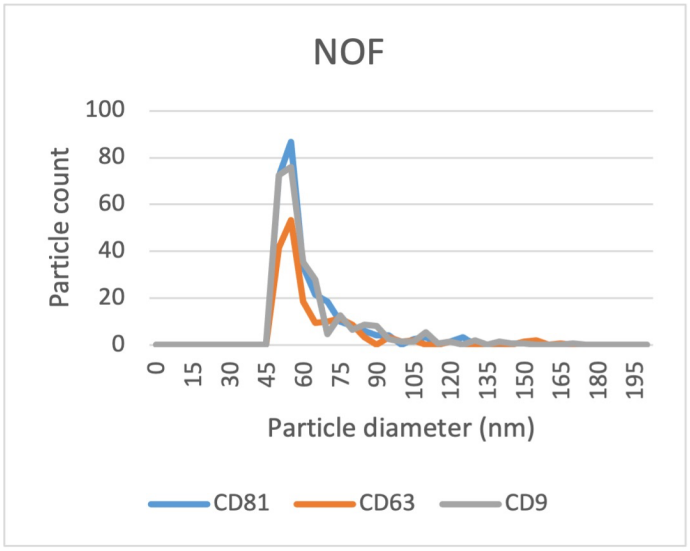
NOF
Particle count
100
80
60
40
20
0
0
15
30
45
60
75
90
105
120
135
150
165
180
195
Particle diameter (nm)
CD81
CD63
CD9

Figure 3.11.Characterisation of NOF derived-EV by ExoView. EV tetraspanin markers (A) CD81(blue), (B) CD63 (red), (C) CD9 (green) (D) Murine IgG negative control. (E) EV population size distribution showed an amplified expression in EV with a size range of 45 to 70 nm, with a specific EV profile of CD9 (53.4 nm), CD63 (57.7 nm), and CD81 (53.1 nm)

3.8.5 Zetapotential of EVs

Electrostatic interactions have been shown to play an important role in the incorporation of the drug into polymer materials and their release kinetics (Kim *et al*., 2009). Thus, the zetapotential of EVs was measured to compare them to those of electrospun scaffolds, to examine the role of electrostatic charge in the interaction and release kinetic of EVs. The zeta-potential (ζ-potential) of EVs was measured using a Malvern Zetasizer NanoZS 3000-HA (Malvern Instruments, UK). EV isolated by SEC were diluted at 1:100 in PBS. The diluted PBS buffer solution acted as an electrolyte for the measurements (pH ~ 5.5, 25 °C). All data were averaged over 100 consecutive runs. All EVs exhibited anionic character regardless of the cell type. The ζ-potential of the two primary cells (NOF and HDPS) were both comparable (−19.1 and −22.8 mV respectively). However, the cancer cells-derived EVs (H357) exhibited a ζ-potential of −37.3 mV, significantly lower than the non-cancerous cell derived EVs ($P<0.0001$) **(Figure 3.12).**

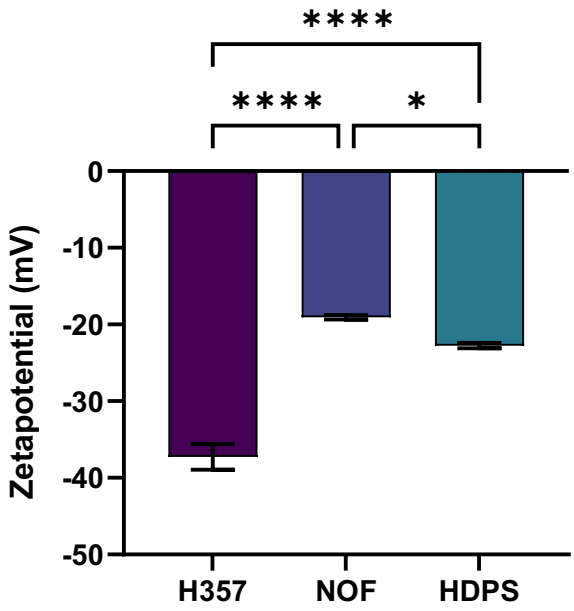

Figure 3.12. ζ-potential measurements of EVs using Zetasizer instrument. All EVs show anionic zetapotential. Following a one-way ANOVA test, H357 exhibited significantly lowest ZP (- 37.3) compared to NOF (-19.1) and HDPS (-22.8) (P<0.0001). ZP of NOF EVs was slightly higher than HDPS(P<0.01). Values are expressed as (mean± SD). Error bar = SD.

3.8.6 Microscopic characterisation

To assess the morphology of EVs and for further examination of their size, EVs isolated by SEC and UC were imaged with SEM, TEM and fluorescence microscopy. Vesicle-like structures were clearly seen under the electron microscope (**Figure 3.13**). The morphologies of the EVs were observed to be heterogenous under TEM. **Figure 3.13** B shows a spherical well-defined single EV that was negatively stained with 1% uranyl acetate sized 100 nm. Multiple EV-like moieties can clearly be observed, with defined outer membranes, in **Figure 3.13** C.

EVs were also visualised by SEM to assess their morphology for future examination when incorporated into scaffolds. After fixation, serial dehydration and gold coating, vesicle-like structures were also clearly seen using SEM (**Figure 3.13** D). EVs were seen to have a cup-shaped structure (**Figure 3.13** E) unlike the more spherical shapes observed under TEM (**Figure 3.13** C). EVs sizes were consistent with the size profile obtained by ZetaView with diameters ranging between 50- 300 nm.

To examine the ability of labelling EVs to be visualised under the fluorescent microscope and also for future use with scaffold, EVs were labelled with CFSE membrane stain as described in **section 2.8.3.1.** Vesicle-like structures were successfully detected by fluorescent microscopy (**Figure 3.13 H-J**). The technical limitations of the resolution of fluorescent microscope precluded the visualisation of individual EV.

Microscopic images using EM and fluorescent microscope showed that EVs isolated by UC tend to aggregate. **Figure 3.13 C, E, I** showed cluster of vesicle like structures isolated by UC. EVs isolated by SEC, however, were found to be more dispersed.

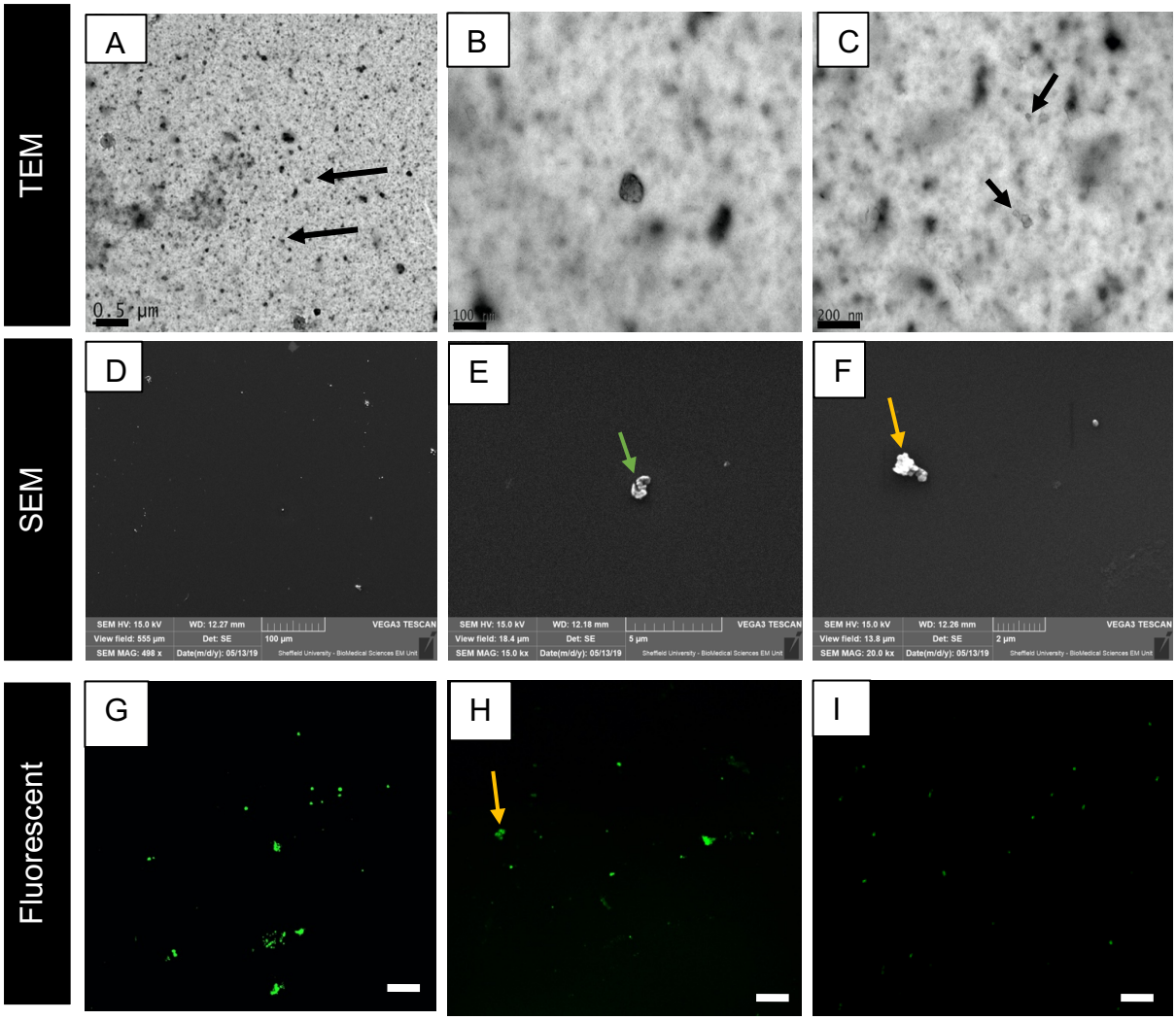
TEM
SEM
Fluorescent
A
B
C
D
E
F
G
H
I
0.5 µm
100 nm
200 nm

Figure 3.13. Microscopic characterization of EVs. (A-B-C) Representative TEM images of EVs. Vesicles like structure can be observed in image (A) indicated with black arrows. (B) single well defied vesicle structure (indicated with black arrow) negatively stained with 1% uranyl acetate sized 100 nm which in consistent with size range obtained by Zetaview (Scale bar :100nm). (C) Cluster of particles like structure of EVs isolated by UC (Scale bar :200nm). (D-E-F) Representative SEM images of EVs on coverslips. (D) low magnification image of EVs. (E) Large cup-shaped like vesicles sized around 500 nm. (F) Cluster vesicles isolated by UC indicated with yellow arrow. (G-H-I) Representative fluorescent images of EVs stained with CFSE (Scale bar :1 µm). (H) Cluster EVs isolated by UC indicated with yellow arrow. (I) Dispersed EVs isolated by SEC (Scale bar :2 µm).

3.9 Discussion

Increasing evidence has suggested that EVs may potentially be used to overcome stem cell tissue engineering challenges including undesirable differentiation and limited circulation due to large size (Holkar *et al*., 2020a). The use of EVs for tissue engineering and regenerative treatments is justified by their role as paracrine mediators during cell-to-cell communication. In this chapter, we studied the ability of isolation and characterisation of EVs to be used in different tissue engineering applications include wound healing, angiogenesis, and osteogenesis.

In this project, EVs were isolated from H357, NOF and HDPS. Although oral cancer cells (H357 in this study) are not an appropriate source of EVs for tissue engineering applications, H357 cells have been used in this study only for optimisation as they represent an abundant source of EVs compared to normal cells (Riches *et al*., 2014) as confirmed by data presented here. NOF and NOF-derived myofibroblast were utilized to study their role in wound healing as previously indicated by Arif *et al*., (2020). Moreover, as the major source of EVs in the context of tissue regeneration is mesenchymal stem cells based on the role of these cells in mediating regeneration, HDPS derived EVs were used to assess their effect in angiogenesis and osteogenesis.

To determine the best isolation method for this project, H357 derived EVs were isolated by UC and SEC for comparison. Our data suggested that EV particle yield was higher in SEC compared to UC. This finding is consistent with that of Takov *et al*., (2019) who found that the total number of EV from UC was negligible compared to peak SEC fractions. When examined under the microscope, UC-EVs were commonly found to be aggregated. The possible cause of this could be the high-speed centrifuge force as suggested by Linares *et al*., (2015). No aggregation was observed in SEC-

EVs. Thus, we decided to use SEC for EV isolation in subsequent experiments in this project.

The data presented in this chapter suggested that all cell lines had comparable SEC elution profiles, with very small variations (Figure 3.5 and Figure 3.6). SEC has the advantage of considerably reducing protein contamination(Suárez *et al*., 2017). In accordance with this, our data showed that SEC was successful in separating soluble proteins from the bulk of eluted EVs. EVs were predominantly found between fractions (4-11) while the majority of proteins were detected starting from fraction 12.

It is important to characterise EVs using a variety of methodologies to evaluate the outcomes of separation methods and determine the possibility that biomarkers or functions relate to EVs rather than other co-isolated materials (Théry *et al*., 2018). Nanoparticle tracking analysis (Zetaview) was used to quantify and determine the size and size distribution of particles isolated by different cell types. However, it is important to say that this is not specific to EVs and may also detect co-isolated particles of similar size including protein aggregates and lipoproteins.

Cancer cells are known to secrete considerably more EVs compared to non-cancerous cells (Riches *et al*., 2014). In keeping with this, using zetaview the human OSCC-derived cell line H357 was found to secrete the highest number of EVs of all cell types analysed. HDPS cells also secreted significantly higher number of EVs compared to fibroblast cells (NOF and NOF-derived myofibroblast). The size range of the isolated EVs in this study (100-170 nm) was consistent with those previously reported in the literature (Kowal *et al.*, 2016; Muralidharan-Chari *et al.*, 2010).

The tetraspanins CD9, CD63, and CD81 are the most commonly reported EV related markers in the literature and have been employed in several investigations for "total" EV capture (Andreu *et al*., 2014). The International Society of Extracellular Vesicles

has recommended using western blot to analyse EV markers in EV research (Lötvall *et al*., 2014). Our western blot data suggested that tetraspanin marker expression wasn't homogenous among EV from different cell types. EV markers CD9 and CD 63 were detected in cancer cells (H357) EVs, only CD63 was detected in NOF EVs. Despite several attempts, no tetraspanins expression was detected in HDPS EVs by western blot.

For further assessment of EV markers, phenotyping of single EV markers was preformed using flow cytometry (nFCM) and Nanoview. To overcome the high threshold of detection of nFCM, mixed antibodies (CD9, CD63 and CD81) were run with EVs from the different cell types. Our nFCM data showed a 7% and 26.3 percent of mixed labelled EVs within H357 and HDPS samples respectively; although seemingly low, this compares favourably with 2% for CD63 and 1% for CD 81 detected in EV from a T lymphocytic cell line (Arab et al., 2021). Nanoview data showed that H357 cells produced 10 times more EV than NOF and both were positive to tetraspanins markers.

Zetapotential (ZP) is the key parameter the controls electrostatic interaction of the nanoparticles and plays an important role of nano-drug delivery system (Honary *et al*., 2013). In addition, the surface charge of the particles determines their stability in the suspension, tendency to aggregate and particle-medium interaction (Midekessa *et al*., 2020) The surface charge of EVs may influence different biological processes (Fröhlich, 2012), it is, however, rarely investigated in the literature.

Our data showed that EVs used in this project demonstrated anionic character irrespective of parental cell type. Despite the multiple factors that may affect the ZP measurements including the ionic strength of the medium and pH, these data were in accordance with previous reports demonstrating negative charge on EVs (Vogel et al.,

2017). The significantly greater negative charge of cancer cell EVs compared to normal cells may have an effect on their functions in cancer progression which needs further investigation. Soares Martins *et al*., (2018) suggested that EVs from different sources could have different zetapotential characters which is broadly in accordance with our results. Although we did not consider the different storage temperatures in this data, Maroto *et al*., (2017) found that particles stored in -80°C expressed less negative charge compared to those stored at 4°C and 18°C. Further zetapotential characterisation is needed because of its crucial role in the stability, pharmacokinetics, and release mechanism of nanoparticles.

We found that a single EV appeared to be spherical under TEM and appeared to be cup-shaped when viewed using SEM which may be explained by the different preparation setup. Chernyshev *et al.* (2015) suggested that the commonly reported cup-shaped appearance of EVs is a likely artefact that occurs due to sample fixation and preparation procedures. Microscopic images using EM and fluorescent microscope showed that EVs isolated by UC tend to aggregate. The aggregation of EVs isolated by UC has been reported by Linares *et al.* (2015), which is similar to our observations. Recently, Bosch *et al.* (2016) reported that using trehalose in EV suspensions may prevent this aggregation and reduce the loss of EVs during isolation and storage.

Despite these promising results, many challenges must still be overcome. First, the isolated EV yields using different isolation methods from routine culture conditions remain low, and a high-yield production method remains to be developed include using a bioreactor-based, large-scale production protocol of clinical-grade EVs (Phan *et al*., 2018). A study reported that a large number of EVs can be obtained from cells under stimulation, such as cells experiencing hypoxia (Zhang *et al*., 2012). However, others

have reported that such conditions may alter the EV cargo (Xie *et al*., 2017b). Second, the aggregation of EVs isolated by UC was observed in this study, which may affect the distribution of EVs within the scaffold. We observed that isolation by SEC prevented aggregation, which was also reported by Linares *et al.* (2015).

3.10 Conclusion

In this chapter, we aimed to isolate, optimise and characterize EVs for variety of cell types for future use in tissue engineering. Firstly, EVs were successfully isolated for H357 cancer cells to optimise isolation and characterisation methods. We found that EVs isolated by UC aggregated, most probably due to the high centrifugation force, in comparison to dispersed EVs isolated by SEC. It was therefore decided to utilise SEC as the isolation method for this project.

In addition, we successfully isolated NOF and NOF-derived myofibroblast EV using SEC and characterised their concentration, size and size distribution to be used for wound healing functional experiment. HDPS EVs were also isolated and characterised to be used for wound healing, angiogenesis and osteogenesis assays. Furthermore, we measured the zetapotential of EVs to study the surface charge and future assessment of the effect of electrostatic interaction on the incorporation of EVs into electrospun scaffold. EVs used in this project demonstrated anionic character irrespective of parental cell type.

Chapter 4

Scaffold and EV-modified scaffold: Analysis and characterisation

4.1 Introduction

Fibrous scaffolds are a promising biomaterial option for tissue engineering applications due to their capacity to mimic the native reticular structure of the extracellular matrix in terms of high porosity, fibre distribution (Li *et al*., 2014) and promoting tissue regeneration by integration with surrounding cells (Sarkar *et al*., 2006). To attain the conditions required to make an electrospun jet, a balance between polymer solution and processing parameters is required. Surface tension, electrostatic interactions, and solvent characteristics, on the other hand, regulate the majority of electrochemical processes that result in a stable and consistent polymer jet. The viscosity of the polymer solution is also important for fibre morphology and depending on working polymers and solvent systems, it is feasible to modify the consistency of the solutions and load relevant organic and inorganic substances into fibres for targeting specific applications (Luraghi *et al*., 2021).

There is a wide range of surface functionalization options for electrospun scaffolds, which means they can be use in very diverse due to the potential to customise scaffolds for various applications such as wound healing, tissue regeneration and drug delivery (Feng *et al*., 2019).

Plasma treatment is a common surface functionalisation method that has been used to increase material wettability, accelerate degradation, and modify drug release kinetics (Petlin *et al*., 2017). Heparin-based delivery systems have proven useful for the delivery of a wide range of growth factors for diverse biomedical applications since a significant number of growth factors bind to heparin with either moderate or high affinity (Sakiyama-Elbert, 2014).

Incorporating EVs into biomaterial devices as delivery systems has the potential to enhance the effects of EVs by increasing bioavailability at the target location. Although electrospun scaffolds are commonly used in tissue engineering and as drug delivery platforms, only a few studies have assessed the ability of electrospun scaffolds to be modified with extracellular vesicles.

4.2 Aim and objectives

The aim of this experimental chapter is to fabricate PCL scaffold and examine the feasibility of combining EVs with the scaffold by comparing different functionalisation routes then study EVs attachment and release kinetics. In order to achieve this aim, the following objectives were established:

1. Fabrication of 10% PCL scaffold using electrospinning technique.
2. Treatment of the surface of scaffolds with air plasma and heparin to enhance wettability.
3. Study the fibre morphology and diameter of PCL, plasma heparin treated PCL scaffolds.
4. Assess microporosity of PCL, plasma and heparin treated PCL scaffolds .
5. Investigate the hydrophilicity of PCL, plasma and heparin-treated PCL scaffolds.
6. Measure the surface zetapotential of PCL, plasma and heparin-treated PCL scaffolds.
7. Modify different scaffolds with EVs and assess the attachment of EVs to the scaffolds.
8. Characterize the EVs attachment and the release kinetics from the scaffolds.

4.3 Experimental approach

According to the objectives above, the experimental approach was established and performed according to the schematic diagram illustrated below **(Figure 4.1)**.

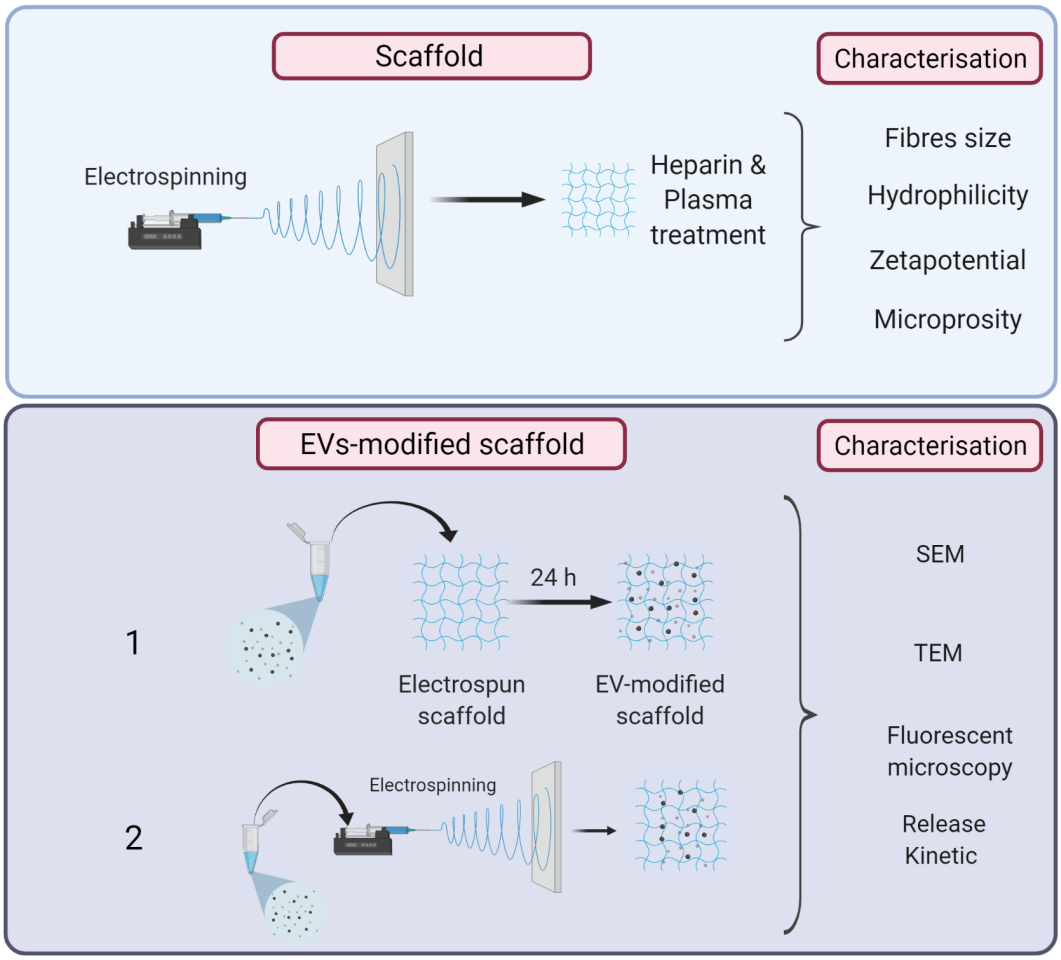

Figure 4.1. schematic diagram illustrating the methodology of fabrication and characterisation of scaffold and EVs-modifieds scaffold.

4.4 Characterisation of electrospun scaffolds

To assess the feasibility of combining EVs with electrospun scaffolds, Polycaprolactone (PCL) was used to manufacture the scaffold using electrospinning as described in **Section 2.4**. After preparing the polymer solution for spinning, it was divided into three groups: plain PCL, EV-spun PCL (polymer solution + 500 µl of EV suspension) and PBS-PCL (polymer solution + 500 µl of PBS). The plain PCL was then treated with air plasma and/or heparin.

Following the successful fabrication of each scaffold, a series of characterisation techniques were used to include fibres diameter, fibres morphology, porosity, zeta potential and hydrophilicity.

4.4.1 Fibre diameter and fibre morphology

Using SEM micrographs, fibre diameter was measured as described in **Section2.6.1**. The average fibre diameter of plain PCL scaffold (PCL) was 1.4 µm ± 0.6 µm. No significant difference was observed in the fibre diameter of plasma, heparin and heparin-plasma treated scaffold compared to PCL scaffold. Adding the EV suspension or PBS to polymer solution before spinning significantly altered the fibre diameter of the scaffold as illustrated in **Figure 4.2.** The morphology of electrospun fibres under SEM was heterogeneous with no apparent defects or beads formation on their surface. SEM images also show the random orientation of the fibres (**Figure 4.2).**

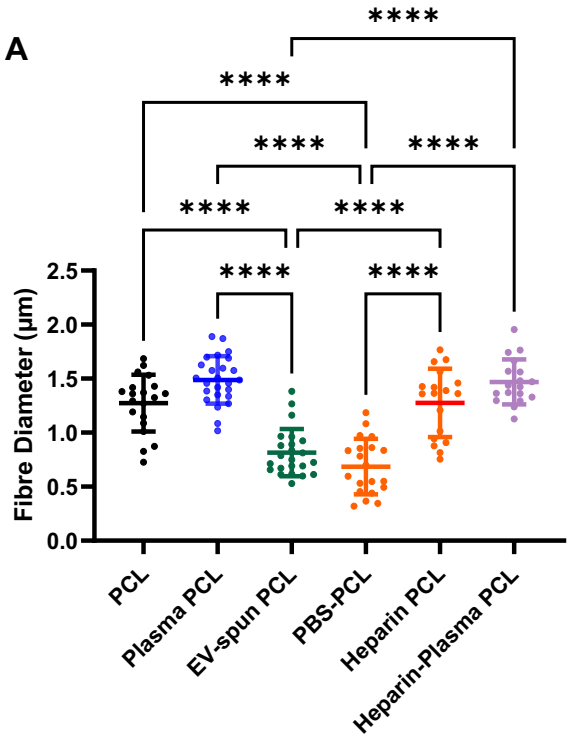
A
****
****
****
****
****
****
****
Fibre Diameter (µm)
2.5
2.0
1.5
1.0
0.5
0.0
PCL
Plasma PCL
EV-spun PCL
PBS-PCL
Heparin PCL
Heparin-Plasma PCL

B

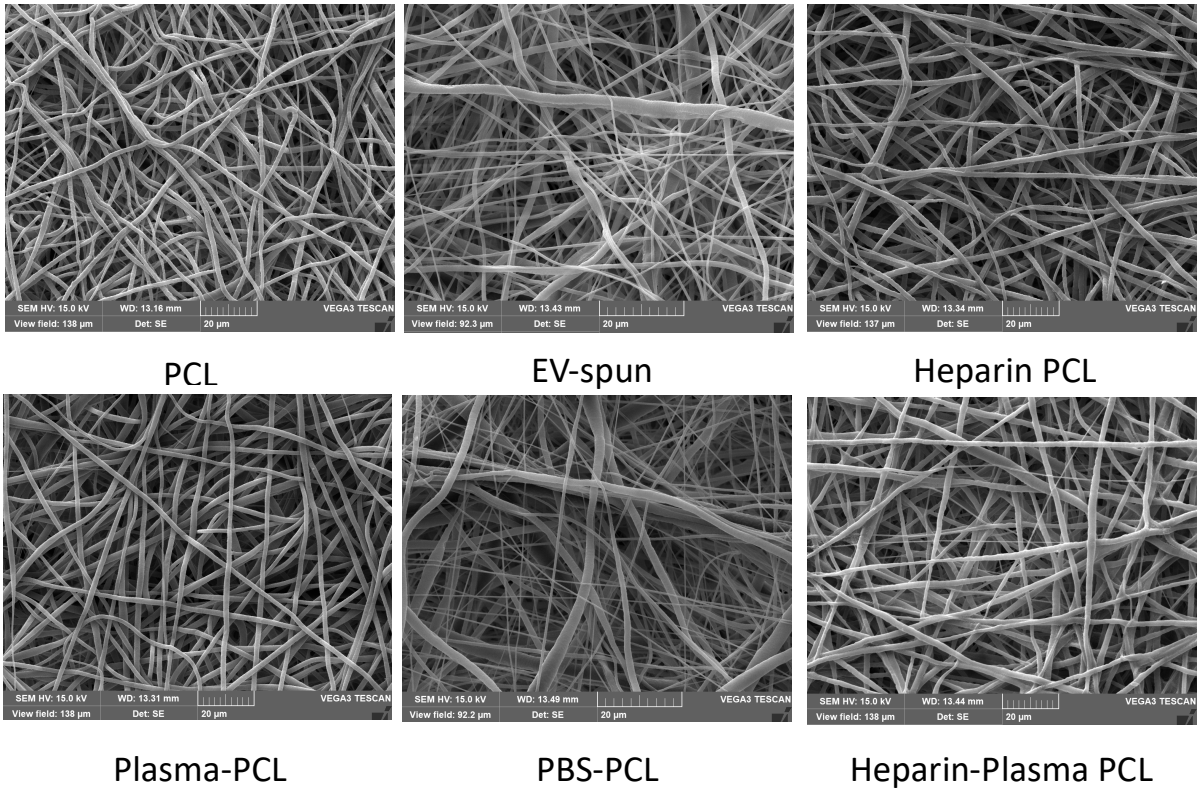
PCL
EV-spun
Heparin PCL
Plasma-PCL
PBS-PCL
Heparin-Plasma PCL

Figure 4.2. Fibre diameter measurements of PCL and treated PCL scaffolds using SEM micrographs. (A) Scatter plot of fibre diameter of PCL and treated PCL scaffold showing a significant reduction in the fibre diameter of EV-spun and PBS-PCL scaffolds compared to other groups following one-ANOVA statistical analysis (**p<0.0001). (B) Representative micrographs of scaffolds used to measure the fibre diameter. Data = mean ± SD. N=3, n=20.**

4.4.2 Mercury intrusion porosimetry (MIP)

Mercury intrusion porosimetry was used to examine the pore characteristics of electrospun scaffolds; these included pore volume, size, size distribution and density. The total porosity of the PCL scaffold was 78.5% which slightly increased after plasma treatment (85.5 %). Heparin treatment tended to reduce the total porosity of the scaffold which can be explained by the effect of the chemicals used during heparinisation include EDA and EDC on the topography of the scaffold (**Table 4.1).** MIP could not measure the porosity of the EV spun scaffold.

The pore size distribution of scaffolds ranged between 5 to 8 µm for PCL and plasma-treated PCL and 9-11 µm for heparin and heparin-plasma PCL (**Figure 4.3)**.

Table 4.1. Porosity and density of scaffolds in comparison to fibre diameters.

Scaffold	Avg. fibre diameter (µm)	Porosity (%)
PCL	1.4 ± 0.6	78.5
Plasma PCL	1.5 ± 0.5	85.5
EV-spun PCL	0.9 ± 0.6	0000
Heparin PCL	1.4 ± 0.5	64.8
Heparin-Plasma PCL	1.6 ± 0.6	60.7

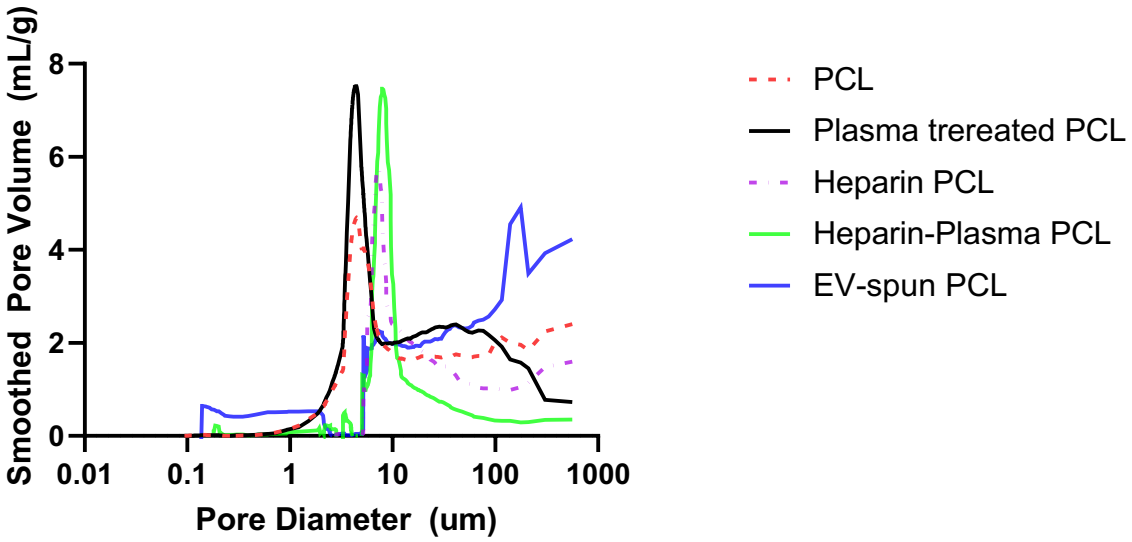

Figure 4.3. Mercury intrusion porosimetry plot showing the pore size distribution of the scaffolds. During the measurement, the samples are placed in an evacuated chamber mercury penetrometer then the mercury is introduced into the chamber. Under increasing pressure up to a maximum of 414 MPa, mercury is forced to penetrate the pores of the sample and measurements were obtained using a MicroActive AutoPore. The plot shows the pore size distribution of each scaffold with each peak represent the average pore size.

4.4.3 Hydrophilicity-contact angle measurements

Contact angle measurements were utilised to assess the change in hydrophilicity after plasma and heparin treatment. Contact angle of non-treated PCL was 141.6° ± 5° which was more hydrophobic compared to treated samples. Plasma and heparin treatment significantly increase the hydrophilicity of the samples (**Figure 4.4**). The results suggest that plasma and heparin treatment made the scaffold more hydrophilic which would improve the EVs attachment.

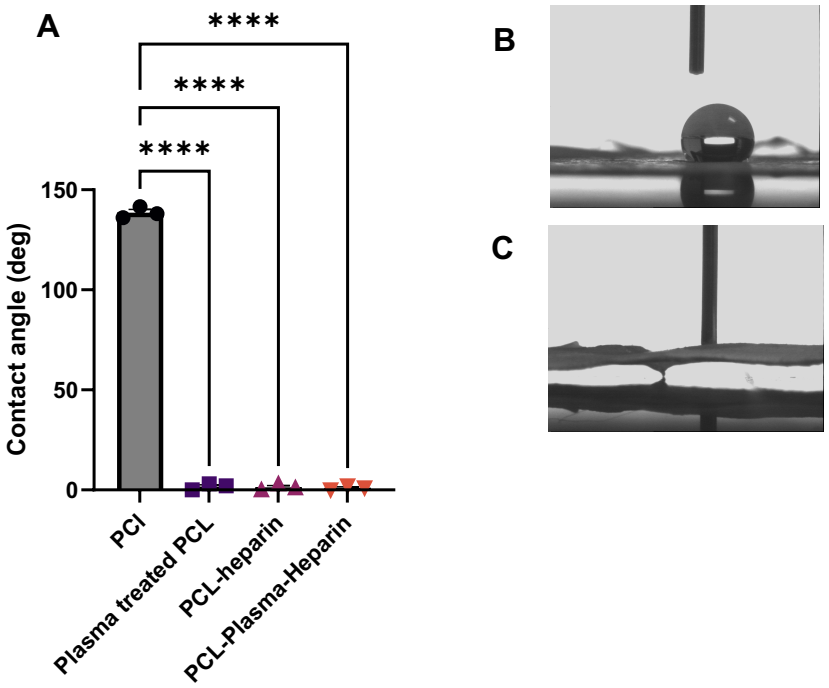

Figure 4.4. Contact angle measurements of PCL and treated PCL scaffolds. After manufacturing the PCL scaffolds using elecrospinning, it was treated with air plasma and/or heparin. Contacts angle measurements were performed using DSA instruments. (A) bar chart of contact angle shows a highly hydrophobic PCL scaffold with contact angle around 141.6° was changed to significantly high hydrophilic after air plasma and heparin treatments (**p<0.0001) following one-ANOVA statistical analysis. (B) Representative images of water contact angle of PCL scaffolds. (C) Representative image of water contact of plasma and heparin treated PCL scaffolds. Data = mean ± SD.**

4.4.4 Zetapotential measurements of the scaffolds

The surface zetapotential of the scaffolds was analysed using Zetasizer instrument to assess the effect of the surface charge of the scaffold on the EVs attachment by comparing that with the zetapotential of EVs. Non-treated PCL scaffold showed almost neutral surface zetapotential (-0.3 mV). Heparin treated scaffold showed to induce anionic character of the surface (-45.8 mV). In contrast, the plasma PCL scaffold exhibited a positive surface charge (+19.6 mV). **Figure 4.5** shows the effect of different treatments on the zetapotential of the scaffold

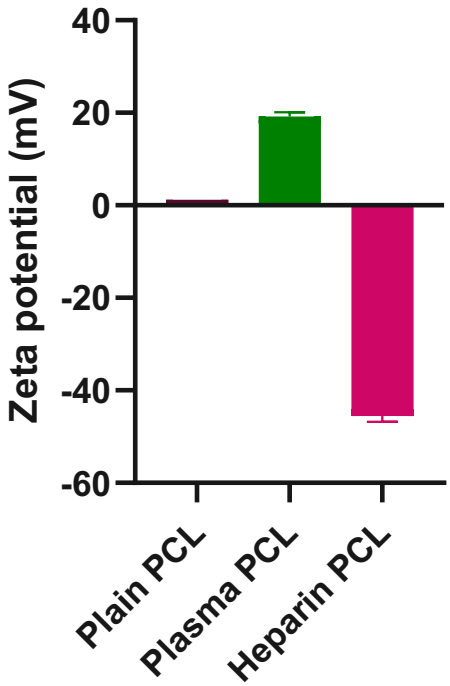

Figure 4.5. Surface zetapotential measurements of the scaffold using Zetasizer instruments. Using neutral nanoparticles, instrument was set up to perform five slow-field reversal measurements at four distances from the sample surface. Data = mean ± SD.

4.5 Manufacture of EVs-modified scaffolds

Utilizing biomaterials to deliver EVs for tissue regeneration has been found to increase EVs bioavailability at the target site (Pinheiro *et al*., 2018). To utilise electrospun scaffold to deliver EVs, the manufacture of EV-modified scaffolds was performed in two ways. First, adding EV suspension to the working polymer solution before spinning to manufacture EV-spun scaffolds. Second, incubating EVs suspensions with PCL and (plasma/heparin) treated PCL scaffolds (after the electrospinning process). Next, qualitative analysis of EVs modified scaffolds using SEM, TEM and fluorescent microscope was conducted to assess the attachment of EVs on the scaffold's fibres. Finally, quantitative analysis of EVs attachment and release kinetics were performed using NTA (Zetaview).

4.6 Characterisation of EVs-modified scaffold

4.6.1 Scanning electron microscope (SEM)

After 24 h of incubation H357 EVs with scaffold at room temperature as described in **Section 2.7.1**, EV-modified scaffold samples including negative controls (PCL scaffolds in PBS) were examined under SEM. UC-EVs were found aggregated on untreated PCL scaffold **Figure 4.6 (A).** At this point we decided to use SEC EVs, to examine whether these showed less aggregation. Few SEC EVs were found attached to untreated PCL **Figure 4.6 (A).** On plasma treated scaffolds, high numbers of EVs were found evenly distributed among the fibres **Figure 4.6 (B)**. Surprisingly, no EVs were found attached to heparin nor heparin-plasma treated scaffolds **Figure 4.6 (C-D)**. No EV-like structures were detected attached to negative control samples.

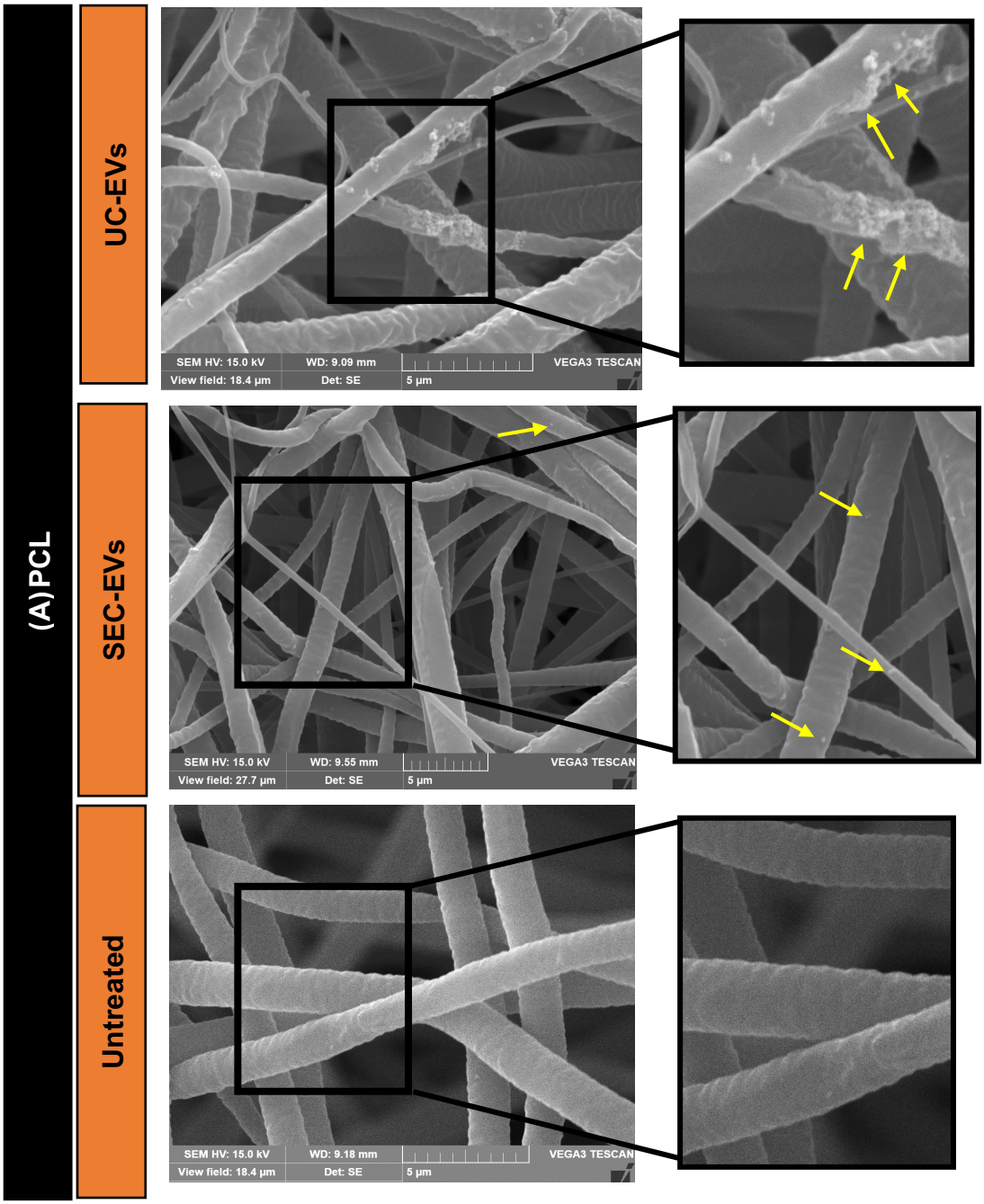
(A)PCL
UC-EVs
SEC-EVs
Untreated
SEM HV: 15.0 kV
WD: 9.09 mm
VEGA3 TESCAN
View field: 18.4 µm
Det: SE
5 µm
SEM HV: 15.0 kV
WD: 9.55 mm
VEGA3 TESCAN
View field: 27.7 µm
Det: SE
5 µm
SEM HV: 15.0 kV
WD: 9.18 mm
VEGA3 TESCAN
View field: 18.4 µm
Det: SE
5 µm

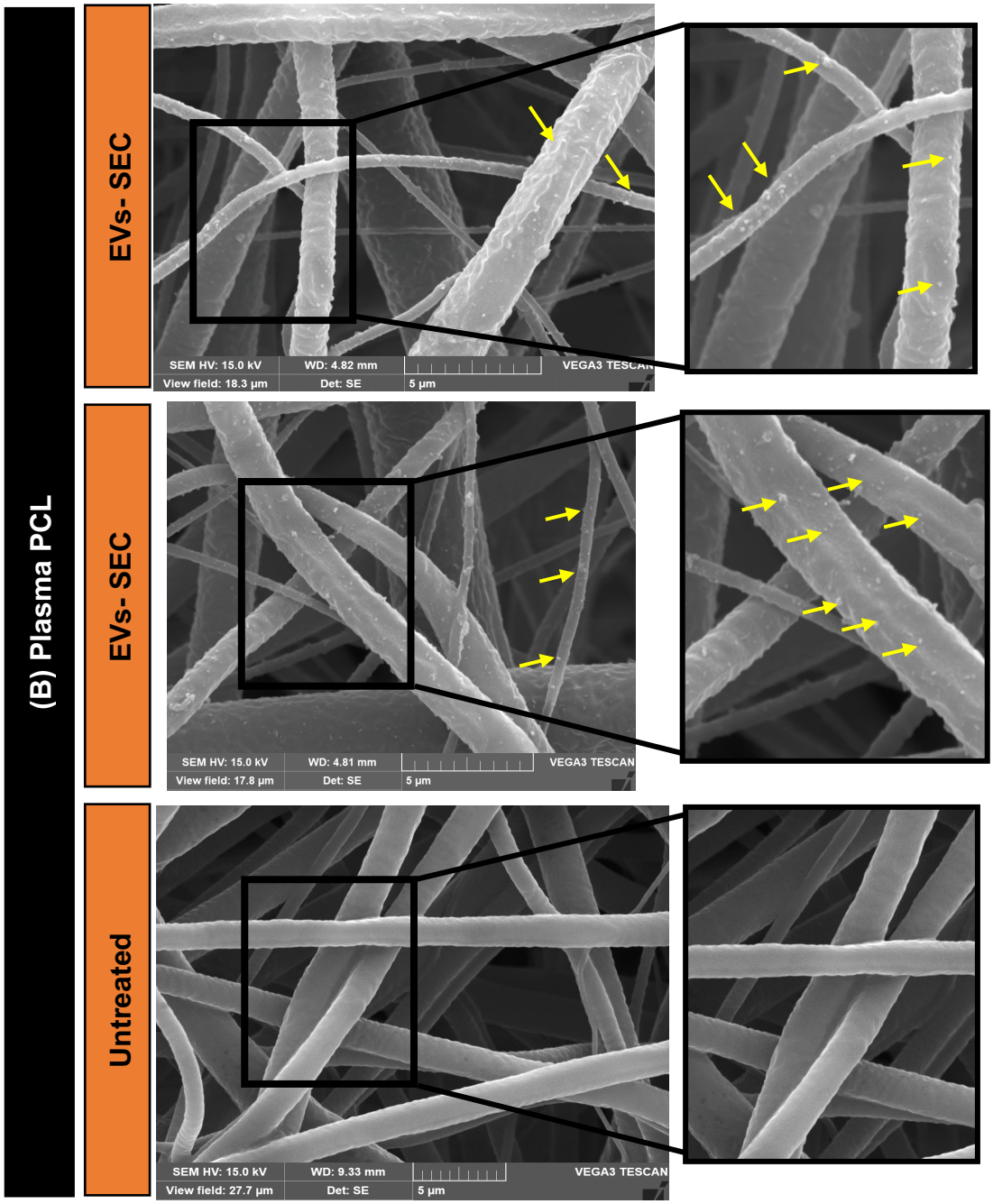
(B) Plasma PCL
EVs- SEC
SEM HV: 15.0 kV
WD: 4.82 mm
View field: 18.3 µm
Det: SE
5 µm
EVs- SEC
SEM HV: 15.0 kV
WD: 4.81 mm
VEGA3 TESCAN
View field: 17.8 µm
Det: SE
5 µm
Untreated
SEM HV: 15.0 kV
WD: 9.33 mm
VEGA3 TESCAN
View field: 27.7 µm
Det: SE
5 µm

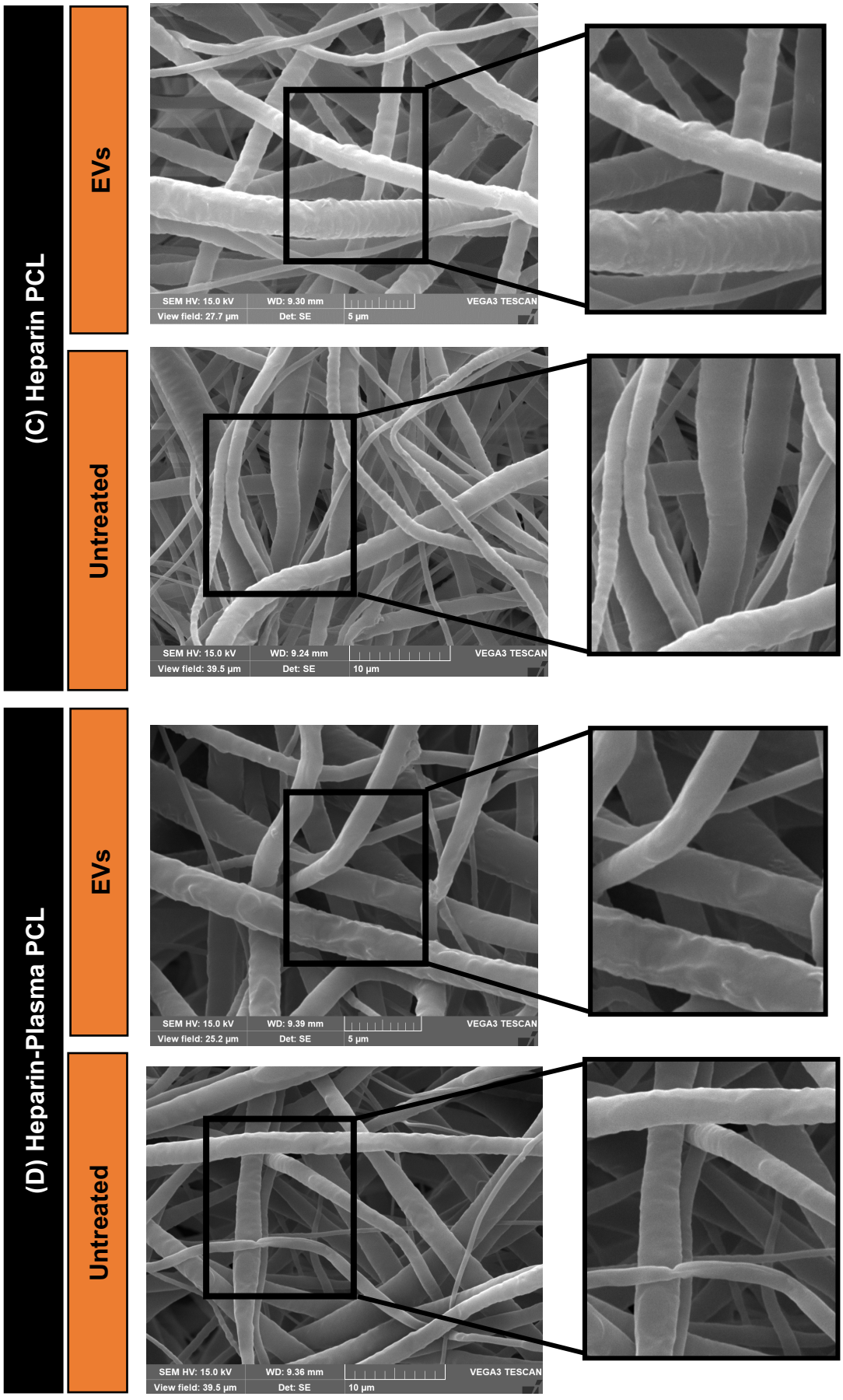
(C) Heparin PCL
EVs
Untreated
(D) Heparin-Plasma PCL
EVs
Untreated
SEM HV: 15.0 kV
WD: 9.30 mm
VEGA3 TESCAN
View field: 27.7 µm
Det: SE
5 µm
SEM HV: 15.0 kV
WD: 9.24 mm
VEGA3 TESCAN
View field: 39.5 µm
Det: SE
10 µm
SEM HV: 15.0 kV
WD: 9.39 mm
VEGA3 TESCAN
View field: 25.2 µm
Det: SE
5 µm
SEM HV: 15.0 kV
WD: 9.36 mm
VEGA3 TESCAN
View field: 39.5 µm
Det: SE
10 µm

Figure 4.6. SEM micrographics of EV-modified scaffolds. H357 EVs were used to assess the attachability of EVs to electrospun scaffolds (A) Representative SEM images show high number of aggregated EVs isolated by UC attached to PCL fibres in comparison to untreated scaffold. (B) Representative images show EVs isolated by SEC were uniformly attached to plasma treated PCL scaffold in comparison to untreated scaffold. (C-D) No EVs were detected attached to the fibres of heparin and plasma treated heparin scaffolds. Arrows indicate EVs.

4.6.2 SEM- Immunogold

To have better visualization of EVs under SEM, EVs modified PCL scaffolds were incubated in (primary antibody (recombinant Anti-CD9) and secondary antibody (goat anti-rabbit IgG H&L [20 nm gold]) before imaging as described in **section 2.8.1.4**. Immunogold labelled EVs were observed attached to electrospun fibres **Figure 4.7 (A-B)**. No EVs were observed in the negative control samples **Figure 4.7 (C-D)**.

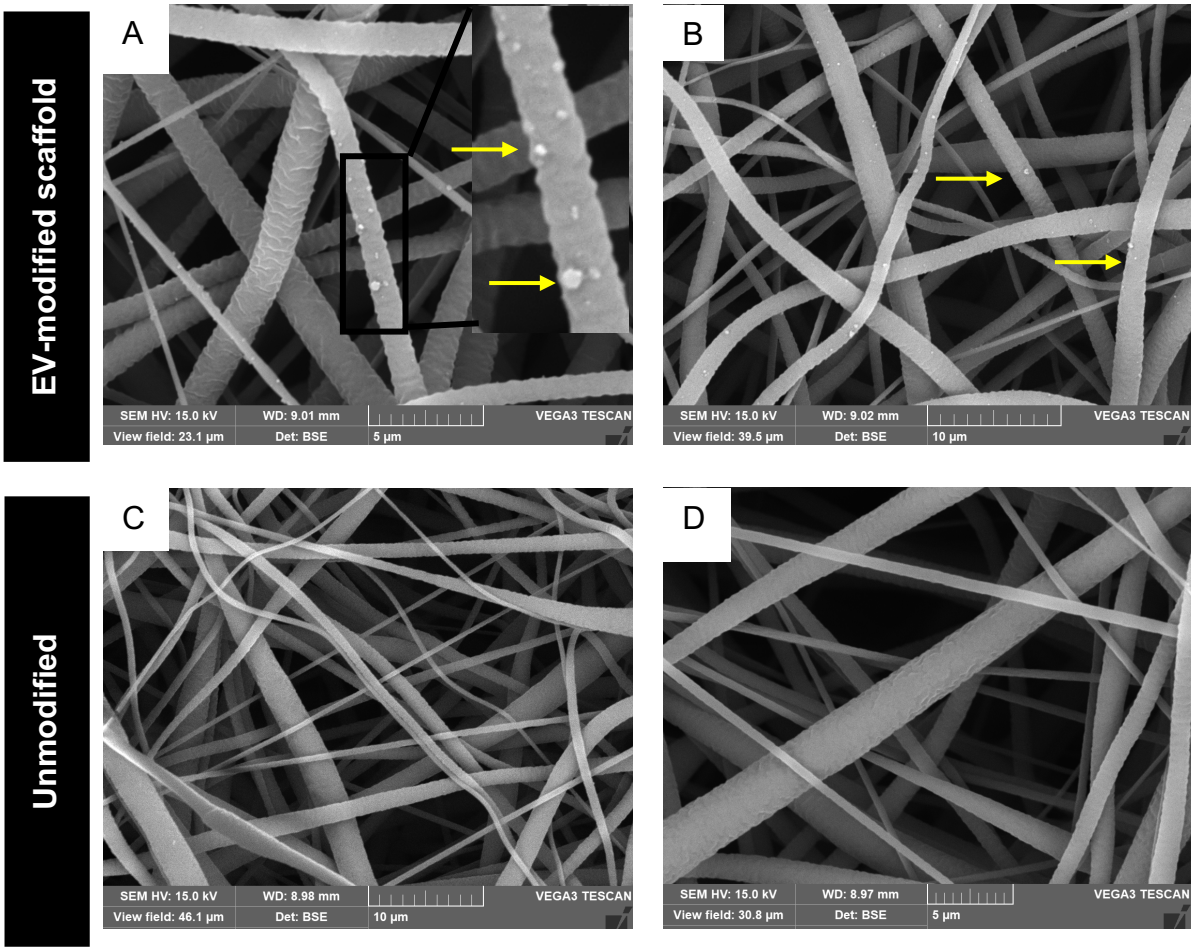

Figure 4.7. Characterisation of Immunogold labelled EV-modified scaffold by SEM. (A-B) Representative images show few labelled EVs attached to electrospun fibres. (C-D) Representative SEM images show the absences of EVs in the unmodified scaffold. Arrows indicate EVs.

4.6.3 Transmission electron microscope

To assess the attachment of EVs across individual fibre, EV-modified scaffolds mounted on resin were sectioned to 60 nm thickness to allow cross-sectional examination of the fibres using TEM. Aggregated EV-like structures were observed attached to electrospun fibres **Figure 4.8 (A)**. EV-like structure within the range of EVs measured by NTA sized 150 nm incorporated to single fibre **Figure 4.8 (B)**. In EV-spun scaffold, EV-like structures were found embedded within the fibres **Figure 4.8 (C-D)**. No vesicle like structures were detected attached to fibre of untreated scaffold **Figure 4.8 (E-F)**.

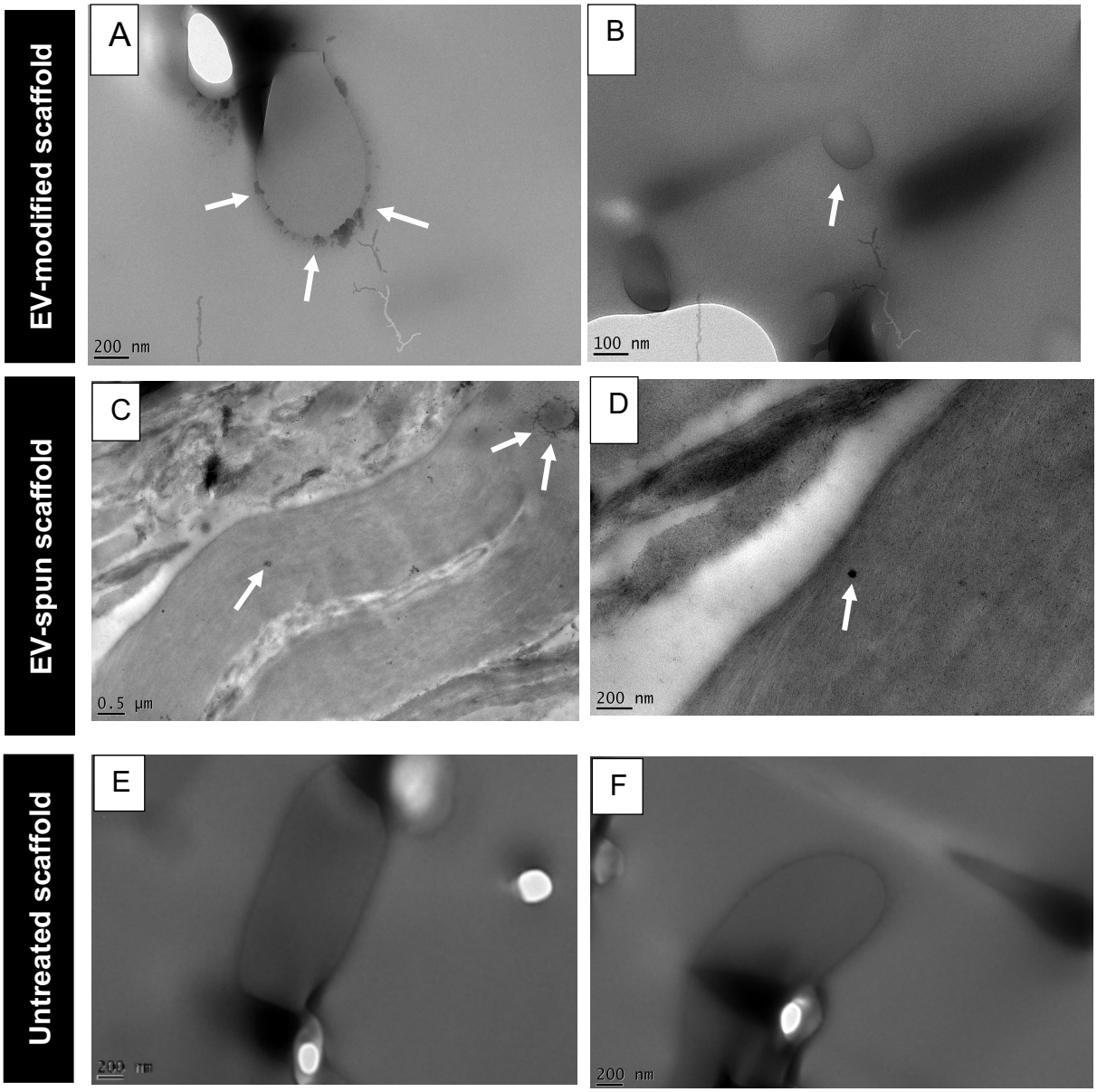

Figure 4.8. Characterisation of EV-modified scaffold by TEM. (A) Representative cross-sectional Image of electrospun fibre shows the attachment of aggregated EVs around the fibre. (B) Representative cross-sectional Image of electrospun fibre shows individual EV attached to electrospun fibre. (C-D) Representative image of EV-spun scaffold with EV like structure embedded within the fibre. (E-F) Representative images show the absence of EVs in the unmodified scaffold. Arrows indicate EVs.

4.6.4 Visualisation of EV in scaffolds using fluorescence microscopy

After isolation of EVs using SEC, EVs were successfully labelled with carboxyfluorescein diacetate succinimidyl ester (CFSE) before being incubated with the scaffolds. After 24 hours, samples were inspected under a fluorescent microscope to determine the distribution of EVs within the scaffolds. Serial Z-stack fluorescent images show the attachment of labelled EVs to the scaffolds (**Figure 4.9)**. **Figure 4.10** shows the distribution of labelled EVs within the electrospun scaffolds.

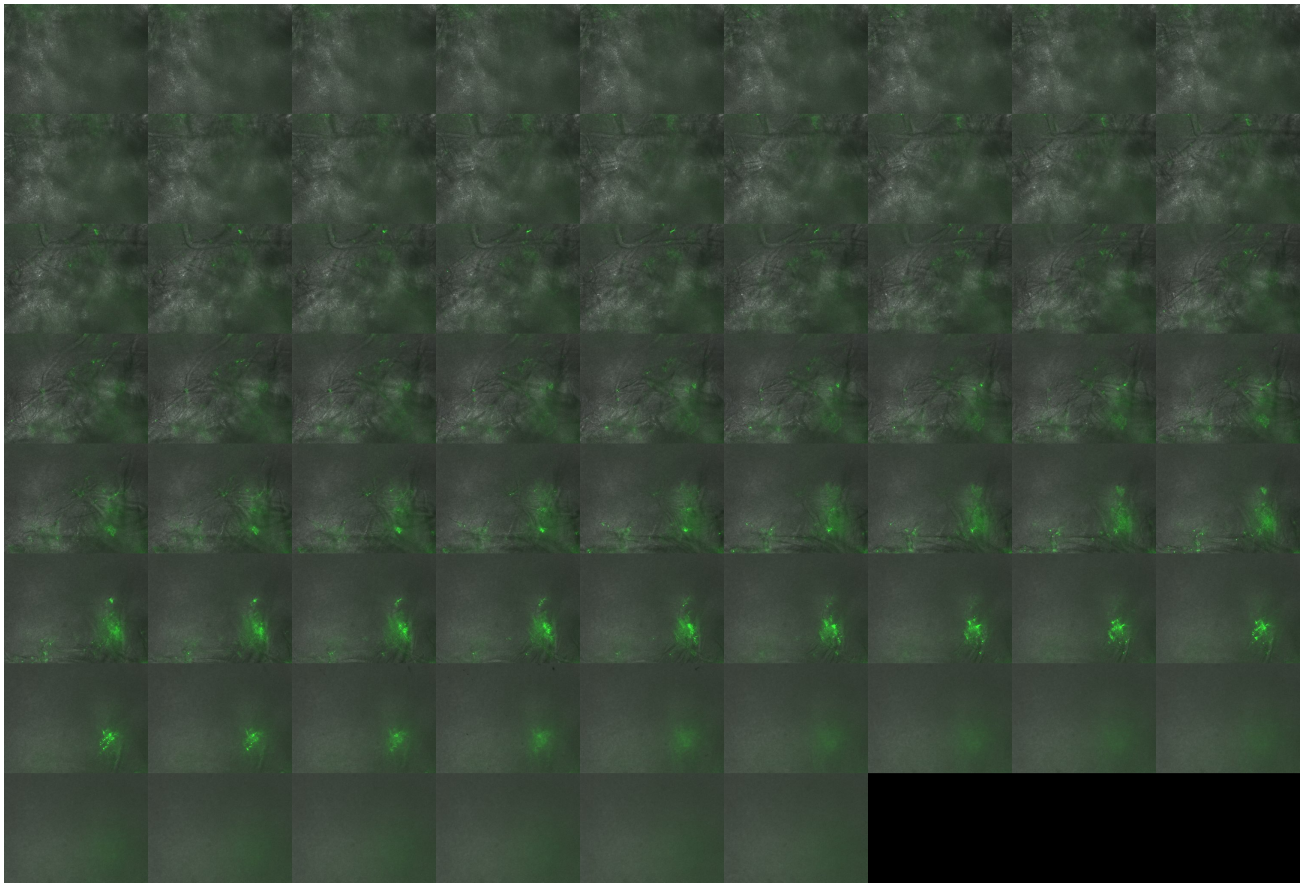

Figure 4.9. Z- Stack fluorescent images show the attachment distribution of labelled EVs at different level of scaffold. Green staining indicates labelled EVs.

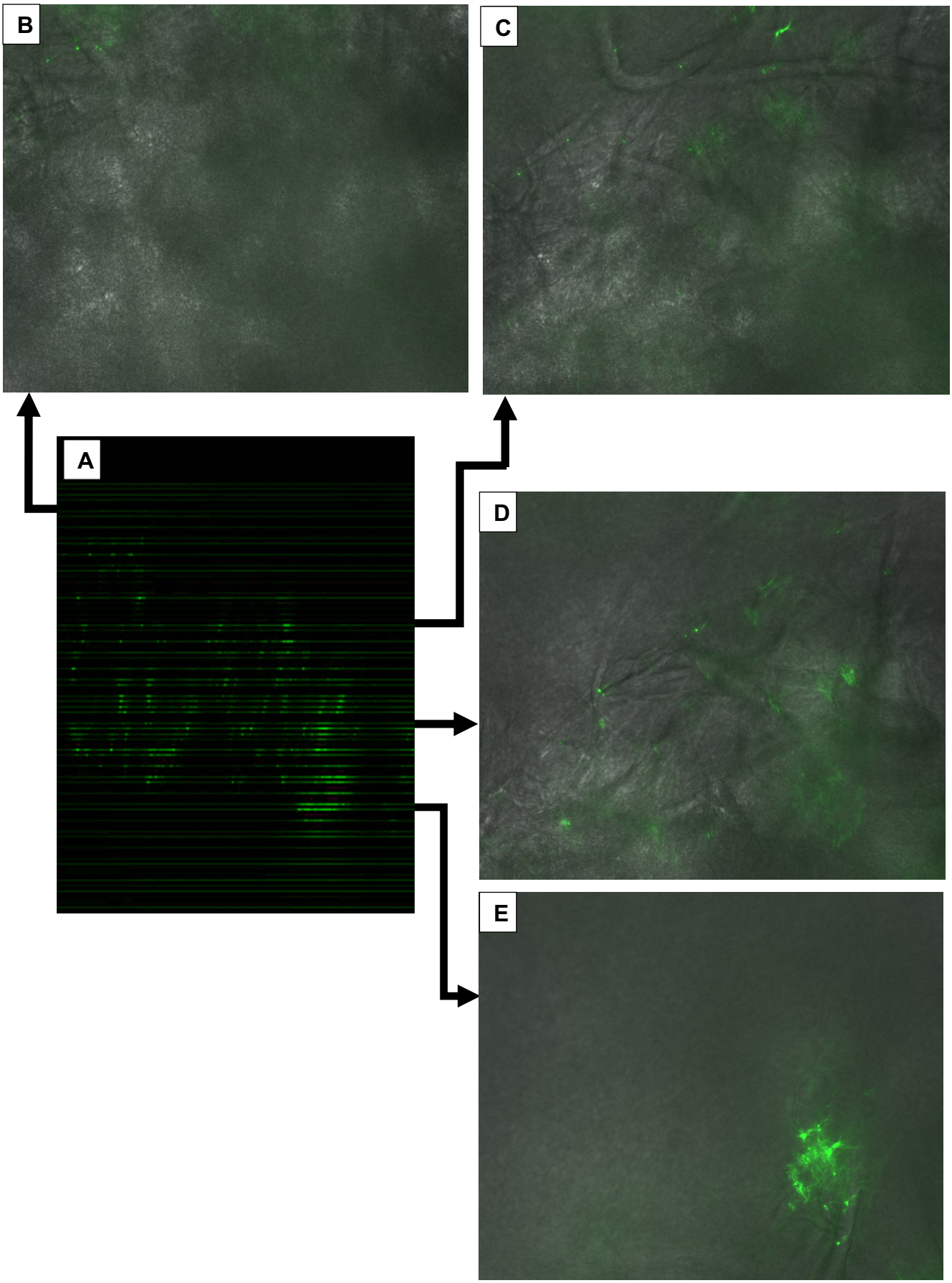
B
C
A
D
E

Figure 4.10. Distribution of labelled EVs (green) within the scaffold. (A) Distribution of EVs within the Z-axis of the scaffold (B) Representative image shows the attachment of few EVs on the top part of the scaffold. (C-D) show the attachment of EVs on the middle part of the scaffold. (E) Shows a high number of EVs accumulate in the bottom part of the scaffold. (Green) dots indicate labelled EVs .

4.7 Attachment and release kinetic of EVs

After successfully incorporating EVs to the electrospun scaffolds which were approved by SEM data, quantitative data of EVs attachment and release was measured to assess the attachability of EVs and study the ability of the scaffold to provide sustained release. The number of EVs attached to each group of scaffolds and their release kinetic over 21 days was assessed using NTA (ZetaView). The quantity of incorporated and released EVs was calculated as described in **section 2.9**. In accordance with SEM data, the highest number of EVs were detected attached to plasma PCL scaffolds retained, with 49.3% of incubated EVs. The lowest attachability was found in heparin-plasma treated scaffold **Figure 4.11 (A)**.

Release kinetics data shows the highest release from plasma-treated scaffolds, with 40% of attached EVs released over 21 days **Figure 4.11 (B)**. Cumulative release plot shows sustained release of EVs from plasma-treated scaffold in comparison to no or poor release from PCL controls, EVs-spun and heparin treated scaffold. Heparin-plasma treated scaffold released 13% of attached EVs by day 4 then only a further 2% between day 5 to 21. These data suggested that plasma-treated scaffold provides a promising platform for EVs delivery.

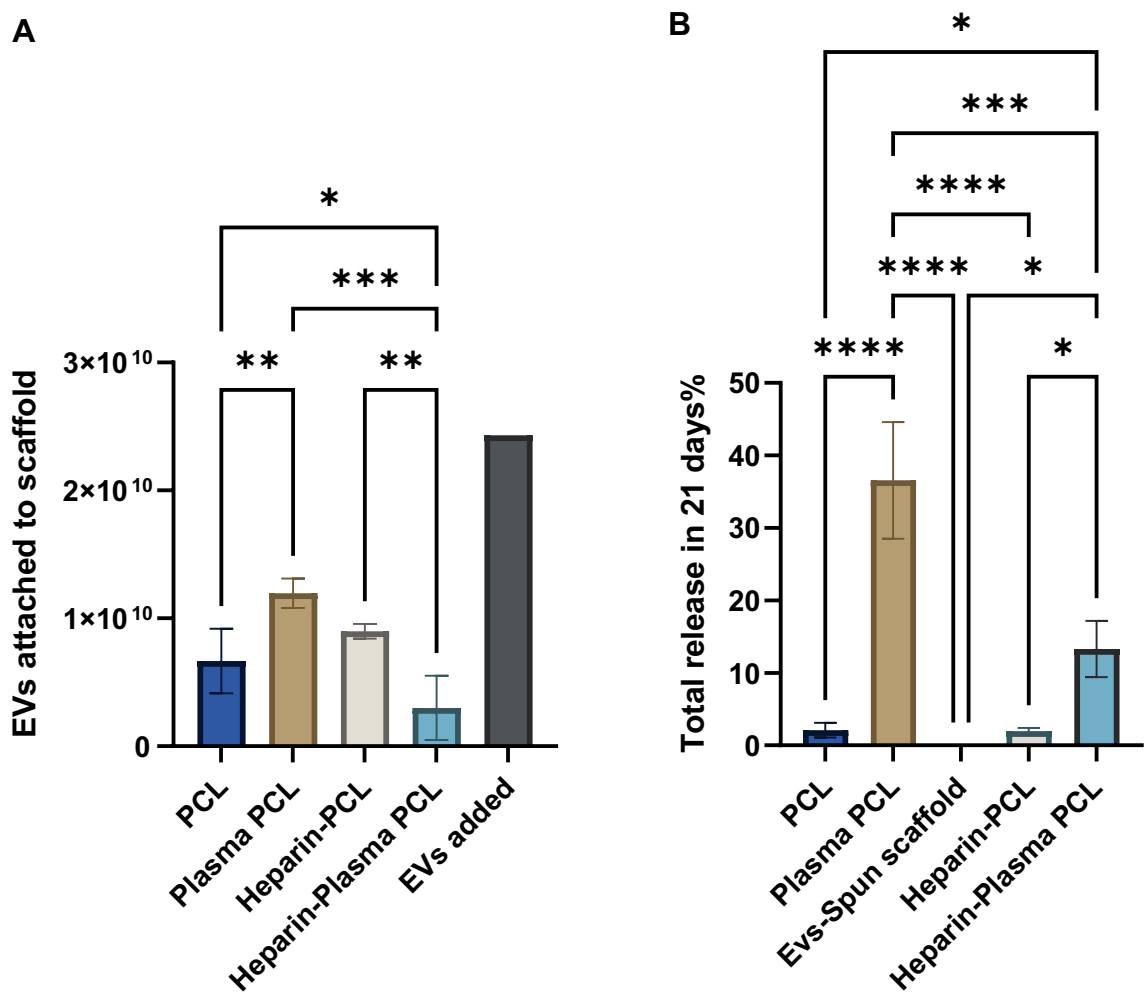

Figure 4.11. EVs attachment and release kinetics measurements using Zetaview instrument. Each scaffold was incubated with EVs suspension for 24 hours. The following day, EVs suspension was removed and fresh PBS was added. (A) Number of EVs that incubated with scaffold ($2.4x10^{10}$ EVs/ml) and number of attached EVs to each scaffold after incubation. (B) The percentage of EVs released form each scaffold in 21 days. Error bar = STDV. *$p<0.05$ was considered significant, following a one-way ANOVA test.

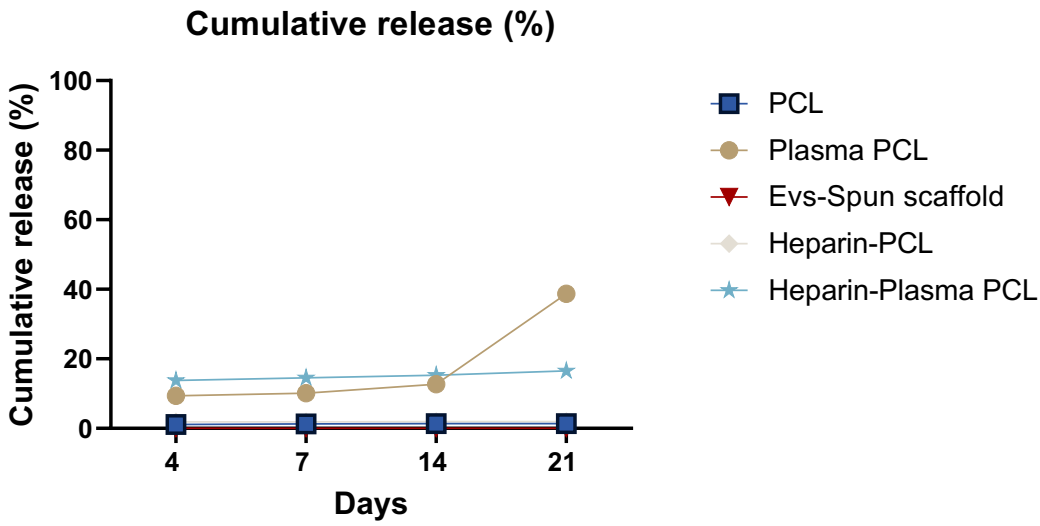

Figure 4.12. *In vitro* cumulative release of EVs from scaffolds over 21 days. Plasma treated scaffold show sustain release with the highest release between day 7 and day 14 (30%). Less than 2% of EVs were released from PCL and heparin PCL scaffold. Heparin-plasma PCL scaffold released 13% of attached EVs by day 4 then 2% between day 7-21.

4.8 Discussion

Electrospinning is a flexible manufacturing technology that has been employed for a variety of tissue engineering applications and biomolecule delivery. In this chapter, we fabricated the PCL electrospun scaffolds and assessed the ability to modify them by incorporating extracellular vesicles, with the intention of developing a platform for use in different tissue engineering applications.

Here, we fabricated electrospun scaffolds using polycaprolactone PCL, one of the most commonly used polymers in the fields of tissue engineering and regenerative medicine (Woodruff *et al*., 2010). PCL is a liner aliphatic polyester, with a melting point between 50–60°C. Bioresorbability, biocompatibility and optimal mechanical properties for different medical applications are the primary advantages of PCL. In addition, PCL has been approved by the US Food and Drug Administration (FDA) and has been successfully used in clinical applications since the 1980s (Cipitria *et al*., 2011). Furthermore, PCL can be easily electrospun using different parameters which can be tailored to fabricate scaffolds with specific fibre diameter and mechanical properties (Christen *et al*., 2020).

The electrospinning process of PCL has been reported using different solvents (Van der Schueren *et al*., 2011). Here, we utilised DCM and DMF due to their high acceptance for medical applications according to the European Medicines Agency (European Medicines Agency, 2019). In addition, previous data from our group showed that electrospun scaffolds fabricated using the DCM:DMF solvent system demonstrated substantially lower solvent values, below the clinical use limits (Navarrete, 2020). PCL dissolves better in DCM than DMF (Woodruff *et al*., 2010). DMF, however, has more conductivity than DCM (Du *et al*., 2016). Therefore,

DCM:DMF system has the overall effect of increasing the conductivity and reducing the instability which leads to the production of regular fibres.

PCL has a slow degradation rate (2-4 years), due to its hydrophobic nature and semi-crystallinity (Nair *et al*., 2007). The hydrophobicity of PCL scaffolds can lead to poor wettability, which results in a lack of cell attachment. Surface modifications to the scaffold, through plasma treatments or chemical treatment (with NaOH), have been shown to increase both wettability and cell attachment (Cipitria *et al*., 2011). Although successful to a degree, Chemical treatments have been shown to negatively affect the structure and elasticity of the scaffolds (Morent *et al*., 2011). Alternatively, non-thermal plasma treatment has shown to be a promising method for increasing the hydrophilicity of the scaffold without affecting its bulk properties and creating a promising platform for the delivery of complex biomolecules(Yildirim *et al*., 2008). In addition, Heparin modification of biomaterials has been extensively studied in the literature and shown to increase the hydrophilicity and biocompatibility of the materials (Tsai *et al*., 2001). Contact angle measurements confirmed the effect of both plasma and heparin treatments used in this study to improve the hydrophilicity of the PCL scaffold.

Fibre diameter for electrospun scaffolds used for tissue engineering applications is an important factor affecting not only the mechanical properties of the scaffold but also the cell migration within their fibres (Liu *et al*., 2009). Here, the fibre diameter of the 10% PCL scaffold was within the range of 0.5-1.8 μm which give a very high surface area-to-volume ratio, which is desired for improving active compound delivery even at high loadings. No significant effect was observed for air plasma (2 min, 10 Watt) and heparin treatments on the fibre diameter of the scaffolds within the parameters we used in this project. In contrast, adding the EV suspension or PBS to polymer solution before spinning to fabricate EV spun scaffold significantly altered the fibre diameter of

the scaffold.Prabhakaran *et al*., (2008) treated electrospun PCL scaffolds with air plasma at 30 W for 1 minute and found no morphological or fibre diameter alterations. In addition, Can-Herrera *et al*., (2016) found air plasma treatment of PCL scaffolds using different power and treatment times showed no significant effect on the fibre dimeter of the scaffold. Similarly, the diameter and morphology of the fibres were preserved after heparin functionalization (Braghirolli *et al*. 2017). The changes in the morphology and fibre diameter of the EV-spun scaffold and PCL-PBS scaffold can most likely be explained by the change in the viscosity and concentration of the polymer solution.

The surface zetapotential of the biomaterials plays important role not only in the interaction between the materials and its surrounding but also affects cells responses and ultimately cell differentiation (Metwally and Stachewicz, 2019). In addition, materials surface charge found affect not only the adsorption of nanoparticles but also their distribution on the surface (Hu *et al*., 2017). Kalasin *et al*., (2009) found that the surface charges of biomaterials play an important role on biomolecule adsorption. Thus, surface zetapotential of the scaffolds used in this project may explain the behaviour of EVs attachment and release. Our data showed that surface zeta potential of PCL scaffolds presented almost neutral charge (-0.3 mV). Various zetapotential values have been reported in the literature for PCL. Metwally *et al*., (2020)reported that the surface zeta of PCL was 220.6 ± 6.7 mV. They also measured the surface charge of PCL electrspun scaffolds that were manufactured with positive or negative external electric field and reported 74 ± 41 mV for PCL (+) and 145 ± 46 mV for PCL (-) (Metwally, Karbowniczek, *et al*., 2019). This outcome is contrary to that reported by Vaquette *et al*., (2008) who showed a negative surface charge of PCL electrospun scaffolds, reporting values around –28 ± 1 mV.

Different treatments of PCL have been found to alter the surface zetapotential. Our heparin-treated scaffolds showed a negative zetapotential (- 45.8 mV) which was consistent with that of previous studies (Nguyen *et al*. 2017; Mammadov *et al*., 2011). Here, we found that a low-pressure air plasma treatment induced a positive charge on the scaffold surface (19.6 mV). To our knowledge, no study has measured the zetapotential of air plasma treated PCL electrospun scaffold. Other studies, however, measured the surface potential of other materials treated with plasma. Guo *et al*., (2009) found a negative charge of woven polyester (PET) treated with air plasma. Another study found a positive charge of cotton fabric treated with O_2 plasma (28.8 mV) and a slightly negative charge of the one treated with N_2 plasma (−0.6 mV). Further studies are needed to fully elucidate the effect of plasma treatment on the surface charge of scaffolds

Utilizing biomaterials to deliver EVs has been found to increase EVs bioavailability at the target site (Pinheiro *et al*., 2018). Some studies have investigated EV-modifications using different types of scaffolds. Xie *et al.* (2017) used mesenchymal stem cell (MSC) -derived EVs to modify a decalcified bone matrix scaffold to enhance bone regeneration. For wound healing, Tao *et al.* (2017) incorporated EVs derived from synovium MSCs into a chitosan hydrogel, whereas Shi *et al.* (2017) used gingival MSC-derived EVs with a chitosan/silk hydrogel. These studies showed promising results and suggested that EV-modified scaffolds may be useful for the promotion of regeneration and angiogenesis within target organs.

In this study, we designed a novel method for EV-modification using porous, electrospun scaffolds that have the potential to be adapted for use in different tissue engineering and regenerative medicine applications. We compared our method of treating the scaffold with plasma treatment before the incubation with EVs with

previously published methods. (Wei *et al*., 2019)treated the scaffold with heparin before incubation with EVs and Trindade *et al*., (2021) added the EVs to the polymer solution before spinning. We observed from microscopic images and NTA data that EVs attached more to plasma-treated scaffolds in comparison to all other scaffolds. These data may be explained by our zetapotential data which found negatively charged EVs attached more to positively charged plasma PCL in comparison to neutral PCL and negatively charged heparin PCL.

Regarding the release kinetic of EVs, we found that the plasma treatment induces the sustained release of EVs with 40% of EVs released within 21 days. These data are consistent with prior reports showing that plasma treatment improves the sustained release of certain drugs (Petlin *et al*., 2017). Costoya *et al*., (2016) found HMDSO-plasma coated electrospun fibres provided sustained release of antifungal drug (Fluconazole) and prevented burst release. Although heparin treatment is reported to improve the sustained release of biomolecules (Copes *et al*., 2019), our data were not able to support this, most likely explained by the observation of low attachment of EVs to heparin treated scaffold in our system.

Many challenges must still be overcome before the widespread use of EV-modified scaffolds becomes possible. First, further optimisation of the effect of different surface treatments of the scaffold is needed for a better understanding of the mechanism of EV attachment and release. Although plasma treatment showed promising effects on the release kinetic of EVs, research is also needed to improve the understanding of the precise mechanism to utilise that tailor the release according to the intended application.

4.9 Conclusion

In this chapter, we focused on the development, characterisation, and optimisation of electrospun scaffolds and we explored the inclusion of extracellular vesicles within them. We used PCL as a working polymer according to previous promising data from our group. Moreover, we studied and characterized the effect of plasma and heparin surface treatments on the PCL electrospun mats and we found no negative effect on the chemical and physical properties of the scaffolds. We also demonstrated that the surface zetapotential of the scaffold was affected by the different nature of the surface treatment. The plasma treatment was found to induce a positive charge in comparison to the highly negative charge induced by heparin treatment. The plain PCL scaffold was found to be neutral.

In essence, the plasma treatment was the most reliable method for the attachment of EVs to the scaffold and provided a sustained release. Heparin treatment, however, did not induce sufficient attachment of EVs to the scaffold. Moreover, spinning of EVs with the polymer solution was found to alter the fibre dimeter, porosity and morphology of the scaffold. Thus, we selected plasma-treated scaffolds to be used for our functional assays to assess the functionality of EVs modified scaffolds in enhancing wound healing, angiogenesis and osteogenesis, as described in chapter 5.

Chapter 5

Assessing the functionality of EVs and EVs-modified scaffolds in wound healing, Angiogenesis and osteogenesis

5.1 Introduction

The paracrine effect of EVs in altering the phenotype of recipient cells is the rationale for employing EVs in tissue engineering and regenerative therapies. Mesenchymal stem cells, because of their role in promoting regeneration, are the most common source of EVs in this context (Marolt Presen *et al*., 2019). However, the utilisation of MSC cells for regenerative therapies is limited due to undesired differentiation, limited circulation due to their large size, and diminished activity due to freeze/thaw cycles (Holkar *et al*., 2020b). In addition, EVs from other cell types were utilised the induce tissue regeneration including myofibroblast (Merjaneh *et al*., 2017) and adipose tissue (Huang *et al*., 2021).

Wound healing is a multicellular physiological process involving many different cell types which include fibroblasts and myofibroblasts that play an important part in the creation of new tissue by secreting and modifying the extracellular matrix (Desmouliere *et al*., 2014). Due to the increasing evidence about the role of EVs in wound healing, myofibroblast-derived EVs are thought to have some role in this context. Merjaneh *et al*., (2017) found that dermal myofibroblast-derived EVs were able to induce endothelial cell migration and capillary formation. A similar study found that skin myofibroblast EVs stimulate the migration of skin fibroblast (Arif *et al*. 2020). Stem cells may be extracted from the body and have differentiation capacity as well as the ability to self-renew. Their function in the adult body is to maintain tissue viability by allowing cell turnover of old, damaged, or dying cells. The dental pulp of permanent teeth, which consists of the soft tissue within a tooth that contains a variety of cells, including vascular cells, fibroblasts, and odontoblasts, is a well-documented source of adult stem cells (Gronthos *et al*., 2000). Human dental pulp stem cells (HDPSC) are derived from neural crest cells, which have a high potential for multi-directional

differentiation, and studies have demonstrated that stem cells can fulfill biological functions by secreting a range of growth factors (Jin *et al*., 2020). HDPS cells have been used in various regenerative medicine applications including angiogenesis (Nakashima *et al*., 2009), muscle regeneration (Martínez-Sarrà *et al*., 2017) and dental pulp regeneration (Moonesi Rad *et al*., 2019).

Angiogenesis (the formation of new blood vessels) is one of the crucial steps for successful tissue regeneration (Mastrullo *et al*., 2020). Among the various methods usually used to assess the angiogenic response of biomaterials (Stryker *et al*., 2019), the chorioallantoic membrane (CAM) assay is considered a simple and cost-effective screening tool for the angiogenic properties of stem cells and their associated potential in the tissue engineering field (Merckx, Tay, *et al*., 2020).

5.2 Aim and objectives

The aim of this experimental chapter is to assess the functionality of myofibroblast and HDPS EVs, and EV-modified scaffolds, in wound healing, angiogenesis and osteogenesis assays. To achieve this aim, the following objectives were established:

1- Differentiate normal oral fibroblast (NOF) cells to myofibroblast using TGFβ and determine myofibroblastic phenotype by examining αSMA expression using immunofluorescence.
2- Examine the effect of myofibroblast EVs on fibroblast migration.
3- Assess the ability of myofibroblast-derived EVs to induce myofibroblastic differentiation of NOF cells using qPCR and immunofluorescence.
4- Evaluate the MSC phenotype of human dental pulp stem cells by their osteogenic capacity and by examining their expression of the STRO-1 MSC marker.

5- Examine the ability of HDPS EVs and conditioned media to induce angiogenesis using chorioallantoic membrane (CAM) assay.

6- Study the ability of HDPS EVs and conditioned media to induce osteogenic differentiation of rat MCS cells.

5.3 Experimental approach

According to the objectives above, the experimental approach was established and performed according to the schematic diagram illustrated below (**Figure 5.1)**.

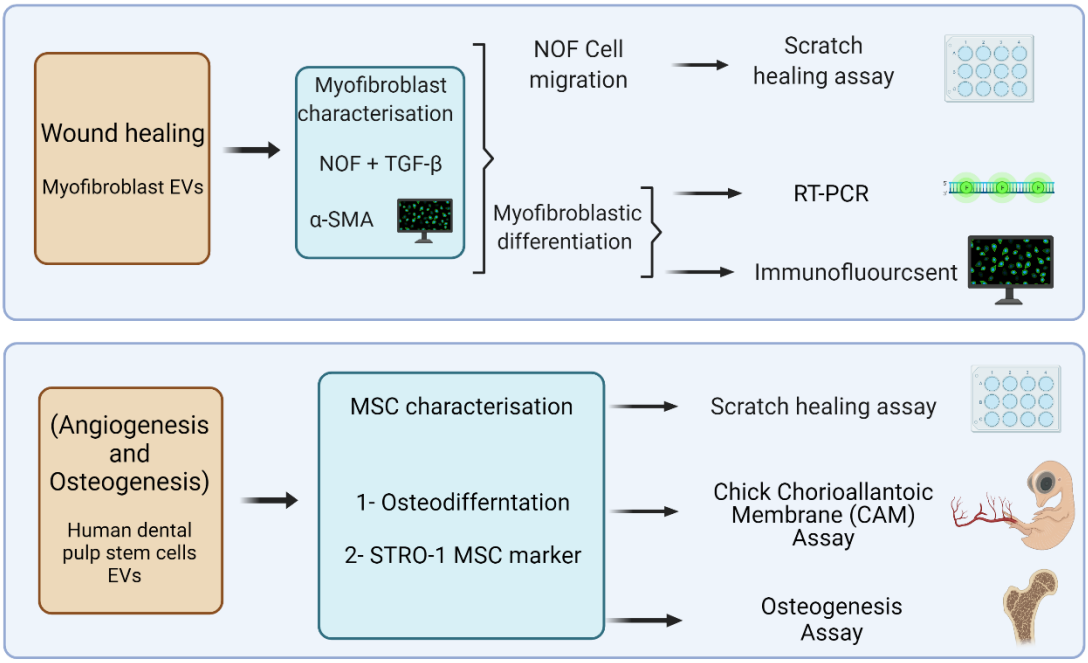

Figure 5.1. Schematic diagram illustrating the methodology of the assays used to assess the functionality of EVs and EVs modified scaffold

5.4 Exploring the role of myofibroblast EVs in wound healing

5.4.1 Fibroblast treated with TGFβ-1 express stromal marker αSMA

Myofibroblasts can be identified *in vitro* by visualising their prominent cytoskeletal α-SMA stress fibres using immunofluorescence (IF). To assess the ability of normal oral fibroblasts (NOF) to differentiate to myofibroblasts, NOF cells were treated with 5 ng/ml of TGFβ and then analysed for intracellular αSMA expression using a FITC conjugated monoclonal antibody. TGFβ-treated fibroblasts exhibited stromal marker α-SMA (Figure 5.2 A, B). Expression was barely detectable in untreated normal oral fibroblast (Figure 5.2 C).

A

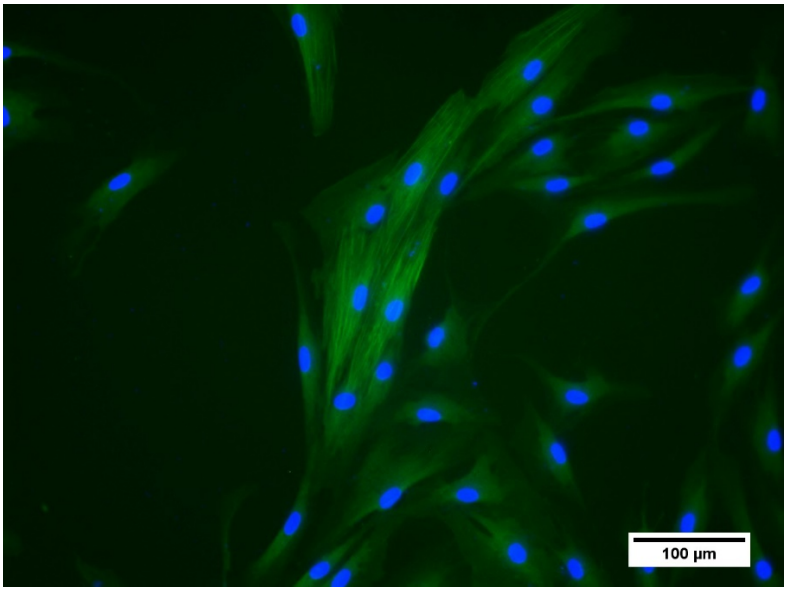

B

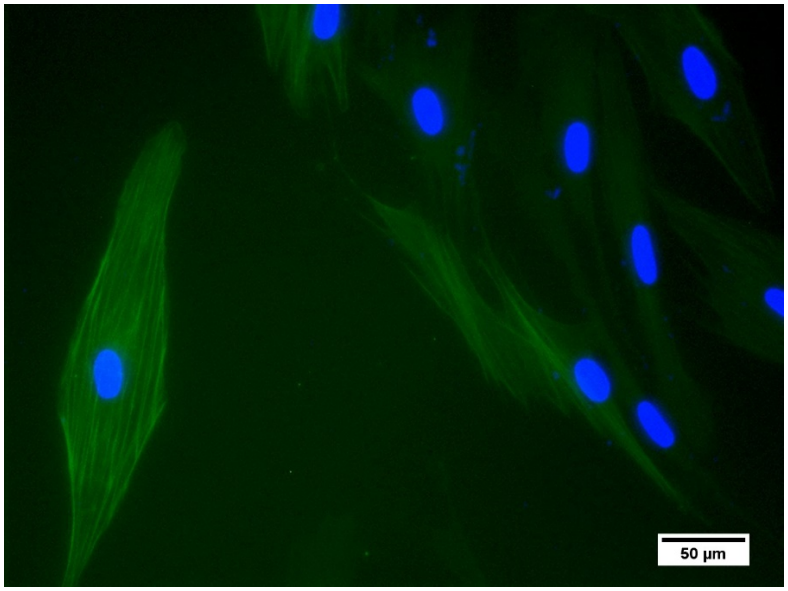

C

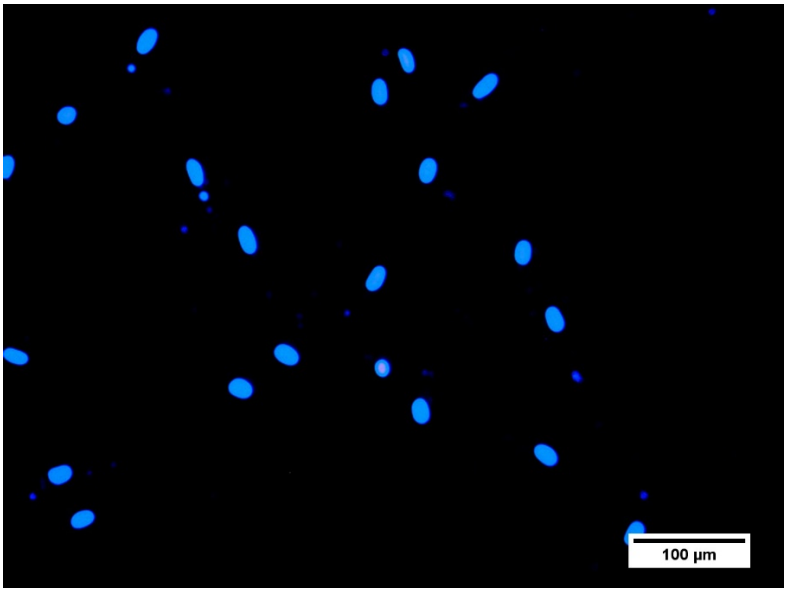

Figure 5.2. Immunofluorescence detection of αSMA contractile features in NOF cells treated with TGFβ. Following treating NOF cells with 5ng/ml TGFβ, cells were stained with 1:100 FITC-conjugated αSMA. (A-B) NOF treated with 5ng/ml TGFβ for 48 hours expressing αSMA stromal marker. (C) Negative control, NOF in serum free media.

5.4.2 Effect of the Myofibroblast- derived EVs on the migration of NOF cells

The differentiation of fibroblasts to myofibroblasts plays an important role in wound healing by inducing wound contraction and connective tissue restoration (Grotendorst *et al*., 2004). To investigate whether EV released by myofibroblasts would be able to induce the migration of normal oral fibroblast (part of the wound healing response), a scratch assay was utilised as described in **Section 2.12**. Upon reaching confluency, the monolayer of NOF was 'scratched' - to create a gap in the monolayer of consistent width - then exposed to EVs and EVs-modified scaffolds. No significant difference was detected between treated and untreated groups after 24 h (**Figure 5.3 A,B).**

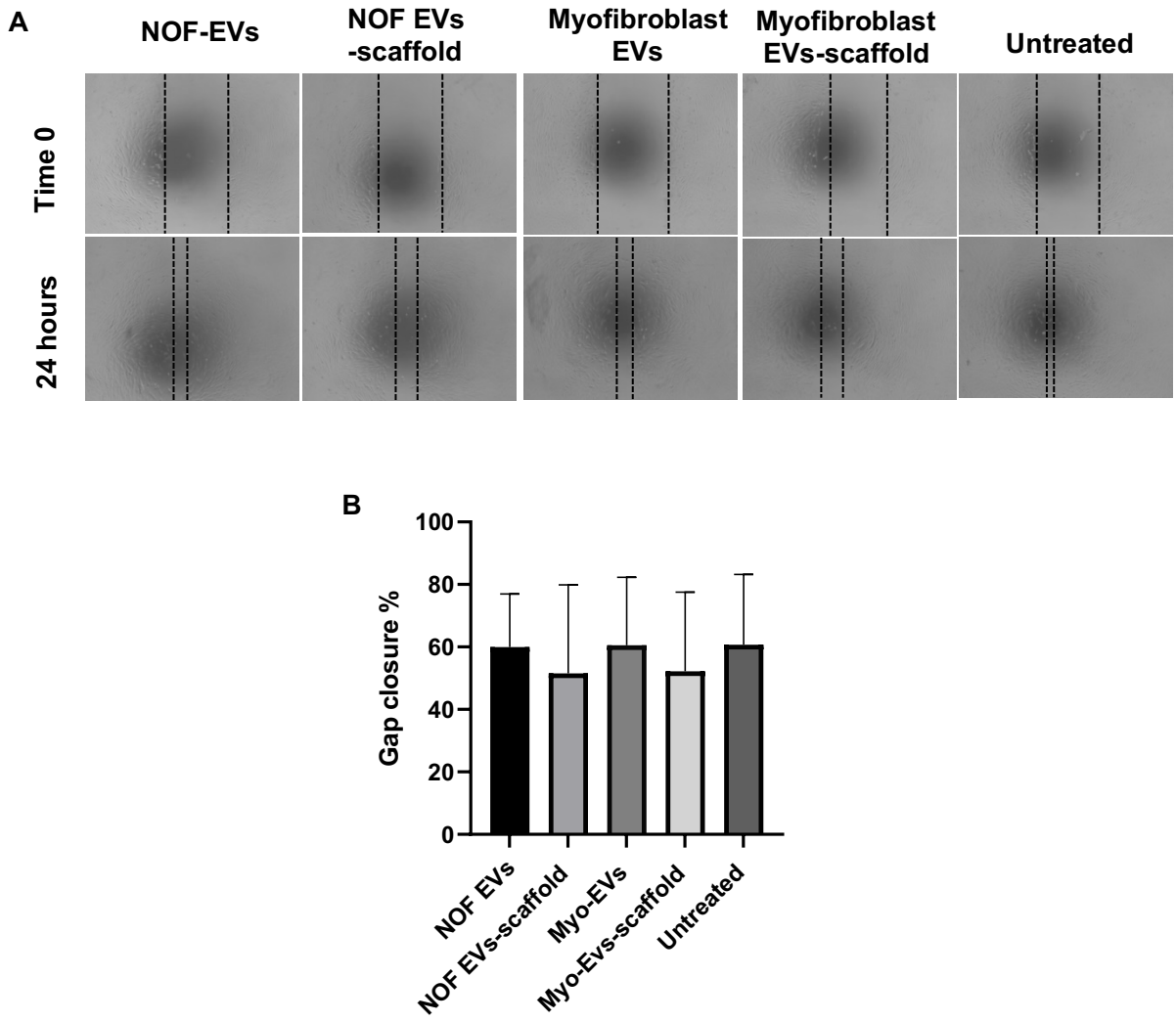

Figure 5.3. Scratch healing assay to study the effect of NOF and myofibroblast-derived EVs on the migration NOF cells. NOF cells were cultured in 24 well plate for 24 h to reach confluency. Next day, cells were scratched using a 200 µl pipette tip and then incubated with EVs and EVs-modified scaffolds for 24 h. The percentage of gap closure was accessed. (A) Representative images of the migration of NOF cells were taken at 0 h (immediately following the creation of the wound) and 24 h after the creation of the wound. Images were taken at x5 magnification. (B) Bar chart shows no significant effect was found of the EVs and EVs-modified scaffold on the migration of NOF cells. Values are expressed as (mean± SD). Error bar = SD. Data represent N=5 and n=3.

5.4.3 Evaluation the gene expression of a-SMA and VCAN myofibroblast markers by NOF treated with myofibroblast EVs

To further investigate the ability of myofibroblast EVs to induce the myofibroblast phenotype of NOF cells, the alpha smooth muscle actin (α-SMA) and versican (VCAN) gene expression were investigated using qPCR. After measuring the migration of NOF cells using the scratch assay, gene expression was measured using qPCR. No significant differences were found in the expression of α-SMA and VCNA gene between the EVs and EVs-modified scaffold treated group and the untreated group **(Figure 5.4).**

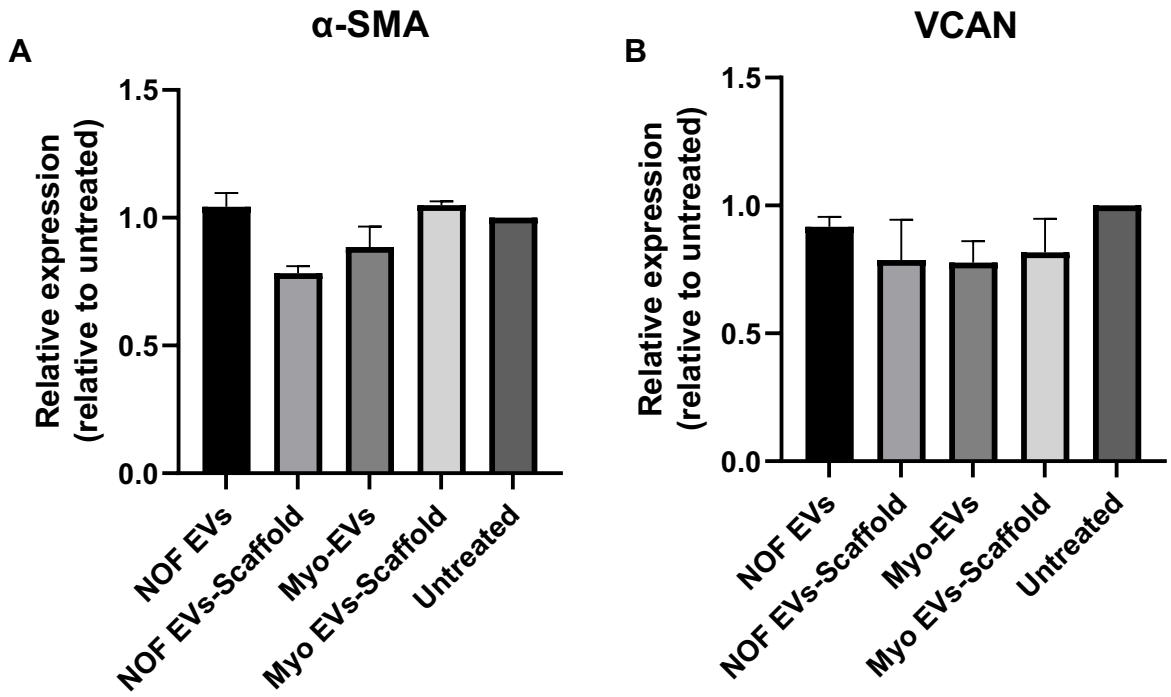

Figure 5.4. Expression data for the α-SMA and matrix marker VCAN in NOF treated with EVs and EVs-modified scaffold. NOF 2D monolayers were treated with NOF and Myofibroblast EVs and EVs-modified scaffold for 24h and the gene expression for (A) α-SMA and (B) VCAN were determined by qPCR. Data is expressed as fold change relative to untreated group, with mean ± SD.

5.4.4 Evaluation of the expression of myofibroblast marker αSMA of NOF treated with myofibroblast EVs

The contractility feature of myofibroblast contributes to wound contraction. To assess whether the myofibroblast EVs are able to express the αSMA stromal marker in NOF, cells were cultured for 24 hours and then treated with TGF-β1 (10 ng/ml) and myofibroblast EVs for 48 hours. Cells were then stained with 1:100 FITC-conjugated αSMA. The treatment of NOF with myofibroblast EVs was not able to change the phenotype of the fibroblast (**Figure 5.5 B)**. TGFβ significantly induced the contractile feature of myofibroblast (**Figure 5.5 A)**. No detectable change was found in untreated NOF (**Figure 5.5 C)**.

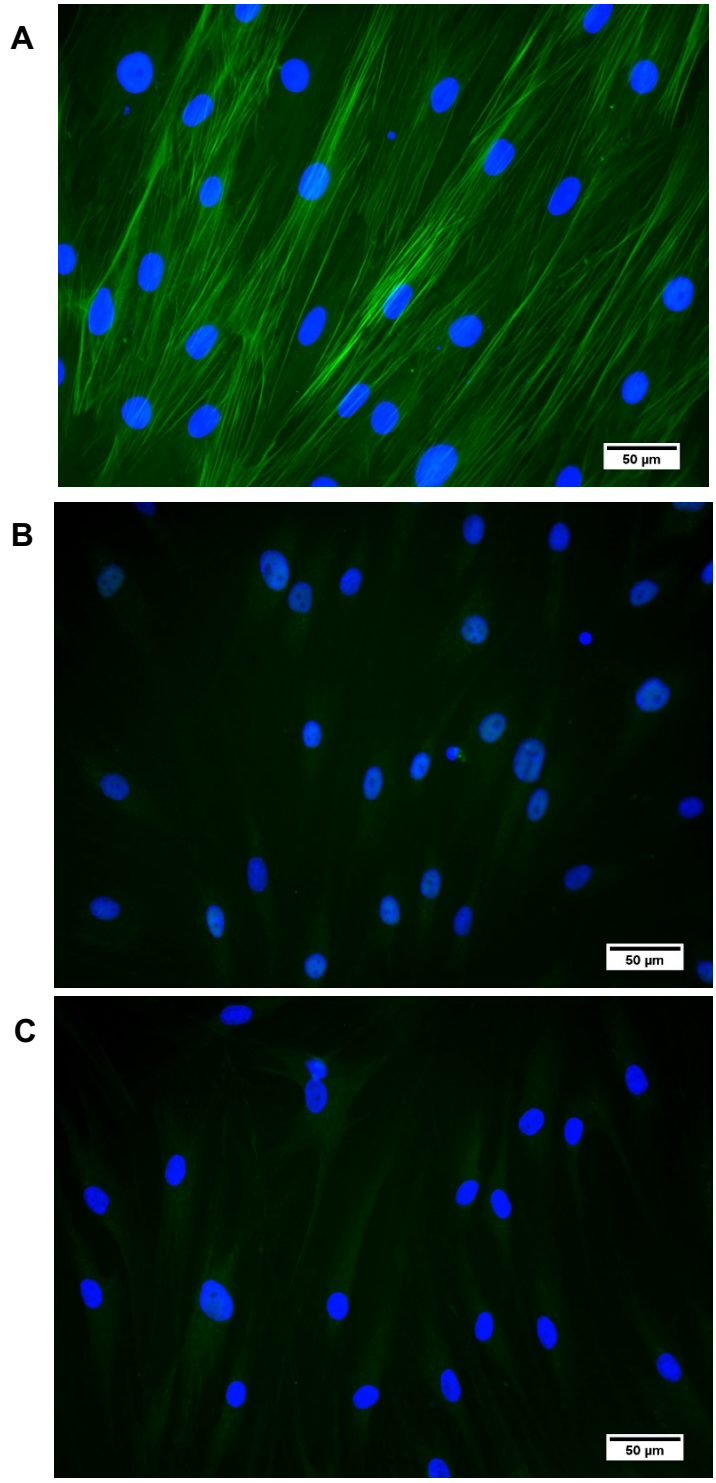

Figure 5.5. Immunofluorescence detection of αSMA stromal marker in NOF treated with myofibroblast EVs compared to TGFβ. NOF cells were treated with TGFβ (10ng/ml) and Myofibroblast EVs. (A) Representative image of NOF treated with TGFb shows the αSMA stromal marker. (B) Representative image of NOF treated with myofibroblast EVs with little or no detectable αSMA. (C) Representative image of untreated NOF with little or no αSMA.

5.5 Human dental pulp stem cells EVs and their role in angiogenesis and osteogenesis

5.5.1 Characterisation of HDPS cells

According to the International Society for Cellular Therapy (ISCT), three criteria should be used to define MSC subpopulations: adherence to plastic, specific surface antigen, and trilineage mesenchymal differentiation (Dominici *et al*., 2006). Thus, we characterised the osteo-differentiation and STRO-1 MSC marker as a specific surface antigen to define the MSC phenotype of human dental pulp stem (HDPS) cells.

5.5.1.1 Osteogenesis differentiation of human dental pulp stem cells

Human dental pulp cells (HDPS) were isolated from non-carious molar teeth from patients at the Charles Clifford Dental Hospital, Sheffield. HDPS cells showed a spindle-shaped morphologically at initial culture **(Figure 5.6).** To examine the capacity of HDPS for osteo-differentiation cells were cultured with osteogenic media for 21 days. Alizarine red staining showed significant calcium deposition of cells cultured with osteogenic media **(Figure 5.7, A)** compared to those cultured with basal media **(Figure 5.7, B).**

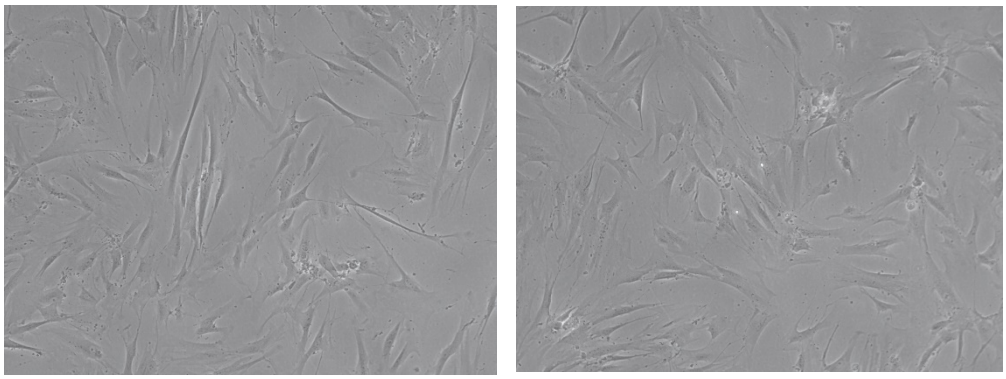

Figure 5.6. Cell morphology of HDPSCs at initial cultures show morphologically spindle shape at initial culture and evidence of their ability to stick to culture plastic. Magnification x10.

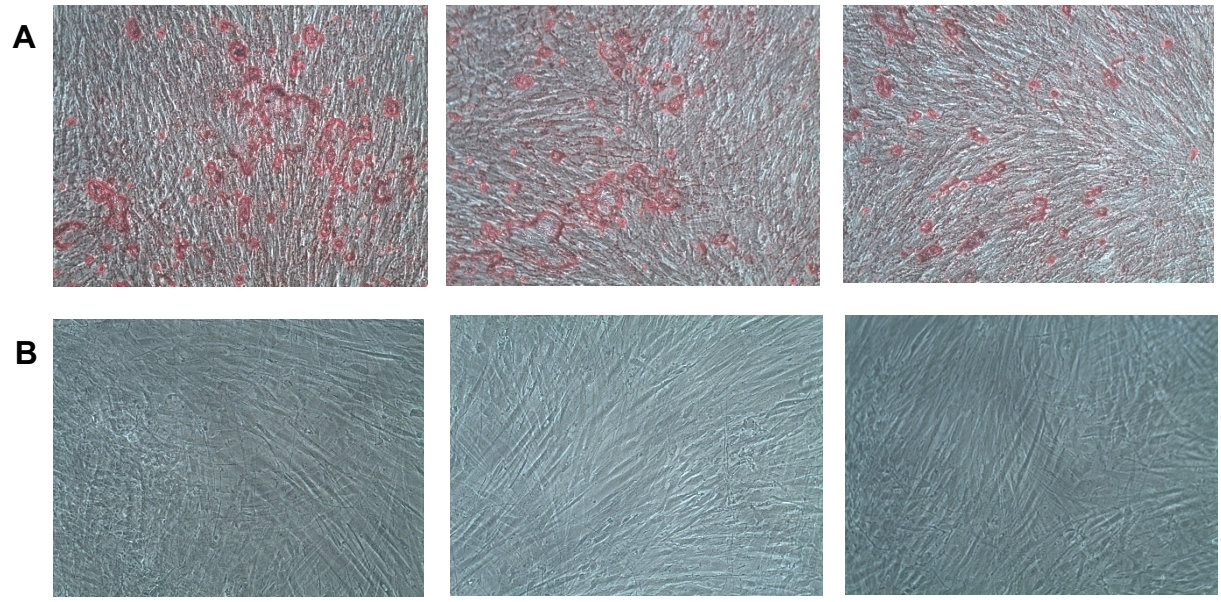

Figure 5.7. Osteogenic differentiation of HDPS cells. HPDS cells were cultured to reach 70% confluency then cultured with osteogenic and basal media for 21 days. Cells then were stained with Alizarine red. (A) Representative images show osteo-differentiation of HDPS cells cultured with osteogenic media. (B) HDPS cultured with basal media with no sign of differentiation. Magnification x10.

5.5.1.2 HDPS cells express mesenchymal stem cells marker (STRO-1)

Stro-1 is the best-known mesenchymal stem cell marker (Lin *et al*., 2011). The expression of STRO-1 was examined by immunofluorescence to further assess the mesenchymal stem cell phenotype of HDPS cells according to ISCT guidelines (Viswanathan *et al*., 2019). After incubation the cells with STRO-1 primary antibody then with DNK anti-mouse FITC secondary antibody, cells were imaged with epi-fluorescent microscope. STRO-1 was expressed in the stained cells (**Figure 5.8, A**). No detectable STRO-1 was found in the cells incubated with secondary antibody only (**Figure 5.8, B**).

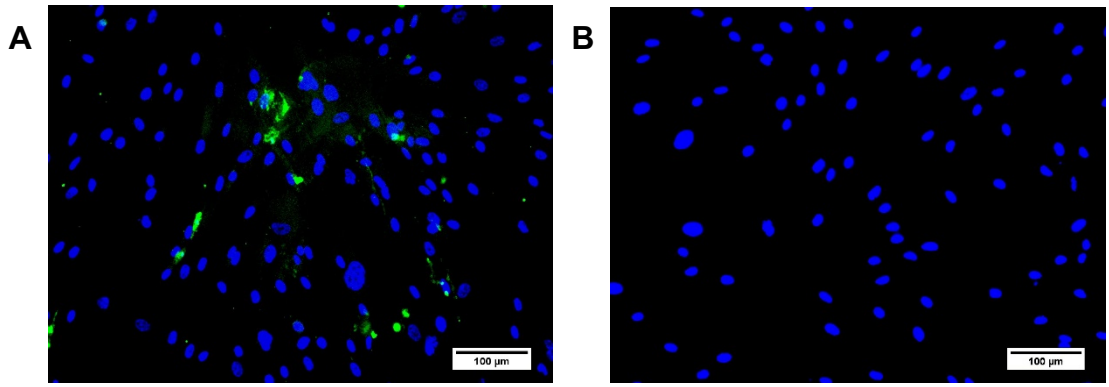

Figure 5.8. Immunofluorescence detection mesenchymal stem cells marker (STRO-1). (A) HDPS cells stained with STRO-1 antibody showed positive STRo-1 marker. (B) No detectable marker in HDPS cells stained with DNK anti-mouse FITC secondary antibody. Magnification 20x.

5.5.2 Role of HDPS derived EVs in inducing the migration of HUVEC cells

Endothelial cell migration is crucial step for vascularisation and angiogenesis (Lamalice *et al*., 2007). Human dental pulp stem (HDPS) cells have been reported to play a role in inducing vasculogenesis (Luzuriaga *et al*., 2020). After successful characterisation of HDPS-derived EVs as described in **Chapter 1****Chapter 3**, they were utilised to examine their ability to induce endothelial cell migration.

Human umbilical vein endothelial cells (HUVEC) are primary cells isolated from the vein of the umbilical cord. Scratch healing assays were utilized to assess the migration of HUVEC cells as described in **Section2.10.3**. Cells were cultured to reach 70% confluency; a scratch was made and then treated with HDPS-derived EVs and EVs-modified scaffold as described in **Table 5.1** below.

Table 5.1. Method of EV delivery and concentration used in HUVEC cells scratch healing assay

Group	Concentration
HDPS EVS	$5.8x10^8$ EVs/ml
HDPS EVs- scaffold	$5.8x10^8$ EVs/ml (incubated with the scaffolds for 24 hours)
Untreated	N/A

With the concentration used in this experiment, no significant effect of HDPS EVs and HDPS EV-modified scaffold on the migration of HUVEC cells was observed compared to the untreated group (**Figure 5.9 A, B**)

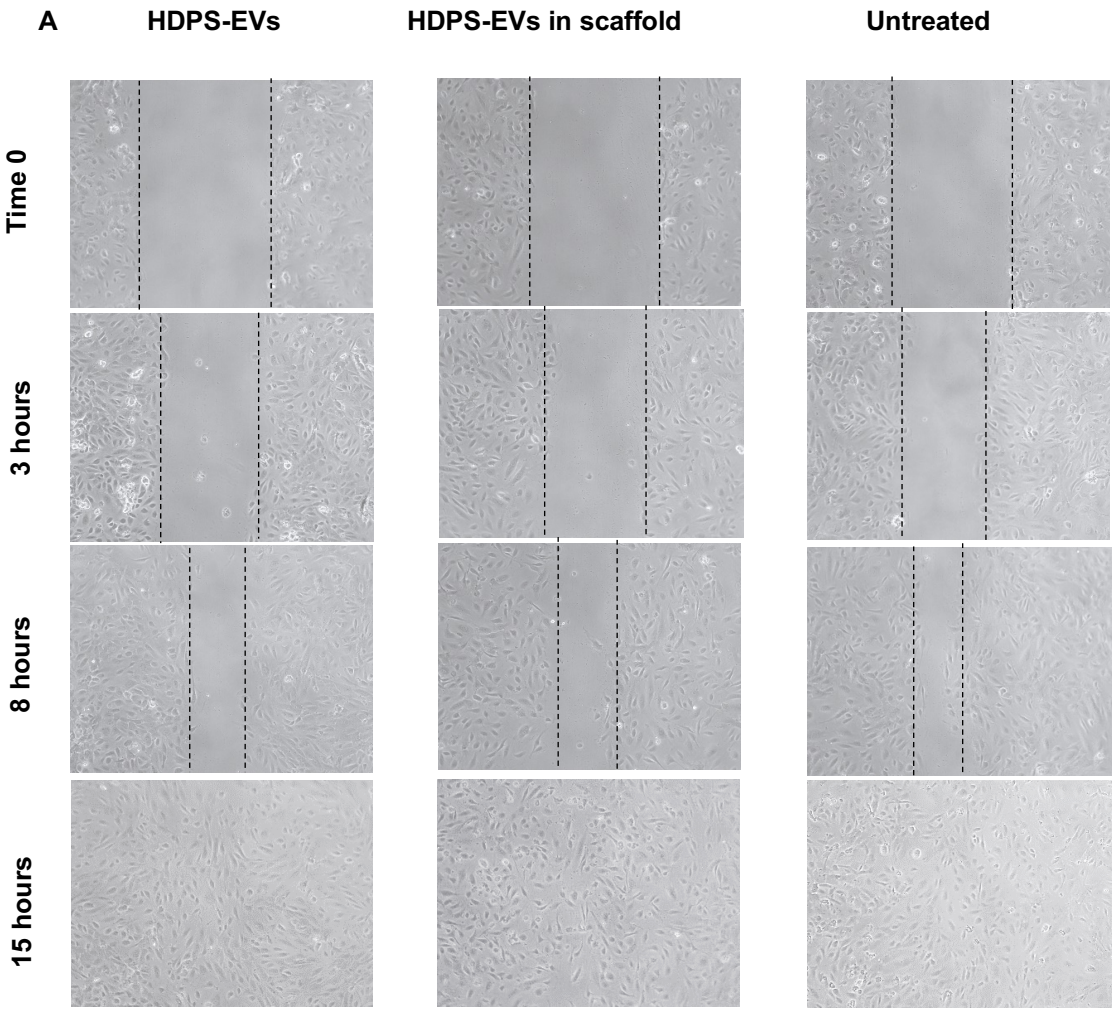
A
HDPS-EVs
HDPS-EVs in scaffold
Untreated
Time 0
3 hours
8 hours
15 hours

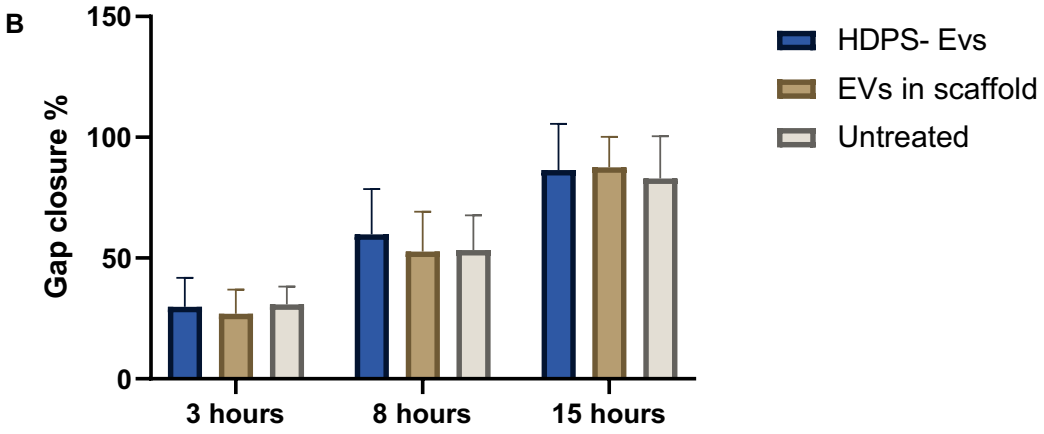
B
Gap closure %
150
100
50
0
3 hours
8 hours
15 hours
HDPS- Evs
EVs in scaffold
Untreated

Figure 5.9. Scratch healing assay to study the effect of HDPS-derived EVs on the migration of HUVEC cells. HUVEC cells were cultured in 24-well plates for 24 h to reach confluency. The next day, cells were scratched using a 200 µl pipette tip and then incubated with EVs and EVs-modified scaffolds for 24 h. The percentage of gap closure was assessed. (A) Representative images of the migration of HUVEC cells were taken at time 0 (immediately following the creation of the wound) and 3,8 and 15 h after the creation of the wound. Images were taken at x10 magnification. (B) No significant effect was found of the EVs and EVs-modified scaffold on the migration of HUVEC cells. Values are expressed as (mean± SD). Error bar = SD

5.1 *Ex-Ovo* study of angiogenic response using a Chorioallantoic membrane (CAM) assay

Chorioallantoic membrane (CAM) assay was used to examine the angiogenic potential of EVs and EVs-modified scaffolds as described in **Section 2.12.** Vascular endothelial growth factor (VEGF) was used as positive control because of its known pro-angiogenic role (Shibuya, 2011). **Figure 5.10** shows a comparison of representative composite images from the CAM assay displays the angiogenic response. The analysis of the vascular density of the area around the samples is shown in **Figure 5.11**.

VEGF showed a high angiogenic effect with a slightly different pattern of vascularization compared to other samples **Figure 5.10 A** VEGF induced the highest amount of vascularisation (21.2% ± 1.8) which was significantly higher than all other groups **Figure 5.11**. HDPS EVs-modified scaffold induced vascularisation around the scaffold with some vessels integrated with scaffold **Figure 5.10 B**. The vascular density around the EVs-modified scaffold was 19.1% ± 0.9 which was comparable to VEGF and significantly higher than HDPS EVs, plasma-treated PCL and PCL scaffold

Figure 5.11. It is noteworthy that HDPS cells derived EVs alone, in the absence of scaffold, showed a low angiogenic response (**Figure 5.10 F, Figure 5.11)**.

The conditioned media of HDPS cells was obtained from confluent cells cultured for three days also showed an angiogenic response in the CAM assay **Figure 5.10 C**. The vascular density was 16.5% ± 2.7 which was significantly higher than both HDPS EVs and PCL scaffold **Figure 5.11**.

The plasma treatment of PCL scaffold showed an increased angiogenic response **Figure 5.10** compared to the untreated scaffold. The vascular density in response to the plasma-treated scaffold was 14.8 ± 1.9, comparable to the response to conditioned media. The lowest vascular density was shown around PCL scaffold **Figure 5.10 E** which was around 9.8% ± 0.5 **Figure 5.11**.

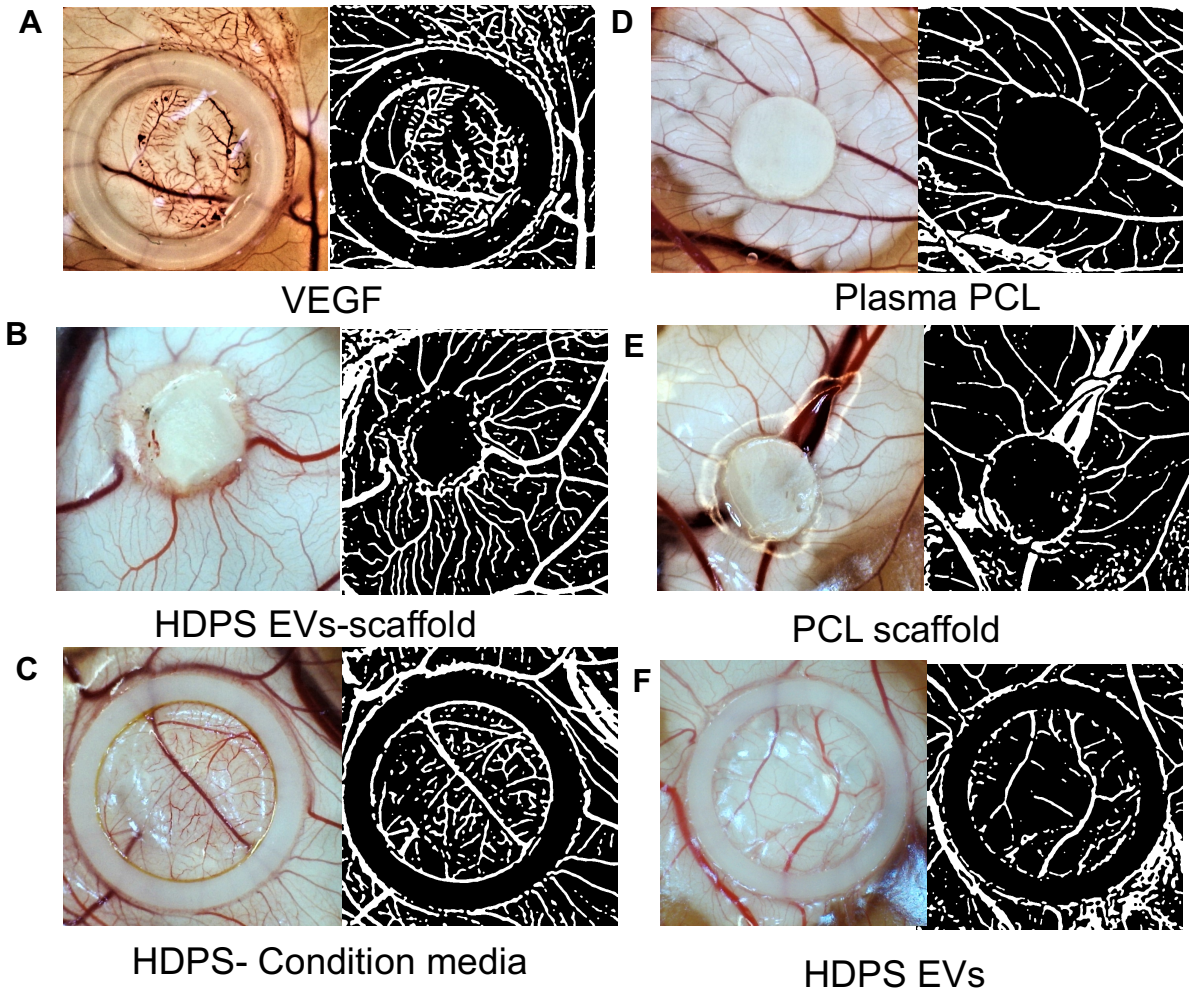

Figure 5.10. Angiogenic response of CAM when cultured with EVs and EVs-modified scaffold. Following cultured the samples with CAM at EDD 7 for 5 days, images were taken at EDD 12 to assess the vascular density. Representative images show the vascularisation response of each group at time of imaging (Left image) and capillary network profile used for analysis (Right images). Silicon rings were used to hold VEGF, EVs and conditioned media.

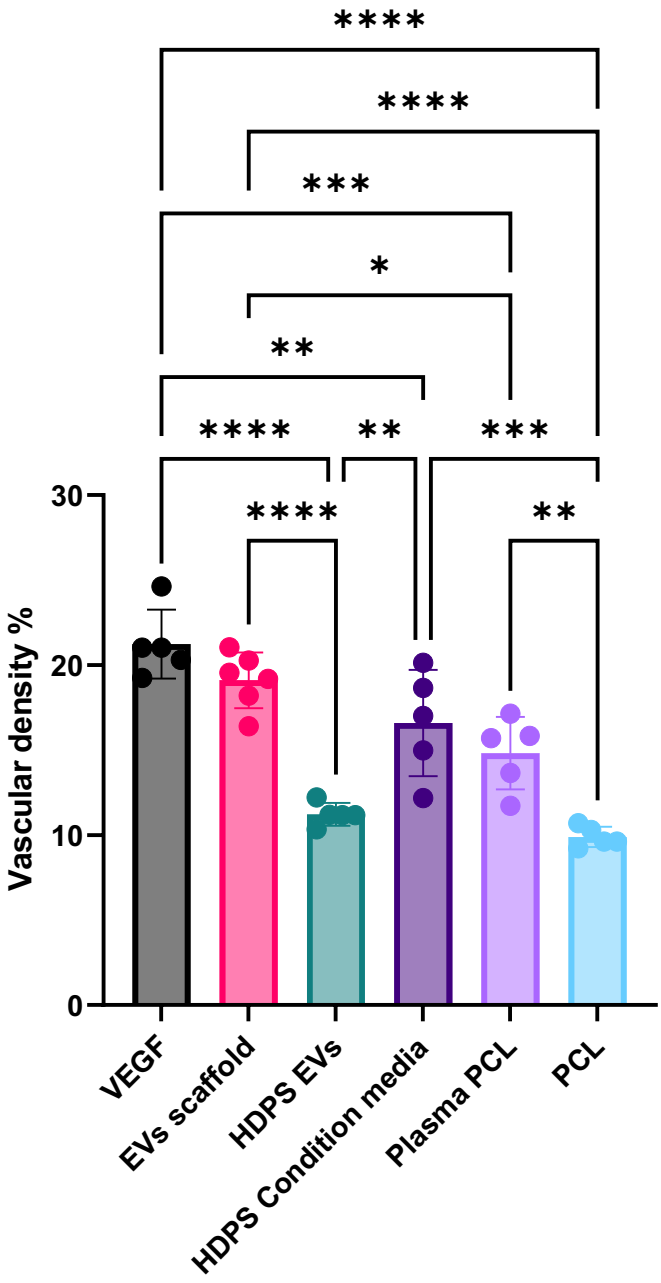

Figure 5.11. Vascular density of CAM assay when cultured with EVs and EVs-modified scaffold. Vascularisation response was assessed using the CAM capillary network profile images taken at EDD 12. Highly significant angiogenic response of HDPS EVs-modified scaffold comparable to VEGF. Data represented n=5, mean ± STDV following One-way ANOVA statistical analysis with Tukey comparison test. **** p < 0.0001 , *** p < 0.001, ** p < 0.01, * p < 0.05. Error bar = STDV.

5.6 Assessment of the ability of EVs and EVs-modified scaffolds to induce osteogenic differentiation

The functionality of human dental pulp stem (HDPS) cells EVs was further assessed by examining the ability to stimulate osteo-differentiation of MSC. Rat MSCs were cultured to reach confluency then treated with media and EVs as described in **section 2.13**. Alizarine red staining and alkaline phosphatase activity were used to examine the ability of the samples to differentiate MSC cells towards a mineralising phenotype. Alizarine red staining data (**Figure 5.12**) showed that osteogenic media significantly induced osteo-differentiation of rMSC. No detectable effect was observed of HDPS condition media, HDPS EVs HDPS EVs-modified scaffold on inducing the mineralization which was comparable to the basal media (negative control). Likewise, ALP activity assay (**Figure 5.13**) showed significant mineralization in response to osteogenic media group on days 7, 14 and 21, but little or no mineralization was detected in response to either EV alone, EV-modified scaffold or scaffold alone (**Figure 5.13**).

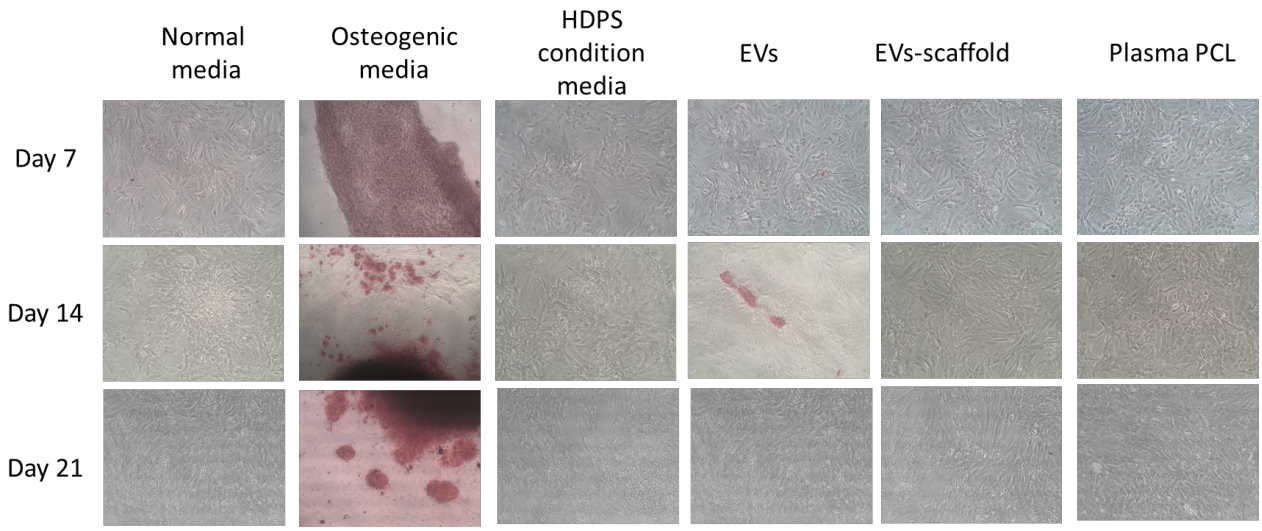

Figure 5.12. Representative photomicrographs of alizarin red stained rat MSC following exposure to osteogenic media, HDPS EVS and HDPS modified scaffold for 21 days. Rat MSCs cells were cultured to reach confluency then treated with osteogenic media, HDPS EVs, HDPS condition media, HDPS EVs-modified scaffold. On day 7, 14 and 21, cells were fixed, stained with Alizarine Red staining and imaged under a light microscope. Cells treated with Osteogenic media showed a high level of mineralization. No detectable mineralization was found in other groups except minor differentiation on EVs group in day 14. Magnification 10x.

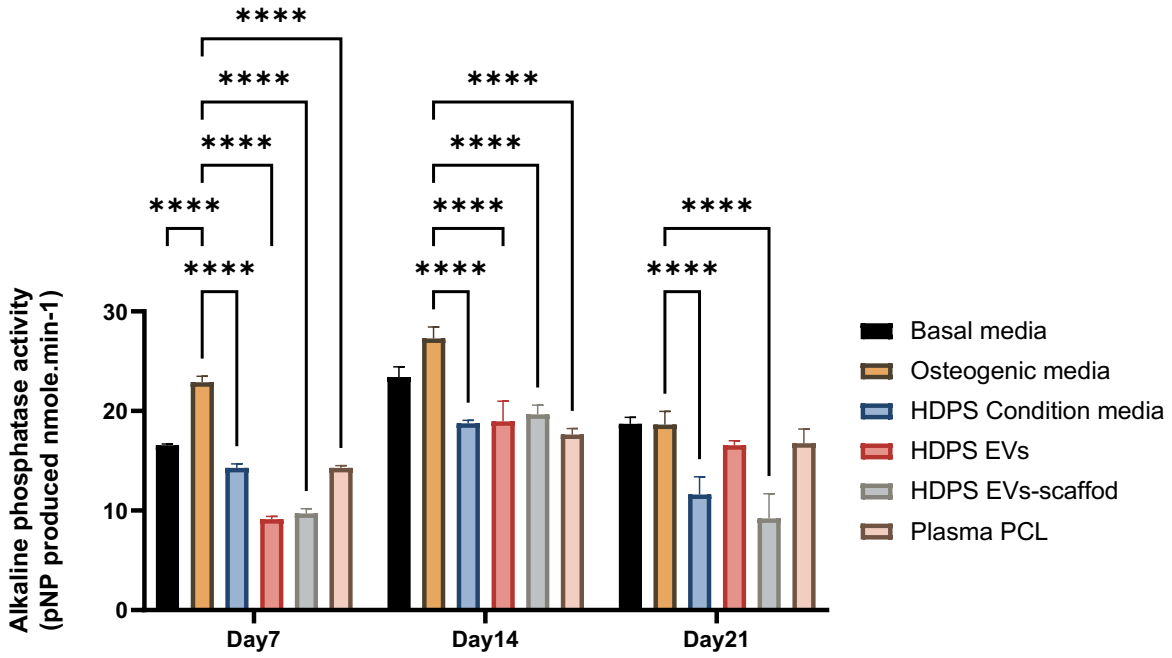

Figure 5.13. Alkaline phosphatase activity of rat MSCs following exposure to osteogenic media, HDPS EVs and HDPS EVs-modified scaffold for 21 days. Rat MSCs were cultured to reach confluency then treated with osteogenic media, HDPS EVs, HDPS condition media, HDPS EVs-modified scaffold. On days 7, 14 and 21, ALP activity was assessed. Cells treated with Osteogenic media showed the highest level of ALP activity. No significant mineralization was found in the other groups. Data represented n=3, mean ± STDV following Two-way ANOVA statistical analysis with Tukey's multiple comparison test. **** p < 0.0001. Error bar = STDV.

5.7 Discussion

Increased understanding of the diversity of physiological and pathological roles of EV has sparked significant interest in their potential in cells-free tissue engineering (Alqurashi *et al*., 2021) and as therapeutic agents (Claridge *et al*., 2021) in recent years. In the previous chapter (**Chapter 4**), EVs were successfully incorporated with plasma-treated electrospun scaffolds and showed promising release kinetic data. To investigate the functionality of EVs from different cell types when incorporated into electrospun scaffolds, in this chapter, we examined the effect of myofibroblast-derived EVs in wound healing and HDPS EVs in wound healing, angiogenesis and osteogenesis.

Wound healing is a sophisticated physiological process involving various cell types, extracellular matrix (ECM) components, and other elements that occurs in four partially overlapping interdependent stages (hemostasis, inflammation, granulation tissue development, and remodelling) (Takeo *et al*., 2015). Fibroblasts and myofibroblasts play a critical part in the development of new tissue in healing wounds by secreting and remodelling the extracellular matrix. In granulation tissue, a key phase in wound healing, stimulated fibroblasts gain α-SMA expression and transform into myofibroblasts (Desmouliere *et al*., 2014). Myofibroblasts exhibit contractile properties, because α-SMA is expressed in microfilament bundles, and play an important role in the contraction of the wound edges (Hinz *et al*., 2003).

Transforming growth factor (TGF)-β1 is the prototypic inducer of myofibroblast differentiation from all precursor cell types (Scharenberg *et al*., 2014). Similarly, our data showed that TGF-β induced differentiation of normal oral fibroblast (NOF) cells and exhibited myofibroblastic characteristics as α-SMA stromal marker.

Myofibroblast secreted EVs have been reported to play a role in wound healing. Merjaneh *et al*., (2017) found that dermal myofibroblast-derived EVs induced endothelial cell migration and capillary formation. Similarly, Arif *et al*. (2020) showed that skin myofibroblast EVs stimulated that migration of skin fibroblast cells. Although establishing direct comparison between the studies is difficult due the different cell source and method of EVs isolation, our data showed that NOF (normal oral fibroblast) derived myofibroblast EVs failed to induce the migration of NOF cells using scratch healing assay.

In order to further examine whether treatment of NOF with myofibroblast EVs could induce myofibroblast differentiation, NOF-derived myofibroblast EVs did not modify the phenotype of NOF cells as assessed by expression of α-SMA stromal marker compared to TGF-β. Likewise, Arif *et al*. (2020) found dermal myofibroblast EVs failed to induce myofibroblast differentiation of cutaneous fibroblast.

In vitro, MSCs are characterized by their ability to adhere to plastic, their expression of a variety of surface antigens (positive: CD90, CD73, CD105; negative: CD34, CD45, CD11b), and their adipogenic, osteogenic, and chondrogenic capabilities (Pera *et al*., 2004). The mesenchymal stem cells phenotype of HDPS cells used in this project have been characterized previously by Solis-Castro *et al*., (2020), they found that HDPS cells were able to differentiate *in-vitro* into neural-like cells and expressed neural crest-related marker. Our results also suggested the ability of HDPS cells to differentiate to bone-like cells. In addition, some HDPS cells were positive to mesenchymal stem cells marker (STRO-1). This data shows that HDPS can be referred as stem cells according to the definition of the International Society for Cellular Therapy (ISCT) (Viswanathan *et al*., 2019).

Due to an established understanding of the regenerative role of HDPS cells, several studies have examined the role of HDPS-derived EVs in tissue regeneration. Merckx, Hosseinkhani, *et al*., (2020) found a positive paracrine effect of HDPS EVs on the migration of endothelial cells. Similarly, using a scratch healing assay, Zhou *et al*., (2020) found that HDPS EVs induced the migration of HUVEC cells. Our data suggested that HDPS EVs, at the concentration used in this project, did not influence the migration of HUVEC cells. Further dose-dependent studies could provide a greater understanding of the effect of HDPS EVs on the migration of HUVEC cells.

Regarding the angiogenetic potential of HDPS EVs and HDPS EVs modified scaffold, an ex-ovo CAM assay was utilised according to the protocol published by Mangir *et al*. (2019). In comparison to other ex vivo, the CAM assay is considered a simple and inexpensive angiogenic screening technique (Merckx, Tay, *et al*., 2020).

Proangiogenic growth factors, such as VEGF or bFGF, are essential regulators released by host tissue cells in response to inflammation or damage. Increasing microvascular permeability and encouraging endothelial cell migration and proliferation are the primary functions of VEGF in the angiogenic process (Abhinand *et al*., 2016). Our data suggested that VEGF positive control induced vascular formation in the CAM model which showed the highest vascular density compared to other samples which also has been proved by previous data within our group (Rodriguez, 2021). Exogenous VEGF usage, on the other hand, has been linked to cancer (Oka et al., 2007), where leaky, permeable, and hemorrhagic blood vessels are found. Thus, it is worthwhile to explore other techniques, such as the prevascularization of tissue engineering scaffolds using pro-angiogenic biomolecules, to induce angiogenesis.

To our knowledge, this is the first time that the CAM model has been employed to examine the functionality of EV in electrospun scaffolds. Interestingly, our data showed a high vascular density induced by HDPS modified scaffold, comparable to the VEGF positive control. This data suggested that the plasma-treated scaffold, which showed sustained release of EVs over 21 days as discussed in Chapter 4, can provide a promising delivery platform of HDPS EVs to induce angiogenesis. This result also suggests that the concentration of EVs incubated with the scaffold used in this project was sufficient to generate an angiogenic response. A further dose-dependent study is needed to obtain a better understanding of the optimal number of EVs for this experiment.

Interestingly, our data also showed that the HDPS conditioned media promoted vascular formation in the CAM assay in excess of the response to HDPS EV alone, which did not induce a statistically significant response. The low vascular activity of HDPS EVs in comparison to HPDS EVs modified scaffold might be explained by that scaffold platform allowing the sustained release of EVs in comparison to an EVs suspension which tend to disperse after application. Future studies may compare EVs modified scaffolds to other EVs delivery platform including hydrogel to draw a better understanding, and also examine other responses with therapeutic potential to scaffolds containing EV, such as osteogenesis and neurogenesis

Unfortunately, because the angiogenic response is often quantified using different methods such as image analysis, histology, or a qualitative grading scale, a direct comparison of CAM data between studies is not always possible. Merckx, Hosseinkhani, *et al*., (2020) used Matrigel to test the angiogenic potential of HDPS EVs in comparison to bone marrow (BM) MSC-derived EVs and their conditioned

media. They found that only bone marrow MSC conditioned media was able to encourage vascular formation on CAM assay.

Plasma treatment of PCL scaffold has shown to increase the cells attachment *in vitro* (Cipitria *et al*., 2011). In CAM assay, our data showed a significant increase in the vascular formation around plasma-treated scaffold compared to untreated PCL scaffold. This could be explained by the increase in the hydrophilicity of plasma-treated scaffold. Gigliobianco et al., (2015) found that following plasma treatment, coating PCL electrospun scaffold with polyethyleneImine (PEI) and polyacrylic Acid (PAC) and one with alternative layers of PEI and heparin showed strong angiogenic activity. Collagen-coated PCL loaded with VEGF was shown to increase vascular formation in CAM assay compared to the scaffolds without VEGF(Singh et al., 2012).

Although non-specific inflammatory reactions are typically considered negligible before embryonic day 15 due to the chicken embryo's immature immune system (Ribatti, 2016), minor inflammation and an associated secondary angio-proliferative response cannot be ruled out as contributors to the effects reported in this thesis.

Regarding the osteogenic potential of HDPS EVs and conditioned media, rat bone MSCs (rBM-MSC) cells were selected to test the ability of HDPS EVS to stimulate osteo-differentiation. Osteogenic media significantly induced the differentiation of rMSC. Our data, however, found no significant effect of HDPS EVs nor the conditioned media on the osteo-differentiation rBM-MSC. To the best of our knowledge, no other study has tested the osteo-differentiation of rBM-MSC using HDPS EVs. However, using different cells, Jin *et al*., (2020) found that HDPS-EVs induced the osteo-differentiation of human adipose-derived stem cells. Qin *et al*., (2016) examined the effect of human BM-MSC EVs on the mineralization and osteoblastic differentiation of human osteoblasts. They found that BM-MSC EVs increased the calcium deposition

and ALP activity was highly induced comparable to the osteogenic media group. The source of EVs used in this project was form human and test in rat cells, future experiments may consider species-specific effects and study the osteogenesis effect using a different source of EVs on various cells to reach to better understanding of the best source of EVs and optimal cells to test the osteogenesis.

Despite the promising results of this project of using HDPS EVs to induce angiogenesis, further studies are needed to establish a better understanding of EVs and EVs modified scaffolds. First, future work would involve re-working these experiments using dose-dependent EVs to determine the optimal dose of EVs needed for tackling the regeneration process. Additionally, as HDPS cells used in this project are able to differentiate into sensory neuron-like cells, this work will provide a platform from which to assess the effect of HDPS EVs, and the potential application of the scaffolds developed here, in the context of neurological pathology and pain. Furthermore, further research into the mechanism of EV cargo delivery would provide a better understanding of the interaction between vesicles and cells *in vitro* and *in vivo*. In addition, the precise mechanism by which HDPS EVs scaffolds induce angiogenesis remains to be elucidated. More research may include other EVs delivery platforms and EVs from other cell types to draw better conclusion in comparison to plasma treated scaffold.

5.8 Conclusion

In the previous chapter, successful manufacturing of EVs-modified scaffolds was achieved using plasma-treated scaffold to provide sustained release of EVs. In this chapter, we focused on the assessment of the functionality of this platform *in vitro* and ex *vivo*. First, we started by examining the potential role of myofibroblast EVs in wound

healing. Initially, NOF cells were found able to differentiate to myofibroblast using TGFβ, as indicated by the expression of α-SMA stress fibres. Then, we examined the ability of myofibroblast EVs to induce the migration of NOF cells. No effect of myofibroblast EVs or EVs modified scaffold on the migration of NOF cells were found. In addition, myofibroblast EVs were found to be unable to induce the myofibroblast differentiation (as assessed by α-SMA and VCAN expression) of NOF.

Next, the functionality of human dental pulp stem cells derived EVs was assessed in the field of wound healing, angiogenesis and osteogenesis. First, HDPS cells were shown to exhibit MSC phenotype by their capacity for osteogenic differentiation and expression of the MSc marker STRO-1. In a CAM assay angiogenesis model, HDPS EVs modified scaffold was able to induce vascular formation to a comparable level to the positive control, VEGF. Moreover, HDPS conditioned media showed a significant ability to induce angiogenesis. In addition, it was observed that plasma-treated PCL scaffold exhibited significant vascular formation in comparison to untreated PCL. No significant effect of HDPS EVs nor the conditioned media on the osteo-differentiation rBM-MSC

In this chapter, we provide evidence that HDPS EVs can be incorporated into the plasma-treated scaffold and provide a promising platform for inducing angiogenesis which can be used in various tissue engineering applications.

Chapter 6

General discussion and conclusion

6.1 General discussion

The aim of this project was to examine the ability to produce a novel electrospun membrane by combining EVs with polycaprolactone fibres and study its potential use for wound healing, angiogenesis and osteogenesis. The research work conducted to achieve this aim was divided into three sections:

1- The isolation and characterization of EVs (EVs)
2- The fabrication and characterisation of elecrospun scaffolds and modifying electrospun scaffolds with EVs and study the EVs attachment and release kinetics
3- The study of the functionality of EVs- modified scaffold on wound healing, angiogenesis and osteogenesis.

6.2 Extracellular vesicles for cell-free tissue engineering

Tissue engineering combines material science, bioengineering, and transplantation principles with engineering designs to restore, preserve, and enhance cell activities for the regeneration of damaged tissues. One of the most commonly used approaches in tissue engineering is using mesenchymal stem cells due to their function in promoting regeneration (Pittenger *et al*., 2019). Many challenges, however, are faced using stem cells which include but are not limited to increased risk of contamination and damage to genetic material during isolation and expansion (Røsland *et al*., 2009), undesirable differentiation and limited circulation due to large size (Holkar *et al.*, 2020). EVs may offer a higher safety profile than their parent cells since their lack of a nucleus renders them incapable of self-replication and eliminates the possibility of uncontrolled proliferation upon administration. For these reasons, the concept of cell-free tissue engineering using EVs has become of interest as a novel alternative that overcomes

the above highlighted limitations. This approach can be justified by the role of EVs as paracrine mediators during cell-to-cell communication by delivering biomolecules, such as cytokines, proteins, mRNA, and regulatory micro RNAs, to target cells and modulate their behaviours (Yáñez-Mó *et al*., 2015).

One of the current main challenges lies in the development of EV therapies is the absence of a standard technology to isolate and characterise EVs. Thus, The MISEV 2018 recommendation emphasised the need to use multiple, complementary methodologies to assess isolated EVs (Théry *et al*., 2018). In this project, we used two isolation methods and multiple characterisation techniques to assess EVs. Size exclusion chromatography (SEC) was selected to be the isolation method for this project after high levels of aggregation were observed for EVs isolated by Ultracentrifugation (UC). Following the characterisation of SEC fraction, high purity of EVs found by BCA data and EVs markers were detected in SEC fractions 4-11 using western blot, Nanoview and Nano-flowcytometry (nFCM). We have also measured the zetapotential of EVs to understand the role electrostatic charge in interaction and release kinetic of EVs. Interestingly, cancer cells EVs (H357, derived from carcinoma of the tongue) exhibited significantly higher anionic charge compared to non-cancerous primary cells. To the best of our knowledge, this study is the first to report the difference in the zetapotential between cancer and noncancerous derived EVs. Additionally, direct pharmaceutical modification of EV-potential has been demonstrated to have promising anti-cancer benefits (Skalska *et al*., 2019). This may highlight the potential roles of the EVs zetapotential in biotherapeutic field.

6.3 Electrospun scaffold as EVs delivery platform

Due to the multiple challenges of systemic delivery of EVs through intravenous (IV), oral, intranasal, intraperitoneal, and subcutaneous administration include short half-life of EVs in circulation (Takahashi *et al*., 2013) and lacks of tissue specificity (Imai *et al*., 2015), local delivery may overcome these challenges. Particularly, utilising biomaterials to deliver EVs has been found to increase EVs bioavailability at the target site (Pinheiro *et al*., 2018).

Electrospinning has been utilised in this project as an EVs delivery platform due to several key advantages. Firstly, it is a versatile system that can accommodate a wide variety of compounds and offers the ability to incorporate multiple polymers and bioactive compounds. Moreover, due to the nanoscale fibre diameter and high porosity, it gives a very high surface area-to-volume ratio, which is desired for improving active compound delivery even at high loadings (Bhardwaj *et al*., 2010). In addition, polycaprolactone (PCL) was selected as one of the most commonly used polymers in the fields of tissue engineering and regenerative medicine (Woodruff *et al*., 2010).

As PCL is a hydrophobic material, a surface treatment is generally needed to induce hydrophilicity which is reported to increase biocompatibility and cell attachment (Cipitria *et al*., 2011). Plasma and heparin surface treatment are commonly used surface modification techniques in the field of biomaterials. For the application of EVs delivery, Wei *et al*. (2019) used heparin to induce the attachment of EVs to electrospun scaffolds. In addition, Trindade *et al*. (2020) suggested that spinning EVs with polymer solution preserved their structure and function. In this project, we have performed a comprehensive experiment comparing these three techniques (plasma treatment, heparin treatment, incorporating EVs within the electrospinning solution) to assess the

effect of different treatment on the fibre diameter, porosity, and fibre morphology, as well as the EVs attachment and release kinetic.

The data reported here indicate that plasma treatment increased the hydrophilicity of PCL electrospun scaffolds without altering the fibre diameter, morphology or porosity of the scaffold. Interestingly, plasma treatment induced a positive charge on the surface of the scaffold which may explain the high attachment of negatively charged EVs. Additionally, release kinetic data showed that plasma treatment provides sustained release of the EVs from the scaffold. To our knowledge, the data of this project is the first to study a plasma-treated PCL scaffold to be used as EVs delivery platform. In contrast, spinning EVs with polymer changed the fibre morphology of the scaffolds, and heparin treatment was not able to enhance EVs attachment, indicating these are less suitable approaches than plasma-treated PCL.

Nevertheless, future work may need to assess different scaffold materials and compare them to PCL (these could include other polyesther based materials with different degradation profiles, for example, Polylactide-co-glycolide or Polylactic acid). In addition, although air plasma treatment within the parameters used in the project showed promising results, different parameters of air plasma and other forms of plasma treatment including O_2, NH_3, SO_2, CO_2 or other organic compounds would need to be examined for achieving a better understanding regarding EVs delivery mechanisms. In depth understanding of the mechanism of the attachment of EVs to the scaffold also requires further investigation. For example, Quartz Crystal Microbalance with Dissipation Monitoring (QCM-D) (Tonda-Turo *et al*., 2018) may offer more precise data about EVs attachment and release kinetics.

6.4 EVs- modified scaffold for cells free tissue engineering

Following successful fabrication of the EVs-modified scaffolds with encouraging EVs attachment and release, it was important to test the biological functionality of this platform. First, myofibroblast EVs were selected due to the established knowledge about the role of myofibroblast cells in wound healing (Desmouliere *et al*., 2014), and our experience in assessing myofibroblast phenotype(Melling *et al*., 2018). Similarly, human dental pulp stem cells (HDPS) were approved to have an impact on wound healing (Martínez-Sarrà *et al*., 2017), angiogenesis (Bronckaers *et al*., 2013) and osteogenesis (Mortada *et al*. 2018). Thus, this project aimed to assess the regenerative effect of EVs derived from these cells as well as the EVs modified scaffold.

Wound healing occurs in three interconnected dynamic stages that overlap in time. These phases are described based on morphological changes that occur throughout the healing process: the inflammatory phase, the proliferative phase (the production of granulation tissue), and the regeneration phase, which includes maturation, scar formation, and re-epithelialization (Ian *et al*. 2014). In the proliferative phase, fibroblasts are activated, they express alpha smooth muscle actin (α-SMA) and develop into myofibroblasts which produce and deposit ECM components that play an important role in the wound contraction (Hinz *et al*., 2003) and restoration of the wound bed. Despite data by Arif *et al*. (2020) that indicated skin myofibroblast EVs stimulated the migration of skin fibroblast cells, the data of this thesis did not show any effect of myofibroblast derived EVs on the migration of fibroblast cells or their differentiation to myofibroblast.

Angiogenesis is the formation of new blood vessels from pre-existing vessels. To deliver nutrition and oxygen to the interior tissue, the tissue must be vascularised. An inadequate vascular network can lead to infection, loss of function and necrosis(Schreml *et al*., 2010). Tissue engineers have examined using angiogenic and prevascularisation (also known as inosculation of blood vessels) techniques to accelerate the process of vascularizing a tissue construct (Laschke *et al*., 2012), which might otherwise be rejected. Novel methodologies are being used to investigate the utilisation of electrospun scaffold in combination with angiogenic agents to promote angiogenesis (Nazarnezhad *et al*., 2020). For most clinical applications, VEGF continues to be the gold standard for inducing fast and efficient vascularization. Here, the angiogenic effect of HDPS EVs and EVs-modified scaffold was examined.

The Chorioallantoic membrane (CAM) assay is regarded as a straightforward and cost-effective angiogenic screening technique (Merckx *et al*. 2020). Our data showed that our novel HDPS EVs-modified scaffold platform expressed high angiogenic potential comparable to VEGF, the gold standard technique for inducing angiogenesis. Knowing that angiogenesis is the pillar of successful regeneration response (Jahani *et al*. 2020) and challenges facing current approaches to tissue regeneration, this platform may provide a promising way to promote vascularization, which can be used for various tissue engineering applications.

Bone is a highly vascularized tissue that relies on the intimate spatial and temporal interaction between blood vessels and bone cells. Thus, angiogenesis plays a pivotal role in skeletal development and bone fracture repair. Relying on the promising angiogenic potential of HDPS EVs-modified scaffold, we tested the ability of the scaffolds to provoke osteogenesis. Due to the lack of evidence about the best type of cells for osteogenesis assay in this context, we selected the rat bone MSCs (rBM-

MSC) cells due to their availability in our lab, acknowledging the potential for species-specific effects. No significant effect of HDPS EVs nor the conditioned media was observed on the osteo-differentiation of rBM-MSC. These data must be interpreted with caution because of the multiple confounders including the type of cells and number of EVs needed for this *in vitro* experiment and as noted, species differences. In future investigations, it might be possible to use a different source of EVs on various cells with considering species differences, to reach to a better understanding of the best source of EVs and optimal cells to test the osteogenesis.

6.5 Challenges and final thoughts

Despite stem cells' immense therapeutic promise for treating a wide range of critical illnesses, there remain concerns about unanticipated and possibly fatal side effects of such treatments. When it comes to clinical translation, factors like tumorigenesis and immunogenicity must be carefully considered (Herberts *et al*., 2011). Extracellular vesicle treatments, however, avoid some of these difficulties and constraints associated with the use of live cells while maintaining the therapeutic benefit of complex biological agents. Furthermore, EVs have several features that make them attractive for the development of medicinal solutions. Their small size enables for simple filtration sterilising of samples, and their lipidic membrane protects the biologically active cargo, perhaps allowing for a longer shelf-life and half-life in patients.

However, from a regulatory standpoint, EVs are to be regarded as a biological medicinal product. The European Medicines Agency (EMA) and agencies on other continents have already established manufacturing and clinical trial procedures. Thus, regulatory compliance is crucial in the development of extracellular vesicle

therapeutics to get a manufacturing licence and eventually a market authorisation. In a position paper, the international association of extracellular vesicles (ISEV) illustrated the regulatory aspects of EV-based therapeutics including safety and manufacturing requirements which should be carefully considered before using EVs in clinical trials (Lener *et al*., 2015).

Finally, despite there currently being no defined composition and therapeutic mechanism of action for each proposed EV use, EVs may provide a tempting off-the-shelf, cell-free treatment alternative that may be safer, more successful, cost-effective compared to employing stem cells.

6.6 Conclusion

The aim of this project was to optimise the functionalisation of electrospun scaffolds with EVs and to evaluate biological functionality for their future use in tissue engineering applications. The conclusions of this project are as follow:

1) EVs were successfully isolated from H357, NOF and HDPS cells *in vitro*.
2) The characterization of EVs including quantification, EV marker, zetapotential and microscopic morphology showed that:
    a. Cancer cells produce more EV than normal primary cells.
    b. EVs isolated by ultracentrifugation tend to aggregate in comparison to dispersed EVs isolated by size exclusion chromatography
    c. EVs isolated by SEC express high purity.
    d. EVs isolated from different cell types expressed EVs marker CD9, CD 63 and CD81.
    e. All EVs exhibited anionic character regardless of the cell type with a significantly higher anionic character of H357 EVs compared to primary cells EVs.
3) PCL electrospun scaffold was successfully fabricated using a DCM and DMF solvent system and treated with air plasma and heparin.
    A. Plasma and heparin treatment did not alter fibre diameter or porosity of PCL scaffolds.
    B. Plasma-treated scaffolds exhibited a positive zetapotential in comparison to the neutral charge of PCL and highly negative charge of heparin-treated scaffold which may explain the high attachment of negatively charged EVs to plasma-treated scaffolds.

4) Upon modifying the scaffolds with EVs, plasma treatment was the most reliable method for the attachment of EVs to the scaffold. Heparin treatment, however, did not induce sufficient attachment of EVs to the scaffold.
5) Plasma-treated scaffold provided sustained release of EVs.
6) No effect of myofibroblast EVs or EVs-modified scaffold on the migration of NOF cells. In addition, Myofibroblast EVs were found unable to induce the myofibroblast differentiation of NOF cells.
7) HDPS cells were found to exhibit an MSC phenotype by their ability to undergo osteogenic differentiation and by expressing STRO-1 MSC marker.
8) In the CAM assay angiogenesis model, HDPS EVs modified scaffolds were able to induce vascular formation at a level comparable to VEGF. Moreover, HDPS conditioned media showed a significant ability to induce angiogenesis. We also found that plasma treated PCL scaffold exhibited significant vascular formation in comparison to untreated PCL.
9) Osteogenesis assay showed no significant effect of HDPS EVs nor the conditioned media on the osteo-differentiation rat bone marrow MSCs Cells.

6.7 Future work

The data presented in this thesis have demonstrated the potential of plasma-treated PCL electrospun scaffolds to be modified with EVs and offer sustained release as well as provide a promising platform for inducing angiogenesis, and possibly other regenerative responses, which can be used in various tissue engineering applications. However, additional work needs to be done to expand our knowledge regarding the manufacturing process, EVs delivery and functionality. The following research activities are suggested as a continuation of the work presented in this thesis:

1- More studies in EVs isolation to increase consistency and the yield of EVs to be used for biotherapeutics.
2- The significantly greater negative charge of cancer cell EVs compared to normal cells may influence their role in cancer progression which needs further investigation.
3- Further optimisation of the effect of different surface treatments of the scaffold includes Ar, O_2 plasma treatment and others on the surface zetapotential.
4- In depth understanding of the mechanism of the attachment of EVs to the scaffold and release kinetic.
5- Functionalize the EVs by modifying gene expression (for example, by incorporating specific microRNA) and study the cell response.
6- Loading EVs with antimicrobials such as linezolid and studying antimicrobial activity of EV modified scaffold *in vitro*.
7- Study the angiogenic potential of EVs modified scaffold *in vivo*.
8- Study other biological functions with relevance to regenerative medicine, such as neurogenesis

COVID-19 impact statement

COVID-19 pandemic has affected the whole world and altered many plans. Due to the complete lockdown from March 2020 to August 2020 and limited lab access with maximum 10 hours per week from August 2020 to April 2021, we were not able to complete some of the planned objectives of this project. The future work section 6.7 includes some of the objectives that were affected by COVID restriction.

References

Abels, Erik R. and Breakefield, Xandra O. (2016), Introduction to Extracellular Vesicles: Biogenesis, RNA Cargo Selection, Content, Release, and Uptake. *Cellular and Molecular Neurobiology*, 36(3): 301–312.

Abhinand, Chandran S., Raju, Rajesh, Soumya, Sasikumar J., Arya, Prabha S. and Sudhakaran, Perumana R. (2016), VEGF-A/VEGFR2 Signaling Network in Endothelial Cells Relevant to Angiogenesis. *Journal of Cell Communication and Signaling*, 10(4): 347–354.

Admyre, Charlotte, Johansson, Sara M., Qazi, Khaleda Rahman, Filén, Jan-Jonas, Lahesmaa, Riitta, Norman, Mikael, Neve, Etienne P. A., Scheynius, Annika and Gabrielsson, Susanne (2007), Exosomes with Immune Modulatory Features Are Present in Human Breast Milk. *The Journal of Immunology*, 179(3): 1969–1978.

Agarwal, Seema, Wendorff, Joachim H. and Greiner, Andreas (2008), Use of Electrospinning Technique for Biomedical Applications. *Polymer*, 49(26): 5603–5621.

Akers, Johnny C., Gonda, David, Kim, Ryan, Carter, Bob S. and Chen, Clark C. (2013), Biogenesis of Extracellular Vesicles (EV): Exosomes, Microvesicles, Retrovirus-like Vesicles, and Apoptotic Bodies. *Journal of Neuro-Oncology*, 113(1): 1–11.

Aliotta, Jason M., Sanchez-Guijo, Fermin M., Dooner, Gerri J., Johnson, Kevin W., Dooner, Mark S., Greer, Kenneth A., Greer, Deborah, Pimentel, Jeffrey, Kolankiewicz, Luiz M., Puente, Napoleon, Faradyan, Sam, Ferland, Paulette, Bearer, Elaine L., Passero, Michael A., Adedi, Mehrdad, Colvin, Gerald A. and Quesenberry, Peter J. (2007), Alteration of Marrow Cell Gene Expression, Protein Production, and Engraftment into Lung by Lung-Derived Microvesicles:

A Novel Mechanism for Phenotype Modulation. *STEM CELLS*.

Alqurashi, Hatim, Ortega Asencio, Ilida and Lambert, Daniel W. (2021), The Emerging Potential of Extracellular Vesicles in Cell-Free Tissue Engineering and Regenerative Medicine. *Tissue Engineering Part B: Reviews*, 27(5): 530–538.

Alvarez-Erviti, Lydia, Seow, Yiqi, Yin, HaiFang, Betts, Corinne, Lakhal, Samira and Wood, Matthew J A (2011), Delivery of SiRNA to the Mouse Brain by Systemic Injection of Targeted Exosomes. *Nature Biotechnology*, 29(4): 341–345.

Anderson, H. C. (1969), VESICLES ASSOCIATED WITH CALCIFICATION IN THE MATRIX OF EPIPHYSEAL CARTILAGE. *The Journal of Cell Biology*, 41(1): 59–72.

Andreu, Zoraida and YÃ¡Ã±ez-MÃ^{3}, MarÃ-a (2014), Tetraspanins in Extracellular Vesicle Formation and Function. *Frontiers in Immunology*, 5.

Arab, Tanina, Mallick, Emily R., Huang, Yiyao, Dong, Liang, Liao, Zhaohao, Zhao, Zezhou, Gololobova, Olesia, Smith, Barbara, Haughey, Norman J., Pienta, Kenneth J., Slusher, Barbara S., Tarwater, Patrick M., Tosar, Juan Pablo, Zivkovic, Angela M., Vreeland, Wyatt N., Paulaitis, Michael E. and Witwer, Kenneth W. (2021), Characterization of Extracellular Vesicles and Synthetic Nanoparticles with Four Orthogonal Single-particle Analysis Platforms. *Journal of Extracellular Vesicles*, 10(6).

Arif, Syrine, Larochelle, Sébastien and Moulin, Véronique J. (2020), PLGF-1 Contained in Normal Wound Myofibroblast-Derived Microvesicles Stimulated Collagen Production by Dermal Fibroblasts. *Journal of Cell Communication and Signaling*, 14(4): 427–438.

Asran, A. Sh, Salama, M., Popescu, C. and Michler, G. H. (2010), Solvent Influences the Morphology and Mechanical Properties of Electrospun Poly(L-Lactic Acid)

Scaffold for Tissue Engineering Applications. *Macromolecular Symposia*, 294(1): 153–161.

Balkom, Bas W.M.van, Jong, Olivier G.de, Smits, Michiel, Brummelman, Jolanda, Ouden, Krista den, Bree, Petra M.de, Eijndhoven, Monique A.J.van, Pegtel, D. Michiel, Stoorvogel, Willem, Würdinger, Thomas and Verhaar, Marianne C. (2013), Endothelial Cells Require MiR-214 to Secrete Exosomes That Suppress Senescence and Induce Angiogenesis in Human and Mouse Endothelial Cells. *Blood*, 121(19): 3997–4006.

Bauer, T. W. (2007), Bone Graft Substitutes. *Skeletal Radiology*, 36(12): 1105–1107.

Berthiaume, François, Maguire, Timothy J. and Yarmush, Martin L. (2011), Tissue Engineering and Regenerative Medicine: History, Progress, and Challenges. *Annual Review of Chemical and Biomolecular Engineering*, 2(1): 403–430.

Beyar, R., 2011. Challenges in organ transplantation. Rambam Maimonides medical journal, 2(2).

Bhardwaj, Nandana and Kundu, Subhas C. (2010), Electrospinning: A Fascinating Fiber Fabrication Technique. *Biotechnology Advances*, 28(3): 325–347.

Bhowmick, Neil A., Chytil, Anna, Plieth, David, Gorska, Agnieszka E., Dumont, Nancy, Shappell, Scott, Washington, M. Kay, Neilson, Eric G. and Moses, Harold L. (2004), TGF-ß Signaling in Fibroblasts Modulates the Oncogenic Potential of Adjacent Epithelia. *Science*, 303(5659): 848–851.

Böing, Anita N., van der Pol, Edwin, Grootemaat, Anita E., Coumans, Frank A.W., Sturk, Auguste and Nieuwland, Rienk (2014), Single-Step Isolation of Extracellular Vesicles by Size-Exclusion Chromatography. *Journal of Extracellular Vesicles*, 3(1).

Boland, Eugene D., Telemeco, Todd A., Simpson, David G., Wnek, Gary E. and

Bowlin, Gary L. (2004), Utilizing Acid Pretreatment and Electrospinning to Improve Biocompatibility of Poly(Glycolic Acid) for Tissue Engineering. *Journal of Biomedical Materials Research - Part B Applied Biomaterials*, 71(1): 144–152.

Bosch, Steffi, De Beaurepaire, Laurence, Allard, Marie, Mosser, Mathilde, Heichette, Claire, Chrétien, Denis, Jegou, Dominique and Bach, Jean Marie (2016), Trehalose Prevents Aggregation of Exosomes and Cryodamage. *Scientific Reports*, 6(May): 1–11.

Breakefield, Xandra O and Abels, Erik R (2016), Introduction to Extracellular Vesicles: Biogenesis, RNA Cargo Selection, Content, Release, and Uptake. *Cellular and molecular neurobiology*, 36(3): 3301–312.

Brennan, Meadhbh Á, Renaud, Audrey, Gamblin, Anne-laure, D'Arros, Cyril, Nedellec, Steven, Trichet, Valerie and Layrolle, Pierre (2015), 3D Cell Culture and Osteogenic Differentiation of Human Bone Marrow Stromal Cells Plated onto Jet-Sprayed or Electrospun Micro-Fiber Scaffolds. *Biomedical Materials*, 10(4): 045019.

Bronckaers, Annelies, Hilkens, Petra, Fanton, Yanick, Struys, Tom, Gervois, Pascal, Politis, Constantinus, Martens, Wendy and Lambrichts, Ivo (2013), Angiogenic Properties of Human Dental Pulp Stem Cells (S. Shi, Ed.). *PLoS ONE*, 8(8): e71104.

Can-Herrera, L.A., Ávila-Ortega, A., de la Rosa-García, S., Oliva, A.I., Cauich-Rodríguez, J.V. and Cervantes-Uc, J.M. (2016), Surface Modification of Electrospun Polycaprolactone Microfibers by Air Plasma Treatment: Effect of Plasma Power and Treatment Time. *European Polymer Journal*, 84: 502–513.

Chen, Carol W., Wang, Leo L., Zaman, Samir, Gordon, Jon, Arisi, Maria F., Venkataraman, Chantel M., Chung, Jennifer J., Hung, George, Gaffey, Ann C.,

Spruce, Lynn A., Fazelinia, Hossein, Gorman, Robert C., Seeholzer, Steven H., Burdick, Jason A. and Atluri, Pavan (2018), Sustained Release of Endothelial Progenitor Cell-Derived Extracellular Vesicles from Shear-Thinning Hydrogels Improves Angiogenesis and Promotes Function after Myocardial Infarction. *Cardiovascular Research*, 114(7): 1029–1040.

Chen, Yuxin, Huang, Junfei, Chen, Ruosi, Yang, Lunan, Wang, Jin, Liu, Bingcheng, Du, Lijuan, Yi, Yanhua, Jia, James, Xu, Yanwei, Chen, Qian, Ngondi, Djakaya Guydidier, Miao, Yong and Hu, Zhiqi (2020), Sustained Release of Dermal Papilla-Derived Extracellular Vesicles from Injectable Microgel Promotes Hair Growth. *Theranostics*, 10(3): 1454–1478.

Chernyshev, Vasiliy S., Rachamadugu, Rakesh, Tseng, Yen Hsun, Belnap, David M., Jia, Yunlu, Branch, Kyle J., Butterfield, Anthony E., Pease, Leonard F., Bernard, Philip S. and Skliar, Mikhail (2015), Size and Shape Characterization of Hydrated and Desiccated Exosomes. *Analytical and Bioanalytical Chemistry*, 407(12): 3285–3301.

Chew, Jacob Ren Jie, Chuah, Shang Jiunn, Teo, Kristeen Ye Wen, Zhang, Shipin, Lai, Ruenn Chai, Fu, Jia Hui, Lim, Lum Peng, Lim, Sai Kiang and Toh, Wei Seong (2019), Mesenchymal Stem Cell Exosomes Enhance Periodontal Ligament Cell Functions and Promote Periodontal Regeneration. *Acta Biomaterialia*, 89: 252–264.

Chiang, Chun Yi and Chen, Chihchen (2019), Toward Characterizing Extracellular Vesicles at a Single-Particle Level Tse-Hua Tan. *Journal of Biomedical Science*, 26(1): 1–10.

Chong, M.S.K., Lee, C.N. and Teoh, S.H. (2007), Characterization of Smooth Muscle Cells on Poly(ε-Caprolactone) Films. *Materials Science and Engineering: C*,

27(2): 309–312.

Christen, Marie-Odile and Vercesi, Franco (2020), Polycaprolactone: How a Well-Known and Futuristic Polymer Has Become an Innovative Collagen-Stimulator in Esthetics. *Clinical, Cosmetic and Investigational Dermatology*, Volume 13: 31–48.

Cipitria, A., Skelton, A., Dargaville, T. R., Dalton, P. D. and Hutmacher, D. W. (2011), Design, Fabrication and Characterization of PCL Electrospun Scaffolds - A Review. *Journal of Materials Chemistry*, 21(26): 9419–9453.

Claridge, Bethany, Lozano, Jonathan, Poh, Qi Hui and Greening, David W. (2021), Development of Extracellular Vesicle Therapeutics: Challenges, Considerations, and Opportunities. *Frontiers in Cell and Developmental Biology*, 9(September).

Colombo, Marina, Raposo, Graça and Théry, Clotilde (2014), Biogenesis, Secretion, and Intercellular Interactions of Exosomes and Other Extracellular Vesicles. *Annual Review of Cell and Developmental Biology*, 30(1): 255–289.

Conde, Ian, Shrimpton, Corie N, Thiagarajan, Perumal and Lo, A (2015), Tissue-Factor – Bearing Microvesicles Arise from Lipid Rafts and Fuse with Activated Platelets to Initiate Coagulation. *Bloodjournal*, 106(5): 1604–1612.

Copes, Francesco, Chevallier, Pascale, Loy, Caroline, Pezzoli, Daniele, Boccafoschi, Francesca and Mantovani, Diego (2019), Heparin-Modified Collagen Gels for Controlled Release of Pleiotrophin: Potential for Vascular Applications. *Frontiers in Bioengineering and Biotechnology*, 7.

Costa Verdera, Helena, Gitz-Francois, Jerney J., Schiffelers, Raymond M. and Vader, Pieter (2017), Cellular Uptake of Extracellular Vesicles Is Mediated by Clathrin-Independent Endocytosis and Macropinocytosis. *Journal of Controlled Release*, 266(July): 100–108.

Costoya, Alejandro, Ballarin, Florencia Montini, Llovo, Jose, Concheiro, Angel, Abraham, Gustavo A. and Alvarez-Lorenzo, Carmen (2016), HMDSO-Plasma Coated Electrospun Fibers of Poly(Cyclodextrin)s for Antifungal Dressings. *International Journal of Pharmaceutics*, 513(1–2): 518–527.

Creasey, Rhiannon, Sharma, Shiwani, Gibson, Christopher T., Craig, Jamie E., Ebner, Andreas, Becker, Thomas, Hinterdorfer, Peter and Voelcker, Nicolas H. (2011), Atomic Force Microscopy-Based Antibody Recognition Imaging of Proteins in the Pathological Deposits in Pseudoexfoliation Syndrome. *Ultramicroscopy*, 111(8): 1055–1061.

Cunnane, Eoghan M., Weinbaum, Justin S., O'Brien, Fergal J. and Vorp, David A. (2018), Future Perspectives on the Role of Stem Cells and Extracellular Vesicles in Vascular Tissue Regeneration. *Frontiers in Cardiovascular Medicine*, 5(July): 1–12.

D'Souza-Schorey, Crislyn and Schorey, Jeffrey S. (2018), Regulation and Mechanisms of Extracellular Vesicle Biogenesis and Secretion. *Essays In Biochemistry*, 62(2): 125–133.

Desmouliere, Alexis, Darby, Ian Andrew, Laverdet, Betty and Bonté, Frédéric (2014), Fibroblasts and Myofibroblasts in Wound Healing. *Clinical, Cosmetic and Investigational Dermatology*: 301.

Van Deun, Jan, Mestdagh, Pieter, Sormunen, Raija, Cocquyt, Veronique, Vermaelen, Karim, Vandesompele, Jo, Bracke, Marc, De Wever, Olivier and Hendrix, An (2014), The Impact of Disparate Isolation Methods for Extracellular Vesicles on Downstream RNA Profiling. *Journal of Extracellular Vesicles*, 3(1).

Diomede, Francesca, D'Aurora, Marco, Gugliandolo, Agnese, Merciaro, Ilaria, Ettorre, Valeria, Bramanti, Alessia, Piattelli, Adriano, Gatta, Valentina, Mazzon,

Emanuela, Fontana, Antonella and Trubiani, Oriana (2018), A Novel Role in Skeletal Segment Regeneration of Extracellular Vesicles Released from Periodontal-Ligament Stem Cells. *International Journal of Nanomedicine*, 13: 3805–3825.

Doherty, Gary J. and McMahon, Harvey T. (2009), Mechanisms of Endocytosis. *Annual Review of Biochemistry*, 78(1): 857–902.

Dominici, M., Le Blanc, K., Mueller, I., Slaper-Cortenbach, I., Marini, F.C, Krause, D.S., Deans, R.J., Keating, A., Prockop, D.J. and Horwitz, E.M. (2006), Minimal Criteria for Defining Multipotent Mesenchymal Stromal Cells. The International Society for Cellular Therapy Position Statement. *Cytotherapy*, 8(4): 315–317.

Dragovic, R. A., Collett, G. P., Hole, P., Ferguson, D. J.P., Redman, C. W., Sargent, I. L. and Tannetta, D. S. (2015), Isolation of Syncytiotrophoblast Microvesicles and Exosomes and Their Characterisation by Multicolour Flow Cytometry and Fluorescence Nanoparticle Tracking Analysis. *Methods*, 87: 64–74.

Dragovic, Rebecca A., Gardiner, Christopher, Brooks, Alexandra S., Tannetta, Dionne S., Ferguson, David J.P., Hole, Patrick, Carr, Bob, Redman, Christopher W.G., Harris, Adrian L., Dobson, Peter J., Harrison, Paul and Sargent, Ian L. (2011), Sizing and Phenotyping of Cellular Vesicles Using Nanoparticle Tracking Analysis. *Nanomedicine: Nanotechnology, Biology, and Medicine*, 7(6): 780–788.

Du, Lei, Xu, Huaizhong, Zhang, Ying and Zou, Fengyuan (2016), Electrospinning of Polycaprolatone Nanofibers with DMF Additive: The Effect of Solution Proprieties on Jet Perturbation and Fiber Morphologies. *Fibers and Polymers*, 17(5): 751–759.

Elfarnawany, Mai H (2015), Signal Processing Methods for Quantitative Power

Doppler Microvascular Angiography. *Electronic Thesis and Dissertation Repository*, (August).

Enderle, Daniel, Spiel, Alexandra, Coticchia, Christine M., Berghoff, Emily, Mueller, Romy, Schlumpberger, Martin, Sprenger-Haussels, Markus, Shaffer, Jonathan M., Lader, Eric, Skog, Johan and Noerholm, Mikkel (2015), Characterization of RNA from Exosomes and Other Extracellular Vesicles Isolated by a Novel Spin Column-Based Method. *PLoS ONE*, 10(8): 1–19.

Escrevente, Cristina, Keller, Sascha, Altevogt, Peter and Costa, Júlia (2011), Interaction and Uptake of Exosomes by Ovarian Cancer Cells. *BMC Cancer*, 11(1): 108.

European Medicines Agency (2019), ICH Guideline Q3C (R6) on Impurities: Guideline for Residual Solvents. *International Conference on Harmonization of Technical Requirements for Registration of Pharmaceuticals for Human Use*, 31(August): 24.

Feng, Du, Zhao, Wen Long, Ye, Yun Ying, Bai, Xiao Chen, Liu, Rui Qin, Chang, Lei Fu, Zhou, Qiang and Sui, Sen Fang (2010), Cellular Internalization of Exosomes Occurs through Phagocytosis. *Traffic*, 11(5): 675–687.

Feng, Xiangru, Li, Jiannan, Zhang, Xi, Liu, Tongjun, Ding, Jianxun and Chen, Xuesi (2019), Electrospun Polymer Micro/Nanofibers as Pharmaceutical Repositories for Healthcare. *Journal of Controlled Release*, 302: 19–41.

Ferreira, Andrea da Fonseca and Gomes, Dawidson Assis (2018), Stem Cell Extracellular Vesicles in Skin Repair. *Bioengineering*, 6(1): 4.

Formhals, Anton (1934), US Patent 1,975,504. : 1–4.

Fröhlich, Eleonore (2012), The Role of Surface Charge in Cellular Uptake and Cytotoxicity of Medical Nanoparticles. *International Journal of Nanomedicine*:

5577.

Gardiner, Chris, Ferreira, Yannick J., Dragovic, Rebecca A., Redman, Christopher W.G. and Sargent, Ian L. (2013), Extracellular Vesicle Sizing and Enumeration by Nanoparticle Tracking Analysis. *Journal of Extracellular Vesicles*, 2(1).

Gardiner, Chris, Vizio, Dolores Di, Sahoo, Susmita, Théry, Clotilde, Witwer, Kenneth W., Wauben, Marca and Hill, Andrew F. (2016), Techniques Used for the Isolation and Characterization of Extracellular Vesicles: Results of a Worldwide Survey. *Journal of Extracellular Vesicles*, 5(1): 1–6.

Gigliobianco, Giulia, Chong, Chuh K and MacNeil, Sheila (2015), Simple Surface Coating of Electrospun Poly-L-Lactic Acid Scaffolds to Induce Angiogenesis. *Journal of Biomaterials Applications*, 30(1): 50–60.

Glowacki, Julie and Mizuno, Shuichi (2008), Collagen Scaffolds for Tissue Engineering. *Biopolymers*, 89(5): 338–344.

Gould, Stephen J. and Raposo, Graça (2013), As We Wait: Coping with an Imperfect Nomenclature for Extracellular Vesicles. *Journal of Extracellular Vesicles*, 2(1).

Graham, John M. (2001), Purification of a Crude Mitochondrial Fraction by Density-Gradient Centrifugation, , in: *Current Protocols in Cell Biology*.

Grant, Barth D. and Donaldson, Julie G. (2009), Pathways and Mechanisms of Endocytic Recycling. *Nature Reviews Molecular Cell Biology*, 10(9): 597–608.

Gronthos, S., Mankani, M., Brahim, J., Robey, P. Gehron and Shi, S. (2000), Postnatal Human Dental Pulp Stem Cells (DPSCs) in Vitro and in Vivo. *Proceedings of the National Academy of Sciences*, 97(25): 13625–13630.

Grotendorst, Gary R., Rahmanie, Hamed and Duncan, Matthew R. (2004), Combinatorial Signaling Pathways Determine Fibroblast Proliferation and Myofibroblast Differentiation. *The FASEB Journal*, 18(3): 469–479.

Guo, Lamei, Campagne, Christine, Perwuelz, Anne and Leroux, F. (2009), Zeta Potential and Surface Physico-Chemical Properties of Atmospheric Air-Plasma-Treated Polyester Fabrics. *Textile Research Journal*, 79(15): 1371–1377.

Gupta, Pankaj, Elkins, Casey, Long, Timothy E. and Wilkes, Garth L. (2005), Electrospinning of Linear Homopolymers of Poly(Methyl Methacrylate): Exploring Relationships between Fiber Formation, Viscosity, Molecular Weight and Concentration in a Good Solvent. *Polymer*, 46(13): 4799–4810.

Haghi, A. K. and Akbari, M. (2007), Trends in Electrospinning of Natural Nanofibers. *Physica Status Solidi (A) Applications and Materials Science*, 204(6): 1830–1834.

Hankins, Hannah M., Baldridge, Ryan D., Xu, Peng and Graham, Todd R. (2015), Role of Flippases, Scramblases and Transfer Proteins in Phosphatidylserine Subcellular Distribution. *Traffic*, 16(1): 35–47.

Harding, Clifford and Stahl, Philip (1983), Transferrin Recycling in Reticulocytes: PH and Iron Are Important Determinants of Ligand Binding and Processing. *Biochemical and Biophysical Research Communications*, 113(2): 650–658.

Harding, Clifford V., Heuser, John E. and Stahl, Philip D. (2013), Exosomes: Looking Back Three Decades and into the Future. *Journal of Cell Biology*, 200(4): 367–371.

He, Fanzhen, Li, Lu, Fan, Ruyi, Wang, Xiaoqian, Chen, Xu and Xu, Yan (2021), Extracellular Vesicles: An Emerging Regenerative Treatment for Oral Disease. *Frontiers in Cell and Developmental Biology*, 9.

Hearnden, Vanessa, Lomas, Hannah, MacNeil, Sheila, Thornhill, Martin, Murdoch, Craig, Lewis, Andrew, Madsen, Jeppe, Blanazs, Adam, Armes, Steve and Battaglia, Giuseppe (2009), Diffusion Studies of Nanometer Polymersomes

Across Tissue Engineered Human Oral Mucosa. *Pharmaceutical Research*, 26(7): 1718–1728.

Herberts, Carla A., Kwa, Marcel S.G. and Hermsen, Harm P.H. (2011), Risk Factors in the Development of Stem Cell Therapy. *Journal of Translational Medicine*, 9.

Hinz, Boris and Gabbiani, Giulio (2003), Cell-Matrix and Cell-Cell Contacts of Myofibroblasts: Role in Connective Tissue Remodeling. *Thrombosis and Haemostasis*, 90(12): 993–1002.

Holkar, Ketki, Vaidya, Anuradha, Pethe, Prasad, Kale, Vaijayanti and Ingavle, Ganesh (2020a), Biomaterials and Extracellular Vesicles in Cell-Free Therapy for Bone Repair and Regeneration: Future Line of Treatment in Regenerative Medicine. *Materialia*, 12(February): 100736.

Holkar, Ketki, Vaidya, Anuradha, Pethe, Prasad, Kale, Vaijayanti and Ingavle, Ganesh (2020b), Biomaterials and Extracellular Vesicles in Cell-Free Therapy for Bone Repair and Regeneration: Future Line of Treatment in Regenerative Medicine. *Materialia*, 12: 100736.

Honary, S and Zahir, F (2013), Effect of Zeta Potential on the Properties of Nano-Drug Delivery Systems - A Review (Part 2). *Tropical Journal of Pharmaceutical Research*, 12(2).

Hu, D. M., Cao, Q. Q. and Zuo, C. C. (2017), Effect of Charge Distribution on the Electrostatic Adsorption of Janus Nanoparticles onto Charged Surface. *AIP Advances*, 7(3): 035006.

Huang, Chun Chieh, Narayanan, Raghuvaran, Alapati, Satish and Ravindran, Sriram (2016), Exosomes as Biomimetic Tools for Stem Cell Differentiation: Applications in Dental Pulp Tissue Regeneration. *Biomaterials*, 111: 103–115.

Huang, Zhe and Xu, Aimin (2021), Adipose Extracellular Vesicles in Intercellular and

Inter-Organ Crosstalk in Metabolic Health and Diseases. *Frontiers in Immunology*, 12.

Im, Ji S., Bai, Byong Ch. and Lee, Young-Seak (2010), The Effect of Carbon Nanotubes on Drug Delivery in an Electro-Sensitive Transdermal Drug Delivery System. *Biomaterials*, 31(6): 1414–1419.

Imai, Takafumi, Takahashi, Yuki, Nishikawa, Makiya, Kato, Kana, Morishita, Masaki, Yamashita, Takuma, Matsumoto, Akihiro, Charoenviriyakul, Chonlada and Takakura, Yoshinobu (2015), Macrophage-Dependent Clearance of Systemically Administered B16BL6-Derived Exosomes from the Blood Circulation in Mice. *Journal of Extracellular Vesicles*, 4(1): 26238.

Jang, Su Chul, Kim, Oh Youn, Yoon, Chang Min, Choi, Dong-Sic, Roh, Tae-Young, Park, Jaesung, Nilsson, Jonas, Lötvall, Jan, Kim, Yoon-Keun and Gho, Yong Song (2013), Bioinspired Exosome-Mimetic Nanovesicles for Targeted Delivery of Chemotherapeutics to Malignant Tumors. *ACS Nano*, 7(9): 7698–7710.

Jella, Kishore Kumar, Nasti, Tahseen H., Li, Zhentian, Malla, Sudarshan R., Buchwald, Zachary S. and Khan, Mohammad K. (2018), Exosomes, Their Biogenesis and Role in Inter-Cellular Communication, Tumor Microenvironment and Cancer Immunotherapy. *Vaccines*, 6(4).

Jin, Qiaoqiao, Li, Peilun, Yuan, Keyong, Zhao, Fen, Zhu, Xiaohan, Zhang, Pengfei and Huang, Zhengwei (2020), Extracellular Vesicles Derived from Human Dental Pulp Stem Cells Promote Osteogenesis of Adipose-Derived Stem Cells via the MAPK Pathway. *Journal of Tissue Engineering*, 11: 204173142097556.

Johnstone, R. M., Adam, M., Hammond, J. R., Orr, L. and Turbide, C. (1987), Vesicle Formation during Reticulocyte Maturation. Association of Plasma Membrane Activities with Released Vesicles (Exosomes). *Journal of Biological*

Chemistry, 262(19): 9412–9420.

Jordens, Ingrid, Fernandez-Borja, Mar, Marsman, Marije, Dusseljee, Simone, Janssen, Lennert, Calafat, Jero, Janssen, Hans, Wubbolts, Richard and Neefjes, Jacques (2001), The Rab7 Effector Protein RILP Controls Lysosomal Transport by Inducing the Recruitment of Dynein-Dynactin Motors. *Current Biology*, 11(21): 1680–1685.

Jung, Min Kyo and Mun, Ji Young (2018), Sample Preparation and Imaging of Exosomes by Transmission Electron Microscopy. *Journal of Visualized Experiments*, 2018(131): 1–6.

Kalasin, Surachate and Santore, Maria M. (2009), Non-Specific Adhesion on Biomaterial Surfaces Driven by Small Amounts of Protein Adsorption. *Colloids and Surfaces B: Biointerfaces*, 73(2): 229–236.

Kaszuba, Michael, Corbett, Jason, Watson, Fraser Mcneil and Jones, Andrew (2010), High-Concentration Zeta Potential Measurements Using Light-Scattering Techniques. *Philosophical Transactions of the Royal Society A: Mathematical, Physical and Engineering Sciences*, 368(1927): 4439–4451.

Kerr, Markus C. and Teasdale, Rohan D. (2009), Defining Macropinocytosis. *Traffic*, 10(4): 364–371.

Ki, Chang Seok, Baek, Doo Hyun, Gang, Kyung Don, Lee, Ki Hoon, Um, In Chul and Park, Young Hwan (2005), Characterization of Gelatin Nanofiber Prepared from Gelatin-Formic Acid Solution. *Polymer*, 46(14): 5094–5102.

Kim, Jong Oh, Kabanov, Alexander V. and Bronich, Tatiana K. (2009), Polymer Micelles with Cross-Linked Polyanion Core for Delivery of a Cationic Drug Doxorubicin. *Journal of Controlled Release*, 138(3): 197–204.

Kim, Seon Hee, Bianco, Nicole, Menon, Rajasree, Lechman, Eric R., Shufesky,

William J., Morelli, Adrian E. and Robbins, Paul D. (2006), Exosomes Derived from Genetically Modified DC Expressing FasL Are Anti-Inflammatory and Immunosuppressive. *Molecular Therapy*, 13(2): 289–300.

Konoshenko, Maria Yu, Lekchnov, Evgeniy A., Vlassov, Alexander V. and Laktionov, Pavel P. (2018), Isolation of Extracellular Vesicles: General Methodologies and Latest Trends. *BioMed Research International*, 2018.

Kopeček, Jindřich (2007), Hydrogel Biomaterials: A Smart Future? *Biomaterials*, 28(34): 5185–5192.

Kowal, Joanna, Arras, Guillaume, Colombo, Marina, Jouve, Mabel, Morath, Jakob Paul, Primdal-Bengtson, Bjarke, Dingli, Florent, Loew, Damarys, Tkach, Mercedes and Théry, Clotilde (2016), Proteomic Comparison Defines Novel Markers to Characterize Heterogeneous Populations of Extracellular Vesicle Subtypes. *Proceedings of the National Academy of Sciences of the United States of America*, 113(8): E968–E977.

Lai, Charles P., Mardini, Osama, Ericsson, Maria, Prabhakar, Shilpa, Maguire, Casey A., Chen, John W., Tannous, Bakhos A. and Breakefield, Xandra O. (2014), Dynamic Biodistribution of Extracellular Vesicles in Vivo Using a Multimodal Imaging Reporter. *ACS Nano*, 8(1): 483–494.

Lai, Ruenn Chai, Tan, Soon Sim, Yeo, Ronne Wee Yeh, Choo, Andre Boon Hwa, Reiner, Agnes T., Su, Yan, Shen, Yang, Fu, Zhiyan, Alexander, Lezhava, Sze, Siu Kwan and Lim, Sai Kiang (2016), MSC Secretes at Least 3 EV Types Each with a Unique Permutation of Membrane Lipid, Protein and RNA. *Journal of Extracellular Vesicles*, 5(1): 29828.

Lamalice, Laurent, Le Boeuf, Fabrice and Huot, Jacques (2007), Endothelial Cell Migration During Angiogenesis. *Circulation Research*, 100(6): 782–794.

Lamichhane, Tek N., Sokic, Sonja, Schardt, John S., Raiker, Rahul S., Lin, Jennifer W. and Jay, Steven M. (2015), Emerging Roles for Extracellular Vesicles in Tissue Engineering and Regenerative Medicine. *Tissue Engineering - Part B: Reviews*, 21(1): 45–54.

Langer, Robert and Vacanti, Joseph P (1993), Tissue Engineering. *Science*, 260(May): 920–926.

Laschke, M.W. and Menger, M.D. (2012), Vascularization in Tissue Engineering: Angiogenesis versus Inosculation. *European Surgical Research*, 48(2): 85–92.

Lee, Changjin, Mitsialis, S. Alex, Aslam, Muhammad, Vitali, Sally H., Vergadi, Eleni, Konstantinou, Georgios, Sdrimas, Konstantinos, Fernandez-Gonzalez, Angeles and Kourembanas, Stella (2012), Exosomes Mediate the Cytoprotective Action of Mesenchymal Stromal Cells on Hypoxia-Induced Pulmonary Hypertension. *Circulation*, 126(22): 2601–2611.

Lener, Thomas, Gimona, Mario, Aigner, Ludwig, Börger, Verena, Buzas, Edit, Camussi, Giovanni, Chaput, Nathalie, Chatterjee, Devasis, Court, Felipe A., Portillo, Hernando A. del, O'Driscoll, Lorraine, Fais, Stefano, Falcon-Perez, Juan M., Felderhoff-Mueser, Ursula, Fraile, Lorenzo, Gho, Yong Song, Görgens, André, Gupta, Ramesh C., Hendrix, An, Hermann, Dirk M., Hill, Andrew F., Hochberg, Fred, Horn, Peter A., Kleijn, Dominique de, Kordelas, Lambros, Kramer, Boris W., Krämer-Albers, Eva-Maria, Laner-Plamberger, Sandra, Laitinen, Saara, Leonardi, Tommaso, Lorenowicz, Magdalena J., Lim, Sai Kiang, Lötvall, Jan, Maguire, Casey A., Marcilla, Antonio, Nazarenko, Irina, Ochiya, Takahiro, Patel, Tushar, Pedersen, Shona, Pocsfalvi, Gabriella, Pluchino, Stefano, Quesenberry, Peter, Reischl, Ilona G., Rivera, Francisco J., Sanzenbacher, Ralf, Schallmoser, Katharina, Slaper-Cortenbach, Ineke, Strunk,

Dirk, Tonn, Torsten, Vader, Pieter, Balkom, Bas W. M. van, Wauben, Marca, Andaloussi, Samir El, Théry, Clotilde, Rohde, Eva and Giebel, Bernd (2015), Applying Extracellular Vesicles Based Therapeutics in Clinical Trials – an ISEV Position Paper. *Journal of Extracellular Vesicles*, 4(1): 30087.

Li, Dan and Xia, Younan (2004), Electrospinning of Nanofibers: Reinventing the Wheel? *Advanced Materials*, 16(14): 1151–1170.

Li, Guo, Zhang, Tong, Li, Meng, Fu, Na, Fu, Yao, Ba, Kai, Deng, Shuwen, Jiang, Yan, Hu, Jing, Peng, Qiang and Lin, Yunfeng (2014), Electrospun Fibers for Dental and Craniofacial Applications. *Current Stem Cell Research & Therapy*, 9(3): 187–195.

Lin, Guiting, Liu, Gang, Banie, Lia, Wang, Guifang, Ning, Hongxiu, Lue, Tom F. and Lin, Ching-Shwun (2011), Tissue Distribution of Mesenchymal Stem Cell Marker Stro-1. *Stem Cells and Development*, 20(10): 1747–1752.

Linares, Romain, Tan, Sisareuth, Gounou, Céline, Arraud, Nicolas and Brisson, Alain R. (2015), High-Speed Centrifugation Induces Aggregation of Extracellular Vesicles. *Journal of Extracellular Vesicles*, 4(1).

Liu, Xiaolin, Yang, Yunlong, Li, Yan, Niu, Xin, Zhao, Bizeng, Wang, Yang, Bao, Chunyan, Xie, Zongping, Lin, Qiuning and Zhu, Linyong (2017), Integration of Stem Cell-Derived Exosomes with in Situ Hydrogel Glue as a Promising Tissue Patch for Articular Cartilage Regeneration. *Nanoscale*, 9(13): 4430–4438.

Liu, Ying, Ji, Yuan, Ghosh, Kaustabh, Clark, Richard A. F., Huang, Lei and Rafailovich, Miriam H. (2009), Effects of Fiber Orientation and Diameter on the Behavior of Human Dermal Fibroblasts on Electrospun PMMA Scaffolds. *Journal of Biomedical Materials Research Part A*, 90A(4): 1092–1106.

Liu, Zhanguo, Cauvi, David M., Bernardino, Erika M.A., Lara, Bernardo, Lizardo,

Radhames E., Hawisher, Dennis, Bickler, Stephen and De Maio, Antonio (2018), Isolation and Characterization of Human Urine Extracellular Vesicles. *Cell Stress and Chaperones*, 23(5): 943–953.

Livshts, Mikhail A., Khomyakova, Elena, Evtushenko, Evgeniy G., Lazarev, Vassili N., Kulemin, Nikolay A., Semina, Svetlana E., Generozov, Edward V. and Govorun, Vadim M. (2015), Isolation of Exosomes by Differential Centrifugation: Theoretical Analysis of a Commonly Used Protocol. *Scientific Reports*, 5(November): 1–14.

Loh, Qiu Li and Choong, Cleo (2013), Three-Dimensional Scaffolds for Tissue Engineering Applications: Role of Porosity and Pore Size. *Tissue Engineering - Part B: Reviews*, 19(6): 485–502.

Lopez-Verrilli, María Alejandra, Picou, Frederic and Court, Felipe A. (2013), Schwann Cell-Derived Exosomes Enhance Axonal Regeneration in the Peripheral Nervous System. *Glia*, 61(11): 1795–1806.

Lötvall, Jan, Hill, Andrew F., Hochberg, Fred, Buzás, Edit I., Di Vizio, Dolores, Gardiner, Christopher, Gho, Yong Song, Kurochkin, Igor V., Mathivanan, Suresh, Quesenberry, Peter, Sahoo, Susmita, Tahara, Hidetoshi, Wauben, Marca H., Witwer, Kenneth W. and Théry, Clotilde (2014), Minimal Experimental Requirements for Definition of Extracellular Vesicles and Their Functions: A Position Statement from the International Society for Extracellular Vesicles. *Journal of Extracellular Vesicles*, 3(1): 26913.

Luong, Nguyen Dang, Moon, Ik Sang and Nam, Jae Do (2009), A Solvent-Assisted Compression Molded of Poly(L-Lactide)/Hydroxyapatite Electrospun Fibers for Robust Engineered Scaffold Systems. *Macromolecular Materials and Engineering*, 294(10): 699–704.

Luraghi, Andrea, Peri, Francesco and Moroni, Lorenzo (2021), Electrospinning for Drug Delivery Applications: A Review. *Journal of Controlled Release*, 334: 463–484.

Luzuriaga, Jon, Irurzun, Jon, Irastorza, Igor, Unda, Fernando, Ibarretxe, Gaskon and Pineda, Jose R. (2020), Vasculogenesis from Human Dental Pulp Stem Cells Grown in Matrigel with Fully Defined Serum-Free Culture Media. *Biomedicines*, 8(11): 483.

Madison, Marisa, Welch, Jennifer and Okeoma, Chioma (2017), Isolation of Exosomes from Semen for in Vitro Uptake and HIV-1 Infection Assays. *Bio-Protocol*, 7(7).

Mammadov, Rashad, Mammadov, Busra, Toksoz, Sila, Aydin, Bahri, Yagci, Ramazan, Tekinay, Ayse B. and Guler, Mustafa O. (2011), Heparin Mimetic Peptide Nanofibers Promote Angiogenesis. *Biomacromolecules*, 12(10): 3508–3519.

Mangir, Naşide, Dikici, Serkan, Claeyssens, Frederik and MacNeil, Sheila (2019), Using Ex Ovo Chick Chorioallantoic Membrane (CAM) Assay To Evaluate the Biocompatibility and Angiogenic Response to Biomaterials. *ACS Biomaterials Science & Engineering*, 5(7): 3190–3200.

Maniatopoulos, C., Sodek, J. and Melcher, A.H. (1988), Bone Formation in Vitro by Stromal Cells Obtained from Bone Marrow of Young Adult Rats. *Cell and Tissue Research*, 254(2).

Marolt Presen, Darja, Traweger, Andreas, Gimona, Mario and Redl, Heinz (2019), Mesenchymal Stromal Cell-Based Bone Regeneration Therapies: From Cell Transplantation and Tissue Engineering to Therapeutic Secretomes and Extracellular Vesicles. *Frontiers in Bioengineering and Biotechnology*,

7(November): 1–20.

Maroto, Rosario, Zhao, Yingxin, Jamaluddin, Mohammad, Popov, Vsevolod L., Wang, Hongwang, Kalubowilage, Madumali, Zhang, Yueqing, Luisi, Jonathan, Sun, Hong, Culbertson, Christopher T., Bossmann, Stefan H., Motamedi, Massoud and Brasier, Allan R. (2017), Effects of Storage Temperature on Airway Exosome Integrity for Diagnostic and Functional Analyses. *Journal of Extracellular Vesicles*, 6(1): 1359478.

Martínez-Sarrà, Ester, Montori, Sheyla, Gil-Recio, Carlos, Núñez-Toldrà, Raquel, Costamagna, Domiziana, Rotini, Alessio, Atari, Maher, Luttun, Aernout and Sampaolesi, Maurilio (2017), Human Dental Pulp Pluripotent-like Stem Cells Promote Wound Healing and Muscle Regeneration. *Stem Cell Research & Therapy*, 8(1): 175.

Mastrullo, Valeria, Cathery, William, Velliou, Eirini, Madeddu, Paolo and Campagnolo, Paola (2020), Angiogenesis in Tissue Engineering: As Nature Intended? *Frontiers in Bioengineering and Biotechnology*, 8.

Masyuk, Anatoliy I., Huang, Bing Q., Ward, Christopher J., Gradilone, Sergio A., Banales, Jesus M., Masyuk, Tatyana V., Radtke, Brynn, Splinter, Patrick L. and LaRusso, Nicholas F. (2010), Biliary Exosomes Influence Cholangiocyte Regulatory Mechanisms and Proliferation through Interaction with Primary Cilia. *American Journal of Physiology-Gastrointestinal and Liver Physiology*, 299(4): G990–G999.

Mateescu, Bogdan, Kowal, Emma J.K., van Balkom, Bas W.M., Bartel, Sabine, Bhattacharyya, Suvendra N., Buzás, Edit I., Buck, Amy H., de Candia, Paola, Chow, Franklin W.N., Das, Saumya, Driedonks, Tom A.P., Fernández-Messina, Lola, Haderk, Franziska, Hill, Andrew F., Jones, Jennifer C., Van Keuren-

Jensen, Kendall R., Lai, Charles P., Lässer, Cecilia, di Liegro, Italia, Lunavat, Taral R., Lorenowicz, Magdalena J., Maas, Sybren L.N., Mäger, Imre, Mittelbrunn, Maria, Momma, Stefan, Mukherjee, Kamalika, Nawaz, Muhammed, Pegtel, D. Michiel, Pfaffl, Michael W., Schiffelers, Raymond M., Tahara, Hidetoshi, Théry, Clotilde, Tosar, Juan Pablo, Wauben, Marca H.M., Witwer, Kenneth W. and Nolte-'t Hoen, Esther N.M. (2017), Obstacles and Opportunities in the Functional Analysis of Extracellular Vesicle RNA - An ISEV Position Paper. *Journal of Extracellular Vesicles*, 6(1).

McCullough, J., Fisher, R. D., Whitby, F. G., Sundquist, W. I. and Hill, C. P. (2008), ALIX-CHMP4 Interactions in the Human ESCRT Pathway. *Proceedings of the National Academy of Sciences*, 105(22): 7687–7691.

Melling, Genevieve E, Flannery, Sarah E, Abidin, Siti A, Clemmens, Hannah, Prajapati, Priyanka, Hinsley, Emma E, Hunt, Stuart, Catto, James W F, Coletta, Ricardo Della, Mellone, Massimiliano, Thomas, Gareth J, Parkinson, E Ken, Prime, Stephen S, Paterson, Ian C, Buttle, David J and Lambert, Daniel W (2018), A MiRNA-145/TGF-B1 Negative Feedback Loop Regulates the Cancer-Associated Fibroblast Phenotype. *Carcinogenesis*, 39(6): 798–807.

Merckx, Greet, Hosseinkhani, Baharak, Kuypers, Sören, Deville, Sarah, Irobi, Joy, Nelissen, Inge, Michiels, Luc, Lambrichts, Ivo and Bronckaers, Annelies (2020), Angiogenic Effects of Human Dental Pulp and Bone Marrow-Derived Mesenchymal Stromal Cells and Their Extracellular Vesicles. *Cells*, 9(2): 312.

Merckx, Greet, Tay, Hanna, Lo Monaco, Melissa, van Zandvoort, Marc, De Spiegelaere, Ward, Lambrichts, Ivo and Bronckaers, Annelies (2020), Chorioallantoic Membrane Assay as Model for Angiogenesis in Tissue Engineering: Focus on Stem Cells. *Tissue Engineering Part B: Reviews*, 26(6):

519–539.

Merjaneh, Mays, Langlois, Amélie, Larochelle, Sébastien, Cloutier, Chanel Beaudoin, Ricard-Blum, Sylvie and Moulin, Véronique J. (2017), Pro-Angiogenic Capacities of Microvesicles Produced by Skin Wound Myofibroblasts. *Angiogenesis*, 20(3): 385–398.

Metwally, Sara, Ferraris, Sara, Spriano, Silvia, Krysiak, Zuzanna J., Kaniuk, Łukasz, Marzec, Mateusz M., Kim, Sung Kyun, Szewczyk, Piotr K., Gruszczyński, Adam, Wytrwal-Sarna, Magdalena, Karbowniczek, Joanna E., Bernasik, Andrzej, Kar-Narayan, Sohini and Stachewicz, Urszula (2020), Surface Potential and Roughness Controlled Cell Adhesion and Collagen Formation in Electrospun PCL Fibers for Bone Regeneration. *Materials & Design*, 194: 108915.

Metwally, Sara, Karbowniczek, Joanna E., Szewczyk, Piotr K., Marzec, Mateusz M., Gruszczyński, Adam, Bernasik, Andrzej and Stachewicz, Urszula (2019), Single-Step Approach to Tailor Surface Chemistry and Potential on Electrospun PCL Fibers for Tissue Engineering Application. *Advanced Materials Interfaces*, 6(2): 1801211.

Metwally, Sara and Stachewicz, Urszula (2019), Surface Potential and Charges Impact on Cell Responses on Biomaterials Interfaces for Medical Applications. *Materials Science and Engineering: C*, 104: 109883.

Midekessa, Getnet, Godakumara, Kasun, Ord, James, Viil, Janeli, Lättekivi, Freddy, Dissanayake, Keerthie, Kopanchuk, Sergei, Rinken, Ago, Andronowska, Aneta, Bhattacharjee, Sourav, Rinken, Toonika and Fazeli, Alireza (2020), Zeta Potential of Extracellular Vesicles: Toward Understanding the Attributes That Determine Colloidal Stability. *ACS Omega*, 5(27): 16701–16710.

Miller, Michael J. and Patrick, Charles W. (2003), *Tissue Engineering*.

Möbius, Wiebke, Ohno-Iwashita, Yoshiko, Donselaar, Elly G. van, Oorschot, Viola M.J., Shimada, Yukiko, Fujimoto, Toyoshi, Heijnen, Harry F.G., Geuze, Hans J. and Slot, Jan W. (2002), Immunoelectron Microscopic Localization of Cholesterol Using Biotinylated and Non-Cytolytic Perfringolysin O. *Journal of Histochemistry & Cytochemistry*, 50(1): 43–55.

Mohammadi, Mohammad, Shokrgozar, Mohammad Ali and Mofid, Rasool (2007), Culture of Human Gingival Fibroblasts on a Biodegradable Scaffold and Evaluation of Its Effect on Attached Gingiva: A Randomized, Controlled Pilot Study. *Journal of Periodontology*, 78(10): 1897–1903.

Moharamzadeh, K., Brook, I. M., Van Noort, R., Scutt, A. M. and Thornhill, M. H. (2007), Tissue-Engineered Oral Mucosa: A Review of the Scientific Literature. *Journal of Dental Research*, 86(2): 115–124.

Mol, Emma A., Goumans, Marie-José, Doevendans, Pieter A., Sluijter, Joost P.G. and Vader, Pieter (2017), Higher Functionality of Extracellular Vesicles Isolated Using Size-Exclusion Chromatography Compared to Ultracentrifugation. *Nanomedicine: Nanotechnology, Biology and Medicine*, 13(6): 2061–2065.

Monguió-Tortajada, Marta, Gálvez-Montón, Carolina, Bayes-Genis, Antoni, Roura, Santiago and Borràs, Francesc E. (2019), Extracellular Vesicle Isolation Methods: Rising Impact of Size-Exclusion Chromatography. *Cellular and Molecular Life Sciences*, 76(12): 2369–2382.

Moonesi Rad, Reza, Atila, Deniz, Akgün, Elif Ece, Evis, Zafer, Keskin, Dilek and Tezcaner, Ayşen (2019), Evaluation of Human Dental Pulp Stem Cells Behavior on a Novel Nanobiocomposite Scaffold Prepared for Regenerative Endodontics. *Materials Science and Engineering: C*, 100: 928–948.

Morales-Kastresana, Aizea, Telford, Bill, Musich, Thomas A., McKinnon, Katherine,

Clayborne, Cassandra, Braig, Zach, Rosner, Ari, Demberg, Thorsten, Watson, Dionysios C., Karpova, Tatiana S., Freeman, Gordon J., Dekruyff, Rosemarie H., Pavlakis, George N., Terabe, Masaki, Robert-Guroff, Marjorie, Berzofsky, Jay A. and Jones, Jennifer C. (2017), Labeling Extracellular Vesicles for Nanoscale Flow Cytometry. *Scientific Reports*, 7(1): 1–10.

Morelli, Adrian E., Larregina, Adriana T., Shufesky, William J., Sullivan, Mara L.G., Stolz, Donna Beer, Papworth, Glenn D., Zahorchak, Alan F., Logar, Alison J., Wang, Zhiliang, Watkins, Simon C., Falo, Louis D. and Thomson, Angus W. (2004), Endocytosis, Intracellular Sorting, and Processing of Exosomes by Dendritic Cells. *Blood*, 104(10): 3257–3266.

Morent, Rino, De Geyter, Nathalie, Desmet, Tim, Dubruel, Peter and Leys, Christophe (2011), Plasma Surface Modification of Biodegradable Polymers: A Review. *Plasma Processes and Polymers*, 8(3): 171–190.

Morse, Michael A., Garst, Jennifer, Osada, Takuya, Khan, Shubi, Hobeika, Amy, Clay, Timothy M., Valente, Nancy, Shreeniwas, Revati, Sutton, Mary Ann, Delcayre, Alain, Hsu, Di Hwei, Le Pecq, Jean Bernard and Lyerly, H. Kim (2005), A Phase I Study of Dexosome Immunotherapy in Patients with Advanced Non-Small Cell Lung Cancer. *Journal of Translational Medicine*, 3: 1–8.

Mulcahy, Laura Ann, Pink, Ryan Charles and Carter, David Raul Francisco (2014), Routes and Mechanisms of Extracellular Vesicle Uptake. *Journal of Extracellular Vesicles*, 3(1).

Muralidharan-Chari, Vandhana, Clancy, James W., Sedgwick, Alanna and D'Souza-Schorey, Crislyn (2010), Microvesicles: Mediators of Extracellular Communication during Cancer Progression. *Journal of Cell Science*, 123(10):

1603–1611.

Murtey, Mogana Das (2016), Immunogold Techniques in Electron Microscopy, , in: *Modern Electron Microscopy in Physical and Life Sciences*.

Nair, Karthik, Whiteside, Benjamin, Grant, Colin, Patel, Rajnikant, Tuinea-Bobe, Cristina, Norris, Keith and Paradkar, Anant (2015), Investigation of Plasma Treatment on Micro-Injection Moulded Microneedle for Drug Delivery. *Pharmaceutics*, 7: 471–485.

Nair, Lakshmi S. and Laurencin, Cato T. (2007), Biodegradable Polymers as Biomaterials. *Progress in Polymer Science (Oxford)*, 32(8–9): 762–798.

Nakashima, Misako, Iohara, Koichiro and Sugiyama, Masahiko (2009), Human Dental Pulp Stem Cells with Highly Angiogenic and Neurogenic Potential for Possible Use in Pulp Regeneration. *Cytokine & Growth Factor Reviews*, 20(5–6): 435–440.

Navarrete, D. S. Villanueva (2020), Design and Fabrication of Microstructured and Mechanicallycontrolled Electrospun Corneal Membranes.

Nazarnezhad, Simin, Baino, Francesco, Kim, Hae-Won, Webster, Thomas J. and Kargozar, Saeid (2020), Electrospun Nanofibers for Improved Angiogenesis: Promises for Tissue Engineering Applications. *Nanomaterials*, 10(8): 1609.

Oka, Naoki, Soeda, Akio, Inagaki, Akihito, Onodera, Masafumi, Maruyama, Hidekazu, Hara, Akira, Kunisada, Takahiro, Mori, Hideki and Iwama, Toru (2007), VEGF Promotes Tumorigenesis and Angiogenesis of Human Glioblastoma Stem Cells. *Biochemical and Biophysical Research Communications*, 360(3): 553–559.

Pan, Bin Tao and Johnstone, Rose M. (1983), Fate of the Transferrin Receptor during Maturation of Sheep Reticulocytes in Vitro: Selective Externalization of

the Receptor. *Cell*, 33(3): 967–978.

Parolini, Isabella, Federici, Cristina, Raggi, Carla, Lugini, Luana, Palleschi, Simonetta, De Milito, Angelo, Coscia, Carolina, Iessi, Elisabetta, Logozzi, Mariantonia, Molinari, Agnese, Colone, Marisa, Tatti, Massimo, Sargiacomo, Massimo and Fais, Stefano (2009), Microenvironmental PH Is a Key Factor for Exosome Traffic in Tumor Cells. *Journal of Biological Chemistry*, 284(49): 34211–34222.

Pasquet, Jean-Max, Dachary-Prigent, Jeanne and Nurden, Alan T. (1996), Calcium Influx Is a Determining Factor of Calpain Activation and Microparticle Formation in Platelets. *European Journal of Biochemistry*, 239(3): 647–654.

Pavani, Krishna Chaitanya, Hendrix, An, Van Den Broeck, Wim, Couck, Liesbeth, Szymanska, Katarzyna, Lin, Xiaoyuan, De Koster, Jenne, Van Soom, Ann and Leemans, Bart (2019), Isolation and Characterization of Functionally Active Extracellular Vesicles from Culture Medium Conditioned by Bovine Embryos in Vitro. *International Journal of Molecular Sciences*, 20(1): 1–22.

Pera, Martin F. and Trounson, Alan O. (2004), Human Embryonic Stem Cells: Prospects for Development. *Development*, 131(22): 5515–5525. r

Petlin, D.G., Tverdokhlebov, S.I. and Anissimov, Y.G. (2017), Plasma Treatment as an Efficient Tool for Controlled Drug Release from Polymeric Materials: A Review. *Journal of Controlled Release*, 266: 57–74.

Pham, Quynh P., Sharma, Upma and Mikos, Antonios G. (2006), Electrospinning of Polymeric Nanofibers for Tissue Engineering Applications: A Review. *Tissue Engineering*, 12(5): 1197–1211.

Phan, Jennifer, Kumar, Priyadarsini, Hao, Dake, Gao, Kewa, Farmer, Diana and Wang, Aijun (2018), Engineering Mesenchymal Stem Cells to Improve Their

Exosome Efficacy and Yield for Cell-Free Therapy. *Journal of Extracellular Vesicles*, 7(1).

Pignataro, Bruno, Steinem, Claudia, Galla, Hans Joachim, Fuchs, Harald and Janshoff, Andreas (2000), Specific Adhesion of Vesicles Monitored by Scanning Force Microscopy and Quartz Crystal Microbalance. *Biophysical Journal*, 78(1): 487–498.

Pinheiro, Alice, Silva, Andreia M., Teixeira, José H., Gonçalves, Raquel M., Almeida, Maria I., Barbosa, Mário A. and Santos, Susana G. (2018), Extracellular Vesicles: Intelligent Delivery Strategies for Therapeutic Applications. *Journal of Controlled Release*, 289(September): 56–69.

van der Pol, E., Coumans, F. A.W., Grootemaat, A. E., Gardiner, C., Sargent, I. L., Harrison, P., Sturk, A., van Leeuwen, T. G. and Nieuwland, R. (2014), Particle Size Distribution of Exosomes and Microvesicles Determined by Transmission Electron Microscopy, Flow Cytometry, Nanoparticle Tracking Analysis, and Resistive Pulse Sensing. *Journal of Thrombosis and Haemostasis*, 12(7): 1182–1192.

Van Der Pol, E., Van Gemert, M. J.C., Sturk, A., Nieuwland, R. and Van Leeuwen, T. G. (2012), Single vs. Swarm Detection of Microparticles and Exosomes by Flow Cytometry. *Journal of Thrombosis and Haemostasis*, 10(5): 919–930.

Prabhakaran, Molamma P., Venugopal, J., Chan, Casey K. and Ramakrishna, S. (2008), Surface Modified Electrospun Nanofibrous Scaffolds for Nerve Tissue Engineering. *Nanotechnology*, 19(45).

Prime, Stephen S., Nixon, Sally V. R., Crane, Isabel J., Stone, Andrea, Matthews, John B., Maitland, Norman J., Remnant, Lucy, Powell, Susan K., Game, Stephen M. and Scully, Crispian (1990), The Behaviour of Human Oral

Squamous Cell Carcinoma in Cell Culture. *The Journal of Pathology*, 160(3): 259–269.

Process, Electrospinning, Doshi, Jayesh and Reneker, Darrell H (1995), Proceedings of the 1993 IEEE Industry Applications Society Meeting. *Journal of Electrostatics*, 35(2–3): 151–296.

Pusic, Aya D., Pusic, Kae M., Clayton, Benjamin L.L. and Kraig, Richard P. (2014), IFNγ-Stimulated Dendritic Cell Exosomes as a Potential Therapeutic for Remyelination. *Journal of Neuroimmunology*, 266(1–2): 12–23.

Qin, Yunhao, Wang, Lian, Gao, Zhengliang, Chen, Genyin and Zhang, Changqing (2016), Bone Marrow Stromal/Stem Cell-Derived Extracellular Vesicles Regulate Osteoblast Activity and Differentiation in Vitro and Promote Bone Regeneration in Vivo. *Scientific Reports*, 6(1): 21961.

Raposo G, Nijman HW, Stoorvogel W, Liejendekker R, Harding CV, Melief CJ, Geuze HJ (1996), B Lymphocytes Secrete Antigen-PresentingVesicles. *Journal of Experimental Medicine*, 183(March): 1161–1172.

Raposo, Graça and Stoorvogel, Willem (2013), Extracellular Vesicles: Exosomes, Microvesicles, and Friends. *Journal of Cell Biology*, 200(4): 373–383.

Reneker, Darrell H. and Chun, Iksoo (1996), Nanometre Diameter Fibres of Polymer, Produced by Electrospinning. *Nanotechnology*, 7(3): 216–223.

Rezaie, Jafar, Ajezi, Saeed, Avci, r. Biray, Karimipour, Mohammad, Geranmayeh, Mohammad Hossein, Nourazarian, Alireza, Sokullu, Emel, Rezabakhsh, Aysa and Rahbarghazi, Reza (2018), Exosomes and Their Application in Biomedical Field: Difficulties and Advantages. *Molecular Neurobiology*, 55(4): 3372–3393.

Ribatti, Domenico (2016), The Chick Embryo Chorioallantoic Membrane (CAM). A Multifaceted Experimental Model. *Mechanisms of Development*, 141: 70–77.

Riches, Andrew, Campbell, Elaine, Borger, Eva and Powis, Simon (2014), Regulation of Exosome Release from Mammary Epithelial and Breast Cancer Cells – A New Regulatory Pathway. *European Journal of Cancer*, 50(5): 1025–1034.

Rodriguez, David Hiram Ramos (2021), Development of Topographically Controlled Electrospun Scaffolds to Stimulate Wound Healing for Skin Tissue Engineering.

Rosario-Meléndez, Roselin, Lavelle, Linda, Bodnar, Stanko, Halperin, Frederick, Harper, Ike, Griffin, Jeremy and Uhrich, Kathryn E. (2011), Stability of a Salicylate-Based Poly(Anhydride-Ester) to Electron Beam and Gamma Radiation. *Polymer Degradation and Stability*, 96(9): 1625–1630.

Røsland, Gro Vatne, Svendsen, Agnete, Torsvik, Anja, Sobala, Ewa, McCormack, Emmet, Immervoll, Heike, Mysliwietz, Josef, Tonn, Joerg-Christian, Goldbrunner, Roland, Lønning, Per Eystein, Bjerkvig, Rolf and Schichor, Christian (2009), Long-Term Cultures of Bone Marrow–Derived Human Mesenchymal Stem Cells Frequently Undergo Spontaneous Malignant Transformation. *Cancer Research*, 69(13): 5331–5339.

Rudt, S. and Müller, R. H. (1993), In Vitro Phagocytosis Assay of Nano- and Microparticles by Chemiluminescence. III. Uptake of Differently Sized Surface-Modified Particles, and Its Correlation to Particle Properties and in Vivo Distribution. *European Journal of Pharmaceutical Sciences*, 1(1): 31–39.

Rupert, Déborah L.M., Claudio, Virginia, Lässer, Cecilia and Bally, Marta (2017), Methods for the Physical Characterization and Quantification of Extracellular Vesicles in Biological Samples. *Biochimica et Biophysica Acta - General Subjects*, 1861(1): 3164–3179.

Sakiyama-Elbert, Shelly E. (2014), Incorporation of Heparin into Biomaterials. *Acta*

Biomaterialia, 10(4): 1581–1587.

Sakiyama-Elbert, Shelly E (2013), Incorporation of Heparin into Biomaterials.

Salomon, Carlos, Ryan, Jennifer, Sobrevia, Luis, Kobayashi, Miharu, Ashman, Keith, Mitchell, Murray and Rice, Gregory E. (2013), Exosomal Signaling during Hypoxia Mediates Microvascular Endothelial Cell Migration and Vasculogenesis. *PLoS ONE*, 8(7): 1–24.

Sandoval-Castellanos, Ana M., Claeyssens, Frederik and Haycock, John W. (2020), Biomimetic Surface Delivery of NGF and BDNF to Enhance Neurite Outgrowth. *Biotechnology and Bioengineering*, 117(10): 3124–3135.

Santocildes-Romero, Martin E., Crawford, Aileen, Hatton, Paul V., Goodchild, Rebecca L., Reaney, Ian M. and Miller, Cheryl A. (2015), The Osteogenic Response of Mesenchymal Stromal Cells to Strontium-Substituted Bioactive Glasses. *Journal of Tissue Engineering and Regenerative Medicine*, 9(5): 619–631.

Sarkar, Sumona, Lee, George Y., Wong, Joyce Y. and Desai, Tejal A. (2006), Development and Characterization of a Porous Micro-Patterned Scaffold for Vascular Tissue Engineering Applications. *Biomaterials*, 27(27): 4775–4782.

Savina, Ariel, Furlán, Marcelo, Vidal, Michel and Colombo, Maria I. (2003), Exosome Release Is Regulated by a Calcium-Dependent Mechanism in K562 Cells. *Journal of Biological Chemistry*, 278(22): 20083–20090.

Scharenberg, Matthias A., Pippenger, Benjamin E., Sack, Ragna, Zingg, Dominik, Ferralli, Jacqueline, Schenk, Susanne, Martin, Ivan and Chiquet-Ehrismann, Ruth (2014), TGF-β-Induced Differentiation into Myofibroblasts Involves Specific Regulation of Two MKL1 Isoforms. *Journal of Cell Science*.

Schreml, S, Szeimies, R-M, Karrer, S, Heinlin, J, Landthaler, M and Babilas, P

(2010), The Impact of the PH Value on Skin Integrity and Cutaneous Wound Healing. *Journal of the European Academy of Dermatology and Venereology*, 24(4): 373–378.

Singh, S., Wu, B.M. and Dunn, J.C., 2012. Delivery of VEGF using collagen-coated polycaprolactone scaffolds stimulates angiogenesis. Journal of Biomedical Materials Research Part A, 100(3), pp.720-727.

Van der Schueren, Lien, De Schoenmaker, Bert, Kalaoglu, Özlem I. and De Clerck, Karen (2011), An Alternative Solvent System for the Steady State Electrospinning of Polycaprolactone. *European Polymer Journal*, 47(6): 1256–1263.

Seeram Ramakrishna, Zamani, Maedeh and Molamma P Prabhakaran (2013), Advances in Drug Delivery via Electrospun and Electrosprayed Nanomaterials. *International Journal of Nanomedicine*: 2997.

Shandilya, Shruti, Rani, Payal, Onteru, Suneel Kumar and Singh, Dheer (2017), Small Interfering RNA in Milk Exosomes Is Resistant to Digestion and Crosses the Intestinal Barrier in Vitro. *Journal of Agricultural and Food Chemistry*, 65(43): 9506–9513.

Shi, Quan, Qian, Zhiyong, Liu, Donghua, Sun, Jie, Wang, Xing, Liu, Hongchen, Xu, Juan and Guo, Ximin (2017), GMSC-Derived Exosomes Combined with a Chitosan/Silk Hydrogel Sponge Accelerates Wound Healing in a Diabetic Rat Skin Defect Model. *Frontiers in Physiology*, 8(NOV): 1–16.

Shibuya, M. (2011), Vascular Endothelial Growth Factor (VEGF) and Its Receptor (VEGFR) Signaling in Angiogenesis: A Crucial Target for Anti- and Pro-Angiogenic Therapies. *Genes & Cancer*, 2(12): 1097–1105.

Sidhom, Karim, Obi, Patience O. and Saleem, Ayesha (2020), A Review of

Exosomal Isolation Methods: Is Size Exclusion Chromatography the Best Option? *International Journal of Molecular Sciences*, 21(18): 6466.

Sill, Travis J. and von Recum, Horst A. (2008), Electrospinning: Applications in Drug Delivery and Tissue Engineering. *Biomaterials*, 29(13): 1989–2006.

Singh, Shivani, Wu, Benjamin M. and Dunn, James C. Y. (2012), Delivery of VEGF Using Collagen-Coated Polycaprolactone Scaffolds Stimulates Angiogenesis. *Journal of Biomedical Materials Research Part A*, 100A(3): 720–727.

Skalnikova, Bohuslavova, Turnovcova, Juhasova, Juhas, Rodinova and Vodicka (2019), Isolation and Characterization of Small Extracellular Vesicles from Porcine Blood Plasma, Cerebrospinal Fluid, and Seminal Plasma. *Proteomes*, 7(2): 17.

Skalska, Julia, Oliveira, Filipa D., Figueira, Tiago N., Mello, Érica O., Gomes, Valdirene M., McNaughton-Smith, Grant, Castanho, Miguel A. R. B. and Gaspar, Diana (2019), Plant Defensin Pv D 1 Modulates the Membrane Composition of Breast Tumour-Derived Exosomes. *Nanoscale*, 11(48): 23366–23381.

Skotland, Tore, Sandvig, Kirsten and Llorente, Alicia (2017), Lipids in Exosomes: Current Knowledge and the Way Forward. *Progress in Lipid Research*, 66: 30–41.

Smyth, Tyson, Kullberg, Max, Malik, Noeen, Smith-Jones, Peter, Graner, Michael W. and Anchordoquy, Thomas J. (2015), Biodistribution and Delivery Efficiency of Unmodified Tumor-Derived Exosomes. *Journal of Controlled Release*, 199: 145–155.

Soares Martins, Tânia, Catita, José, Martins Rosa, Ilka, A. B. da Cruz e Silva, Odete and Henriques, Ana Gabriela (2018), Exosome Isolation from Distinct Biofluids

Using Precipitation and Column-Based Approaches (G.-C. Fan, Ed.). *PLOS ONE*, 13(6): e0198820.

Solis-Castro, Oscar O., Boissonade, Fiona M. and Rivolta, Marcelo N. (2020), Establishment and Neural Differentiation of Neural Crest-Derived Stem Cells from Human Dental Pulp in Serum-Free Conditions. *Stem Cells Translational Medicine*, 9(11): 1462–1476.

Stenmark, Harald (2009), Rab GTPases as Coordinators of Vesicle Traffic. *Nature Reviews Molecular Cell Biology*, 10(8): 513–525.

Stephens, Len, Ellson, Chris and Hawkins, Phillip (2002), Roles of PI3Ks in Leukocyte Chemotaxis and Phagocytosis. *Current Opinion in Cell Biology*, 14(2): 203–213.

Stoorvogel, Willem, Strous, Ger J., Geuze, Hans J., Oorschot, Viola and Schwartzt, Alan L. (1991), Late Endosomes Derive from Early Endosomes by Maturation. *Cell*, 65(3): 417–427.

Stryker, Zachary I., Rajabi, Mehdi, Davis, Paul J. and Mousa, Shaker A. (2019), Evaluation of Angiogenesis Assays. *Biomedicines*, 7(2): 37.

Suárez, Henar, Gámez-Valero, Ana, Reyes, Raquel, López-Martín, Soraya, Rodríguez, María Josefa, Carrascosa, José L., Cabañas, Carlos, Borràs, Francesc E. and Yáñez-Mó, María (2017), A Bead-Assisted Flow Cytometry Method for the Semi-Quantitative Analysis of Extracellular Vesicles. *Scientific Reports*, 7(1): 11271.

Szatanek, Rafał, Baj-Krzyworzeka, Monika, Zimoch, Jakub, Lekka, Małgorzata, Siedlar, Maciej and Baran, Jarek (2017), The Methods of Choice for Extracellular Vesicles (EVs) Characterization. *International Journal of Molecular Sciences*, 18(6).

Takahashi, Yuki, Nishikawa, Makiya, Shinotsuka, Haruka, Matsui, Yuriko, Ohara, Saori, Imai, Takafumi and Takakura, Yoshinobu (2013), Visualization and in Vivo Tracking of the Exosomes of Murine Melanoma B16-BL6 Cells in Mice after Intravenous Injection. *Journal of Biotechnology*, 165(2): 77–84.

Takeo, M., Lee, W. and Ito, M. (2015), Wound Healing and Skin Regeneration. *Cold Spring Harbor Perspectives in Medicine*, 5(1): a023267–a023267.

Takov, Kaloyan, Yellon, Derek M. and Davidson, Sean M. (2019), Comparison of Small Extracellular Vesicles Isolated from Plasma by Ultracentrifugation or Size-Exclusion Chromatography: Yield, Purity and Functional Potential. *Journal of Extracellular Vesicles*, 8(1).

Tao, Shi-Cong, Guo, Shang-Chun, Li, Min, Ke, Qin-Fei, Guo, Ya-Ping and Zhang, Chang-Qing (2017), Chitosan Wound Dressings Incorporating Exosomes Derived from MicroRNA-126-Overexpressing Synovium Mesenchymal Stem Cells Provide Sustained Release of Exosomes and Heal Full-Thickness Skin Defects in a Diabetic Rat Model. *STEM CELLS Translational Medicine*, 6(3): 736–747.

Teo, W. E. and Ramakrishna, S. (2006), A Review on Electrospinning Design and Nanofibre Assemblies. *Nanotechnology*, 17(14).

Théry, Clotilde, Clayton, Aled, Amigorena, Sebastian and Raposo, Graca (2006), Isolation and Characterization of Exosomes from Cell Culture Supernatants. *Current Protocols in Cell Biology*, supplement: 1–29.

Théry, Clotilde, Witwer, Kenneth W., Aikawa, Elena, Alcaraz, Maria Jose, et al. (2018), Minimal Information for Studies of Extracellular Vesicles 2018 (MISEV2018): A Position Statement of the International Society for Extracellular Vesicles and Update of the MISEV2014 Guidelines. *Journal of Extracellular*

Vesicles, 7(1).

Tian, Tian, Zhu, Yan Liang, Hu, Fei Hu, Wang, Yuan Yuan, Huang, Ning Ping and Xiao, Zhong Dang (2013), Dynamics of Exosome Internalization and Trafficking. *Journal of Cellular Physiology*, 228(7): 1487–1495.

Tian, Ye, Gong, Manfei, Hu, Yunyun, Liu, Haisheng, Zhang, Wenqiang, Zhang, Miaomiao, Hu, Xiuxiu, Aubert, Dimitri, Zhu, Shaobin, Wu, Lina and Yan, Xiaomei (2020), Quality and Efficiency Assessment of Six Extracellular Vesicle Isolation Methods by Nano-flow Cytometry. *Journal of Extracellular Vesicles*, 9(1): 1697028.

Tonda-Turo, Chiara, Carmagnola, Irene and Ciardelli, Gianluca (2018), Quartz Crystal Microbalance With Dissipation Monitoring: A Powerful Method to Predict the in Vivo Behavior of Bioengineered Surfaces. *Frontiers in Bioengineering and Biotechnology*, 6.

Trams, Eberhard G., Lauter, Carl J., Norman Salem, Jr and Heine, Ursula (1981), Exfoliation of Membrane Ecto-Enzymes in the Form of Micro-Vesicles. *BBA - Biomembranes*, 645(1): 63–70.

Trindade, Rita Pereira, Renault, Nisa, El Harane, Nadia, Menasché, Philippe and Williams, Gareth R. (2021), Extracellular Vesicles Can Be Processed by Electrospinning without Loss of Structure or Function. *Materials Letters*, 282: 128671.

Tsai, Chen-Chi, Chang, Yen, Sung, Hsing-Wen, Hsu, Jer-Chen and Chen, Chiun-Nan (2001), Effects of Heparin Immobilization on the Surface Characteristics of a Biological Tissue Fixed with a Naturally Occurring Crosslinking Agent (Genipin): An in Vitro Study. *Biomaterials*, 22(6): 523–533.

Valadi, Hadi, Ekström, Karin, Bossios, Apostolos, Sjöstrand, Margareta, Lee, James

J. and Lötvall, Jan O. (2007), Exosome-Mediated Transfer of MRNAs and MicroRNAs Is a Novel Mechanism of Genetic Exchange between Cells. *Nature Cell Biology*, 9(6): 654–659.

Vaquette, Cedryck, Babak, Valery G., Baros, Francis, Boulanouar, Omar, Dumas, Dominique, Fievet, Patrick, Kildeeva, Natalia R., Maincent, Philippe and Wang, Xiong (2008), Zeta-Potential and Morphology of Electrospun Nano- and Microfibers from Biopolymers and Their Blends Used as Scaffolds in Tissue Engineering. *Mendeleev Communications*, 18(1): 38–41.

Vijayalakshmi, K A, Mekala, M, Yoganand, C P and Pandiyaraj, K Navaneetha (2011), Studies on Modification of Surface Properties in Polycarbonate (PC) Film Induced by DC Glow Discharge Plasma. *International Journal of Polymer Science*, 2011.

Viswanathan, S., Shi, Y., Galipeau, J., Krampera, M., Leblanc, K., Martin, I., Nolta, J., Phinney, D.G. and Sensebe, L. (2019), Mesenchymal Stem versus Stromal Cells: International Society for Cell & Gene Therapy (ISCT®) Mesenchymal Stromal Cell Committee Position Statement on Nomenclature. *Cytotherapy*, 21(10): 1019–1024.

van der Vlist, Els J., Nolte-'t Hoen, Esther N.M., Stoorvogel, Willem, Arkesteijn, Ger J.A. and Wauben, Marca H.M. (2012), Fluorescent Labeling of Nano-Sized Vesicles Released by Cells and Subsequent Quantitative and Qualitative Analysis by High-Resolution Flow Cytometry. *Nature protocols*, 7(7): 1311–1326.

Vogel, Robert, Pal, Anoop K., Jambhrunkar, Siddharth, Patel, Pragnesh, Thakur, Sachin S., Reátegui, Eduardo, Parekh, Harendra S., Saá, Paula, Stassinopoulos, Adonis and Broom, Murray F. (2017), High-Resolution Single

Particle Zeta Potential Characterisation of Biological Nanoparticles Using Tunable Resistive Pulse Sensing. *Scientific Reports*, 7(1): 17479.

Wang, Chenggui, Wang, Min, Xu, Tianzhen, Zhang, Xingxing, Lin, Cai, Gao, Weiyang, Xu, Huazi, Lei, Bo and Mao, Cong (2019), Engineering Bioactive Self-Healing Antibacterial Exosomes Hydrogel for Promoting Chronic Diabetic Wound Healing and Complete Skin Regeneration. *Theranostics*, 9(1): 65–76.

Wang, Xuefen, Um, In Chul, Fang, Dufei, Okamoto, Akio, Hsiao, Benjamin S. and Chu, Benjamin (2005), Formation of Water-Resistant Hyaluronic Acid Nanofibers by Blowing-Assisted Electro-Spinning and Non-Toxic Post Treatments. *Polymer*, 46(13): 4853–4867.

Wang, Zhexiang, Sun, Bin, Zhang, Min, Ou, Lailiang, Che, Yongzhe, Zhang, Jun and Kong, Deling (2013), Functionalization of Electrospun Poly(ε-Caprolactone) Scaffold with Heparin and Vascular Endothelial Growth Factors for Potential Application as Vascular Grafts. *Journal of Bioactive and Compatible Polymers*, 28(2): 154–166.

Wannatong, Ladawan, Sirivat, Anuvat and Supaphol, Pitt (2004), Effects of Solvents on Electrospun Polymeric Fibers: Preliminary Study on Polystyrene. *Polymer International*, 53(11): 1851–1859.

Webber, Jason and Clayton, Aled (2013), How Pure Are Your Vesicles? *Journal of Extracellular Vesicles*, 2(1): 1–6.

Wei, Yongzhen, Wu, Yifan, Zhao, Runxia, Zhang, Kaiyue, Midgley, Adam C., Kong, Deling, Li, Zongjin and Zhao, Qiang (2019), MSC-Derived SEVs Enhance Patency and Inhibit Calcification of Synthetic Vascular Grafts by Immunomodulation in a Rat Model of Hyperlipidemia. *Biomaterials*, 204(January): 13–24.

Wei, Zhiyun, Batagov, Arsen O., Carter, David R.F. and Krichevsky, Anna M. (2016), Fetal Bovine Serum RNA Interferes with the Cell Culture Derived Extracellular RNA. *Scientific Reports*, 6: 1–6.

Wolf, P. (1967), The Nature and Significance of Platelet Products in Human Plasma. *British journal of haematology*, 13(3): 269–288.

Woodruff, Maria Ann and Hutmacher, Dietmar Werner (2010), The Return of a Forgotten Polymer - Polycaprolactone in the 21st Century. *Progress in Polymer Science (Oxford)*, 35(10): 1217–1256.

Xie, Hui, Wang, Zhenxing, Zhang, Liming, Lei, Qian, Zhao, Aiqi, Wang, Hongxiang, Li, Qiubai, Cao, Yilin, Jie Zhang, Wen and Chen, Zhichao (2017a), Extracellular Vesicle-Functionalized Decalcified Bone Matrix Scaffolds with Enhanced Pro-Angiogenic and Pro-Bone Regeneration Activities. *Scientific Reports*, 7(March): 1–13.

Xie, Hui, Wang, Zhenxing, Zhang, Liming, Lei, Qian, Zhao, Aiqi, Wang, Hongxiang, Li, Qiubai, Cao, Yilin, Jie Zhang, Wen and Chen, Zhichao (2017b), Extracellular Vesicle-Functionalized Decalcified Bone Matrix Scaffolds with Enhanced Pro-Angiogenic and Pro-Bone Regeneration Activities. *Scientific Reports*, 7(1): 45622.

Xin, Hongqi, Li, Yi, Buller, Ben, Katakowski, Mark, Zhang, Yi, Wang, Xinli, Shang, Xia, Zhang, Zheng Gang and Chopp, Michael (2012), Exosome-Mediated Transfer of MiR-133b from Multipotent Mesenchymal Stromal Cells to Neural Cells Contributes to Neurite Outgrowth. *Stem Cells*, 30(7): 1556–1564.

Xin, Hongqi, Li, Yi, Cui, Yisheng, Yang, James J., Zhang, Zheng Gang and Chopp, Michael (2013), Systemic Administration of Exosomes Released from Mesenchymal Stromal Cells Promote Functional Recovery and Neurovascular

Plasticity after Stroke in Rats. *Journal of Cerebral Blood Flow and Metabolism*, 33(11): 1711–1715.

Xu, C. Y., Inai, R., Kotaki, M. and Ramakrishna, S. (2004), Aligned Biodegradable Nanofibrous Structure: A Potential Scaffold for Blood Vessel Engineering. *Biomaterials*, 25(5): 877–886.

Yao, Qingqing, Cosme, Jaqueline G.L., Xu, Tao, Miszuk, Jacob M., Picciani, Paulo H.S., Fong, Hao and Sun, Hongli (2017), Three Dimensional Electrospun PCL/PLA Blend Nanofibrous Scaffolds with Significantly Improved Stem Cells Osteogenic Differentiation and Cranial Bone Formation. *Biomaterials*, 115: 115–127.

Ye, Lin, Wu, Xin, Duan, Hong-Yong, Geng, Xue, Chen, Bing, Gu, Yong-Quan, Zhang, Ai-Ying, Zhang, Jian and Feng, Zeng-Guo (2012), The in Vitro and in Vivo Biocompatibility Evaluation of Heparin–Poly(E-caprolactone) Conjugate for Vascular Tissue Engineering Scaffolds. *Journal of Biomedical Materials Research Part A*, 100A(12): 3251–3258.

Yildirim, Eda D., Besunder, Robyn, Guceri, Selcuk, Allen, Fred and Sun, Wei (2008), Fabrication and Plasma Treatment of 3D Polycaprolactane Tissue Scaffolds for Enhanced Cellular Function. *Virtual and Physical Prototyping*, 3(4): 199–207.

Yuan, Xiao Yan, Zhang, Yuan Yuan, Dong, Cunhai and Sheng, Jing (2004), Morphology of Ultrafine Polysulfone Fibers Prepared by Electrospinning. *Polymer International*, 53(11): 1704–1710.

Yuana, Yuana, Koning, Roman I., Kuil, Maxim E., Rensen, Patrick C. N., Koster, Abraham J., Bertina, Rogier M and Osanto, Susanne (2013), Cryo-Electron Microscopy of Extracellular Vesicles in Fresh Plasma. *Journal of Extracellular Vesicles*, 2(1): 21494.

Zeleny, John (1914), The Electrical Discharge from Liquid Points, and a Hydrostatic Method of Measuring the Electric Intensity at Their Surfaces. *Physical Review*, 3(2): 69–91.

Zhang, Chunxue, Yuan, Xiaoyan, Wu, Lili, Han, Yue and Sheng, Jing (2005), Study on Morphology of Electrospun Poly(Vinyl Alcohol) Mats. *European Polymer Journal*, 41(3): 423–432.

Zhang, Hong Chao, Liu, Xin Bin, Huang, Shu, Bi, Xiao Yun, Wang, Heng Xiang, Xie, Li Xian, Wang, Yong Qi, Cao, Xiao Fang, Lv, Jun, Xiao, Feng Jun, Yang, Yang and Guo, Zi Kuan (2012), Microvesicles Derived from Human Umbilical Cord Mesenchymal Stem Cells Stimulated by Hypoxia Promote Angiogenesis Both in Vitro and in Vivo. *Stem Cells and Development*, 21(18): 3289–3297.

Zhang, Jieyuan, Liu, Xiaolin, Li, Haiyan, Chen, Chunyuan, Hu, Bin, Niu, Xin, Li, Qing, Zhao, Bizeng, Xie, Zongping and Wang, Yang (2016), Exosomes/Tricalcium Phosphate Combination Scaffolds Can Enhance Bone Regeneration by Activating the PI3K/Akt Signaling Pathway. *Stem Cell Research and Therapy*, 7(1): 1–14.

Zhang, Kaiyue, Zhao, Xiangnan, Chen, Xiaoniao, Wei, Yongzhen, Du, Wei, Wang, Yuebing, Liu, Linan, Zhao, Weian, Han, Zhibo, Kong, Deling, Zhao, Qiang, Guo, Zhikun, Han, Zhongchao, Liu, Na, Ma, Fengxia and Li, Zongjin (2018), Enhanced Therapeutic Effects of Mesenchymal Stem Cell-Derived Exosomes with an Injectable Hydrogel for Hindlimb Ischemia Treatment. *ACS Applied Materials and Interfaces*, 10(36): 30081–30091.

Zhang, S., Chu, W. C., Lai, R. C., Lim, S. K., Hui, J. H.P. and Toh, W. S. (2016), Exosomes Derived from Human Embryonic Mesenchymal Stem Cells Promote Osteochondral Regeneration. *Osteoarthritis and Cartilage*, 24(12): 2135–2140.

Zhen, Y. and Stenmark, H. (2015), Cellular Functions of Rab GTPases at a Glance. *Journal of Cell Science*, 128(17): 3171–3176.

Zhou, Huan, Li, Xuan, Yin, Yuan, He, Xiao-Tao, An, Ying, Tian, Bei-Min, Hong, Yong-Long, Wu, Li-An and Chen, Fa-Ming (2020), The Proangiogenic Effects of Extracellular Vesicles Secreted by Dental Pulp Stem Cells Derived from Periodontally Compromised Teeth. *Stem Cell Research & Therapy*, 11(1): 110.

Zhou, Yijie, Liu, Shuyun, Zhao, Meng, Wang, Chengshi, Li, Ling, Yuan, Yujia, Li, Lan, Liao, Guangneng, Bresette, William, Zhang, Jie, Chen, Younan, Cheng, Jingqiu, Lu, Yanrong and Liu, Jingping (2019), Injectable Extracellular Vesicle-Released Self-Assembling Peptide Nanofiber Hydrogel as an Enhanced Cell-Free Therapy for Tissue Regeneration. *Journal of Controlled Release*, 316(October): 93–104.

Zhuang, Xiaoying, Xiang, Xiaoyu, Grizzle, William, Sun, Dongmei, Zhang, Shuangqin, Axtell, Robert C., Ju, Songwen, Mu, Jiangyao, Zhang, Lifeng, Steinman, Lawrence, Miller, Donald and Zhang, Huang Ge (2011), Treatment of Brain Inflammatory Diseases by Delivering Exosome Encapsulated Anti-Inflammatory Drugs from the Nasal Region to the Brain. *Molecular Therapy*, 19(10): 1769–1779.

Zitvogel, Laurence, Regnault, Armelle, Lozier, Anne, Wolfers, Joseph, Flament, Caroline, Tenza, Danielle, Ricciardi-Castagnoli, Paola, Raposo, Graça and Amigorena, Sebastian (1998), Eradication of Established Murine Tumors Using a Novel Cell-Free Vaccine: Dendritic Cell-Derived Exosomes. *Nature Medicine*, 4(5): 594–600.

Zlotogorski-Hurvitz, Ayelet, Dayan, Dan, Chaushu, Gavriel, Korvala, Johanna, Salo, Tuula, Sormunen, Raija and Vered, Marilena (2015), Human Saliva-Derived

Exosomes: Comparing Methods of Isolation. *Journal of Histochemistry and Cytochemistry*, 63(3): 181–189.

Appendix: Copyright of text and figures form (Alqurashi *et al*. 2020)